The Influence of Topography upon Rotating Magnetoconvection

by

. Paul A. Coffey

A Thesis submitted in partial fulfilment
of the requirements for the degree of
Doctor of Philosophy

Dept. Mathematics and Statistics

The University of Newcastle upon Tyne

1996

DEDICATED TO LOUISE DUFFY

Acknowledgements

I would like to express my deepest gratitude to my supervisor, Prof. Andrew Soward. Without his constant help and encouragement, this work would not have been possible. I would also like to thank him for making me aware of, and arranging for me to attend, several conferences, including the NATO ASI on Dynamo Theory in Cambridge, 1992, and the twenty first IUGG conference in Boulder, 1995, all of which I enjoyed very much. I am also grateful to Dr.'s Richard Kerswell and Matthew Walker, with whom I had many interesting and helpful conversations regarding the use (and abuse!) of the computing facilities at Newcastle. The secretaries in the department also deserve thanks for all their help while preparing this thesis.

This research was funded by the Engineering and Physical Sciences Research Council, and I am grateful to them for their financial support, and for enabling me to attend the NATO and IUGG conferences.

I would like to thank my parents and family for all the support that they have given me throughout the years. None of this would have been at all possible without you! Last (but definitely not least!) I would like to thank my fiancee, Louise Duffy. Her patience and understanding, not to mention her polite attention while I rabbited on about nonlinear convection and all the problems associated with it, have helped me so many times to sort things out in my head, that she is as much responsible for the completion of this work as I am. This work is therefore dedicated to her.

Abstract

Aspects of thermal convection in the Earth's fluid core in the presence of a strong azimuthal magnetic field may be understood by considering a horizontal plane layer, rotating about the vertical z axis, with gravity acting downwards and containing an applied magnetic field aligned in the y (azimuthal) direction. Since the CMB is not smooth, the effects of adding bumps (with axes perpendicular to the applied magnetic field) to the top boundary of the layer are investigated in the magnetogeostrophic limit. The arbitrary geostrophic flow that arises under this limit is evaluated using a modified Taylor constraint.

The bumps distort the isotherms so that they are not aligned with equipotential surfaces, leading to an imperfect configuration. This means that a hydrostatic balance is not possible, and motion ensues. This motion takes the form of a steady transverse convection roll, with axis parallel to the bumps. The roll exists for all values of the Rayleigh number, except that value for which the corresponding homogeneous problem in the standard plane layer has a solution. The roll obeys Taylor's constraint, and has no associated geostrophic flow.

The stability of this roll to perturbation by oblique rolls (which are preferred for $O(1)$ values of the Elsasser number) is considered. It is found that the most unstable linear mode consists of a pair of these oblique rolls, aligned so that no geostrophic flow is accelerated by their interaction with the basic state. Hence, the stability results obtained here are identical to those found by perturbing the hydrostatic conduction solution with oblique rolls in the standard layer.

Finally, the nonlinear evolution through the Ekman regime of these linear instabilities is considered. It is found that the nonlinear convection behaves similarly to mean field dynamo models which incorporate a geostrophic nonlinearity. Various types of Ekman solution are found, and evolution to Taylor states is observed.

Contents

Chapter I

Introduction

1.1 Convection In The Core

Paleomagnetic data indicate that the Earth's magnetic field has been in existance for in excess of three billion years. Since this exceeds by several orders of magnitude the Ohmic decay time of the Earth (which is on the order of fourteen thousand years), it follows that there must be some regenerative mechanisms operative within the Earth, which maintain the magnetic field against Ohmic losses. These *dynamo* mechanisms are thought to be linked to the motion of the electrically conducting fluid in the outer core of the Earth. Trapped between the solid inner core and the solid mantle, this fluid is driven into motion by two mechanisms: thermal and compositional convection. Compositional convection occurs when the heavy iron part of the fluid freezes onto the inner core, releasing a lighter component. This lighter component contributes to a buoyancy force, which forces motion in the outer core. In addition, the temperature at the inner core boundary is hotter than the temperature at the core mantle boundary. This sets up an adverse temperature gradient across the outer core, which contributes to a thermal buoyancy force, which also forces motion in the outer core.

The fluid flow in the core is characterised by various dimensionless parameters. These parameters are defined using measures of the flow in the core. Let $\mathcal{U}$ be a measure of the fluid velocity in the core, $\mathcal{B}_0$ a measure of the magnetic field strength, Ω a measure of the rotation of the Earth, $\mathcal{D}$ a measure of the dimensions of the core, ν a measure of the viscosity, g a measure of gravity and β a measure of the adverse temperature gradient. Then the Rayleigh number, defined by

$$R = \frac{g\alpha\beta\mathcal{D}^2}{\Omega\kappa}, \tag{1.1a}$$

measures the strength of the adverse temperature gradient in the core β, to thermal diffusion in the core, κ. The constant α is the coefficient of volume expansion in the core. Similarly, the Elsasser number, defined by

$$\Lambda = \frac{\mathcal{B}_0^2}{\Omega \mu_0 \rho_0 \eta}, \tag{1.1b}$$

measures how strong the Lorentz force (which is the force caused by the magnetic field) is compared to the Coriolis force (which is the force caused by the Earth's rotation). The constants μ_0, ρ_0 and η represent the magnetic permeability, density and magnetic diffusivity in the core. The Roberts number,

$$q = \frac{\kappa}{\eta}, \tag{1.1c}$$

measures the relative strength of the thermal diffusivity and the magnetic diffusivity. The Prantl number, defined by

$$P = \frac{\nu}{\kappa}, \tag{1.1d}$$

measures how strong the viscosity of the core is compared to the thermal diffusion of the core. The Ekman number, defined by

$$E = \frac{\nu}{\Omega \mathcal{D}^2}, \tag{1.1ed}$$

measures how strong the viscous force is compared to the Coriolis force. Finally, the Rossby number, defined by

$$Ro = \frac{\mathcal{U}}{\Omega \mathcal{D}}, \tag{1.1f}$$

measures how strong the inertial force is compared to the Coriolis force. Not all of these parameters arise is this work.

The simplest way to model the motion is by the thermal convection of a rotating spherical shell of Boussinesq fluid. Studies of the non-magnetic case by Roberts (1965, 1968), Busse (1970) and more recently by Zhang (1991) have shown that at the onset of instability, the motion consists of convection rolls parallel to the axis of rotation. These rolls propogate azimuthally due to the effects of inertia and the curvature of the boundaries, and are called thermal Rossby waves. They are confined to a thin annular region of the core (the thickness of this annular region

being dependent upon the value taken by the Prantl number P), where the effects of the rapid rotation of the Earth through the Taylor-Proudman theorem (which constrains the fluid motions to be two dimensional, independent of the coordinate parallel to the axis of rotation) are relaxed by a balance between the viscous and buoyancy forces. The lengthscale of the convection in the azimuthal direction is very short, and is given by $E^{-\frac{1}{3}}$. As the thermal driving is increased, the convective motions become stronger, and fill the entire spherical shell.

When the effects of a magnetic field are included, the situation is different. Provided the magnetic field strength is sufficiently large, the constraints of the Taylor-Proudman theorem may be broken by the Lorentz force, and the convection can initially take place on a much larger lengthscale, that of outer core itself (see for example Eltayeb and Kumar 1977; Fearn 1979a,b). The magnetic case will be considered in this work, albeit in a simpler geometry.

1.2 The Dynamo Problem

Discovering if (and how) such fluid motion can support a magnetic field against Ohmic decay is called the dynamo problem. For the Earth, the dynamo problem is difficult to solve for three main reasons. The first is that the equations to be solved constitute a highly nonlinear, coupled set of partial differential equations for the fluid velocity and magnetic field. These equations must be solved in a spherical shell geometry subject to appropriate boundary conditions. The second difficulty is that the dynamo problem is inherently three dimensional. This is a consequence of Cowling's theorem (Cowling 1934), which states that an axisymmetric magnetic field cannot be supported against Ohmic decay by dynamo action. To break the constraints of this theorem, each unknown (e.g. fluid velocity **U**, magnetic field **B** etc.) is regarded as being composed of two parts: a large axisymmetric or mean part, and a smaller asymmetric part, which is added to break the constraints of Cowling's theorem. In the core, these asymmetries are thought to be planetary waves which ride upon the underlying axisymmetric state (Braginsky 1967). It is the presence of the asymmetries that makes the problem three dimensional.

The mean magnetic field is then supported by two mechanisms. The poloidal part of the mean magnetic field is bowed out by the differential rotation of the fluid to form the toroidal part. This is called the ω-effect. To complete the regerative process, the asymmetries combine to produce an α-effect, which creates the

poloidal part of the mean magnetic field from the toroidal part (and to a lesser extent, it also creates toroidal magnetic field from poloidal magnetic field). If there are no asymmetries present, the α-effect is absent, and the poloidal part of the mean magnetic field would decay due to Ohmic losses. With no poloidal mean field to create toroidal mean field, the toroidal part is subject to a similar Ohmic decay. Through the α-effect, the asymmetries regenerate the mean magnetic field. To solve the governing equations for both the mean and asymmetric parts of the solution together is beyond the power of even the most powerful computers today. Usually, the problem is split into two simpler components.

The first component involves solving the equations for the larger mean part of the solution, having prescribed the asymmetries in the form of an α-effect. This is the mean field dynamo problem. Several types of mean field dynamo can occur, depending on what processes are used to sustain the field. In an α^2 dynamo, the α-effect is used to create both the toroidal and poloidal parts of the mean magnetic field. In an $\alpha\omega$ dynamo, the ω-effect is used to create the toroidal part of the mean magnetic field, and the α-effect is used to create the poloidal part. Finally, in an $\alpha^2\omega$ dynamo, both the α-effect and ω-effect create the toroidal part of the mean magnetic field, while the α-effect is also responsible for creating the poloidal part. Examples of all three types of mean field dynamo may be found in Fearn, Roberts and Soward (1988).

The second component of the problem involves solving the equations for the smaller asymmetric part of the solution having prescribed the mean part. This is called the magnetoconvection problem. This problem provides valuable information on the small scale processes that take place to generate the α and ω-effects of the mean field problem. Several types of magnetoconvection problem are described by Chandrasekhar (1961).

1.3 The Magnetogeostrophic Approximation

The third difficulty in solving the dynamo problem in the Earth arises because of the nature of the primary force balance in the outer core, which consists of a balance between the Coriolis, pressure, Lorentz (and buoyancy) forces. This force balance occurs for the following reasons.

The inertial terms are neglected because the Rossby number Ro is $O(10^{-8})$ in

the outer core. This small value indicates that the inertial force is insignificant compared to the Coriolis force. Neglecting the inertial terms filters out inertial waves, whose timescales (on the order of a day) are too short to be of interest to the dynamo problem. Mathematically, neglecting these terms changes the equation of motion from a predictive equation to a diagnostic equation, that is, a condition that must be satisfied by the fluid velocity U for all time.

Comparing the size of the viscous force with the Coriolis force yields the aforementioned Ekman number, E. In the core, E is $O(10^{-16})$, which indicates that the viscous force is also insignificant compared to the Coriolis force. Hence, neglecting viscous and inertial terms from the momentum equation (this is the magnetogeostrophic approximation which gives rise to the primary force balance in the outer core) yields the magnetogeostrophic equation

$$2\mathbf{\Omega} \wedge \mathbf{U} = -\nabla(\frac{P}{\rho_0}) + \frac{1}{\mu_0 \rho_0}(\nabla \wedge \mathbf{B}) \wedge \mathbf{B} + \frac{\rho}{\rho_0}\mathbf{g}. \tag{1.2}$$

By considering the curl of this equation, it can be shown that the velocity U can not be determined uniquely from the magnetogeostrophic equation. It can only be determined up to an arbitrary geostrophic flow,

$$V_g = V_g(s)\hat{\phi}, \tag{1.3}$$

where cylindrical coordinates with z axis parallel to the axis of rotation are employed (see Fearn 1994). This arbitrariness can be traced to the neglect of the viscous term, which has the effect of lowering the order of the momentum equation by two. This situation, where a small parameter (in this case ν, the viscosity) multiplies the highest derivative of an equation, is quite common in singular perturbation theory. That theory suggests that although viscosity is unimportant over the bulk of the core (in which region (1.2) applies), viscosity is important in thin viscous Ekman layers close to the core mantle boundary. The question of how important these Ekman layers are in determining the dynamics of the outer core is of key importance in determining the geostrophic flow.

Taylor (1963) argued that the Ekman layers do not affect the dynamics. In this situation, the solutions of (1.2) can be shown to satisfy the Taylor constraint

$$M = \int \int_{C(s)} \Big[(\nabla \wedge \mathbf{B}) \wedge \mathbf{B} \Big]_{\phi} dS = 0 \quad \forall s, \tag{1.4}$$

where $C(s)$ is a cylinder of radius s coaxial with the axis of rotation, called a geostrophic cylinder. Physically, the Taylor constraint says that there can be no mean torque exerted on geostrophic cylinders by the Lorentz force. Mathematically, the existence of a homogeneous solution V_g of the magnetogeostrophic equation necessitates a solvability condition (i.e. the Taylor constraint) in order to find inhomogeneous solutions (see Fearn and Proctor 1992). Taylor argued that even if the Taylor constraint was not initially satisfied by the magnetic field, the resulting torque on the geostrophic cylinders would set up a torsional oscillation, that is, an oscillation of the geostrophic cylinders, which would ultimately decay in time to leave the Taylor constraint satisfied. In Taylor's prescription, the geostrophic flow is determined implicitly by the requirement that its' effect on the magnetic field (through the ω-effect) should be precisely that needed to ensure that Taylor's constraint is satisfied. A solution which obeys Taylor's constraint is said to be in a Taylor state.

On the other hand, it can be argued that the viscous Ekman layers do influence the dynamics of the outer core through the effects of Ekman suction, where fluid is drawn into the Ekman layers at the poles, and then ejected through the Ekman layers towards the equator. The resulting mass flux through the Ekman layers can be related to the arbitrary geostrophic flow (see Fearn 1994), leading to an alternative form of (1.4), given by

$$2\rho_0 \Big[\frac{\Omega \nu}{\cos\theta} \Big]^{\frac{1}{2}} V_g = \int \int_{C(s)} \frac{1}{\mu_0} \Big[(\nabla \wedge \mathbf{B}) \wedge \mathbf{B} \Big]_{\phi} dS. \tag{1.5}$$

This is called the modified Taylor constraint, and provides an explicit equation for the arbitrary geostrophic flow. The term on the left hand side of (1.5) represents the mass flux through the Ekman layers caused by the Ekman suction effect.

Braginsky (1975) proposed an alternative to the Taylor model. It consists of an $\alpha\omega$ dynamo, in which the effects of the viscous Ekman layers are retained, and where the radial component of the mean magnetic field is assumed to satisfy

$$B_s \ll 1. \tag{1.6}$$

This assumption implies that there is weak coupling between adjacent geostrophic cylinders. Consequently, the torsional oscillations that are driven by the failure of the magnetic field to satisfy the Taylor constraint are not damped to zero (since the damping mechanism relies on B_s being $O(1)$, so there is strong coupling between the geostrophic cylinders). Hence, although the Taylor integral is always small, it never vanishes, and must always be balanced by the Ekman suction term. The model is characterised by the shape of the poloidal part of it's mean magnetic field, which is aligned with the rotation axis. This led Braginsky to call it Model Z. Braginsky was able to show that in the limit $\nu \rightarrow 0$, Taylor's constraint remained unsatisfied, showing that the model always depends upon the value of the viscosity.

1.4 The Taylor Problem

The question of whether or not viscous effects are important in the dynamics of the outer core has received a lot of attention. Specifically, the question asked is whether or not Taylor's constraint can be satisfied in the outer core, and if so, how is it brought about? The failure of Braginsky's Model Z to ever satisfy the Taylor constraint has prompted a more cautious approach. Most authors retain the effect of Ekman suction (through the modified Taylor constraint) and ask whether the magnetic field and geostrophic flow can evolve in such a way that Taylor's constraint can be eventually satisfied.

One possible evolution for α^2 dynamos in a sphere was described by Malkus and Proctor (1975). They show that there is a critical value of α, denoted by α_c, below which the dynamo does not work because the effects of Ohmic dissipation are too strong. Just above α_c, the α-effect is strong enough to overcome the Ohmic dissipation, and the magnetic field strength begins to grow. However, at this point, the magnetic field strength is small, of $O(\nu^{\frac{1}{4}})$. As a result, the most important nonlinearity is that generated by the geostrophic flow and the modified Taylor constraint, all the other nonlinearities being small enough to ignore. Hence, it is the viscosity that limits the field growth through the modified Taylor's constraint. This regime is therefore called the Ekman regime. However, by increasing α, Malkus and Proctor find a second critical value of α, denoted α_T, at which Taylor's constraint becomes satisfied. As α is increased to α_T, the magnetic field and geostrophic flow adjust so that Taylor's constraint becomes satisfied. The Taylor state is characterised by a rapid growth in the strength of the magnetic field,

which goes from $O(\nu^{\frac{1}{4}})$ to $O(1)$, becoming independent of viscosity in the Taylor state. Above α_T, the other nonlinearities of the problem become important, and control the magnetic field strength. This is called the Taylor regime, since Taylor's constraint is satisfied for $\alpha > \alpha_T$. In the Taylor regime, the geostrophic flow is determined implicitly using the method prescribed by Taylor (1963).

This scenario has come to be known as the Malkus-Proctor scenario, and has been verified for α^2 dynamos in various geometries. For instance, the plane layer model of Soward and Jones (1983), the spherical models of Ierley (1985), Hollerbach and Ierley (1991), Barenghi and Jones (1991) and Barenghi (1992a) all exhibit this evolution to a Taylor state. This is not the only behaviour possible, however. A second type of solution occurs where the Taylor states lie on a higher amplitude branch of the solution, which is not connected to the initial bifurcation of the small amplitude Ekman regime. This type of solution has been observed by Soward and Jones (1983), Barenghi and Jones (1991) and Hollerbach and Ierley (1991).

By contrast, the behaviour of $\alpha\omega$ dynamos is not so straightforward. Although the infinite plane layer $\alpha\omega$ dynamo of Abdel-Aziz and Jones (1987) does show the smooth transition to a Taylor regime envisaged by Malkus and Proctor, similar models in confined geometries (e.g. a duct or a sphere) do not show such a well defined transition to a Taylor state.

The difference between α^2 and $\alpha\omega$ dynamos is twofold. Firstly, $\alpha\omega$ dynamos tend to be oscillatory, while α^2 dynamos are usually steady. Secondly, $\alpha\omega$ dynamos are prone to secondary bifurcations which lead to more and more complicated temporal behaviour in the solution. For instance, the $\alpha\omega$ dynamo of Wallace and Jones (1992) in a duct geometry has secondary bifurcations which take the initial solution from oscillatory to vascillatory, frequency locked, chaotic and back to oscillatory again, all in the Ekman regime! These secondary bifurcations do not seem to occur in α^2 dynamos. Because of this complicated bifurcation structure, the transition to a Taylor state is hard to establish. Typically, the solution comes to an end at a subcritical Hopf bifurcation, at which a second frequency is introduced. In some cases (e.g. Barenghi and Jones 1991 in a sphere) an oscillatory Taylor state does become established. However, in the models of Hollerbach, Barenghi and Jones (1991) in a sphere, and Wallace and Jones (1992) in a duct, the solution becomes chaotic after this point, and the dependence of the solution upon the viscosity is hard to establish. Quite why this behaviour occurs is still an open question, and is the subject of ongoing research.

The question of whether or not Taylor's constraint can be satisfied has also arisen in models of magnetoconvection. Just as in the mean field case, it is found that when the amplitude of the magnetoconvection is small, the geostrophic nonlinearity is the most important nonlinearity in the problem, and becomes responsible for equilibrating the amplitude of the solutions. However, the mechanism by which the amplitude is controlled differs from the mean field case, where viscous damping was resposible for controlling the amplitude. In magnetoconvection, the shear generated by the geostrophic flow is responsible for controlling the amplitude of the solutions (see Fearn 1994). The Taylor problem in magnetoconvection has been investigated in various geometries: an infinite plane layer (Roberts and Stewartson 1974, 1975; Soward 1980), a duct (Soward 1986; Jones and Roberts 1990), a cylindrical annulus (Skinner and Soward 1988, 1990) and a sphere (Fearn, Proctor and Sellar 1994).

The Roberts and Stewartson model consists of a horizontal plane layer, which rotates about the vertical axis, with gravity acting downwards. The layer is assumed to contain a horizontal applied mean magnetic field, and the bottom boundary is made hotter than the top to facilitate thermal convection. Roberts and Stewartson find that once the Rayleigh number (which is a dimensionless measure of the adverse temperature gradient) is made large enough to overcome the effects of thermal diffusion, then convection in the form of rolls ensues. For weak applied mean magnetic field strengths, a single convection roll whose axis is perpendicular to the applied mean magnetic field is the preferred mode of convection. Increasing the strength of the applied mean magnetic field however, they find that a pair of oblique convection rolls, aligned at equal but opposite angles to the applied mean magnetic field, become preferred. These rolls can go unstable either singly (called a single oblique roll solution) or in a pair (called a double oblique roll solution).

The single oblique roll solutions obey Taylor's constraint, and constitute the Taylor states that arise in the plane layer. Their nonlinear evolution is investigated in Roberts and Stewartson (1974). Of more interest, however, is the double oblique roll solution, since a pair of oblique rolls taken together do not satisfy the Taylor constraint. To investigate this solution, Roberts and Stewartson (1975) regard one of the oblique rolls in the double roll solution as being very small, and treat it as a perturbation to its' companion. The resulting linear stability problem investigates where the Taylor solutions (i.e. the single oblique roll solutions) are unstable. In the regions where instability occurs, Taylor's constraint is not satisfied, and there is a complicated nonlinear interaction between the two oblique rolls and

the concomitant geostrophic flow accelerated by the interaction of the two rolls through the Taylor integral. Soward (1980) investigates the subsequent nonlinear evolution of this instability.

However, the double oblique roll solution found in the plane layer is degenerate, and arises as a consequence of the infinite geometry. It does not occur in bounded geometries. For instance in a sphere, a single mode which does not satisfy Taylor's constraint typically onsets at criticality. To remedy this, Soward (1986) bounded the infinite plane layer to form a duct. The simplicty of the model enabled him to look for Taylor solutions directly, using the method of Taylor (1963). Soward finds the critical Rayleigh numbers at which Taylor's constraint can be met in the duct model, and investigates the nature of the Taylor states that arise. In Skinner and Soward (1988, 1990) the case of a cylindrical geometry is investigated. Using the modified Taylor's constraint to evaluate the arbitrary geostrophic flow, Skinner and Soward again find that the solution evolves to a Taylor state provided the Rayleigh number is made sufficiently large.

This evolution to a Taylor state does not always occur. Jones and Roberts (1990) modified the duct model of Soward so that the rotation is perpendicular to both gravity and the applied mean magnetic field. They were able to show that (provided the applied mean magnetic field is made strong enough) the solution does not evolve to a Taylor state, no matter how large the Rayleigh number is made. Similarly, in a spherical model of magnetoconvection, Fearn, Proctor and Sellar (1993) were also unable to find Taylor solutions. As the Rayleigh number is increased, the solution becomes more and more complicated temporally, but does not settle down to a Taylor state. These results strike a cautionary note, and indicate that the question of whether a Taylor state will always exist in a given system is far from settled.

1.5 Inhomogeneities On The CMB

A common fact which links all of the models discussed thus far is that in each model, the bounding surfaces are assumed to be homogeneous. However, there is ample evidence to suggest that at least one of the boundaries, the core-mantle boundary, may have inhomogeneities in the form of topography, lateral temperature variations, compositional variations and variations in conductivity. Hide (1967) first pointed out that the presence of these inhomogeneities on the

core-mantle boundary could have a profound effect upon the dynamics of the outer core.

The first indication the the core-mantle boundary is not homogeneous comes from the fact that the length of day on the Earth is not constant: it varies on the order of several milliseconds per decade. This so called decadal variation in the length of day can be traced to changes in the rotation rate of the Earth due to angular momentum exchanges between the core and mantle (Hide 1969). There are three main mechanisms by which the core and mantle exchange angular momentum: viscous coupling, electromagnetic coupling and topographic coupling.

Viscous coupling, caused by friction between the core and the mantle, is universally believed to be too small to account for the decadal variation, due to the small value of the viscosity in the outer core. Electromagnetic coupling, caused by the leakage of currents from the outer core into the mantle, is also not strong enough to account for the observed variations. There are also doubts as to whether the timescale of variations in the magnetic field is the correct one on which the variation in the length of day occurs (see Roberts 1988; Voorhies 1991). This leaves topographic coupling, which is now thought to be the main mechanism responsible for the length of day variations. The mechanisms by which the core and mantle exchange angular momentum through topographic coupling are described in detail by Hide (1989) and Jault and Le Moeul (1989).

Hide (1969) argued that bumps of only 1km height on the core-mantle boundary would produce the torque required to account for the observed length of day variations. By observing that bumps of this height should distort the magnetic field and gravitational potential on the core-mantle boundary, and by then showing that variations in the gravitational potential and magnetic field are correlated on the core-mantle boundary, Hide and Malin (1970) inferred the existance of bumps of height 1km on the core mantle boundary. Several theoretical calculations (see for example Moffat 1978; Bloxham and Gubbins 1993) have confirmed that the topographic torque is large enough to account for the observed length of day variations.

Further evidence of inhomogeneities on the core mantle boundary comes from maps of the radial magnetic field on the core-mantle boundary, produced by downwards extrapolation of the observed poloidal field at the Earths surface. The work of Gubbins and Bloxham (1987) shows the existance of four or five fixed flux lobes at the core-mantle boundary, which have remained static, fixed in one spot

throughout the period 1715-1980. Bloxham and Gubbins (1987) explained these fixed features by saying that the convection rolls in the outer core (which create the flux lobes by sweeping flux up towards the core-mantle boundary) have become locked onto hot and cold spots on the core-mantle boundary, instead of propogating azimuthally as usual. By correlating variations in seismic velocity (which depends on the temperature of the mantle) with variations in the radial magnetic field at the core mantle boundary, Bloxham and Gubbins were able to show that the fixed features of the radial field were indeed located at hot and cold spots on the core-mantle boundary.

Theoretical support for this comes from models of convection in a spherical shell, which is cooled inhomgeneously at the core-mantle boundary. With these temperature variations on the core-mantle boundary, the isotherms no longer line up with surfaces of constant gravitational potential, and so small scale motion is always forced in the shell - this is known as an imperfect configuration. Zhang and Gubbins (1992, 1993) showed that the subsequent convection forced by thermal instability (through an "imperfect" bifurcation) did indeed lock onto the hot and cold spots imposed on the core-mantle boundary. A subsequent investigation by Sun, Schubert and Glatzmaier (1994), which examined this boundary forced convection far into the nonlinear regime (Rayleigh number five times critical) found that the temperature perturbations were locked to the boundary, but deep inside the shell the convection was columner in structure.

However, Gubbins and Richards (1986) have argued that the topography of the core- mantle boundary could also be responsible for locking these convection rolls into place. Using a model of the viscosity in the mantle, together with seismic data, Gubbins and Richards construct a model of the "dynamic" topography on the core-mantle boundary, and find correlation between this topography and the variations in the radial magnetic field at the core mantle boundary. Gubbins and Richards concluded that the topography was just as likely to be responsible as lateral temperature variations for locking the convection rolls into place.

Support for this viewpoint has come from the models of Bell (1993) and Bell and Soward (1995), who use a modified form of Busse's annulus model to examine the effects of topography upon convection. Bell and Soward find several new types of convection mode driven by the bumps, the most interesting being a boundary locked mode, which becomes preferred once the height of the bumps is sufficiently large.

That thermal inhomogeneities and bumps produce similar effects should not be surprising, since the two inhomogeneities are linked in a fundamental way. Hot spots on the core-mantle boundary produce upwelling in the mantle. Similarly, cold spots will produce downwellings in the mantle. Hence, where there are temperature variations, there will also be bumps. Gubbins and Richards stress the need for further work to examine the effects of flow over topography.

1.6 Motivation For The Problem

The results of the previous section indicate that the inhomogeneities on the core-mantle boundary can have a profound effect upon the dynamics of the outer core. The distortion of the isotherms from the equipotential surfaces by the inhomogeneities produces an imperfect configuration, where small scale motion is always forced. This has implications when computing the basic state in such a system. The inhomogeneities produce new effects, such as the locking of convection onto the inhomogeneities, found in the models of Zhang and Gubbins (1992) and Bell and Soward (1995). However, most of the models decribed in the previous section have not included the strong toroidal magnetic field that is thought to be present in the outer core. To remedy this, a model that examines the effects of boundary inhomgeneities on convection in the presence of a strong toroidal magnetic field should be considered. That is the motivation for the problem studied in this work. Due to the similar effects of thermal inhomgeneities and bumps, the inhomogeneity will be assumed to take the form of bumps on the core-mantle boundary.

The plane layer model of Roberts and Stewartson (1974) described earlier, captures all the essential aspects of thermal convection in a spherical shell, but in a much simpler geometry. For this reason, and to isolate the key effects associated with magnetoconvection in the presence of topography, the plane layer model is modified to include the effects of topography. Since the exact details of the topography are not important, the bumps are assumed to take the form of a sinusoidal undulation which varies in the y direction. The bumps will be assumed to be small. In a model such as this, which is to be applied to the core, the magnetogeostrophic approximation must be made, and the arbitrary geostrophic flow evaluated. With regard to the remarks of section 1.3, the arbitrary geostrophic flow will be evaluated by a modified Taylor condition, in the hope that the solutions of the problem

will evolve to a Taylor state as the Rayleigh number is increased (or decreased).

The model is decribed in detail in chapter 2, and the equations and boundary conditions for the topographical convection forced by the bumps are there derived. The linear results of Roberts and Stewartson are reviewed in chapter 3. The distortion of the isotherms by the bumps leads to an imperfect configuration problem. Specifically, a hydrostatic balance is no longer possible in a layer with bumps. The exact basic state must therefore be calculated from the governing equations and boundary conditions, and this is done in chapter 4. Since oblique rolls are the preferred mode of convection in a plane layer when there is a strong toroidal magnetic field, the stability of the basic state to perturbation by these rolls, together with the concomitant geostrophic flow accelerated by the interaction of these rolls with the basic state through the Taylor integral, is considered in chapter 5 (see also Appendix B). Finally, the nonlinear evolution of the resulting instabilities through the Ekman regime is considered in chapter 6. In chapter 7, the conclusions of the research will be presented.

Chapter II

Description Of The Model

2.1 The Modified Plane Layer

The outer core is modelled by a plane layer containing an electrically conducting fluid. The layer is of infinite extent in the horizontal x and y directions, but is bounded in the vertical z direction. The finite geometry of the core is mimicked by seeking solutions which are periodic in the x and y directions, with periods $\frac{2\pi}{l}$ and $\frac{2\pi}{m}$ respectively, where l and m are real constants. The layer is bounded below by

$$z = 0. \tag{2.1}$$

This represents the boundary between the solid inner core and liquid outer core. This boundary is assumed flat for simplicity. To model the bumps which occur on the core-mantle boundary, the traditional plane layer model is modified so that the top boundary lies at

$$z = d + \gamma \cos(my), \tag{2.2}$$

where γ is a real constant. The size of γ governs the size of the bumps, while m governs how they vary laterally; γ and m are assumed to be known a priori. Thus, the periodicity in the y direction is fixed by the bumps. The bumps on the core mantle boundary extend a distance of about 1km into the core (Hide and Malin 1970). Since this is a small figure compared with the dimensions of the outer core, it is assumed that

$$\gamma \ll 1. \tag{2.3}$$

The layer rotates about the vertical with constant angular velocity, and gravity acts downwards, so

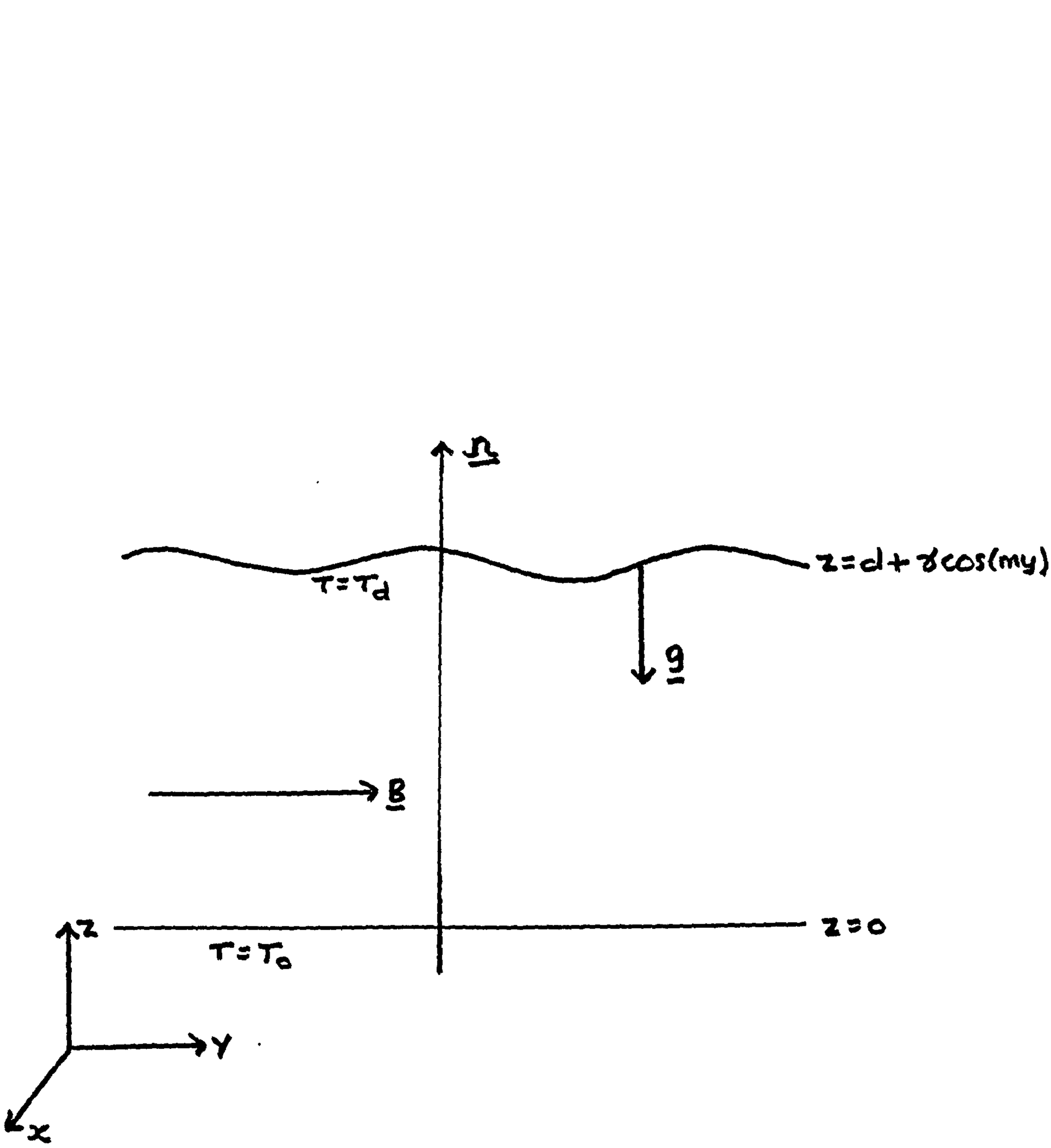

Figure 2.1: The configuration of the model

$$\boldsymbol{\Omega} = \Omega\hat{\mathbf{z}}, \quad \mathbf{g} = -g\hat{\mathbf{z}}, \tag{2.4}$$

where Ω and g are real constants. This orientation of $\boldsymbol{\Omega}$ and $\mathbf{g}$ corresponds to the north polar region of the outer core, but the qualitative behaviour of the system is not altered by choosing arbitrary orientations (Chandrasekhar 1961).

Convection in the outer core is driven by a combination of thermal and compositional effects. As thermal convection is better understood and easier to model, all compositional effects will be ignored. In a thermally driven system, the bottom boundary is maintained at a constant temperature T_0 and the top boundary is maintained at a constant temperature T_d. By choosing

$$T_0 > T_d,$$

the bottom boundary is made hotter than the top, and an adverse temperature gradient

$$\beta = \frac{T_0 - T_d}{d} > 0,$$

is set up across the layer. This arrangement is unstable since hot, light fluid lies beneath cold, heavy fluid. Convection ensues to restore the thermal equilibrium, once the adverse temperature gradient becomes large enough.

The fluid in the layer is assumed to be Boussinesq - that is, temperature and pressure variations across the layer are assumed to be sufficiently small that the density may be treated as a constant ρ_0 everywhere, except where it appears with the buoyancy force. There, it takes the value

$$\rho = \rho_0(1 - \alpha(T - T_0)). \tag{2.5}$$

The constant α is the coefficient of volume expansion, T is the temperature and T_0 is the temperature at the bottom boundary. The fluid has kinematic viscosity ν, thermal conductivity κ, magnetic permeability μ_0, electrical permitivity ϵ_0 and electrical conductivity σ. For simplicity, all these quantities are assumed to be constants. Note that in the core

$$\nu = O(10^{-8}),$$

so the effects of viscosity will be neglected over the bulk of the layer. Viscosity is only important in thin, viscous Ekman layers that lie close to the bounding surfaces.

2.2 The Boundary Conditions

It is assumed that the bounding surfaces are rigid, isothermal and perfectly electrically conducting. Now, these boundary conditions do not reflect the true physics of the core. More accurate boundary conditions would reflect the fact that the lower mantle is (to a high approximation) electrically insulating, and not perfectly electrically conducting. Similarly, a condition on the heat flux through the boundaries would be more realistic than arbitrarily imposing isothermal boundaries. However, of primary concern is isolating the mechanisms by which bumps on the core-mantle boundary affect convection in the outer core. For this reason, these simpler, artificial boundary conditions are adopted to make the problem more tractable, in the hope that they retain all the essential physics of the problem.

These boundary conditions lead to conditions that the velocity $\mathbf{U}$, temperature T, magnetic field $\mathbf{B}$ and electric field $\mathbf{E}$ must satisfy at the boundaries. To obtain these conditions, the normals to the boundaries are required. They are given by

$$\mathbf{n} = \begin{cases} \hat{\mathbf{z}} & \text{on } z = 0, \\ \\ \hat{\mathbf{z}} + \gamma m \sin(my)\hat{\mathbf{y}} & \text{on } z = d + \gamma \cos(my). \end{cases} \tag{2.6}$$

They are obtained by writing the boundaries in the form of a level surface

$$\Phi = \text{constant},$$

so that the normals are given by

$$\mathbf{n} = \nabla\Phi.$$

2.2.1 The Boundary Conditions On The Velocity

At a rigid boundary, the velocity **U** satisfies

$$\mathbf{U}.\mathbf{n} = 0. \tag{2.7}$$

This is the no penetration condition, which says that the fluid in the layer cannot penetrate into the regions outside of the layer. Using (2.6), the conditions at the bounding surfaces are, therefore

$$U_z = 0 \quad \text{on} \quad z = 0, \tag{2.8a}$$

$$U_z + \gamma m \sin(my) U_y = 0 \quad \text{on} \quad z = d + \gamma \cos(my). \tag{2.8b}$$

Because viscosity has been neglected, the no-slip boundary condition on the velocity (namely $\mathbf{n} \wedge \mathbf{U} = 0$) does not have to be satisfied.

2.2.2 The Boundary Conditions On The Temperature

At an isothermal boundary, the temperature T satisfies

$$T = \text{constant},$$

which says that the boundary is maintained at a constant temperature. Recalling that the bottom boundary is kept at a temperature T_0, while the top boundary is kept at a temperature T_d, it follows that T must satisfy

$$T = T_0 \quad \text{on} \quad z = 0, \tag{2.9a}$$

$$T = T_d \quad \text{on} \quad z = d + \gamma \cos(my). \tag{2.9b}$$

Note that $T_0 > T_d$, which sets up the adverse temperature gradient necessary to drive convection in the layer.

2.2.3 Electromagnetic Boundary Conditions

The regions outside the layer are perfectly electrically conducting. Hence

$$\sigma = \infty \quad \text{in} \quad z \leq 0, \quad z \geq d + \gamma \cos(my).$$

However, the fluid in the layer has a finite electrical conductivity, so σ is finite in the layer. This leads to a discontinuity in σ at the boundaries. At a boundary where σ is discontinous, the magnetic field $\mathbf{B}$ and the electric field $\mathbf{E}$ must satisfy

$$[\mathbf{B}.\mathbf{n}] = 0, \quad [\mathbf{n} \wedge \mathbf{E}] = \mathbf{0},$$

where the square brackets denote the jump in value across the boundary (see Gubbins and Roberts in Jacobs 1987). Ignoring any electromagnetic fields outside the layer, $\mathbf{B}$ and $\mathbf{E}$ must satisfy

$$\mathbf{B}.\mathbf{n} = 0, \quad \mathbf{n} \wedge \mathbf{E} = \mathbf{0} \quad \text{on} \quad z = 0 \quad \text{and} \quad z = d + \gamma \cos(my). \tag{2.10}$$

Now, using Ohm's law, the boundary condition on $\mathbf{E}$ can be replaced by an equivalent condition on the electric current, $\mathbf{J} = \frac{1}{\mu_0}(\nabla \wedge \mathbf{B})$. Ohm's law is

$$\frac{1}{\sigma}\mathbf{J} = \mathbf{E} + \mathbf{U} \wedge \mathbf{B}.$$

Taking the cross product with $\mathbf{n}$ and using a standard vector identity, this becomes

$$\frac{1}{\sigma}\mathbf{n} \wedge \mathbf{J} = \mathbf{n} \wedge \mathbf{E} + (\mathbf{n}.\mathbf{B})\mathbf{U} - (\mathbf{n}.\mathbf{U})\mathbf{B}. \tag{2.11}$$

Using (2.7) and (2.10) this says that

$$\mathbf{n} \wedge \mathbf{J} = 0 \quad \text{on} \quad z = 0 \quad \text{and} \quad z = d + \gamma \cos(my). \tag{2.12}$$

Therefore, an equivalent set of boundary conditions is

$$\mathbf{B}.\mathbf{n} = 0, \quad \mathbf{n} \wedge \mathbf{J} = \mathbf{0} \quad \text{on} \quad z = 0 \quad \text{and} \quad z = d + \gamma \cos(my). \tag{2.13}$$

Using (2.6) these become

$$B_z = 0 \quad \text{on} \quad z = 0, \tag{2.14a}$$

$$B_z + \gamma m \sin(my) B_y = 0 \quad \text{on} \quad z = d + \gamma \cos(my), \tag{2.14b}$$

and

$$J_x = 0, \quad J_y = 0 \quad \text{on} \quad z = 0, \tag{2.15a}$$

$$J_x = 0, \quad J_y = \gamma m \sin(my) J_z \quad \text{on} \quad z = d + \gamma \cos(my). \tag{2.15b}$$

Now, $\mathbf{J}$ satisfies the pre-Maxwell equation

$$\nabla.\mathbf{J} = 0.$$

This, together with (2.15), implies that

$$\frac{\partial J_z}{\partial z} = 0 \quad \text{on} \quad z = 0, \tag{2.16a}$$

$$(1 - \gamma^2 m^2 \sin^2(my)) \frac{\partial J_z}{\partial z} + \frac{\partial}{\partial y}(\gamma m \sin(my) J_z) + \gamma m \sin(my) \frac{\partial J_y}{\partial z} = 0$$

$$\text{on} \quad z = d + \gamma \cos(my). \tag{2.16b}$$

The boundary conditions (2.16) are equivalent to (2.15), and will be used instead of (2.15).

2.2.4 Taylor Expansion Of The Boundary Conditions

The boundary conditions on the surface $z = d + \gamma\cos(my)$ are very difficult to apply. However, it is possible to obtain a simpler set of boundary conditions, which (hopefully) retain all the essential features, but which are applied on $z = d$. This is done by Taylor expanding the full set of boundary conditions in γ, using the fact that $\gamma \ll 1$, retaining only $O(1)$ and $O(\gamma)$ terms. This yields the conditions

$$\left.\begin{aligned} U_z &= 0 \\ B_z &= 0 \\ \tfrac{\partial J_z}{\partial z} &= 0 \\ T &= T_0 \end{aligned}\right\} \quad \text{on} \quad z = 0, \tag{2.17a}$$

$$\left.\begin{aligned} U_z + \gamma\cos(my)\tfrac{\partial U_z}{\partial z} &= -\gamma m\sin(my)U_y \\ B_z + \gamma\cos(my)\tfrac{\partial B_z}{\partial z} &= -\gamma m\sin(my)B_y \\ \tfrac{\partial J_z}{\partial z} + \gamma\cos(my)\tfrac{\partial^2 J_z}{\partial z^2} &= -\tfrac{\partial}{\partial y}(\gamma m\sin(my)J_z) - \gamma m\sin(my)\tfrac{\partial J_y}{\partial z} \\ T + \gamma\cos(my)\tfrac{\partial T}{\partial z} &= T_d \end{aligned}\right\} \quad \text{on} \quad z = d. \tag{2.17b}$$

This idealised set of boundary conditions will be applied instead of the full set. However, any effects caused by their imposition will be attributed to the bumps.

2.3 The Equations

The equations that the system must obey are derived from the various physical laws that govern a rotating, Boussinesq fluid in the presence of a magnetic field. The first law is Newton's law of motion, which is used to derive the momentum equation. Now, to model motion in the core, the magnetogeostrophic approximation is made, and the magnetogeostrophic equation is obtained

$$2\boldsymbol{\Omega}\wedge\mathbf{U} = -\nabla(\frac{P}{\rho_0}) + \frac{1}{\mu_0\rho_0}(\mathbf{B}.\nabla)\mathbf{B} + \frac{\rho}{\rho_0}\mathbf{g}, \tag{2.18a}$$

where

$$\rho = \rho_0(1 - \alpha(T - T_0)), \tag{2.18b}$$

$$P = p - \frac{1}{2}\rho_0|\mathbf{\Omega} \wedge \mathbf{x}|^2 + \frac{1}{2\mu_0}\mathbf{B}^2, \tag{2.18c}$$

are the density and modified pressure respectively. The left hand side of (2.18) represents the Coriolis force, while the right hand side represents the pressure force, the Lorentz force and the buoyancy force respectively. Recall from chapter 1 that the fluid velocity **U** cannot be determined uniquely from (2.18). It can only be determined up to an arbitrary flow, $V(x)\hat{\mathbf{y}}$ called the geostrophic flow. This arbitrariness arises as a consequence of the magnetogeostrophic approximation. To determine V, and hence find the flow velocity uniquely, the following equation must be solved

$$2(\Omega\nu)^{\frac{1}{2}}V = \frac{1}{\mu_0\rho_0}\frac{\partial M}{\partial x}, \tag{2.19a}$$

where

$$M = \frac{m}{2\pi d}\int_0^{\frac{2\pi}{m}}\int_0^d B_x B_y dz dy, \tag{2.19b}$$

is the mean Maxwell stress in the y direction (see Soward 1980; Soward and Jones 1983; Abdel-Aziz and Jones 1987). Equation (2.19) represents conservation of mass in the x direction, but includes contributions from the viscous Ekman layers that lie at the boundaries. (This is the only place in the model where the effects of viscosity are important). The second law is conservation of mass. This is embodied in the continuity equation,

$$\nabla.\mathbf{U} = 0. \tag{2.20}$$

The first law of thermodynamics yields the heat equation

$$\frac{\partial T}{\partial t} + (\mathbf{U}.\nabla)T = \kappa\nabla^2 T. \tag{2.21}$$

The left hand side of (2.21) represents advection of heat by the fluid, while the right hand side represents the removal of heat by thermal diffusion. The laws of electrodynamics (namely Faraday's law, Ohm's law and Ampere's law) can be combined to give a single equation for the magnetic field. This is the induction equation, which is given by

$$\frac{\partial \mathbf{B}}{\partial t} + (\mathbf{U}.\nabla)\mathbf{B} = (\mathbf{B}.\nabla)\mathbf{U} + \eta\nabla^2\mathbf{B}, \tag{2.22}$$

where

$$\eta = \frac{1}{\mu_0\sigma},$$

is the magnetic diffusivity. The left hand side of (2.22) represents advection of the field by the flow, while the right hand side represents stretching of the field lines by the motion of the fluid, and destruction of field by Ohmic diffusion. Finally, **B** satisfies a solonoidal condition

$$\nabla.\mathbf{B} = 0. \tag{2.23}$$

This equation arises because magnetic monopoles do not exist in nature. Hence, the flux of **B** through any closed surface must be zero.

2.4 The Formulation Of The Problem

The equations are nondimensionalised by adopting the following scalings

$$\mathbf{x} = \mathcal{D}\mathbf{x}^*, \quad t = \mathcal{T}t^*, \tag{2.24a,b}$$

$$\gamma = \mathcal{D}\gamma^*, \quad m = \frac{1}{\mathcal{D}}m^*, \tag{2.24c,d}$$

$$\nabla = \frac{1}{\mathcal{D}}\nabla^*, \tag{2.24e}$$

where the starred quantities are nondimensional, and

$$\mathcal{D} = \frac{d}{\pi}, \quad \mathcal{T} = \frac{\mathcal{D}^2}{\kappa},$$

have been adopted as length and time scales repectively. As is common in convection problems, time has been scaled on the basis of the thermal diffusion timescale. The velocity, magnetic field and temperature scale as follows

$$\mathbf{U} = \frac{\kappa}{\mathcal{D}}(V^*(x)\hat{\mathbf{y}} + \gamma^*\hat{\mathbf{u}}^*), \tag{2.25a}$$

$$\mathbf{B} = B_0(\hat{\mathbf{y}} + \gamma^* q\hat{\mathbf{b}}^*), \tag{2.25b}$$

$$T = \beta\mathcal{D}(T_0^* - z^* + \gamma^*\hat{\theta}^*), \tag{2.25c}$$

where q is the Roberts number.

The flow $V^*(x)\hat{\mathbf{y}}$ is the geostrophic flow that arises as a consequence of the magnetogeostrophic approximation, but it is corrected by a flow $\gamma^*\mathbf{u}^*$, which is determined to ensure that the geostrophic flow fits into a layer with a bumpy top boundary. The form of the geostrophic flow arises for the following reason. The true geostrophic flow in the bumpy layer takes the form $U^*(x,y,z)\hat{\mathbf{y}}$. Consider the mass flux across the plane $y = \frac{\pi}{2}$, at which the layer has height π. It is given by

$$\mathcal{F} = \pi U^*(x, \frac{\pi}{2}, \pi).$$

This mass flux $\mathcal{F}$ must be the same as the mass flux across any arbitrary plane $y = y_0$, at which the layer has height $z_0 = \pi + \gamma^*\cos(m^* y_0)$. Hence,

$$\mathcal{F} = \pi U^*(x, \frac{\pi}{2}, \pi) = (\pi + \gamma^*\cos(m^* y_0))U^*(x, y_0, z_0).$$

Defining $V^*(x) = U^*(x, \frac{\pi}{2}, \pi)$ the following relation is obtained

$$U^*(x,y,z) = \frac{V^*(x)}{1 + \frac{\gamma^*}{\pi}\cos(m^* y)}.$$

Taylor expanding this in γ^* and retaining terms of $O(\gamma^*)$ alone, we get

$$U^*(x,y,z) = V^*(x) + O(\gamma^*).$$

The $O(\gamma^*)$ correction is absorbed into the flow $\hat{\mathbf{u}}^*$ forced by the bumps, and the above relation is obtained.

Similarly, the magnetic field $\hat{\mathbf{y}}$ represents the strong azimuthal magnetic field thought to be present in the outer core. It is corrected by a field $q\gamma^*\mathbf{b}^*$ to ensure that it also fits into a bumpy layer. Finally, the linear temperature profile set up by the adverse temperature gradient β is corrected by $\gamma^*\theta^*$ to account for the presence of the bumps. Each of these corrections is topographically forced, i.e. they are forced by the presence of the bumps. As $\gamma^* \ll 1$, these corrections will be small. Therefore, substituting (2.25) into the governing equations and boundary conditions, all terms of $O(\gamma^{*2})$ or smaller can be neglected, to obtain the following non-dimensional equations

$$2\hat{\mathbf{z}} \wedge \mathbf{u} = -\nabla P + \Lambda \frac{\partial \mathbf{b}}{\partial y} + R\theta\hat{\mathbf{z}}, \tag{2.26a}$$

$$2V = \Gamma\Lambda q \frac{\partial}{\partial x}\Big\{\frac{m}{2\pi^2}\int_0^{\frac{2\pi}{m}}\int_0^{\pi}(b_x b_y)dzdy\Big\}, \tag{2.26b}$$

$$q\Big(\frac{\partial \mathbf{b}}{\partial t} + V\frac{\partial \mathbf{b}}{\partial y}\Big) = \frac{\partial \mathbf{u}}{\partial y} + qb_x\frac{dV}{dx}\hat{\mathbf{y}} + \nabla^2\mathbf{b}, \tag{2.26c}$$

$$\frac{\partial \theta}{\partial t} + V\frac{\partial \theta}{\partial y} = u_z + \nabla^2\theta, \tag{2.26d}$$

$$\nabla.\mathbf{u} = 0, \tag{2.26e}$$

$$\nabla.\mathbf{b} = 0, \tag{2.26f}$$

(where the stars have been dropped). The boundary conditions become

$$u_z = b_z = \frac{\partial j_z}{\partial z} = \theta = 0 \quad \text{on} \quad z = 0, \tag{2.27a}$$

$$u_z + mV\sin(my) = b_z + \frac{m}{q}\sin(my) = \frac{\partial j_z}{\partial z} = \theta - \cos(my) = 0 \quad \text{on} \quad z = \pi, \tag{2.27b}$$

where

$$\mathbf{j} = \nabla \wedge \mathbf{b}, \tag{2.28}$$

is the electric current forced in the layer by the bumps.

The parameters that arise under this non-dimensionalisation are the Roberts number q, the Elsasser number Λ, the Rayleigh number R, and a modified bump parameter, Γ, defined by

$$\Gamma = \frac{\gamma^2 \mathcal{D}\Omega^{\frac{1}{2}}}{\nu^{\frac{1}{2}}} = \frac{\gamma^2}{E^{\frac{1}{2}}}, \tag{2.29}$$

where E is the Ekman number. Now, under the magnetogeostrophic approximation,

$$E \ll 1,$$

since the viscous force is neglible compared to the Coriolis force. But, in the limit of small bumps, γ satisfies

$$\gamma \ll 1,$$

and so it is expected that Γ will be a *finite* parameter, which ensures that a finite geostrophic flow is obtained. Hence, equations (2.26) and (2.27) are valid in the asymptotic limit

$$\gamma \ll 1, \quad \Gamma \quad \text{finite.} \tag{2.30}$$

The Rayleigh number is the driving parameter of the system. Any increase or decrease in R corresponds to an increase or decrease in the amount of excess heat put in at the bottom boundary, and hence to the thermal forcing on the layer.

Now, define

$$w = u_z,\ b = b_z,\ \zeta = (\nabla \wedge \mathbf{u})_z,\ \xi = (\nabla \wedge \mathbf{b})_z = j_z. \tag{2.31}$$

Then a system of equations for the unknown vector

$$\mathbf{X}^T = \left[\theta \quad w \quad b \quad \xi \quad \zeta \quad b_x \quad b_y \quad u_x \quad u_y\right], \tag{2.32a}$$

(which is a function of x, y, z and t), and the geostrophic flow

$$V = V(x), \tag{2.32b}$$

can be derived from (2.26). This is done by applying the operators $\hat{\mathbf{z}}$.**curl** and $\hat{\mathbf{z}}$.**curl**^{2} to the momentum equation, and the operators $\hat{\mathbf{z}}$. and $\hat{\mathbf{z}}$.**curl** to the induction equation. Using standard vector identities and (2.31), the following system of equations is obtained

$$2\frac{\partial w}{\partial z} + \Lambda\frac{\partial \xi}{\partial y} = 0, \tag{2.33a}$$

$$2\frac{\partial \zeta}{\partial z} - \Lambda\frac{\partial}{\partial y}(\nabla^2 b) - R\nabla_H^2\theta = 0, \tag{2.33b}$$

$$2V = \Gamma\Lambda q\frac{\partial}{\partial x}\left\{\frac{m}{2\pi^2}\int_0^{\frac{2\pi}{m}}\int_0^{\pi}(b_x b_y)dzdy\right\}, \tag{2.33c}$$

$$q\left(\frac{\partial b}{\partial t} + V\frac{\partial b}{\partial y}\right) = \frac{\partial w}{\partial y} + \nabla^2 b = 0, \tag{2.33d}$$

$$q\left(\frac{\partial \xi}{\partial t} + V\frac{\partial \xi}{\partial y}\right) = \frac{\partial \zeta}{\partial y} + \nabla^2\xi + q\left(b_x\frac{d^2V}{dx^2} - \frac{dV}{dx}\left(\frac{\partial b_y}{\partial y} - \frac{\partial b_x}{\partial x}\right)\right), \tag{2.33e}$$

$$\frac{\partial \theta}{\partial t} + V\frac{\partial \theta}{\partial y} = w + \nabla^2\theta, \tag{2.33f}$$

$$\nabla_H^2 b_x = -\frac{\partial^2 b}{\partial x \partial z} - \frac{\partial \xi}{\partial y}, \tag{2.33g}$$

$$\nabla_H^2 b_y = -\frac{\partial^2 b}{\partial y \partial z} + \frac{\partial \xi}{\partial x}, \tag{2.33h}$$

$$\nabla_H^2 u_x = -\frac{\partial^2 w}{\partial x \partial z} - \frac{\partial \zeta}{\partial y}, \tag{2.33i}$$

$$\nabla_H^2 u_y = -\frac{\partial^2 w}{\partial y \partial z} + \frac{\partial \zeta}{\partial x}, \tag{2.33j}$$

where

$$\nabla_H^2 = \frac{\partial^2}{\partial x^2} + \frac{\partial^2}{\partial y^2},$$

is the horizontal Laplacian operator. (Note that the solenoidal conditions on $\mathbf{u}$ and $\mathbf{b}$ have been used together with the definitions of ξ and ζ to derive the last four equations of (2.33)). Using (2.31) the boundary conditions become

$$w = b = \frac{\partial \xi}{\partial z} = \theta = 0 \quad \text{on} \quad z = 0, \tag{2.34a}$$

$$w + mV\sin(my) = b + \frac{m}{q}\sin(my) = \frac{\partial \xi}{\partial z} = \theta - \cos(my) = 0 \quad \text{on} \quad z = \pi. \tag{2.34b}$$

Equations (2.33) will be solved subject to (2.34) in the subsequent chapters.

2.5 A Note On The Choice Of q And m

At various points in this work, it will be necessary to make choices for the values of the parameters q and m. In the core, the value of q is thought to be $O(10^{-6})$. This is an extremely small value, and as the work of Soward (1986) and Skinner and Soward (1988, 1990) shows, the behaviour of solutions of the magnetoconvection problem is extremely complicated in the small q limit. However, since this work is chiefly concerned with isolating the effects of the topography upon the magnetoconvection, it is necessary to isolate those effects from any that might arise as a result of the smallness of q. Hence, this work will not consider small values of q.

Now, the value of m for the core is not known, and therefore it would be advisable to solve the problem over a range of values of m. However, the results of Kelly and Pal (1977) indicate that the critical values of m that arise in the standard plane layer model give rise to the most interesting behaviour in the bumpy layer, since the possibility of resonance between the bumps and the convection in the layer then arises (see also chapter 4 for more details). Therefore, as a matter of expediency, the values of m will be chosen to be the critical values of m that arise in the standard layer, since these appear to give the most interesting behaviour in the bumpy layer. However, the observation that these are but one out of a continuum of values of m should be borne in mind when considering the results of this work.

Chapter III

The No Bump Case

3.1 The No Bump System

Before proceeding to solve the full system, it is enlightening to consider the no bump case, where the top boundary is flat, and given by $z = d$. This is the standard plane layer model of magnetoconvection. The problem involves solving the magneto-geostrophic equations

$$2\Omega \wedge (\mathbf{U} + V(x)\hat{\mathbf{y}}) = -\nabla(\frac{P}{\rho_0}) + \frac{1}{\mu_0\rho_0}(\mathbf{B}.\nabla)\mathbf{B} + \frac{\rho}{\rho_0}\mathbf{g}, \qquad (3.1a)$$

$$2(\Omega\nu)^{\frac{1}{2}}V = \frac{1}{\mu_0\rho_0}\frac{\partial}{\partial x}\Big\{\frac{m}{2\pi d}\int_0^{\frac{2\pi}{m}}\int_0^d B_x B_y dz dy\Big\}, \qquad (3.1b)$$

$$\nabla.(\mathbf{U} + V(x)\hat{\mathbf{y}}) = 0, \qquad (3.1c)$$

$$\frac{\partial T}{\partial t} + (\mathbf{U}.\nabla)T + V\frac{\partial T}{\partial y} = \kappa\nabla^2 T, \qquad (3.1d)$$

$$\frac{\partial \mathbf{B}}{\partial t} + (\mathbf{U}.\nabla)\mathbf{B} + V\frac{\partial \mathbf{B}}{\partial y} = (\mathbf{B}.\nabla)\mathbf{U} + B_x\frac{dV}{dx}\hat{\mathbf{y}} + \eta\nabla^2\mathbf{B}, \qquad (3.1e)$$

$$\nabla.\mathbf{B} = 0, \qquad (3.1f)$$

(where ρ and P, defined by (2.18b,c), are the density and modified pressure respectively). The boundary conditions are as before, namely that the boundaries are rigid, perfectly electrically conducting and isothermal. They lead to the conditions

$$U_z = B_z = \frac{\partial J_z}{\partial z} = T - T_0 = 0 \quad \text{on} \quad z = 0, \tag{3.2a}$$

$$U_z = B_z = \frac{\partial J_z}{\partial z} = T - T_d = 0 \quad \text{on} \quad z = d. \tag{3.2b}$$

In the no bump case, these boundary conditions are exact.

3.2 The Equilibrium Solution

A steady solution of (3.1) subject to (3.2) is

$$\mathbf{U} = 0, \tag{3.3a}$$

$$V = 0, \tag{3.3b}$$

$$\mathbf{B} = B_0 \hat{\mathbf{y}}, \tag{3.3c}$$

$$T = T_0 - \beta z. \tag{3.3d}$$

This is the hydrostatic conduction solution, so called because the fluid in the layer remains at rest, and excess heat at the bottom boundary is carried across the layer by thermal diffusion (Chandrasekhar 1961). Such a motionless solution is possible because the equation of hydrostatic equilibrium is satisfied,

$$\nabla P + \rho g \hat{\mathbf{z}} = \nabla P + \rho_0 (1 - \alpha (T - T_0)) g \hat{\mathbf{z}} = 0.$$

Taking the curl of this equation yields

$$\nabla T \wedge \hat{\mathbf{z}} = 0, \tag{3.4}$$

which says that the surfaces of constant temperature (isotherms) are horizontal. This is the condition that ensures that a hydrostatic balance is possible in a plane layer.

3.3 The Perturbation Equations

To see how motion develops from the hydrostatic basic state, the stability of (3.3) must be considered. This is done by adding small perturbations to **U**, **B** and T and asking whether the perturbations grow or decay with time. If the perturbations decay, then motion does not become established in the layer, and the basic state (3.3) is said to be stable. If, however, the perturbations grow in time, then motion does become established in the layer and (3.3) is said to be unstable. Denoting the perturbations by **u**, **b** and θ, the velocity, magnetic field and temperature take the the following form in the perturbed state

$$\mathbf{U} = \frac{\kappa}{\mathcal{D}}(\mathbf{0} + \delta\mathbf{u}^*), \tag{3.5a}$$

$$\mathbf{B} = B_0(\hat{\mathbf{y}} + \delta q\mathbf{b}^*), \tag{3.5b}$$

$$T = \beta\mathcal{D}(T_0^* - z^* + \delta\theta^*), \tag{3.5c}$$

where q is the Roberts number (defined by (1.1)), $\delta \ll 1$ is a small parameter measuring the size of the perturbations, and the starred quantities are nondimensional. The unknowns have been nondimensionalised by adopting

$$\mathcal{D} = \frac{d}{\pi},$$

$$\mathcal{T} = \frac{\mathcal{D}^2}{\kappa}$$

as length and time scales, respectively. Substituting (3.5) into (3.1) and (3.2), and neglecting all terms of $O(\delta^2)$ or smaller, the nondimensional equations governing departures from hydrostatic equilibrium are obtained. These are given by

$$2\hat{\mathbf{z}} \wedge \mathbf{u} = -\nabla P + \Lambda \frac{\partial \mathbf{b}}{\partial y} + R\theta\hat{\mathbf{z}}, \tag{3.6a}$$

$$\nabla.\mathbf{u} = 0, \tag{3.6b}$$

$$\frac{\partial \theta}{\partial t} = u_z + \nabla^2\theta, \tag{3.6c}$$

$$q\frac{\partial \mathbf{b}}{\partial t} = \frac{\partial \mathbf{u}}{\partial y} + \nabla^2\mathbf{b}, \tag{3.6d}$$

$$\nabla.\mathbf{b} = 0, \tag{3.6e}$$

where here and below the stars are dropped. As well as the Roberts number q, the other parameters of the problem are Λ, the Elsasser number and R, the Rayleigh number. Note that

$$b_x b_y = O(\delta^2),$$

so no Maxwell stress is generated at $O(\delta)$, and hence, no geostrophic flow is accelerated by the perturbations. The boundary conditions on the perturbations are

$$u_z = b_z = \frac{\partial j_z}{\partial z} = \theta = 0 \quad \text{on} \quad z = 0, \pi,$$

where $\mathbf{j} = \nabla \wedge \mathbf{b}$ is the perturbation electric current. Define

$$w = u_z,\ b = b_z,\ \zeta = (\nabla \wedge \mathbf{u})_z,\ \xi = (\nabla \wedge \mathbf{b})_z = j_z.$$

Then, exactly as in chapter 2, a system of equations for the vector

$$\mathbf{X}^T = \begin{bmatrix} \theta & w & b & \xi & \zeta & b_x & b_y & u_x & u_y \end{bmatrix},$$

may be derived from (3.6). They are

$$2\frac{\partial w}{\partial z} + \Lambda\frac{\partial \xi}{\partial y} = 0, \tag{3.7a}$$

$$2\frac{\partial \zeta}{\partial z} - \Lambda\frac{\partial}{\partial y}(\nabla^2 b) - R\nabla_H^2\theta = 0, \tag{3.7b}$$

$$q\frac{\partial b}{\partial t} - \frac{\partial w}{\partial y} - \nabla^2 b = 0, \tag{3.7c}$$

$$q\frac{\partial \xi}{\partial t} - \frac{\partial \zeta}{\partial y} - \nabla^2 \xi = 0, \tag{3.7d}$$

$$\frac{\partial \theta}{\partial t} - w - \nabla^2\theta = 0, \tag{3.7e}$$

$$\nabla_H^2 b_x = -\frac{\partial^2 b}{\partial x \partial z} - \frac{\partial \xi}{\partial y}, \tag{3.7f}$$

$$\nabla_H^2 b_y = -\frac{\partial^2 b}{\partial y \partial z} + \frac{\partial \xi}{\partial x}, \tag{3.7g}$$

$$\nabla_H^2 u_x = -\frac{\partial^2 w}{\partial x \partial z} - \frac{\partial \zeta}{\partial y}, \tag{3.7h}$$

$$\nabla_H^2 u_y = -\frac{\partial^2 w}{\partial y \partial z} + \frac{\partial \zeta}{\partial x}, \tag{3.7i}$$

where ∇_H^2 is the horizontal Laplacian. The boundary conditions become

$$w = b = \frac{\partial \xi}{\partial z} = \theta = 0 \quad \text{on} \quad z = 0 \quad \text{and} \quad z = \pi. \tag{3.8}$$

3.4 Solutions Of The Perturbation Equations

The solutions of (3.7) and (3.8) must be periodic in x and y, with periods $\frac{2\pi}{l}$ and $\frac{2\pi}{m}$ respectively. To satisfy this condition, a solution of (3.7) and (3.8) is sought of the form

$$\mathbf{X} = \mathbf{X}_1(z) \exp(ilx + imy + \lambda t) + c.c., \tag{3.9}$$

where

$$\mathbf{X}_1^T(z) = \Big[T_1(z) \quad W_1(z) \quad B_1(z) \quad X_1(z) \quad Z_1(z)$$

$$B_{x1}(z) \quad B_{y1}(z) \quad U_{x1}(z) \quad U_{y1}(z)\Big], \tag{3.10}$$

represents the z-structure of (3.9) and *c.c.* stands for complex conjugate. (The reason for including a subscript 1 will be made clear later). λ is a complex number defined by

$$\lambda = s + i\omega, \tag{3.11}$$

where s is the growth rate and ω is the frequency of the perturbations. (3.9) represents a convection roll, whose axis is perpendicular to the vector defined by

$$\mathbf{k} = (l, m, 0).$$

Two distinct types of roll can arise, depending on their orientation with the applied magnetic field (which is in the y direction). A solution which has $l \neq 0$ is called an

oblique roll, since it's axis makes an angle less than $\frac{\pi}{2}$ with the applied magnetic field, and a solution which has $l = 0$ is called a transverse roll, because it's axis is perpendicular to the applied magnetic field. Although the transverse roll is a special case of the oblique roll, it has different stability characteristics, and will be discussed in isolation.

Substituting (3.9) into (3.7) the equations for the z-structure of the roll are obtained. These are given by

$$2DW_1 + \Lambda imX_1 = 0, \tag{3.12a}$$

$$2DZ_1 - \Lambda im(D^2 - k^2)B_1 + Rk^2T_1 = 0, \tag{3.12b}$$

$$(D^2 - k^2 - q\lambda)B_1 + imW_1 = 0, \tag{3.12c}$$

$$(D^2 - k^2 - q\lambda)X_1 + imZ_1 = 0, \tag{3.12d}$$

$$(D^2 - k^2 - \lambda)T_1 + W_1 = 0, \tag{3.12e}$$

$$k^2B_{x1} - ilDB_1 - imX_1 = 0, \tag{3.12f}$$

$$k^2B_{y1} - imDB_1 + ilX_1 = 0, \tag{3.12g}$$

$$k^2U_{x1} - ilDW_1 - imZ_1 = 0, \tag{3.12h}$$

$$k^2U_{y1} - imDW_1 + ilZ_1 = 0, \tag{3.12i}$$

where here and below

$$D = \frac{d}{dz},$$

$$k^2 = l^2 + m^2.$$

Substituting (3.9) into (3.8) the boundary conditions become

$$W_1 = B_1 = DX_1 = T_1 = 0 \quad \text{on} \quad z = 0 \quad \text{and} \quad z = \pi. \tag{3.13}$$

The most general solution of (3.12) and (3.13) is given by

$$\mathbf{X}_1(z) = A_1 \mathbf{X}_{1RS}(z), \tag{3.14}$$

where A_1 is a complex constant and

$$\mathbf{X}_{1RS}(z) = \begin{bmatrix} T_{1RS}(z) \\ W_{1RS}(z) \\ B_{1RS}(z) \\ X_{1RS}(z) \\ Z_{1RS}(z) \\ B_{x1RS}(z) \\ B_{y1RS}(z) \\ U_{x1RS}(z) \\ U_{y1RS}(z) \end{bmatrix} = \begin{bmatrix} \sin(z) \\ (1+k^2+\lambda)\sin(z) \\ \frac{im(1+k^2+\lambda)}{1+k^2+q\lambda}\sin(z) \\ \frac{2i(1+k^2+\lambda)}{\Lambda m}\cos(z) \\ \frac{2(1+k^2+q\lambda)(1+k^2+\lambda)}{\Lambda m^2}\cos(z) \\ (\frac{-lm}{k^2(1+k^2+q\lambda)} - \frac{2}{\Lambda k^2})(1+k^2+\lambda)\cos(z) \\ (\frac{-m^2}{k^2(1+k^2+q\lambda)} + \frac{2l}{\Lambda k^2 m})(1+k^2+\lambda)\cos(z) \\ i(\frac{l}{k^2} + \frac{2m(1+k^2+q\lambda)}{\Lambda m^2 k^2})(1+k^2+\lambda)\cos(z) \\ i(\frac{m}{k^2} - \frac{2l(1+k^2+q\lambda)}{\Lambda m^2 k^2})(1+k^2+\lambda)\cos(z) \end{bmatrix}. \tag{3.15}$$

This solution exists if and only if the following relation is satisfied

$$4(q\lambda + 1 + k^2)^2(\lambda + 1 + k^2) + \Lambda^2 m^4(\lambda + 1 + k^2)(1 + k^2)$$

$$-k^2\Lambda m^2(q\lambda + 1 + k^2)R = 0. \tag{3.16}$$

(3.16) is called the dispersion relation. The real and imaginary parts of (3.16) give two equations for the two unknowns s and ω. For fixed values of Λ and q, the solution of these two equations takes the form

$$s = s(R, l^2, m^2), \quad \omega = \omega(R, l^2, m^2).$$

The stability of the basic state (3.3) depends upon the sign of s. If at given values of R, l and m

$$s(R, l^2, m^2) < 0,$$

then the perturbations will decay exponentially in time to leave the basic state as it was. Hence, (3.3) is stable. However, if

$$s(R, l^2, m^2) > 0,$$

then the perturbations will grow exponentially in time, and the basic state will lose stability to the convection roll defined by (3.9). Hence, (3.3) is unstable. The point at which the basic state loses stability for given Λ and q is defined by

$$s(R, l^2, m^2) = 0. \tag{3.17}$$

Now, this defines a relation of the form

$$R = R(l^2, m^2), \tag{3.18}$$

i.e., for given values of l and m it defines the Rayleigh number at which the basic state (3.3) goes unstable to perturbations of the form (3.9). To find where this *first* occurs, (3.18) must be minimised with respect to l^2 and m^2. This is done by solving the simultaneous equations

$$\frac{\partial R}{\partial l^2} = \frac{\partial R}{\partial m^2} = 0.$$

These yield the critical wavenumbers l_c and m_c for which R defined by (3.18) is a minimum. This is the critical Rayleigh number, and is defined by

$$R_c = R(l_c^2, m_c^2).$$

The basic state is stable to the perturbations for $R < R_c$, but loses stability to the perturbations at $R = R_c$. The frequency of the perturbations at criticality is given by

$$\omega_c = \omega(R_c, l_c^2, m_c^2).$$

For the transverse rolls, the above procedure is repeated, but with l set to zero.

3.5 Linear Stability Results

The stability results quoted below were first derived by Roberts and Stewartson (1974). Now, R_c and ω_c can be found directly from (3.16) by setting

$$s = 0,$$

in (3.16). This yields

$$4(qi\omega + 1 + k^2)^2(i\omega + 1 + k^2) + \Lambda^2 m^4(i\omega + 1 + k^2)(1 + k^2)$$
$$-k^2\Lambda m^2(qi\omega + 1 + k^2)R = 0. \qquad (3.19)$$

The real part of (3.19) is

$$(1 + k^2)[4q(q + 2)\omega^2 - \{4(1 + k^2)^2 + \Lambda^2 m^4(1 + k^2) - k^2\Lambda m^2 R\}] = 0, \qquad (3.20)$$

while the imaginary part is

$$\omega[4q^2\omega^2 - \{4(2q+1)(1+k^2)^2 + \Lambda^2 m^4(1+k^2) - k^2\Lambda m^2 qR\}] = 0. \qquad (3.21)$$

These provide two equations for the two unknowns R and ω, from which R_c and ω_c can be found.

3.5.1 The Exchange Of Stabilities

The simplest solution of (3.21) is

$$\omega^2 = 0. \qquad (3.22)$$

This means that the basic state loses stability to steady perturbations, which is called losing stability through the exchange of stabilities (Chandrasekhar 1961). Substituting (3.22) into (3.20) gives

$$R = \frac{4(1+k^2)^2}{\Lambda m^2 k^2} + \frac{\Lambda m^2(1+k^2)}{k^2}. \qquad (3.23)$$

The critical wavenumbers l_c and m_c are found from the simultaneous equations

$$\frac{\partial R}{\partial l^2} = \frac{\partial R}{\partial m^2} = 0.$$

The solution of these equations is given by

$$l_c^2 = 2 - \frac{2\sqrt{3}}{\Lambda}, \quad m_c^2 = \frac{2\sqrt{3}}{\Lambda}. \qquad (3.24)$$

Evaluating (3.23) on these values yield the critical Rayleigh number for an oblique roll

$$R_c = 6\sqrt{3}. \qquad (3.25)$$

Thus, as R is increased from zero, the basic state first loses stability to an oblique roll (whose wavenumbers are given by (3.24)) through the exchange of stabilities once R equals R_c. This result depends upon the value of Λ: if

$$\Lambda < \sqrt{3},$$

then

$$l_c^2 < 0,$$

which cannot happen, since l is real. Therefore, the oblique roll can only go unstable for sufficiently strong magnetic fields, those which satisfy

$$\Lambda \geq \sqrt{3}. \tag{3.26}$$

Setting $l = 0$ in (3.20) yields R for the transverse roll

$$R = \frac{4(1+m^2)^2}{\Lambda m^4} + \Lambda(1+m^2). \tag{3.27}$$

The critical wavenumber m_c for this roll is defined by the solution of

$$\frac{\partial R}{\partial m^2} = 0,$$

that is, as the solution of

$$\Lambda^2 m^6 - 8(1+m^2) = 0. \tag{3.28}$$

(3.28) is regarded as a cubic equation for m^2, and m_c^2 is chosen to be it's positive root. Evaluating (3.27) on m_c yields the critical Rayleigh number for the transverse roll

$$R_c = \frac{4(1+m_c^2)^2}{\Lambda m_c^4} + \Lambda(1+m_c^2),$$

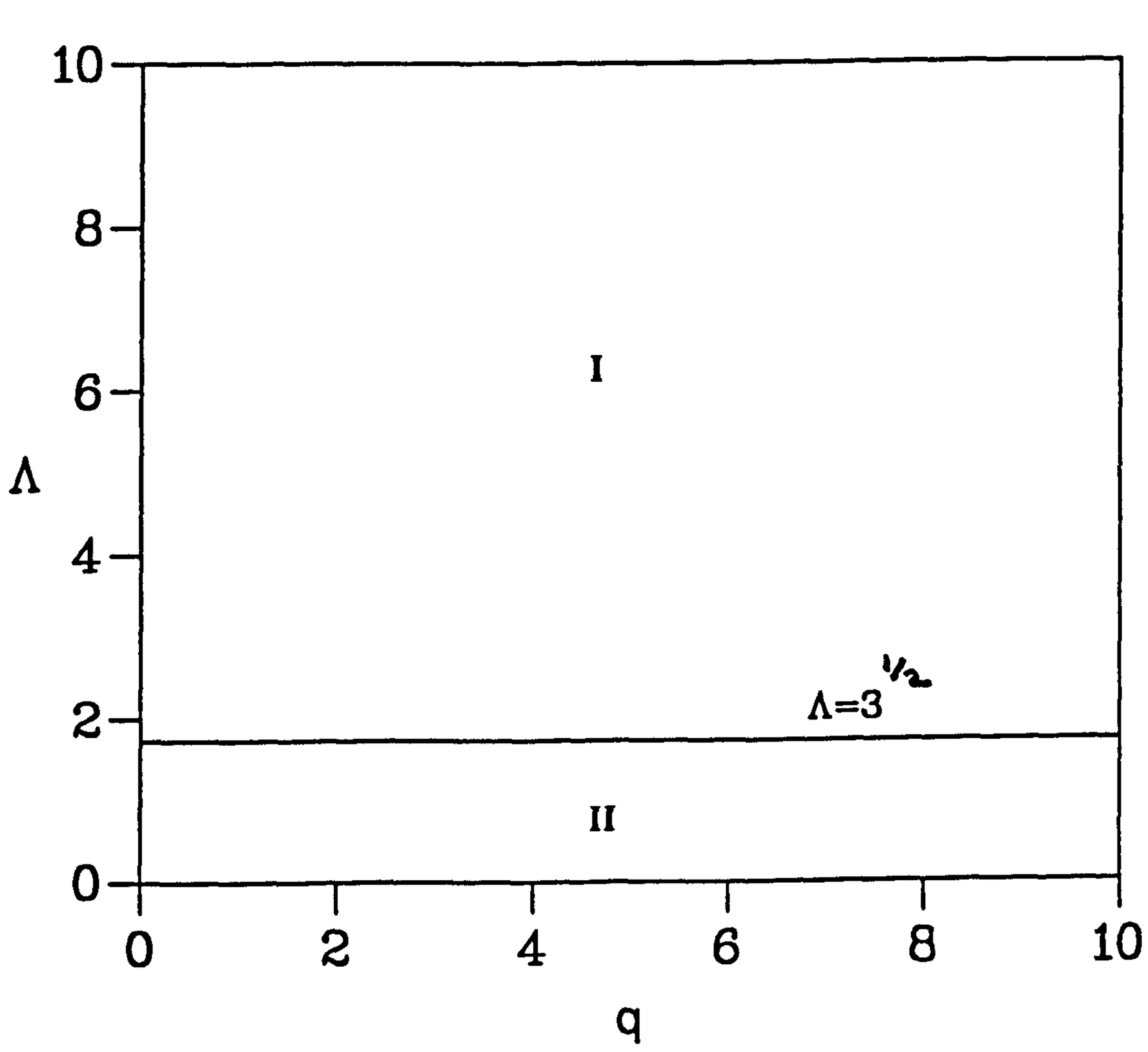

Figure 3.1: Stability boundaries in the (q, Λ) plane for the exchange of stabilities. The oblique roll is preferred in region I, and the transverse roll is preferred in region II.

which after simplifying using (3.28) becomes

$$R_c = \frac{\Lambda}{2}(2 + m_c^2)(1 + m_c^2). \tag{3.29}$$

Thus, as R is increased from zero, the basic state first loses stability to a transverse roll (whose wavenumber is given by m_c) through the exchange of stabilities when R equals R_c. This occurs for all values of Λ.

Now, when $\Lambda \geq \sqrt{3}$, the basic state can lose stability to either a transverse roll or an oblique roll. It actually loses stability to only one - the one with the lowest critical Rayleigh number. This roll is then said to be preferred for $\Lambda \geq \sqrt{3}$. Since $6\sqrt{3}$ is the minimum of

$$R = \frac{4(1 + k^2)^2}{\Lambda m^2 k^2} + \frac{\Lambda m^2 (1 + k^2)}{k^2},$$

over all l and m, including the case $l = 0$, it follows that the oblique roll has a lower critical Rayleigh number that the transverse roll, and is the preferred mode of convection for $\Lambda \geq 3$.

Hence, for weak magnetic fields, i.e. those satisfying

$$\Lambda < \sqrt{3},$$

the basic state loses stability to a transverse roll through the exchange of stabilities. But, once the magnetic field strength (as measured by Λ) increases beyond $\sqrt{3}$, the oblique roll becomes preferred, and the basic state loses stability to an oblique roll through the exchange of stabilities. This is shown in figure 3.1.

3.5.2 Overstability

The second solution of (3.21) is

$$\omega^2 = \frac{4(2q + 1)(1 + k^2)^2 + \Lambda^2 m^4 (1 + k^2) - k^2 \Lambda m^2 q R}{4q^2}. \tag{3.30}$$

Now, ω is real, so

$$\omega^2 \geq 0.$$

When this holds (and conditions will be found to ensure that it does) the basic state loses stability to perurbations that oscillate with frequency ω. This is called losing stability through the mechanism of overstability (Chandasekhar 1961). Substituting (3.30) into (3.20) and simplifying yields

$$R = \frac{2}{q}\left(\frac{4(1+k^2)^2}{\hat{\Lambda}m^2k^2} + \frac{\hat{\Lambda}m^2(1+k^2)}{k^2}\right), \tag{3.31}$$

where

$$\hat{\Lambda} = \frac{\Lambda}{1+q}, \tag{3.32}$$

is a modified Elsasser number. Substituting (3.31) into (3.30) and simplifying yields

$$\omega^2 = \frac{(q^2-1)\hat{\Lambda}^2m^4(1+k^2) - 4(1+k^2)^2}{4q^2}. \tag{3.33}$$

The critical wavenumbers minimising R are found from the simultaneous equations

$$\frac{\partial R}{\partial l^2} = \frac{\partial R}{\partial m^2} = 0.$$

The solution of these equations is given by

$$l_c^2 = 2 - \frac{2\sqrt{3}}{\Lambda}(1+q), \quad m_c^2 = \frac{2\sqrt{3}}{\Lambda}(1+q). \tag{3.34}$$

Evaluating (3.31) and (3.33) on these values yields the critical Rayleigh number and the frequency of the oblique roll, which are given by

$$R_c = \frac{12\sqrt{3}}{q}, \tag{3.35}$$

$$\omega_c^2 = \frac{9(q^2-2)}{q^2}. \tag{3.36}$$

Therefore, as R is increased from zero, the basic state first loses stability to an oblique roll (whose wavenumbers are given by (3.34)) through overstability once R equals R_c. The frequency of the perturbations at criticality is given by ω_c. Notice that ω_c is real only when

$$q \geq \sqrt{2}.$$

Similarly, l_c is real only when

$$\Lambda \geq \Lambda_1(q) = \sqrt{3}(1+q).$$

Thus, an overstable oblique roll is only possible in the region of the (q, Λ) plane defined by

$$q \geq \sqrt{2}, \quad \Lambda \geq \Lambda_1(q), \tag{3.37}$$

since only in this region are both ω_c and l_c real.

Setting $l = 0$ in (3.31) and (3.33) yields the Rayleigh number and the frequency associated with the transverse roll

$$R = \frac{2}{q}\left(\frac{4(1+m^2)^2}{\hat{\Lambda}m^4} + \hat{\Lambda}(1+m^2)\right), \tag{3.38}$$

$$\omega^2 = \frac{(q^2-1)\hat{\Lambda}^2 m^4(1+m^2) - 4(1+m^2)^2}{4q^2}. \tag{3.39}$$

The critical wavenumber minimising R is found from the solution of

$$\frac{\partial R}{\partial m^2} = 0,$$

i.e. from the solution of

$$\Lambda^2 m^6 - 8(1+q)^2(1+m^2) = 0. \tag{3.40}$$

This is again regarded as a cubic im m^2, and m_c^2 is chosen to be it's positive root. Evaluating (3.38) and (3.39) on m_c and simplifying using (3.40) yields the critical Rayleigh number and frequency associated with the transverse roll

$$R_c = \frac{\Lambda}{q(1+q)}(1+m_c^2)(2+m_c^2), \tag{3.41}$$

$$\omega_c^2 = \frac{(1+m_c^2)(2q^2-2-m_c^2)}{q^2 m_c^2}. \tag{3.42}$$

Thus as R is increased from zero, the basic state first loses stability to a transverse roll (whose wavenumber is given by m_c) through overstability once R equals R_c. The frequency of the transverse roll is given by ω_c. This solution exists provided the ω_c is real. The region of the (q, Λ) plane where this is true has a boundary defined by

$$\omega_c^2 = 0.$$

From (3.42), this occurs when

$$m_c^2 = 2(q^2-1). \tag{3.43}$$

Substituting (3.43) into (3.40) and simplifying yields

$$(q^2-1)^3\Lambda^2 - (1+q)^2(2q^2-1) = 0.$$

Define

$$\Lambda_0(q) = \frac{(1+q)(2q^2-1)^{\frac{1}{2}}}{(q^2-1)^{\frac{3}{2}}}. \tag{3.44}$$

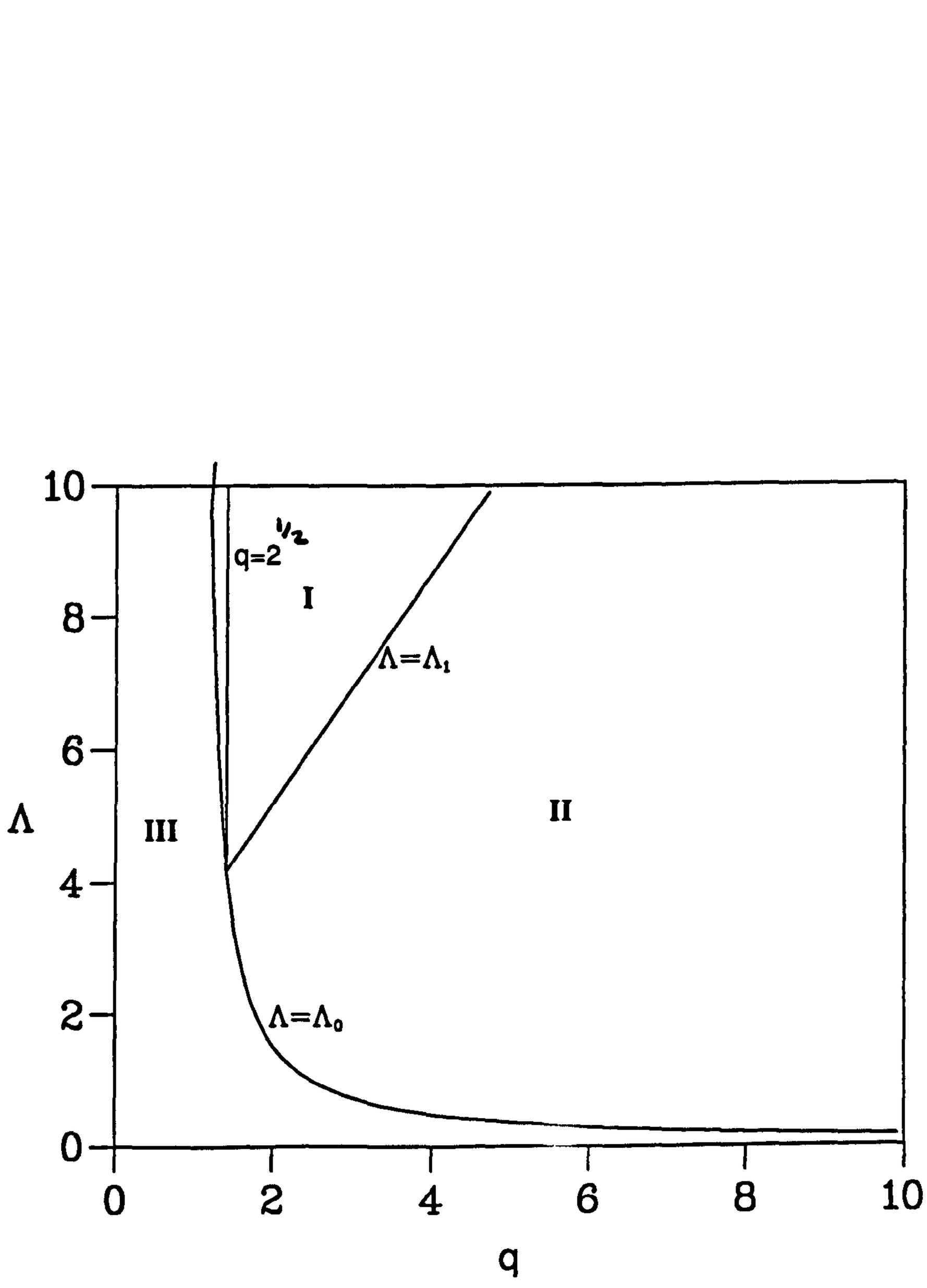

Figure 3.2: Stability boundaries in the (q, Λ) plane in the overstable case. The oblique roll is preferred in region I, while the transverse roll is preferred in region II. Oscillatory solutions are not possible in region III.

Examination of (3.44) reveals that $\Lambda_0(q)$ is real only if $q > 1$. Therefore, an overstable transverse roll is only possible in the region of the (q, Λ) plane defined by

$$q > 1, \quad \Lambda \geq \Lambda_0(q), \tag{3.45}$$

since ω_c is real only in this region.

Now, for q and Λ in the region

$$q \geq \sqrt{2}, \quad \Lambda \geq \Lambda_1(q),$$

the basic state can lose stability to either the oblique roll or the transverse roll through overstability. However, repeating the argument given in the exchange of stabilities case, it can be shown that the oblique roll has a lower critical Rayleigh number than the transverse roll, and hence is preferred in this region. The transverse roll is preferred in the region defined by

$$1 < q < \sqrt{2}, \quad \Lambda \geq \Lambda_0(q),$$

$$q > \sqrt{2}, \quad \Lambda_0(q) \leq \Lambda \leq \Lambda_1(q).$$

This is illustrated in figure 3.2.

3.5.3 Steady Or Oscillatory?

The basic state can lose stability to the perturbations through two mechanisms - the exchange of stabilities or overstability. To find the regions of the (q, Λ) plane where each mechanism is preferred, define

$$R_e = \begin{cases} 6\sqrt{3} & \text{for } \Lambda \geq \sqrt{3}, \\ \\ \frac{\Lambda}{2}(1 + m_e^2)(2 + m_e^2) & \text{for } \Lambda < \sqrt{3}, \end{cases} \tag{3.46}$$

where m_e^2 is the positive root of

$$\Lambda^2 m^6 - 8m^2 - 8 = 0.$$

R_e is the critical Rayleigh number associated with the exchange of stabilities. Similarly, define

$$R_o = \begin{cases} \frac{12\sqrt{3}}{q} & \text{for } q > 2,\ \Lambda > \Lambda_1(q), \\ \\ \frac{\Lambda}{q(1+q)}(1+m_o^2)(2+m_o^2) & \text{for } 1 < q < \sqrt{2},\ \Lambda > \Lambda_0(q), \\ & \text{and } q > \sqrt{2},\ \Lambda_0(q) < \Lambda < \Lambda_1(q), \end{cases} \tag{3.47}$$

where m_o^2 is the positive root of

$$\Lambda^2 m^6 - 8(1+q)^2(1+m^2) = 0.$$

R_o is the critical Rayleigh number associated with overstability. Now, if for given Λ and q, $R_e < R_o$, then the exchange of stabilities is the preferred mechanism; however, if $R_e > R_o$, then overstability is the preferred mechanism of instability. The line in the (q, Λ) plane separating the regions where each mechanism is preferred is given by

$$R_e = R_o.$$

This defines the boundary curve

$$\Lambda = \Lambda_E(q),$$

between the two regions. This curve must be calculated numerically using (3.46) amd (3.47). The graph of Λ_E against q is shown in figure 3.3. The exchange of stabilities is preferred to the left of the curve, while overstability is preferred to the right.

Using this curve together with the stability results obtained earlier, the (q, Λ) plane may be divided into four regions, in which each of the four possible types of

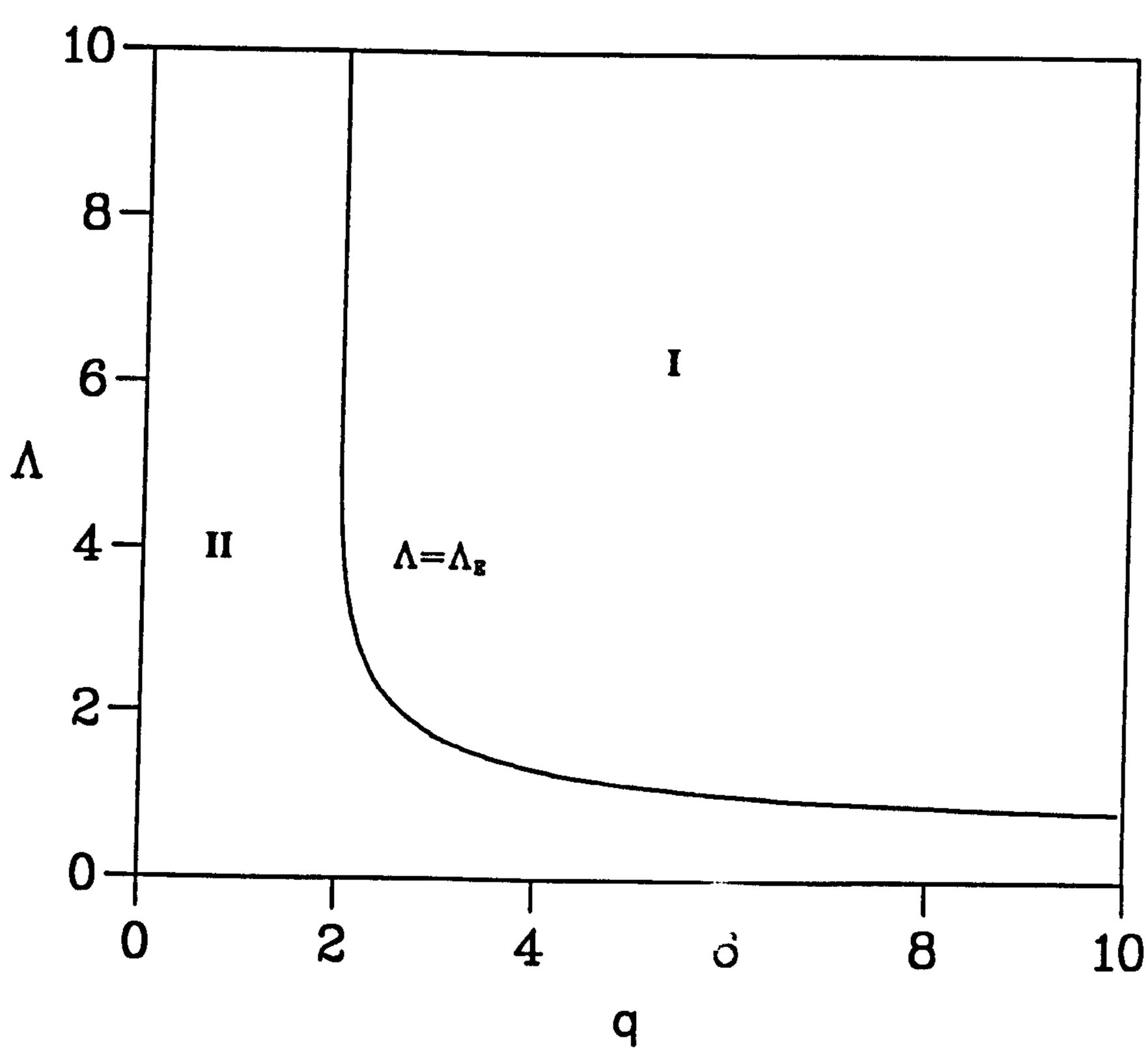

Figure 3.3: The curve $\Lambda = \Lambda_E(q)$ which separates the (q, Λ) plane into regions where the exchange of stabilities or overstability is preferred. Overstability is preferred in region I, while the exchange of stabilities is preferred in region II.

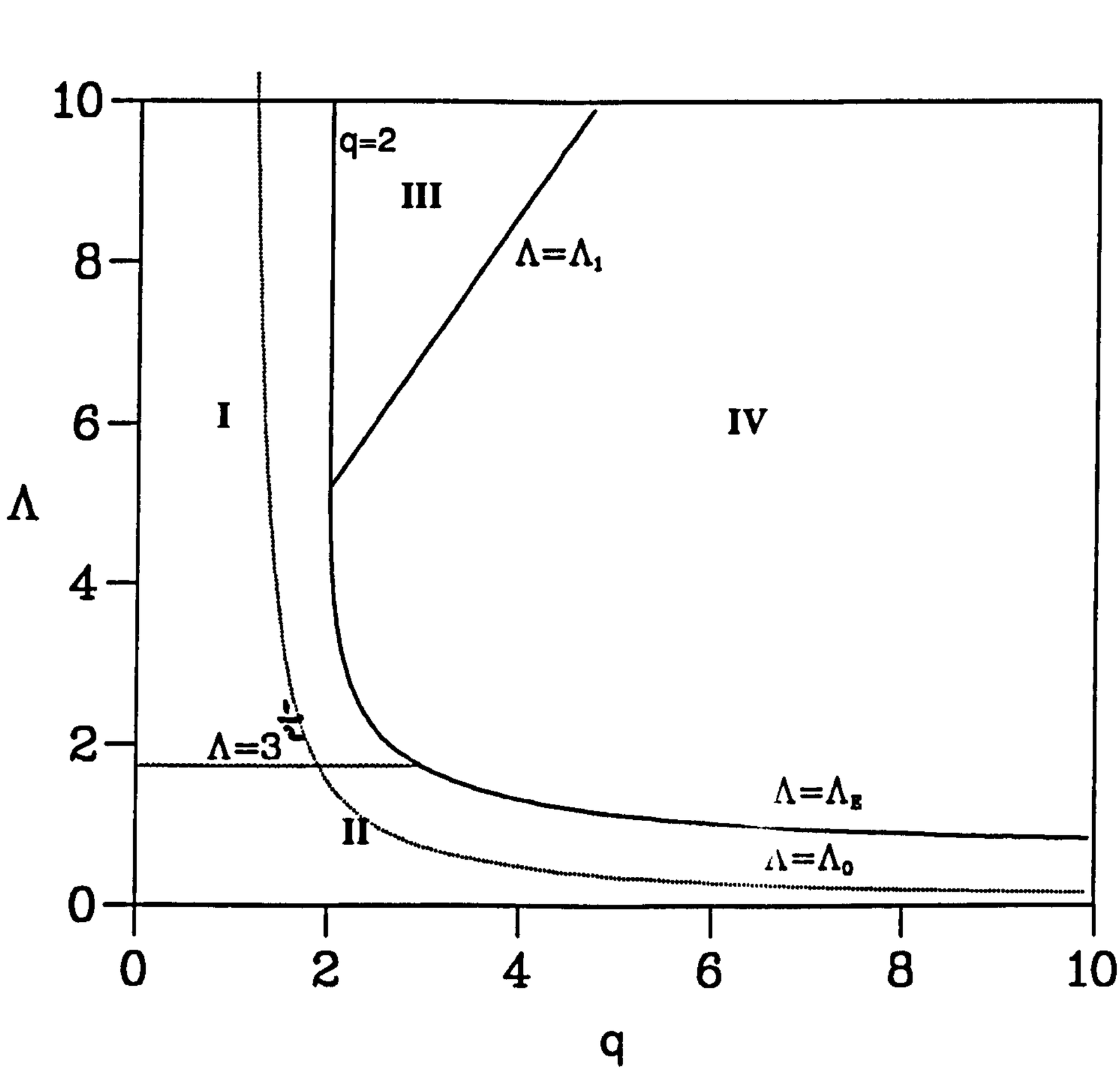

Figure 3.4: The regions of the (q, Λ) plane where each of the four possible types of convection roll are preferred. Region I: Steady oblique roll. Region II: Steady transverse roll. Region III: Overstable oblique roll. Region IV: Overstable transverse roll.

roll (*viz.* steady oblique, steady transverse, overstable oblique, overstable transverse) are preferred. This is shown in figure 3.4, and represents the complete stability diagram for the basic state (3.3).

3.6 Degeneracy Of The Solution

The angle made between the oblique roll solution (3.9) and the applied magnetic field is determined so that the Coriolis force in the layer is best balanced by the Lorentz force (see Roberts and Stewartson 1974). It transpires that this angle is fixed in magnitude but not in sign. That is, there is another solution of the perturbation equations which may be obtained from (3.9) and (3.15) by mapping

$$m \longrightarrow -m.$$

This reverses the angle made by the oblique roll solution (3.9) with the applied magnetic field. The new roll is defined by

$$\mathbf{X} = \mathbf{X}_{-1}(z)\exp(ilx - imy + \lambda t) + c.c.. \tag{3.48}$$

where the z-structure of this roll is given by

$$\mathbf{X}_{-1}(z) = A_{-1}\mathbf{X}_{-1RS}(z),$$

where A_{-1} is a complex constant and

$$\mathbf{X}_{-1RS}(z) = \begin{bmatrix} T_{-1RS}(z) \\ W_{-1RS}(z) \\ B_{-1RS}(z) \\ X_{-1RS}(z) \\ Z_{-1RS}(z) \\ B_{x-1RS}(z) \\ B_{y-1RS}(z) \\ U_{x-1RS}(z) \\ U_{y-1RS}(z) \end{bmatrix} = \begin{bmatrix} \sin(z) \\ (1+k^2+\lambda)\sin(z) \\ \frac{-im(1+k^2+\lambda)}{1+k^2+q\lambda}\sin(z) \\ \frac{-2i(1+k^2+\lambda)}{\Lambda m}\cos(z) \\ \frac{2(1+k^2+q\lambda)(1+k^2+\lambda)}{\Lambda m^2}\cos(z) \\ (\frac{lm}{k^2(1+k^2+q\lambda)} - \frac{2}{\Lambda k^2})(1+k^2+\lambda)\cos(z) \\ (\frac{-m^2}{k^2(1+k^2+q\lambda)} - \frac{2l}{\Lambda k^2 m})(1+k^2+\lambda)\cos(z) \\ i(\frac{l}{k^2} - \frac{2m(1+k^2+q\lambda)}{\Lambda m^2 k^2})(1+k^2+\lambda)\cos(z) \\ i(\frac{-m}{k^2} - \frac{2l(1+k^2+q\lambda)}{\Lambda m^2 k^2})(1+k^2+\lambda)\cos(z) \end{bmatrix}. \tag{3.49}$$

This oblique roll has identical stability characteristics to the roll defined by (3.9) and (3.15). The difference between the two solutions is that the axis of (3.9) makes an angle ϕ with the applied magnetic field, while the axis of (3.48) makes an angle $-\phi$ with the applied magnetic field. Therefore, the two rolls are aligned at equal but opposite angles to the applied magnetic field. The roll (3.9) is called a (+)-roll, while (3.48) is called a (-)-roll. Linearly, there is no way to destinguish between the two rolls.

This means that there are two types of oblique roll solution to the perturbation equations. Either a single (+) or (-)-roll goes unstable at criticality, so either

$$\mathbf{X} = A_1\mathbf{X}_{1RS}(z)\exp(ilx + imy + i\omega_c t) + c.c.,$$

or

$$\mathbf{X} = A_{-1}\mathbf{X}_{-1RS}(z)\exp(ilx - imy + i\omega_c t) + c.c.,$$

at criticality. These are called single roll solutions. The alternative is that a linear combination of a (+)-roll and a (-)-roll goes unstable at criticality, so

$$\mathbf{X} = A_{-1}\mathbf{X}_{-1RS}(z)\exp(ilx - imy + i\omega_c t) + A_1\mathbf{X}_{1RS}(z)\exp(ilx + imy + i\omega_c t) + c.c.,$$

at criticality. This is a double roll solution. The existance of two distinct types of oblique roll solution means that the problem is degenerate. The nonlinear evolution of single roll solutions was examined by Roberts and Stewartson (1974), while Roberts and Stewartson (1975), and Soward (1980), examined the evolution of the double roll solution.

Chapter IV

The Basic State That Arises In A Layer With Bumps

4.1 An Imperfect Configuration

Recall that a hydrostatic balance can only be maintained in a plane layer provided that the isotherms line up with surfaces of constant gravitational potential (see chapter 3). Since the top boundary of the modified layer, $z = \pi + \gamma \cos(my)$, is maintained at a constant temperature T_d, it is an isotherm. However, the surfaces of constant gravitational potential are planes parallel to the bottom boundary, i.e. the planes

$$z = constant,$$

just as in the standard layer. The nonalignment of the isotherms near the top boundary with the surfaces of constant gravitational potential leads to an unbalanced buoyancy torque, which forces small scale motion in the layer. This forcing is independent of the thermal forcing on the bottom boundary, and so motion will be forced irrespective of how strong the adverse temperature gradient is. This situation differs from what occurs in the standard plane layer model. There, motion could only occur when the hydrostatic basic state lost stability to convection rolls once the adverse temperature gradient (as measured by the Rayleigh number) exceeded a certain critical value.

Configurations such as this are called imperfect, and have been studied in various geometries with different types of forcing (e.g. Kuang and Bloxham 1993, in a plane layer with bumps, Bell and Soward 1995, in an annulus with bumps, Sun *et al* 1994, in a sphere with thermal inhomogeneities). The work most relevant to this problem is described in Kelly and Pal (1977), who consider convection in a layer with bumpy top and bottom boundaries in the absence of a magnetic field.

4.2 The Equilibrium Solution

To find what form is taken by the motion forced by bumps, a solution of the following equations is required

$$2\frac{\partial w}{\partial z} + \Lambda\frac{\partial \xi}{\partial y} = 0, \tag{4.1a}$$

$$2\frac{\partial \zeta}{\partial z} - \Lambda\frac{\partial}{\partial y}(\nabla^2 b) - R\nabla_H^2\theta = 0, \tag{4.1b}$$

$$2V = \Gamma\Lambda q\frac{\partial}{\partial x}\Big[\frac{m}{2\pi^2}\int_0^{\frac{2\pi}{m}}\int_0^{\pi}(b_x b_y)dzdy\Big], \tag{4.1c}$$

$$qV\frac{\partial b}{\partial y} = \frac{\partial w}{\partial y} + \nabla^2 b, \tag{4.1d}$$

$$qV\frac{\partial \xi}{\partial y} = \frac{\partial \zeta}{\partial y} + \nabla^2\xi + q\Big(b_x\frac{d^2V}{dx^2} - \frac{dV}{dx}\Big(\frac{\partial b_y}{\partial y} - \frac{\partial b_x}{\partial x}\Big)\Big), \tag{4.1e}$$

$$V\frac{\partial \theta}{\partial y} = w + \nabla^2\theta, \tag{4.1f}$$

$$\nabla_H^2 b_x = -\frac{\partial^2 b}{\partial x\partial z} - \frac{\partial \xi}{\partial y}, \tag{4.1g}$$

$$\nabla_H^2 b_y = -\frac{\partial^2 b}{\partial y\partial z} + \frac{\partial \xi}{\partial x}, \tag{4.1h}$$

$$\nabla_H^2 u_x = -\frac{\partial^2 w}{\partial x\partial z} - \frac{\partial \zeta}{\partial y}, \tag{4.1i}$$

$$\nabla_H^2 u_y = -\frac{\partial^2 w}{\partial y\partial z} + \frac{\partial \zeta}{\partial x}. \tag{4.1j}$$

These are to be solved subject to the boundary conditions

$$w = b = \frac{\partial \xi}{\partial z} = \theta = 0 \quad \text{on} \quad z = 0, \tag{4.2a}$$

$$w + mV\sin(my) = b + \frac{m}{q}\sin(my) = \frac{\partial \xi}{\partial z} = \theta - \cos(my) = 0 \quad \text{on} \quad z = \pi. \tag{4.2b}$$

The solution of (4.1) subject to (4.2) will represent the basic state that arises in a plane layer with a bumpy top boundary.

The boundary conditions suggest the following ansatz for the solution of (4.1) and (4.2),

$$\mathbf{X} = \mathbf{X}_0(z)\exp(imy) + c.c., \tag{4.3}$$

where c.c. stands for complex conjugate and

$$\mathbf{X}_0^T(z) = \Big[T_0(z) \quad W_0(z) \quad B_0(z) \quad X_0(z) \quad Z_0(z)$$
$$B_{x0}(z) \quad B_{y0}(z) \quad U_{x0}(z) \quad U_{y0}(z)\Big], \tag{4.4}$$

represents the z-structure of the solution. (4.3) is a steady, transverse convection roll whose axis is parallel to that of the bumps, and perpendicular to the applied magnetic field. The wavenumber m of this convection roll is equal to the wavenumber of the bumps, and is assumed to be given.

Now, (4.3) gives

$$b_x b_y = B_{x0}(z)B_{y0}(z)e^{2imy} + B_{x0}(z)B_{y0}^*(x) + c.c.,$$

(where the star denotes complex conjugate). Using this, the Maxwell stress M generated by the transverse roll is given by

$$M = \frac{m}{2\pi^2}\int_0^{\frac{2\pi}{m}}\int_0^{\pi}(b_x b_y)dzdy = \frac{1}{\pi}\int_0^{\pi} B_{x0}(z)B_{y0}^*(z)dz + c.c. = const.$$

Hence, the transverse roll forced by the bumps satisfies Taylor's constraint

$$\frac{\partial M}{\partial x} = \frac{\partial}{\partial x}\left[\frac{m}{2\pi^2}\int_0^{\frac{2\pi}{m}}\int_0^{\pi}(b_x b_y)dzdy\right] = 0,$$

and no geostrophic flow is accelerated, so

$$V = 0. \tag{4.5}$$

Substituting (4.3) into (4.1) using (4.5), the equations for the z-structure of the roll are obtained

$$2DW_0 + \Lambda imX_0 = 0, \tag{4.6a}$$

$$2DZ_0 - \Lambda im(D^2 - m^2)B_0 + Rm^2T_0 = 0, \tag{4.6b}$$

$$(D^2 - m^2)B_0 + imW_0 = 0, \tag{4.6c}$$

$$(D^2 - m^2)T_0 + W_0 = 0, \tag{4.6d}$$

$$(D^2 - m^2)X_0 + imZ_0 = 0, \tag{4.6e}$$

$$m^2 B_{x0} = imX_0, \tag{4.6f}$$

$$m^2 B_{y0} = imDB_0, \tag{4.6g}$$

$$m^2 U_{x0} = imZ_0, \tag{4.6h}$$

$$m^2 U_{y0} = imDW_0, \tag{4.6i}$$

where $D = \frac{d}{dz}$. The boundary conditions (4.2) are satisfied by (4.3) provided that

$$W_0 = B_0 = DX_0 = T_0 = 0 \quad \text{on} \quad z = 0, \tag{4.7a}$$

$$W_0 = B_0 - \frac{im}{2q} = DX_0 = T_0 - \frac{1}{2} = 0 \quad \text{on} \quad z = \pi. \tag{4.7b}$$

The solution of (4.6) subject to (4.7) is given by

$$\mathbf{X}_0(z) = \begin{bmatrix} T_0(z) \\ W_0(z) \\ B_0(z) \\ X_0(z) \\ Z_0(z) \\ B_{x0}(z) \\ B_{y0}(z) \\ U_{x0}(z) \\ U_{y0}(z) \end{bmatrix} = \begin{bmatrix} \sum_{n=1}^{6} A_{0n} \exp(\lambda_n z) \\ \sum_{n=1}^{6} (m^2 - \lambda_n^2) A_{0n} \exp(\lambda_n z) \\ \sum_{n=1}^{6} imA_{0n} \exp(\lambda_n z) + \frac{im(1-q)}{2q \sinh(m\pi)} \sinh(mz) \\ \frac{2i}{\Lambda m} \sum_{n=1}^{6} \lambda_n (m^2 - \lambda_n^2) A_{0n} \exp(\lambda_n z) \\ \frac{2}{\Lambda m^2} \sum_{n=1}^{6} \lambda_n (m^2 - \lambda_n^2)^2 A_{0n} \exp(\lambda_n z) \\ \frac{-2}{\Lambda m^2} \sum_{n=1}^{6} \lambda_n (m^2 - \lambda_n^2) A_{0n} \exp(\lambda_n z) \\ -\sum_{n=1}^{6} \lambda_n A_{0n} \exp(\lambda_n z) + \frac{(q-1)m}{2q \sinh(m\pi)} \cosh(mz) \\ \frac{2i}{\Lambda m^3} \sum_{n=1}^{6} \lambda_n (m^2 - \lambda_n^2)^2 A_{0n} \exp(\lambda_n z) \\ \frac{i}{m} \sum_{n=1}^{6} \lambda_n (m^2 - \lambda_n^2) A_{0n} \exp(\lambda_n z) \end{bmatrix}, \tag{4.8}$$

where the A_{0n} are complex constants and the λ_n are the zeros of the polynomial

$$\frac{4}{\Lambda m^2} \lambda^2 (\lambda^2 - m^2)^2 + \Lambda m^2 (\lambda^2 - m^2) + Rm^2 = 0. \tag{4.9}$$

To determine the A_{0n}, the boundary conditions must be applied. These yield

$$\sum_{n=1}^{6} A_{0n} = 0, \tag{4.10a}$$

$$\sum_{n=1}^{6} A_{0n} \exp(\lambda_n \pi) = \frac{1}{2}, \tag{4.10b}$$

$$\sum_{n=1}^{6} A_{0n}(m^2 - \lambda_n^2) = 0, \tag{4.10c}$$

$$\sum_{n=1}^{6} A_{0n}(m^2 - \lambda_n^2) \exp(\lambda_n \pi) = 0, \tag{4.10d}$$

$$\frac{2i}{\Lambda m} \sum_{n=1}^{6} A_{0n} \lambda_n^2 (m^2 - \lambda_n^2) = 0, \tag{4.10e}$$

$$\frac{2i}{\Lambda m} \sum_{n=1}^{6} A_{0n} \lambda_n^2 (m^2 - \lambda_n^2) \exp(\lambda_j \pi) = 0. \tag{4.10f}$$

(4.10) provides six linear equations for the six unknowns A_{0n}. They can be written in matrix form as

$$\mathbf{L}\mathbf{A}_0 = \mathbf{R}, \tag{4.11}$$

where

$$\mathbf{A}_0^T = \begin{bmatrix} A_{01} & A_{02} & A_{03} & A_{04} & A_{05} & A_{06} \end{bmatrix},$$

$$\mathbf{R}^T = \begin{bmatrix} 0 & \frac{1}{2} & 0 & 0 & 0 & 0 \end{bmatrix},$$

and the rows of the 6×6 complex matrix $\mathbf{L}$ are defined by

$$L_{1n} = 1, \tag{4.12a}$$

$$L_{2n} = \exp(\lambda_n \pi), \tag{4.12b}$$

$$L_{3n} = m^2 - \lambda_n^2, \tag{4.12c}$$

$$L_{4n} = (m^2 - \lambda_n^2)\exp(\lambda_n \pi), \tag{4.12d}$$

$$L_{5n} = \frac{2i}{\Lambda m}\lambda_n^2(m^2 - \lambda_n^2), \tag{4.12e}$$

$$L_{6n} = \frac{2i}{\Lambda m}\lambda_n^2(m^2 - \lambda_n^2)\exp(\lambda_j \pi). \tag{4.12f}$$

Once (4.11) has been solved to give the A_{0n}, the solution of (4.1) and (4.2) will be complete, and given by (4.3) and (4.8).

4.3 Parameter Values And Numerical Methods

Completing the solution of (4.1) and (4.2) depends on being able to solve (4.9) for the λ_n and (4.11) for the A_{0n}. To accomplish this, values must be assigned to Λ, q, Γ, m and R, and then numerical methods must be found to solve (4.9) and (4.11).

The value of Λ in the core is thought to be $O(1)$, indicating the presence of a strong azimuthal magnetic field. We choose

$$\Lambda = 4.0, \tag{4.13}$$

since this is a geophysically plausible value. Three values of q are chosen, namely

$$q = 0.1, \quad q = 1.0, \quad q = 10.0, \tag{4.14}$$

to ensure that a large range of values of q is covered.

The vanishing of the geostrophic flow V means that the solution is independent of the value of Γ, since Γ only appears in the equation for V.

The qualitative behaviour of the convection is not dependent upon the value of m - it merely defines the lengthscale on which the bumps vary and the convection takes place. For this reason, m is chosen to be the critical wavenumber associated with a steady transverse convection roll in a standard plane layer, as defined in chapter 3. That is, m^2 is chosen to be the positive root of the polynomial

$$\Lambda^2 m^6 - 8m^2 - 8 = 0, \tag{4.15}$$

which is cubic in m^2. This choice is also made in Kelly and Pal (1977). (4.15) is solved numerically using N.A.G. routine C02AFF. This routine uses a variant of Laguerre's method to find all the zeros of a complex polynomial.

Finally, a range of values of R is chosen. For each value of R in this range, (4.9) is set up, and then solved numerically using N.A.G. routine C02AFF. This yields the λ_n. Using these, the matrix $\mathbf{L}$ is set up, and equations (4.11) are solved using N.A.G. routine F04ADF. This routine uses an LU decomposition of $\mathbf{L}$ to solve (4.11) for $\mathbf{A_0}$.

In this way, the λ_n and A_{0n} are found for each relevant value of the Rayleigh number R. These define $\mathbf{X}_0(z)$, and hence the solution of (4.1) and (4.2) for each value of R.

4.4 The Results

Unlike the hydrostatic basic state that arises in a standard plane layer, the basic state that arises in a layer with a bumpy boundary depends upon the value taken by the Rayleigh number R. To show this dependence, the amplitude of the solution is plotted against R. A convenient measure of the amplitude of the solution was found to be the meansquare heatflux generated at the bottom boundary by

the solution, denoted by H. This measure is used instead of the usual Nusselt number throughout this work. H is defined as follows. The temperature of the roll is given by

$$\theta = \left\{ \sum_{n=1}^{6} A_{0n} \exp(\lambda_n z) \right\} \exp(imy) + c.c..$$

The heatflux is then given by

$$\mathcal{F}(y,z) = \frac{\partial \theta}{\partial z} = \left\{ \sum_{n=1}^{6} \lambda_n A_{0n} \exp(\lambda_n z) \right\} \exp(imy) + c.c..$$

Then, define

$$H = \frac{m}{2\pi^2} \int_0^{\frac{2\pi}{m}} \int_0^{\pi} \mathcal{F}(y,0)^2 dz dy.$$

It transpires that

$$H = 2 \left| \sum_{n=1}^{6} \lambda_n A_{0n} \right|^2. \tag{4.16}$$

(Note that H is independent of q, since the equations that define the λ_n and A_{0n} are independent of q). Figure 4.1 shows a plot of H against R.

The graph of H shows that the convection exists for all values of R (confirming the argument given in section 4.1) except that it is singular at one value of R, which shall be denoted by R_s. The convection can be separated into two regimes. The first is

$$R \ll R_s, \quad \text{or} \quad R \gg R_s,$$

and is called the quasi-conduction regime. Here, the convection is of finite amplitude. The second regime is

$$R \approx R_s,$$

and is called the critical regime. Here, the amplitude of the convection becomes unbounded. R_s is called the critical Rayleigh number, but the phrase is used in a different context to it's use in chapter 3, where it referred to the value of R at which the hydrostatic basic state lost stability to perturbations and convection could take place. Instead, the critical Rayleigh number is used here to define the value of R at which H, and hence the basic state, has a singluarity.

It tranpires that the value of R at which the singularity lies can be calculated analytically. In fact,

$$R_s = R_c,$$

where R_c is the value of the Rayleigh number at which steady, transverse convection rolls go unstable in a standard plane layer. To see this, note that

$$R_c = \frac{4(1+m^2)^2}{\Lambda m^4} + \Lambda(1+m^2), \tag{4.17a}$$

where m^2 is the positive root of the following cubic equation in m^2,

$$\Lambda^2 m^6 - 8(1+m^2) = 0. \tag{4.17b}$$

But, at R_c, (4.9) gives

$$R_c = \frac{4(-\lambda_c^2+m^2)^2(-\lambda_c^2)}{\Lambda m^4} + \Lambda(-\lambda_c^2+m^2), \tag{4.18a}$$

where λ_{cn} denotes the values of the λ_n at R_c and where, again, m^2 is the positive root of the following cubic equation in m^2,

$$\Lambda^2 m^6 - 8(1+m^2) = 0. \tag{4.18b}$$

Subtracting (4.18a) from (4.17a) yields

$$(\lambda_c^2+1)P(\lambda_c) = 0 \quad \text{at} \quad R = R_c,$$

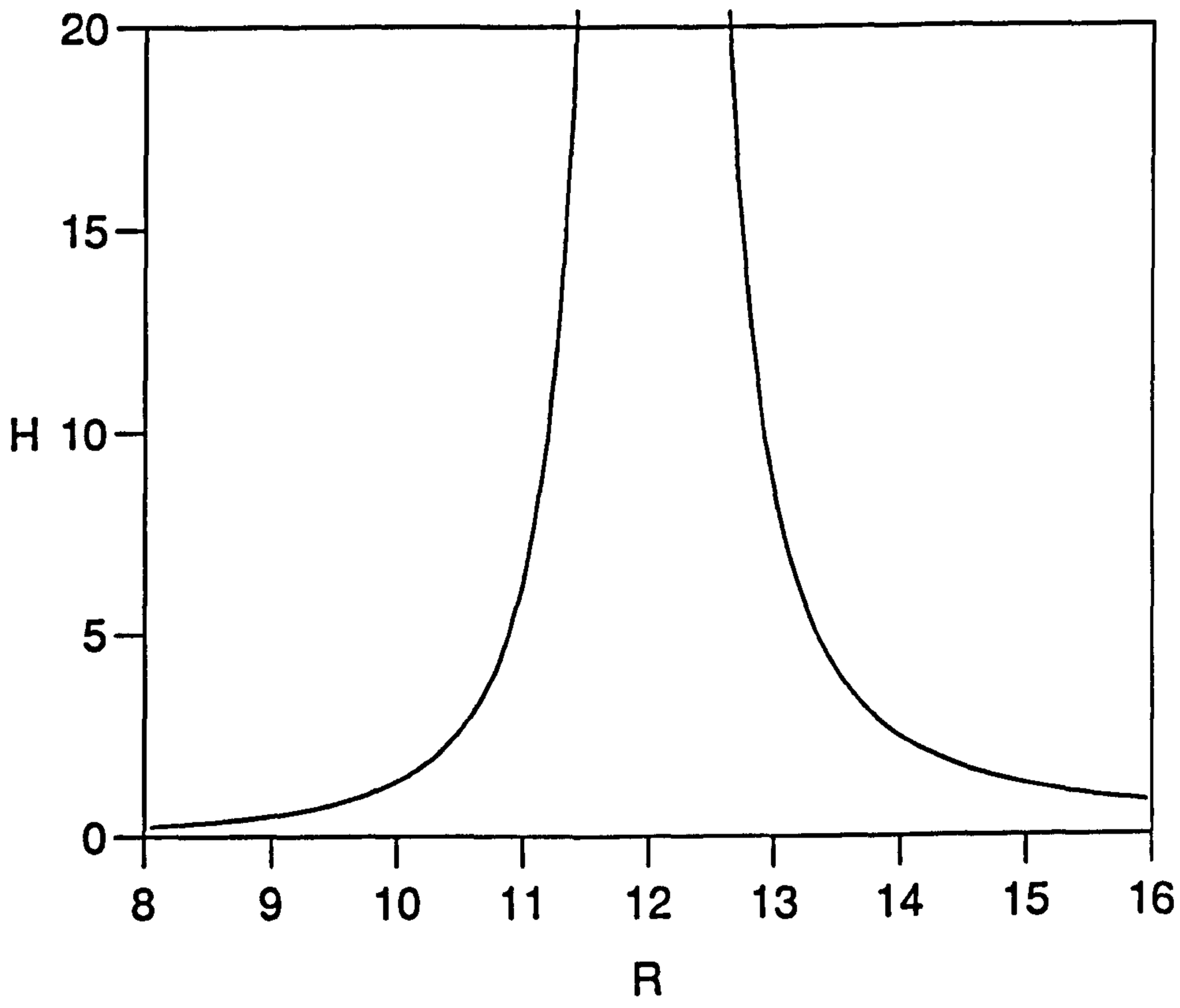

Figure 4.1: The meansquare heatflux at the bottom boundary H, plotted against the Rayleigh number R, for the case $\Lambda = 4.0$. This quantity is independent of q.

where $P(\lambda)$ is a fourth order polynomial in λ. Hence, choosing

$$\lambda_{c1} = i, \lambda_{c2} = -i, \tag{4.19}$$

and substituting (4.19) into (4.12), it turns out that the first two columns of $\mathbf{L}$ are identical when

$$R = R_c.$$

Therefore,

$$\det \mathbf{L} = 0 \quad \text{when} \quad R = R_c, \tag{4.20}$$

and the system of equations defined by (4.11) has no solution. Hence

$$R_s = R_c.$$

Mathematically, the singularity arises because R_s is the eigenvalue of the matrix $\mathbf{L}$ at which the corresponding homogeneous problem that arises in a standard plane layer has a solution. The forced, inhomogeneous problem considered here will not in general have a solution at the points where the homogeneous problem has a solution. (This is known as the Fredholm Alternative). Physically, the singularity arises as a result of resonance - the wavelength of the bumps forcing the motion (namely $\frac{2\pi}{m}$) is the same as the wavelength of the free mode of convection at R_s, the free mode of convection being a steady, transverse convection roll in the standard plane layer. Kelly and Pal (1977) call this resonant wavelength excitation.

In practice, the amplitude of the convection does not become unbounded at R_s. Close to R_s the solution is outside the asymptotic limit in which the governing equations (4.1) are valid, and the nonlinear terms neglected in this limit become important. These nonlinearities prevent the amplitude of the convection from becoming infinite (see Kelly and Pal 1977).

Figures 4.2, 4.3, 4.4, 4.5 and 4.6 show plots of $T_0(z)$, $U_{x0}(z)$, $U_{y0}(z)$, $W_0(z)$, $B_{x0}(z)$, $B_{y0}(z)$, $B_0(z)$, $X_0(z)$ and $Z_0(z)$ against the quantity

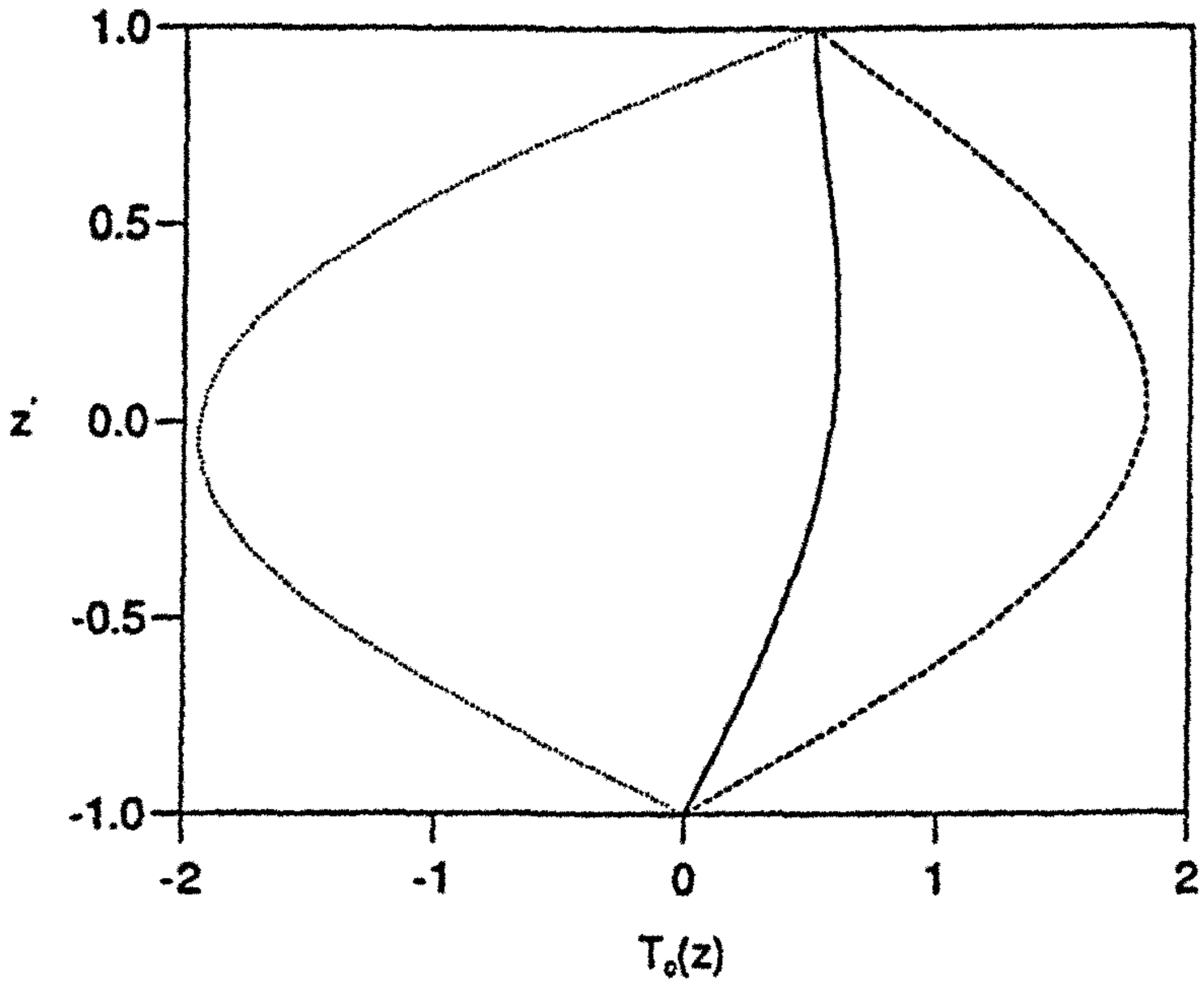

(a)

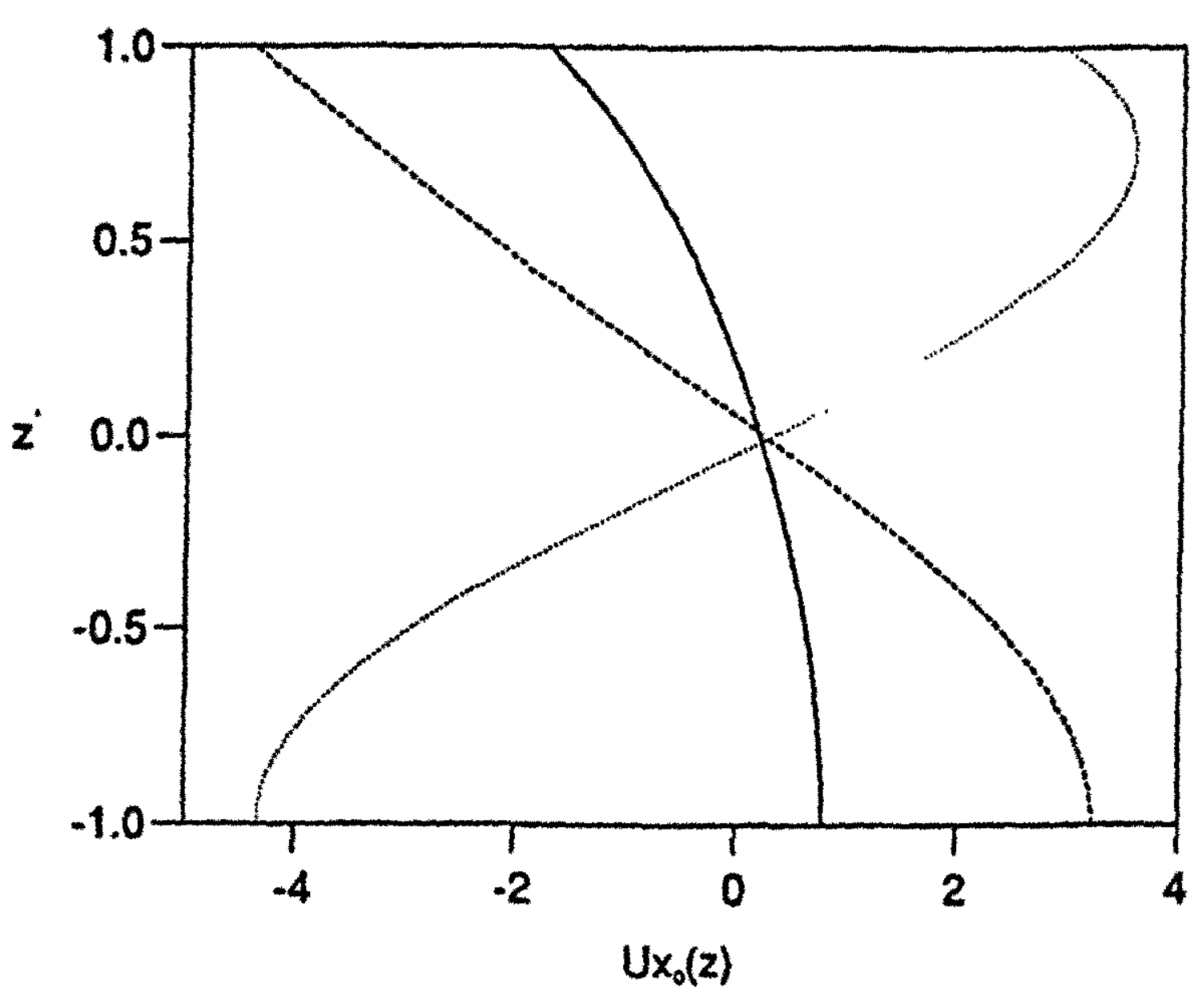

(b)

Figure 4.2: Plots of (a) $T_0(z)$, (b) $U_{x0}(z)$, against $z' = \frac{2z-\pi}{\pi}$ for the case $\Lambda = 4.0$, $q = 0.1$. The values of R shown are: $R = 9.0$ (——), $R = 11.0$ (- - -), and $R = 13.0$ (.....).

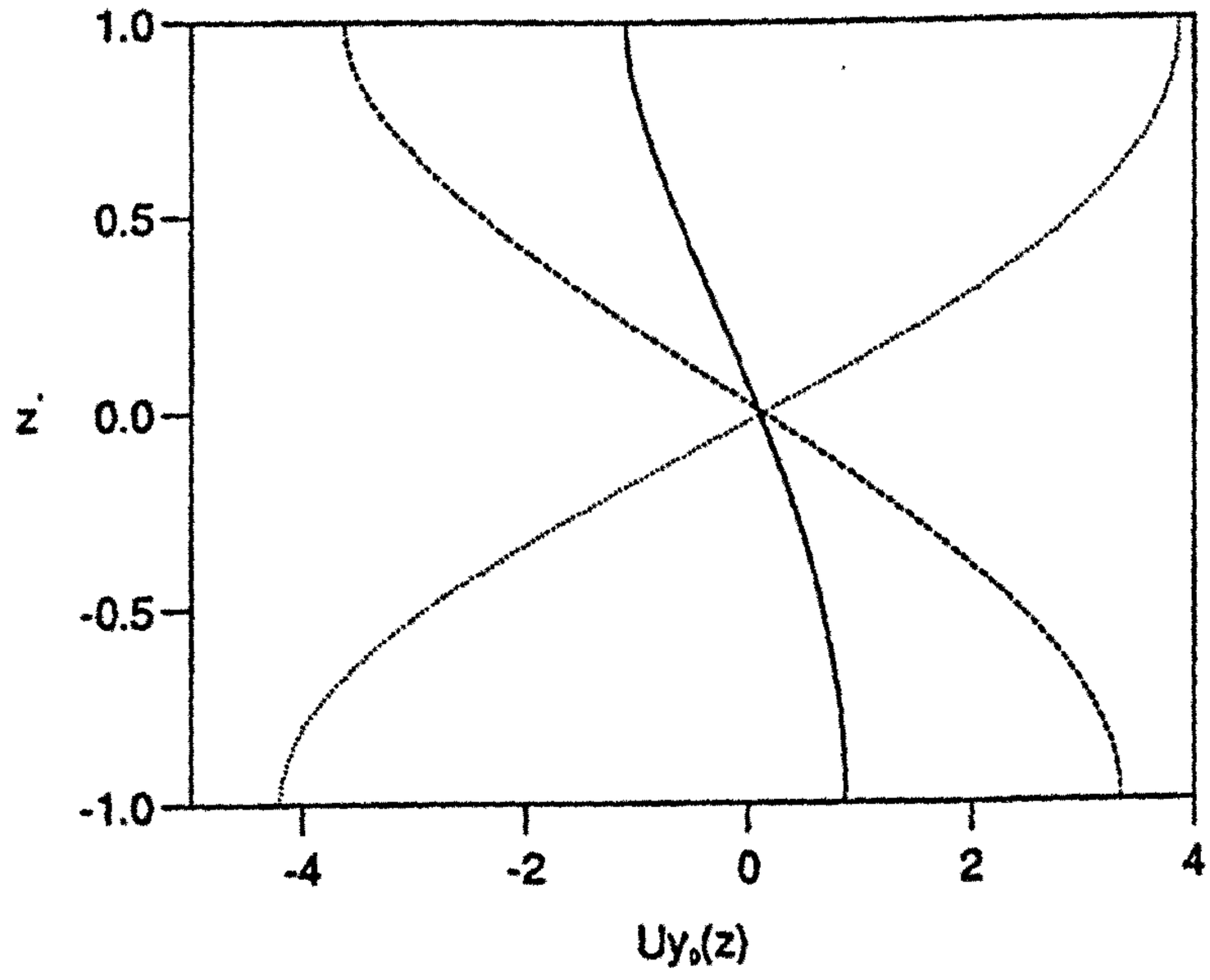

(a)

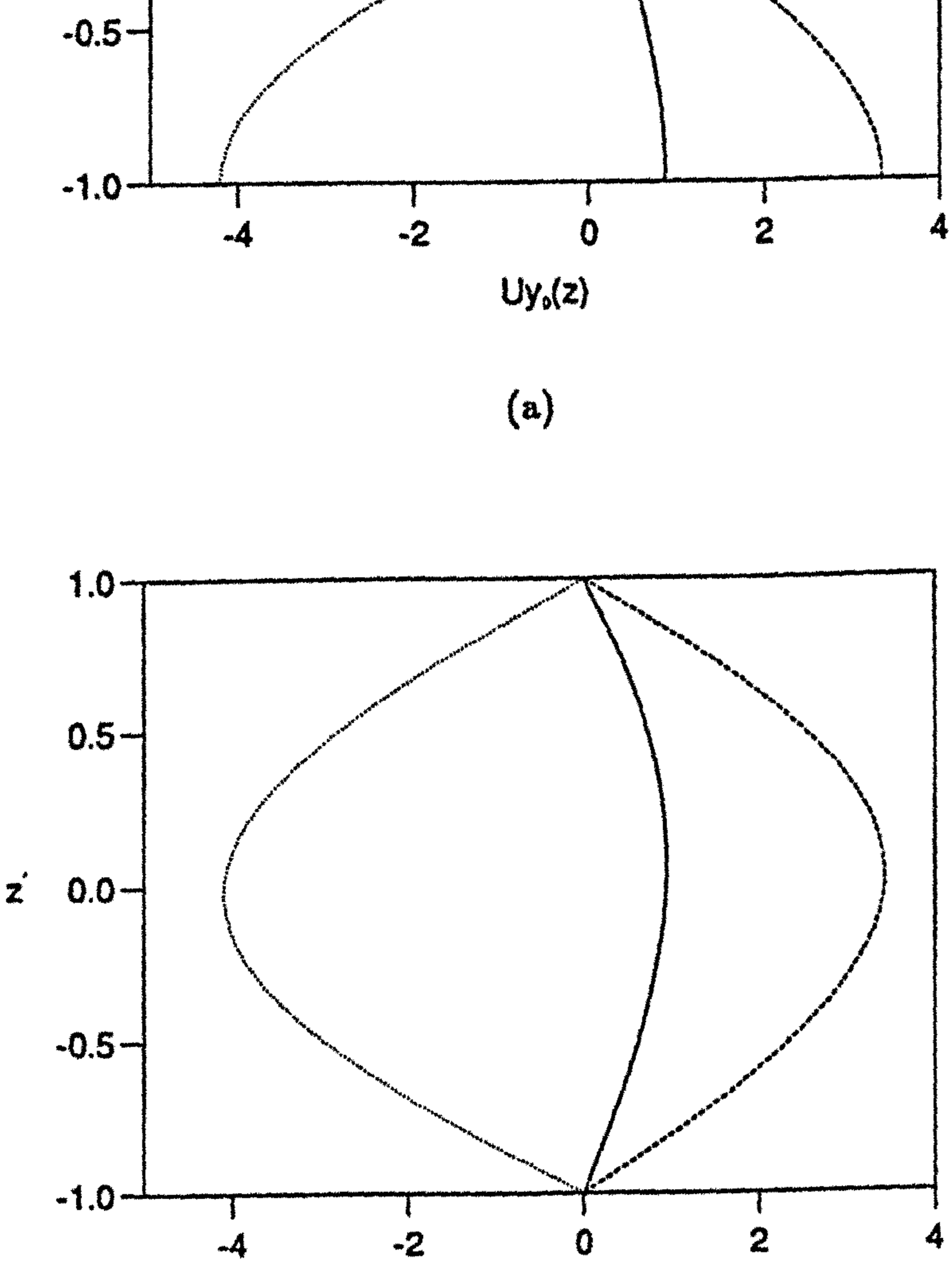

(b)

Figure 4.3: As in figure 4.2, but showing (a) $U_{y0}(z)$, (b) $W_0(z)$.

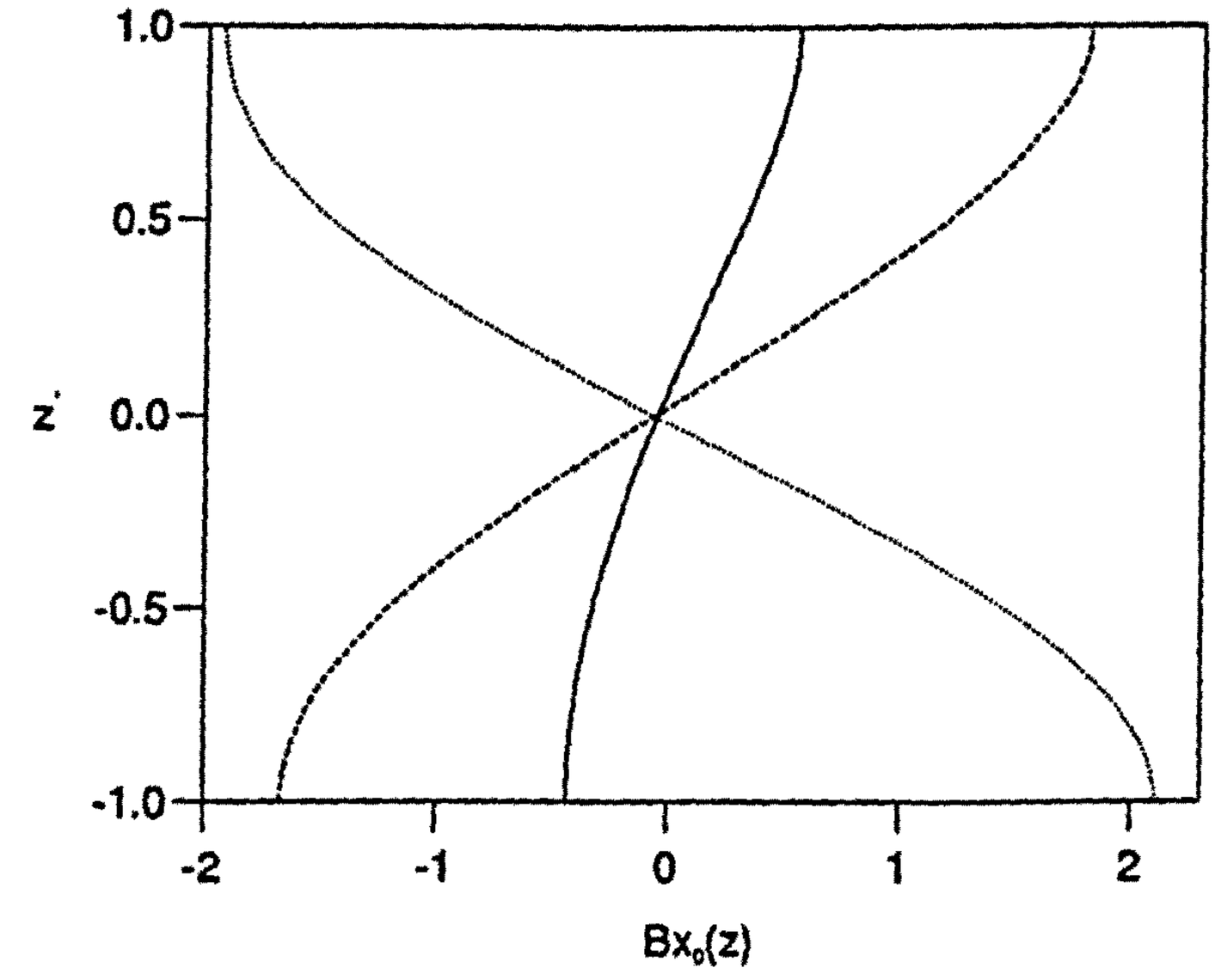

(a)

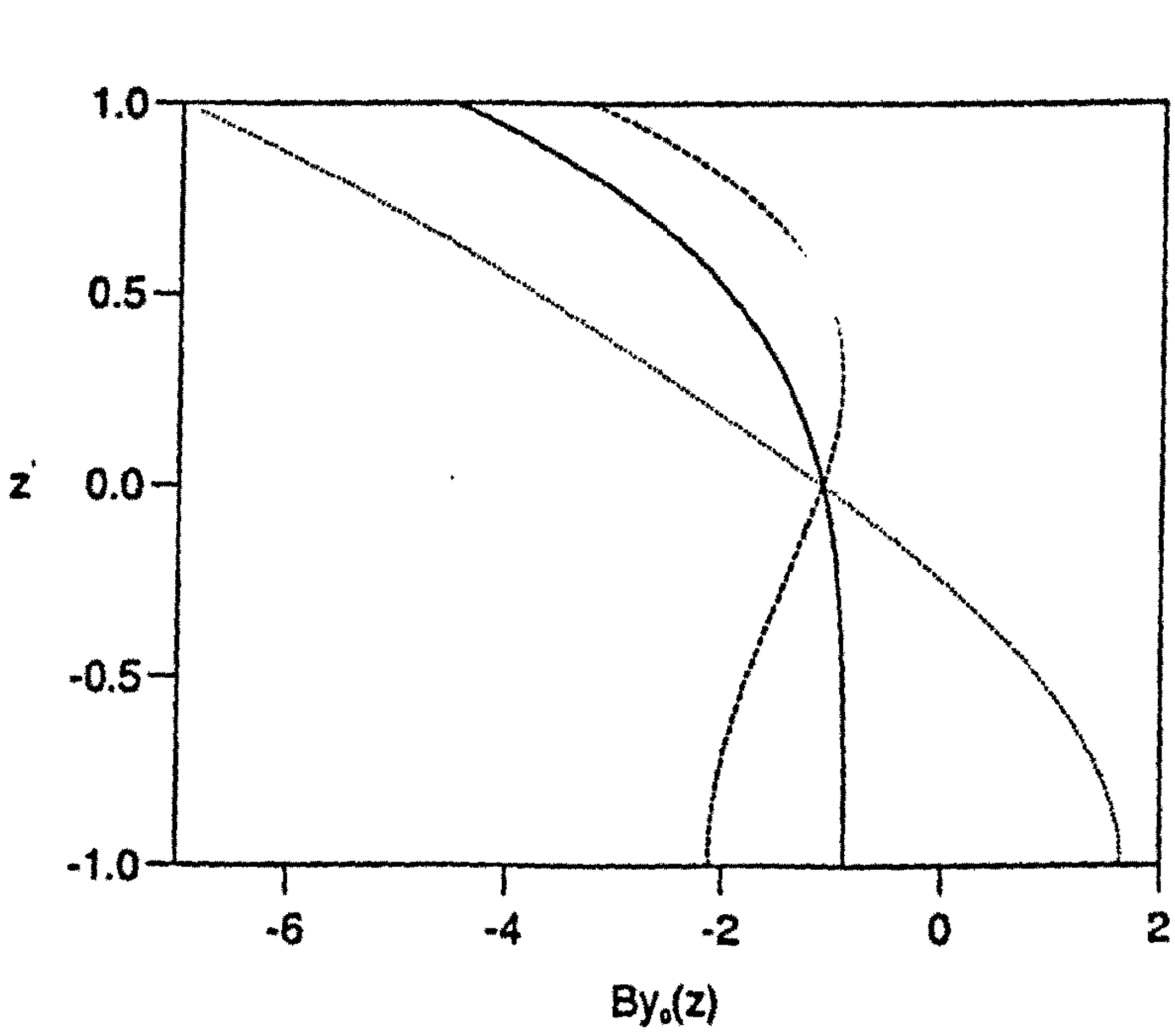

(b)

Figure 4.4: As in figure 4.2, but showing (a) $B_{x0}(z)$, (b) $B_{y0}(z)$.

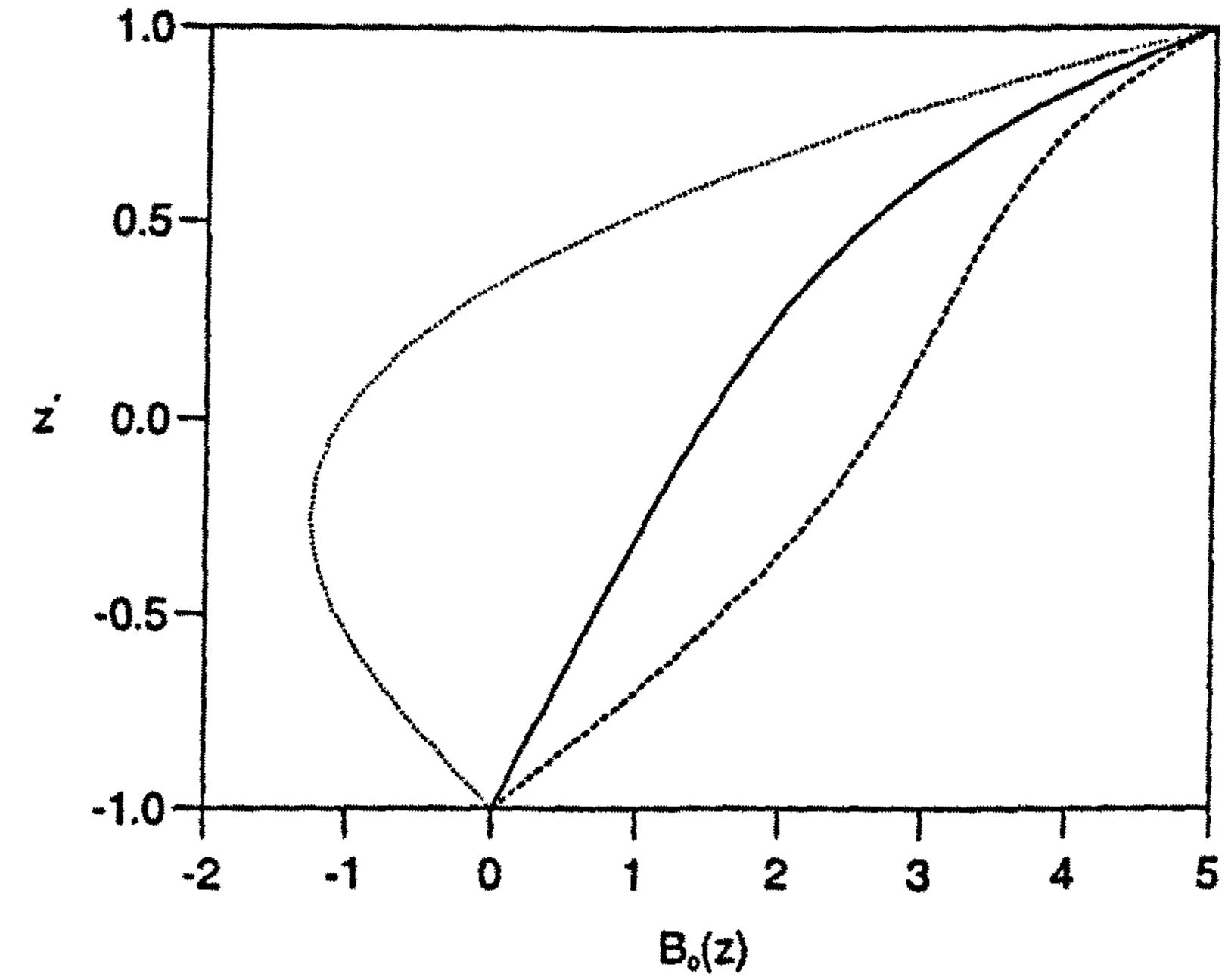

Figure 4.5: As in figure 4.2, but showing (a) $B_0(z)$, (b) $X_0(z)$.

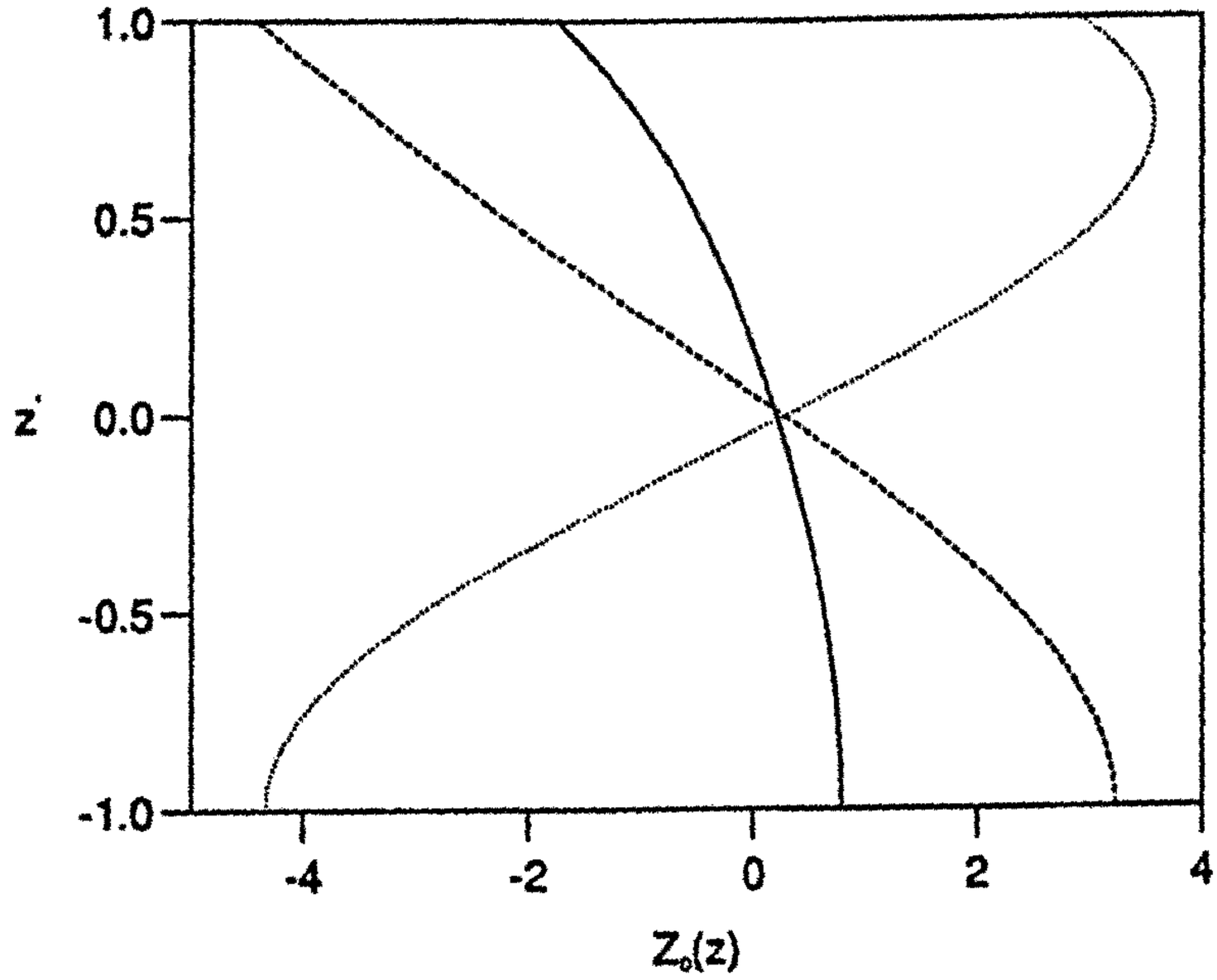

Figure 4.6: As in figure 4.2, but showing $Z_0(z)$.

$$z' = \frac{2z - \pi}{\pi},$$

(which is chosen so that the layer lies on the interval $[-1, 1]$) for various values of R. The unknowns were found to obey the following conditions

$$T_0 = T_0^*,$$

$$U_{x0} = -U_{x0}^*,$$

$$U_{y0} = -U_{y0}^*,$$

$$W_0 = W_0^*,$$

$$B_{x0} = B_{x0}^*, \tag{4.21}$$

$$B_{y0} = B_{y0}^*,$$

$$B_0 = -B_0^*,$$

$$X_0 = -X_0^*,$$

$$Z_0 = Z_0^*,$$

so only the relevant real or imaginary part of each unknown is plotted. Only B_{y0} and B_0 depend upon the value taken by q, and these are shown for $q = 0.1$. The plots show that the transverse roll forced in the layer by the bumps has a more complicated z-structure than the free transverse roll that arises in the

standard plane layer. This is because the inhomogeneities on T_0 and B_0 forbid the solution from adopting a simple sinusoidal z-structure. The plots also show that the convection reverses direction above R_s, since the solutions change sign once the Rayleigh number exceeds R_s.

Chapter V

The Stability Of The Basic State

5.1 The Perturbation Equations

Having computed the basic state that arises in a layer with a bumpy top boundary, the next step is to examine the stability of that basic state. This is done by adding small perturbations to the basic state, and asking whether the perturbations grow or decay in time, for given parameter values. If the perturbations grow in time, then the basic state is unstable to the perturbations. But if the perturbations decay in time, then the basic state is stable to the perturbations. Of key importance will be locating the point at which the basic state first loses stability to the perturbations, and what form the onset of instability takes, i.e. does the basic state lose stability through the exchange of stabilities or through overstability?

Recall, the basic state has the form

$$\mathbf{X} = \hat{\mathbf{X}}(y,z), \quad V = 0. \tag{5.1}$$

Denote the perturbations by $\mathbf{X}_p$ and V_p, and set

$$\mathbf{X} = \hat{\mathbf{X}}(y,z) + \delta\mathbf{X}_p(x,y,z,t), \tag{5.2a}$$

$$V = 0 + \delta V_p(x), \tag{5.2b}$$

where $\delta \ll 1$ is a small parameter governing the size of the perturbations. Substituting (5.2) into the governing equations (2.35), subtracting off the equations satisfied by the basic state, and neglecting all terms of $O(\delta^2)$ or smaller (using the fact that δ is small), the linear equations governing the perturbations are obtained

$$2\frac{\partial w_p}{\partial z} + \Lambda\frac{\partial \xi_p}{\partial y} = 0, \tag{5.3a}$$

$$2\frac{\partial \zeta_p}{\partial z} - \Lambda\frac{\partial}{\partial y}(\nabla^2 b_p) - R\nabla_H^2\theta_p = 0, \tag{5.3b}$$

$$2V_p - \Gamma\Lambda q\frac{\partial}{\partial x}\left\{\frac{m}{2\pi^2}\int_0^{\frac{2\pi}{m}}\int_0^{\pi}(\hat{b}_x b_{yp} + b_{xp}\hat{b}_y)dzdy\right\} = 0, \tag{5.3c}$$

$$q\frac{\partial b_p}{\partial t} + q\left(\frac{\partial \hat{b}}{\partial y}\right)V_p - \frac{\partial w_p}{\partial y} - \nabla^2 b_p = 0, \tag{5.3d}$$

$$q\frac{\partial \xi_p}{\partial t} + q\left(\frac{\partial \hat{\xi}}{\partial y}\right)V_p - \frac{\partial \zeta_p}{\partial y} - \nabla^2\xi_p$$

$$-q(\hat{b}_x)\frac{d^2V_p}{dx^2} - q\left(\frac{\partial \hat{b}_x}{\partial x} - \frac{\partial \hat{b}_y}{\partial y}\right)\frac{dV_p}{dx} = 0, \tag{5.3e}$$

$$\frac{\partial \theta_p}{\partial t} + \left(\frac{\partial \hat{\theta}}{\partial y}\right)V_p - w_p - \nabla^2\theta_p = 0, \tag{5.3f}$$

$$\nabla_H^2 b_{xp} = -\frac{\partial^2 b_p}{\partial x\partial z} - \frac{\partial \xi_p}{\partial y}, \tag{5.3g}$$

$$\nabla_H^2 b_{yp} = -\frac{\partial^2 b_p}{\partial y\partial z} + \frac{\partial \xi_p}{\partial x}, \tag{5.3h}$$

$$\nabla_H^2 u_{xp} = -\frac{\partial^2 w_p}{\partial x\partial z} - \frac{\partial \zeta_p}{\partial y}, \tag{5.3i}$$

$$\nabla_H^2 u_{yp} = -\frac{\partial^2 w_p}{\partial y\partial z} + \frac{\partial \zeta_p}{\partial x}. \tag{5.3j}$$

In a similar manner, the boundary conditions on the perturbations may be obtained from (2.36). They are given by

$$w_p = b_p = \frac{\partial \xi_p}{\partial z} = \theta_p = 0 \quad \text{on} \quad z = 0, \tag{5.4a}$$

$$w_p + mV_p \sin(my) = b_p = \frac{\partial \xi_p}{\partial z} = \theta_p = 0 \quad \text{on} \quad z = \pi. \tag{5.4b}$$

Now, the basic state takes the form of a transverse roll,

$$\hat{\mathbf{X}} = \mathbf{X}_0(z) \exp(imy) + c.c., \tag{5.5}$$

where

$$\mathbf{X}_0^T(z) = \Big[T_0(z) \quad W_0(z) \quad B_0(z) \quad X_0(z) \quad Z_0(z)$$

$$B_{x0}(z) \quad B_{y0}(z) \quad U_{x0}(z) \quad U_{y0}(z)\Big], \tag{5.6}$$

is the solution of equations (4.6) for the z-structure of the basic state. Recall that (5.5) satisfies Taylor's constraint, and has no geostrophic flow associated with it. The perturbations are assumed to take the form

$$\mathbf{X}_p = \mathbf{X}_{-1}(z) \exp(ilx - imy + \lambda t) +$$

$$\mathbf{X}_1(z) \exp(ilx + imy + \lambda t) + c.c., \tag{5.7a}$$

$$V_p = \mathcal{U} \exp(ilx + \lambda t) + c.c., \tag{5.7b}$$

where, for $r = \pm 1$,

$$\mathbf{X}_r^T(z) = \Big[T_r(z) \quad W_r(z) \quad B_r(z) \quad X_r(z) \quad Z_r(z)$$

$$B_{xr}(z) \quad B_{yr}(z) \quad U_{xr}(z) \quad U_{yr}(z)\Big], \tag{5.8}$$

represents the z-structure of the perturbations, and $\mathcal{U}$ is a constant to be determined. λ is a complex number, defined by

$$\lambda = s + i\omega, \tag{5.9}$$

where s is the growth rate and ω is the frequency of the perturbations. (5.7) and (5.8) define a double oblique convection roll (a (+)-roll and a (-)-roll in the notation of chapter 3), together with the geostrophic flow accelerated by the interaction of these rolls with the transverse roll forced in the layer by the bumps. In the standard plane layer model of magnetoconvection, these rolls are the preferred mode of convection for order one values of Λ, and have identical linear stability characteristics. The stability analysis carried out here will ascertain what effect the presence of the transverse roll has upon the stability of these rolls.

Substituting (5.5)and (5.7) into (5.3), the equations for the z-structure of the perturbations are obtained

$$2DW_{-1} - \Lambda imX_{-1} = 0, \tag{5.10a}$$

$$2DZ_{-1} + \Lambda im(D^2 - k^2)B_{-1} + Rk^2T_{-1} = 0, \tag{5.10b}$$

$$(D^2 - k^2 - q\lambda)B_{-1} - imW_{-1} + qimB_0^*\mathcal{U} = 0, \tag{5.10c}$$

$$(D^2 - k^2 - q\lambda)X_{-1} - imZ_{-1} - q(-imX_0^* + l^2B_{x0}^* + lmB_{y0}^*)\mathcal{U} = 0, \tag{5.10d}$$

$$(D^2 - k^2 - \lambda)T_{-1} + W_{-1} + imT_0^*\mathcal{U} = 0, \tag{5.10e}$$

$$k^2B_{x,-1} - ilDB_{-1} + imX_{-1} = 0, \tag{5.10f}$$

$$k^2B_{y,-1} + imDB_{-1} + ilX_{-1} = 0, \tag{5.10g}$$

$$k^2 U_{x,-1} - ilDW_{-1} + imZ_{-1} = 0, \tag{5.10h}$$

$$k^2 U_{y,-1} + imDW_{-1} + ilZ_{-1} = 0, \tag{5.10i}$$

$$2DW_1 + \Lambda imX_1 = 0, \tag{5.10j}$$

$$2DZ_1 - \Lambda im(D^2 - k^2)B_1 + Rk^2 T_1 = 0, \tag{5.10k}$$

$$(D^2 - k^2 - q\lambda)B_1 + imW_1 - qimB_0 \mathcal{U} = 0, \tag{5.10l}$$

$$(D^2 - k^2 - q\lambda)X_1 + imZ_1 - q(imX_0 + l^2 B_{x0} - lmB_{y0})\mathcal{U} = 0, \tag{5.10m}$$

$$(D^2 - k^2 - \lambda)T_1 + W_1 - imT_0 \mathcal{U} = 0, \tag{5.10n}$$

$$k^2 B_{x1} - ilDB_1 - imX_1 = 0, \tag{5.10o}$$

$$k^2 B_{y1} - imDB_1 + ilX_1 = 0, \tag{5.10p}$$

$$k^2 U_{x1} - ilDW_1 - imZ_1 = 0, \tag{5.10q}$$

$$k^2 U_{y1} - imDW_1 + ilZ_1 = 0, \tag{5.10r}$$

where the coefficient of the perturbation geostrophic flow is given by

$$\mathcal{U} = \Gamma \frac{ilq\Lambda}{2\pi} \int_0^\pi (B_{x0}^* B_{y1} + B_{x0} B_{y,-1} + B_{x,-1} B_{y0} + B_{x1} B_{y0}^*) dz. \tag{5.11}$$

As usual, the following definitions have been made

$$D = \frac{d}{dz},$$

$$k^2 = l^2 + m^2.$$

The boundary conditions (5.4) are satisfied provided that

$$W_{-1} = B_{-1} = DX_{-1} = T_{-1} = 0 \quad \text{on} \quad z = 0, \tag{5.12a}$$

$$W_{-1} + \frac{im\mathcal{U}}{2} = B_{-1} = DX_{-1} = T_{-1} = 0 \quad \text{on} \quad z = \pi, \tag{5.12b}$$

$$W_1 = B_1 = DX_1 = T_1 = 0 \quad \text{on} \quad z = 0, \tag{5.12c}$$

$$W_1 - \frac{im\mathcal{U}}{2} = B_1 = DX_1 = T_1 = 0 \quad \text{on} \quad z = \pi. \tag{5.12d}$$

The chief difficulty of solving equations (5.10) and (5.11) is that their coefficients depend upon the basic state $\hat{\mathbf{X}}$, and $\hat{\mathbf{X}}$ depends upon the value of the Rayleigh number R. Thus, for each value of R, the coefficients must first be determined from equations (4.6) before (5.10) and (5.11) can be solved for the perturbations. This means that (5.10) and (5.11) cannot be solved independently of (4.6). Since the solution of (5.10) and (5.11) must be found numerically, this means that (4.6) must also be solved numerically, using the same numerical method.

5.2 The Numerical Method

Equations (4.6), (5.10) and (5.11) will be solved numerically using spectral methods, which involve approximating the solution of a system of ODE's with an expansion of the form

$$\sum_{n=0}^{M} \mathbf{a}_n \phi_n(z),$$

called the spectral expansion. M is a positive integer, the constants $\mathbf{a}_n$ are the spectral coefficients and

$$\{\phi_n \quad : \quad n = 0, 1, 2...\},$$

is a set of known functions, called basis functions. For this problem, it is convenient to choose

$$\phi_n(z) = P_n(z') \quad n = 0, 1, 2, ..., \tag{5.13}$$

where P_n denotes the n^{th} Legendre polynomial, and

$$z' = \frac{2z - \pi}{\pi}, \tag{5.14}$$

is chosen so that the interval

$$0 \leq z \leq \pi,$$

on which the layer lies, is mapped into the interval

$$-1 \leq z' \leq 1,$$

on which the Legendre polynomials are defined.

Legendre polynomials are chosen for two main reasons. The first is that they converge rapidly, so only a few terms of the spectral expansion are needed to give

a good approximation to the exact solution. The second reason is that Legendre polynomials are orthogonal. They satisfy

$$\int_{-1}^{1} P_n(z')P_m(z')dz' = \frac{2\delta_{nm}}{2n+1}, \tag{5.15}$$

where

$$\delta_{nm} = \begin{cases} 1 & n = m, \\ \\ 0 & n \neq m, \end{cases}$$

is the Kronecker delta. This makes evaluating the Taylor integral M much easier, since it can be done analytically using (5.15).

If a function $f(z)$ is expanded in terms of Legendre polynomials as

$$f(z) = \sum_{n=0}^{N} f_n P_n(z'),$$

where N is an integer, and the coefficients f_n are constants, then the derivatives of f have expansions of the form

$$Df = \sum_{n=0}^{N-1} (Df)_n P_n(z'),$$

$$D^2 f = \sum_{n=0}^{N-2} (D^2 f)_n P_n(z'),$$

where $(Df)_n$ and $(D^2 f)_n$ are constants, defined using the recursion relations for Legendre polynomials to be

$$(Df)_n = \frac{2}{\pi}(2n+1) \sum_{\substack{p=n+1, \\ p+n \text{ odd}}}^{N} f_p \quad (0 \leq n \leq N-1), \tag{5.16a}$$

$$(D^2 f)_n = \frac{4}{\pi^2}(n+\frac{1}{2}) \sum_{\substack{p=n+2, \\ p+n \text{ even}}}^{N} (p(p+1) - n(n+1))f_p \quad (0 \leq n \leq N-2). \tag{5.16b}$$

(See Gottlieb and Orzag 1977). Note that the expansions for Df and D^2f have N and and $N-1$ terms respectively, wheras the expansion for f has $N+1$ terms. This is caused because the operator D is a lowering operator. That is, it maps the set of basis functions

$$\{P_n \quad : \quad n = 0, 1, ..., N\},$$

into the set

$$\{P_n \quad : \quad n = 0, 1, ..., N-1\}.$$

The values of f and Df at the boundaries can be obtained using the relations

$$P_n(\pm 1) = (\pm 1)^n, \quad P_n^{'}(\pm 1) = \frac{1}{2} n(n+1)(\pm 1)^{n+1}. \tag{5.17}$$

Now, the problem being solved has inhomogeneous, non-periodic boundary conditions. Therefore, a spectral method called the Tau method (developed by Lanczos, 1956) will be used to obtain the solution (see Gottlieb and Orzag, 1977). To see how the method is applied to a simple equation, see Appendix A.

5.3 The Numerical Solution Of (4.6)

The equations for the z-structure of the basic state are given by (4.6), and they are to be solved subject to (4.7). These equations were solved previously using standard methods for linear ODE's, but here, the Tau method will be used. The unknowns are assumed to have the following spectral expansions

$$\mathbf{X}_0(z) = \begin{bmatrix} T_0(z) \\ W_0(z) \\ B_0(z) \\ X_0(z) \\ Z_0(z) \\ B_{x0}(z) \\ B_{y0}(z) \\ U_{x0}(z) \\ U_{y0}(z) \end{bmatrix} = \begin{bmatrix} \sum_{n=0}^{N+2} T_{0n} P_n(z') \\ \sum_{n=0}^{N+1} W_{0n} P_n(z') \\ \sum_{n=0}^{N+2} B_{0n} P_n(z') \\ \sum_{n=0}^{N+2} X_{0n} P_n(z') \\ \sum_{n=0}^{N} Z_{0n} P_n(z') \\ \sum_{n=0}^{N+1} B_{x0n} P_n(z') \\ \sum_{n=0}^{N+1} B_{y0n} P_n(z') \\ \sum_{n=0}^{N} U_{x0n} P_n(z') \\ \sum_{n=0}^{N} U_{y0n} P_n(z') \end{bmatrix}, \tag{5.18}$$

where N is an integer and the coefficients of the expansions are complex constants. There are $9N + 18$ complex unknowns to be determined using (4.6) and (4.7). The expansions (5.18) are substituted into (4.6) and (4.7) using (5.16) and (5.17), and the Tau method is used to derive the following algebraic equations for the spectral coefficients

$$\frac{4(2n+1)}{\pi} \sum_{\substack{p=n+1 \\ p+n \text{ odd}}}^{N+1} W_{0p} + \Lambda i m X_{0n} = 0 \quad (0 \le n \le N), \tag{5.19a}$$

$$\frac{4(2n+1)}{\pi} \sum_{\substack{p=n+1 \\ p+n \text{ odd}}}^{N} Z_{0p} - \Lambda i m \left\{ \frac{2(2n+1)}{\pi^2} \sum_{\substack{p=n+2 \\ p+n \text{ even}}}^{N+2} [p(p+1) - n(n+1)] B_{0p} - m^2 B_{0n} \right\}$$

$$+ R m^2 T_{0n} = 0 \quad (0 \le n \le N-1), \tag{5.19b}$$

$$\frac{2(2n+1)}{\pi^2}\sum_{\substack{p=n+2\\ p+n\ \text{even}}}^{N+2}[p(p+1)-n(n+1)]B_{0p}-m^2B_{0n}+imW_{0n}=0\quad(0\le n\le N),\tag{5.19c}$$

$$\frac{2(2n+1)}{\pi^2}\sum_{\substack{p=n+2\\ p+n\ \text{even}}}^{N+2}[p(p+1)-n(n+1)]X_{0p}-m^2X_{0n}+imZ_{0n}=0\quad(0\le n\le N),\tag{5.19d}$$

$$\frac{2(2n+1)}{\pi^2}\sum_{\substack{p=n+2\\ p+n\ \text{even}}}^{N+2}[p(p+1)-n(n+1)]T_{0p}-m^2T_{0n}+W_{0n}=0\quad(0\le n\le N),\tag{5.19e}$$

$$m^2B_{x0n}-imX_{0n}=0\quad(0\le n\le N+1),\tag{5.19f}$$

$$m^2B_{y0n}-im\left\{\frac{2(2n+1)}{\pi}\sum_{\substack{p=n+1\\ p+n\ \text{odd}}}^{N+2}B_{0p}\right\}=0\quad(0\le n\le N+1),\tag{5.19g}$$

$$m^2U_{x0n}-imZ_{0n}=0\quad(0\le n\le N),\tag{5.19h}$$

$$m^2U_{y0n}-im\left\{\frac{2(2n+1)}{\pi}\sum_{\substack{p=n+1\\ p+n\ \text{odd}}}^{N+1}W_{0p}\right\}=0\quad(0\le n\le N),\tag{5.19i}$$

$$\sum_{p=0}^{N+1}(-1)^pW_{0p}=0,\tag{5.19j}$$

$$\sum_{p=0}^{N+1}W_{0p}=0,\tag{5.19k}$$

$$\sum_{p=0}^{N+2}(-1)^p T_{0p} = 0, \tag{5.19l}$$

$$\sum_{p=0}^{N+2} T_{0p} = \frac{1}{2}, \tag{5.19m}$$

$$\sum_{p=0}^{N+2}(-1)^p B_{0p} = 0, \tag{5.19n}$$

$$\sum_{p=0}^{N+2} B_{0p} = \frac{im}{2q}, \tag{5.19o}$$

$$\sum_{p=0}^{N+2}\frac{1}{2}(-1)^{p+1}p(p+1)X_{0p} = 0, \tag{5.19p}$$

$$\sum_{p=0}^{N+2}\frac{1}{2}p(p+1)X_{0p} = 0. \tag{5.19q}$$

(5.19) defines $9N+18$ complex equations in the $9N+18$ complex coefficients of the spectral expansions. In matrix notation, (5.19) takes the form

$$\mathbf{L}_0\mathbf{Y}_0 = \mathbf{R}_0, \tag{5.20}$$

where $\mathbf{L}_0$ is a $(9N+18)\times(9N+18)$ complex matrix, $\mathbf{R}_0$ is a $(9N+18)\times 1$ complex vector and $\mathbf{Y}_0$ is the $(9N+18)\times 1$ vector of unknowns defined by

$$\mathbf{Y}_0^T = \Big[T_{00}\,T_{01}\ldots T_{0,N+2}\,W_{00}\,W_{01}\ldots W_{0,N+1}\,B_{00}\,B_{01}\ldots B_{0,N+2}$$

$$X_{00}\,X_{01}\ldots X_{0,N+2}\,Z_{00}\,Z_{01}\ldots Z_{0,N}\,B_{x00}\,B_{x01}\ldots B_{x0,N+1}$$

$$B_{y00}\,B_{y01}\ldots B_{y0,N+1}\,U_{x00}\,U_{x01}\ldots U_{x0,N}\,U_{y00}\,U_{y01}\ldots U_{y0,N}\Big]. \tag{5.21}$$

Once suitable values for Λ, q, m and N have been prescribed, (5.20) can be solved for each value of R using NAG routine F04ADF. This routine uses an LU decomposition of $\mathbf{L}_0$ to solve (5.20) for $\mathbf{Y}_0$.

5.3.1 Comparison With Chapter 4

To check the validity of the numerical method, the analytic results of Chapter 4 are here reproduced using the Tau method. To do this, the values chosen for the parameters in Chapter 4, must also be used here.

Attention is restricted to the case

$$\Lambda = 4, \quad q = 0.1.$$

The wavenumber m is chosen as in Chapter 4: that is, m^2 is chosen to be the positive root of the cubic

$$\Lambda^2 m^6 - 8m^2 - 8 = 0.$$

To choose a value of N, and check for convergence, (5.20) is solved for various values of N at the point $R = 9.0$. At this point, the meansquare heatflux at the bottom boundary is calcualated using the spectral approximation for $T_0(z)$. Recall that

$$H = 2\left|DT_0(0)\right|^2.$$

Substituting

$$T_0(z) = \sum_{n=0}^{N+2} T_{0n} P_n(z'),$$

(where the T_{0n} are obtained from $\mathbf{Y}_0$) into the definition of H, the following result is obtained

$$H = \frac{2}{\pi^2}\left|\sum_{n=0}^{N+2}(-1)^{n+1} n(n+1) T_{0n}\right|^2. \tag{5.22}$$

The value of (5.22) for various N at $R = 9.0$ must be compared to the exact value as calculated in Chapter 4, which is

$$H_{exact} = 0.5048671.$$

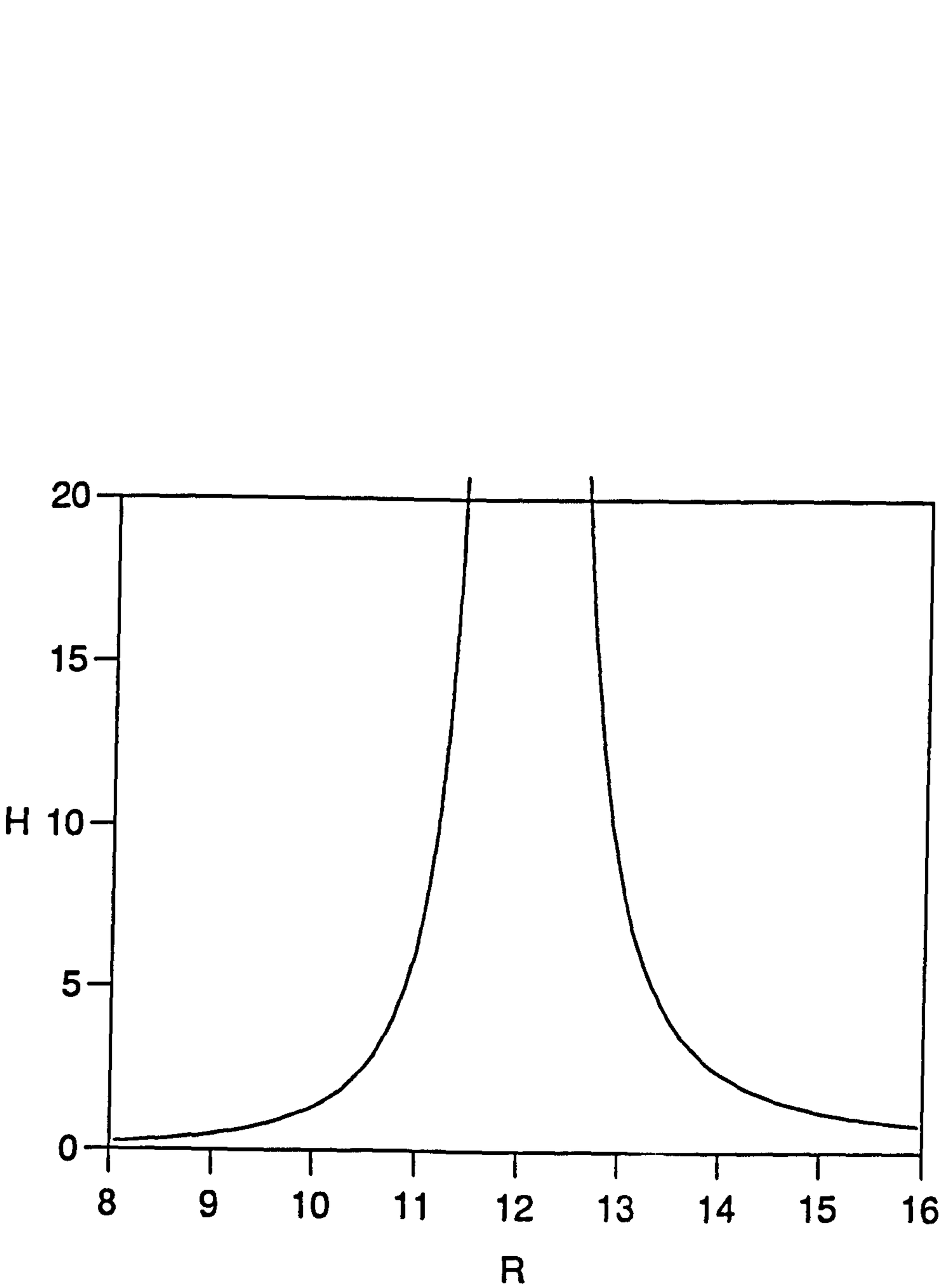

Figure 5.1: The numerically calculated meansquare heatflux at the bottom boundary, plotted against the Rayleigh number R, for the case $\Lambda = 4.0$.

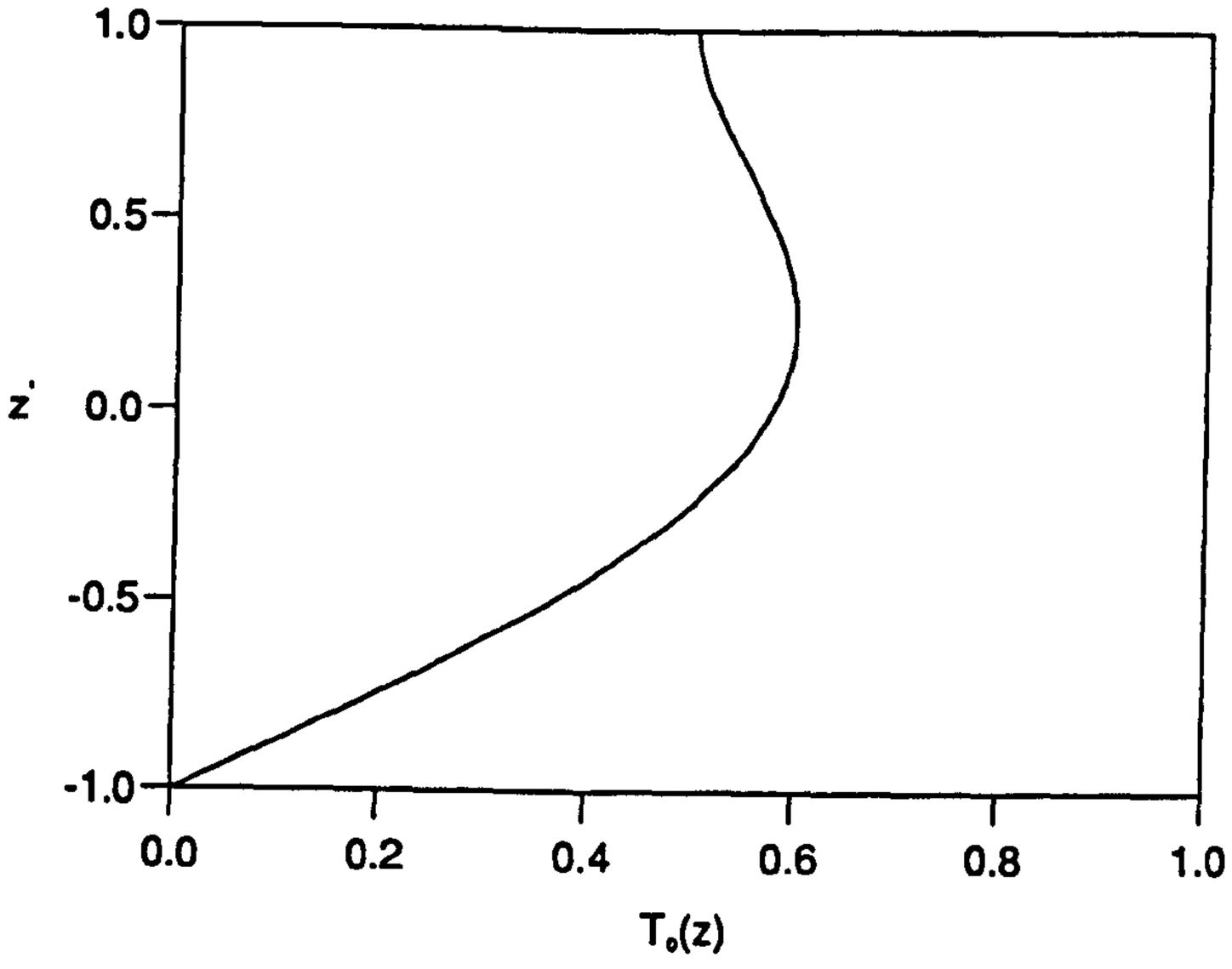

(a)

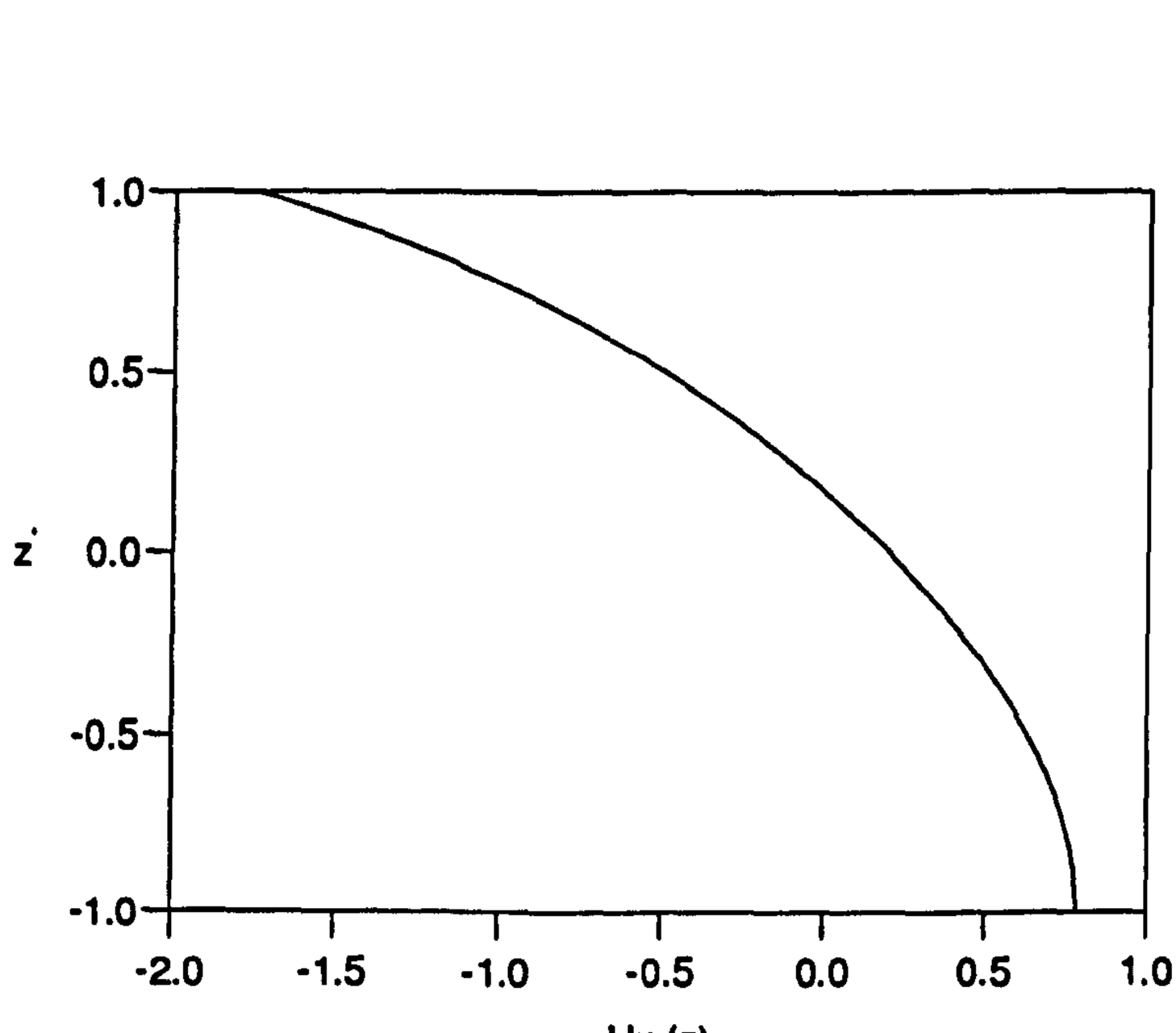

(b)

Figure 5.2: Plots of (a) $T_0(z)$, (b) $U_{x0}(z)$, against z' for the case $\Lambda = 4.0$, $q = 0.1$. The value of R shown is $R = 9.0$

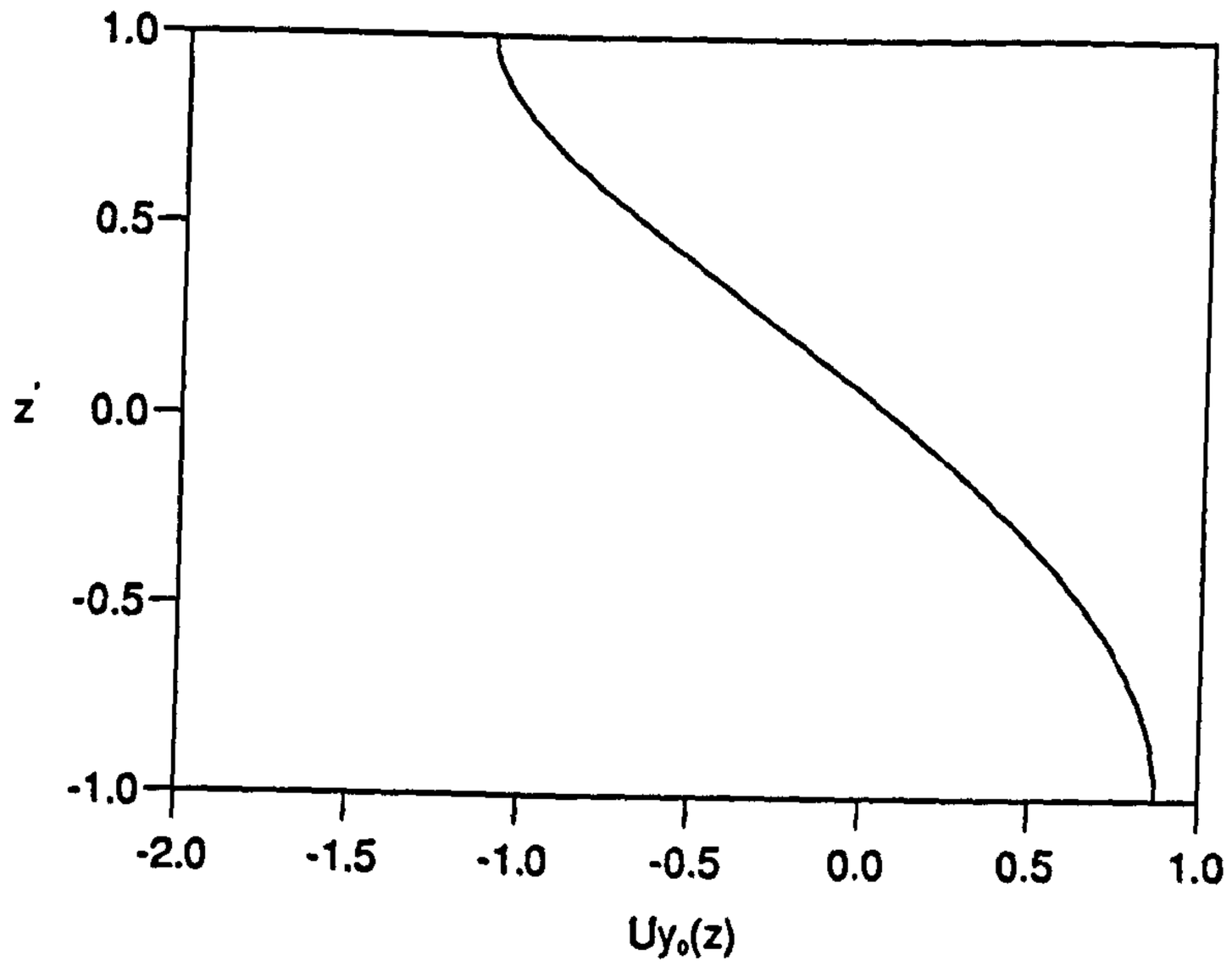

(a)

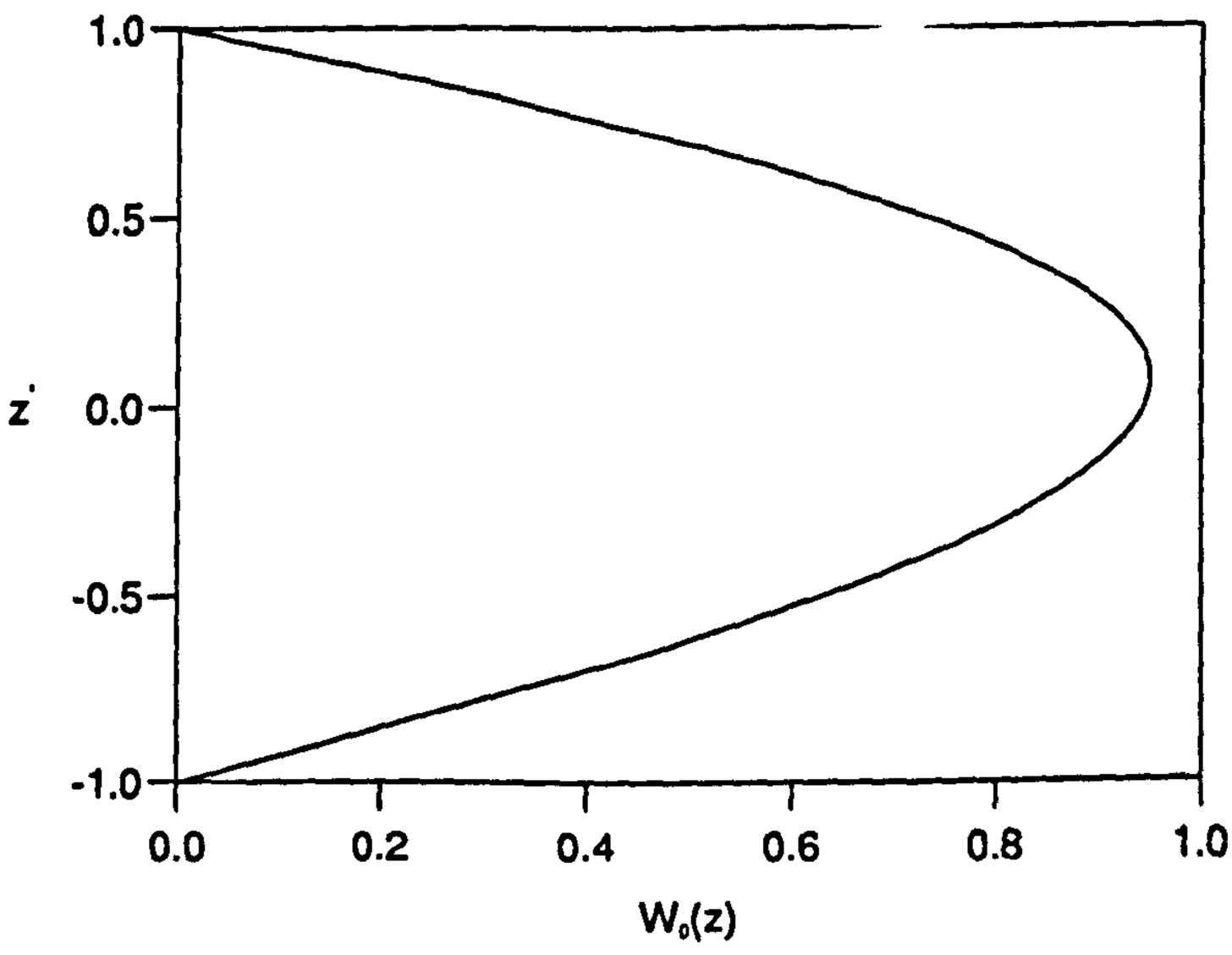

(b)

Figure 5.3: As in figure 5.2, but showing (a) $U_{y0}(z)$, (b) $W_0(z)$.

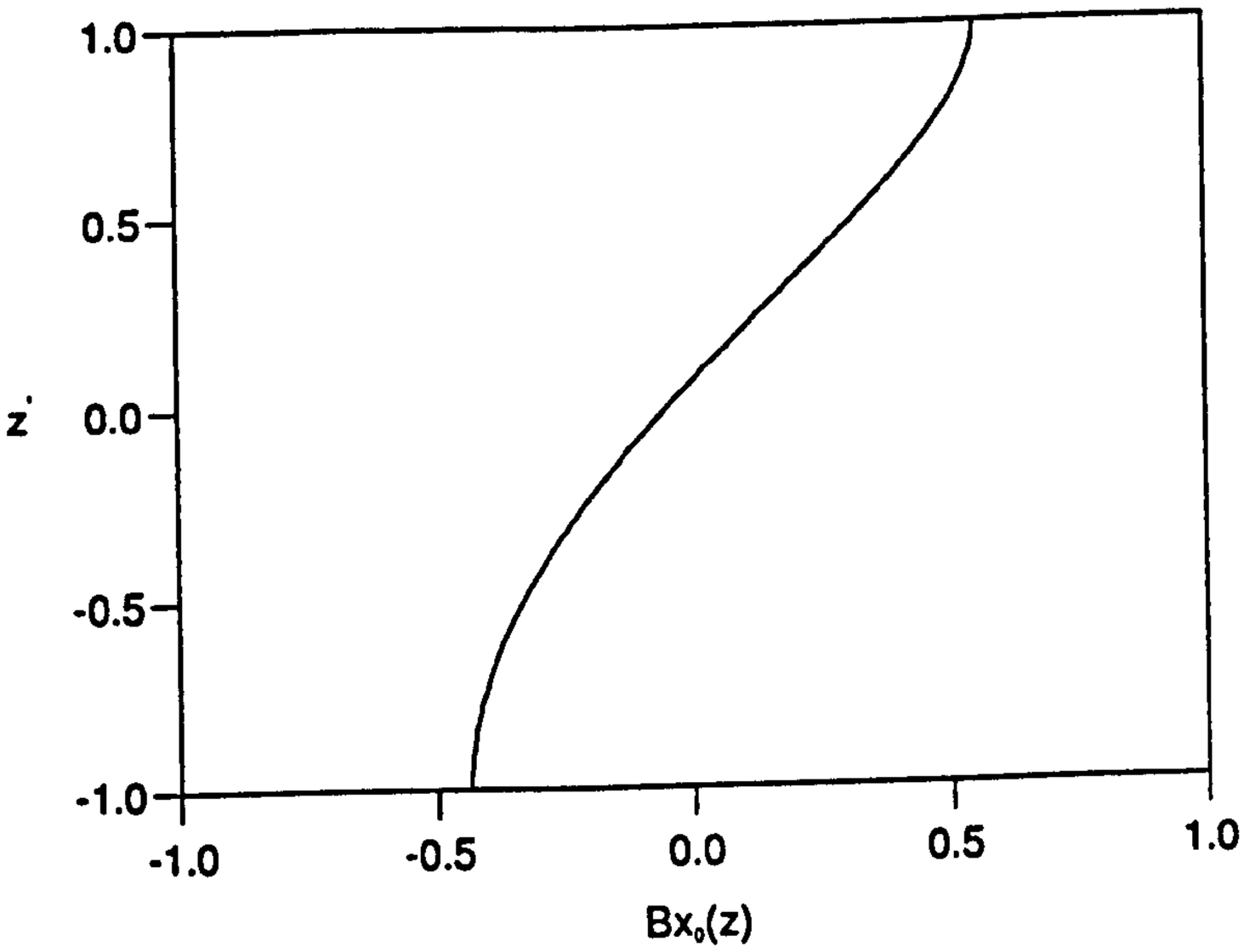

(a)

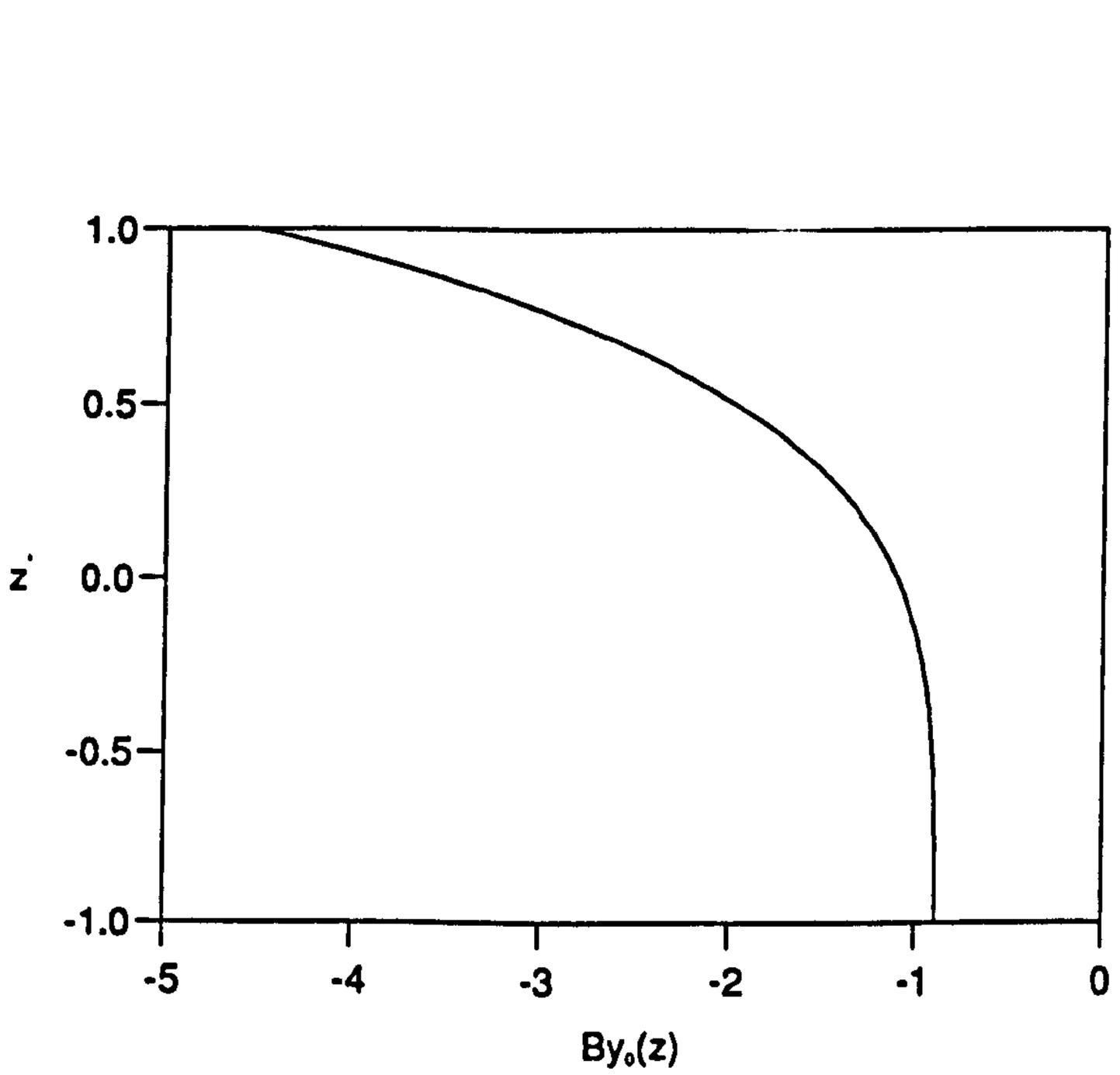

(b)

Figure 5.4: As in figure 5.2, but showing (a) $B_{x0}(z)$, (b) $B_{y0}(z)$.

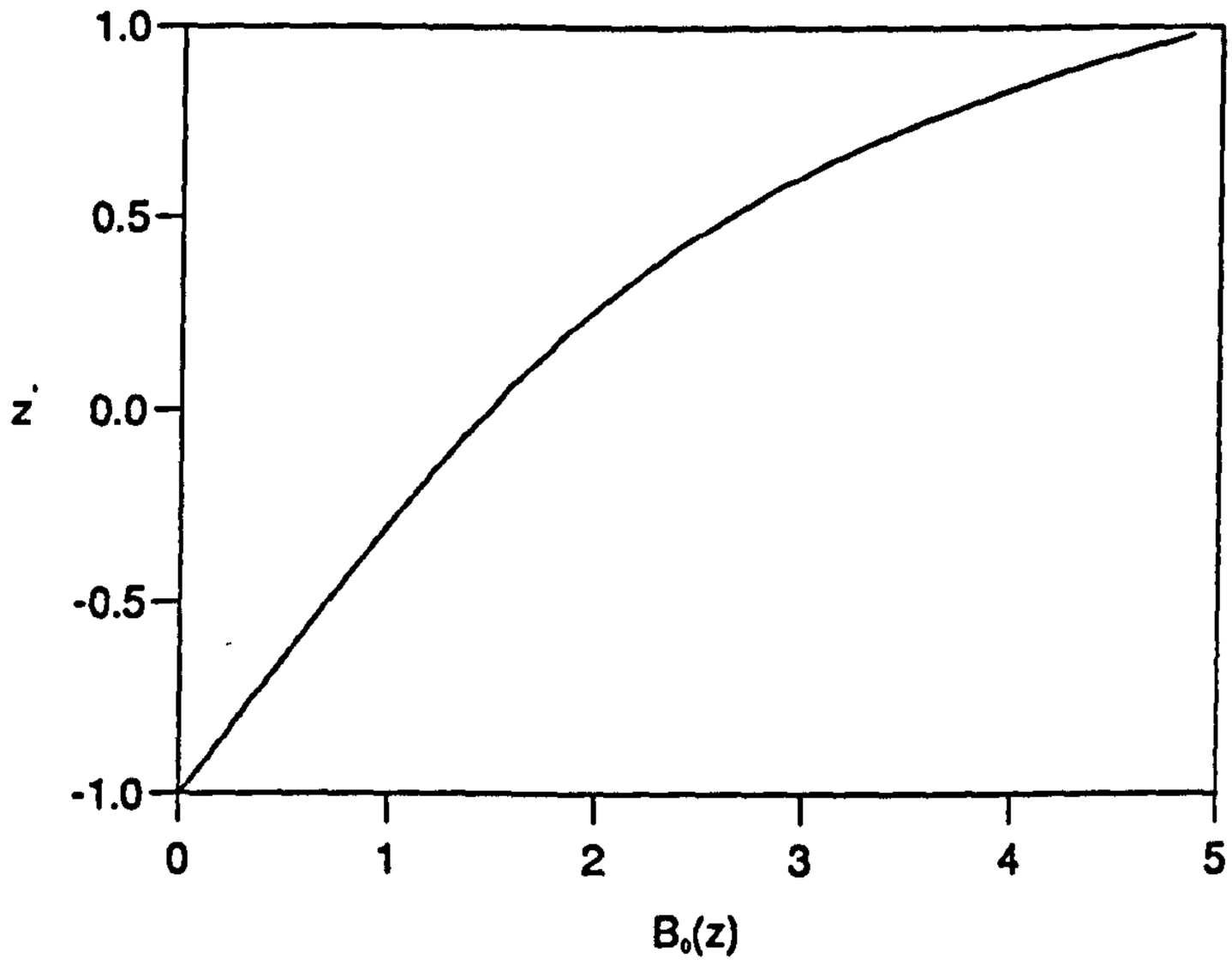

(a)

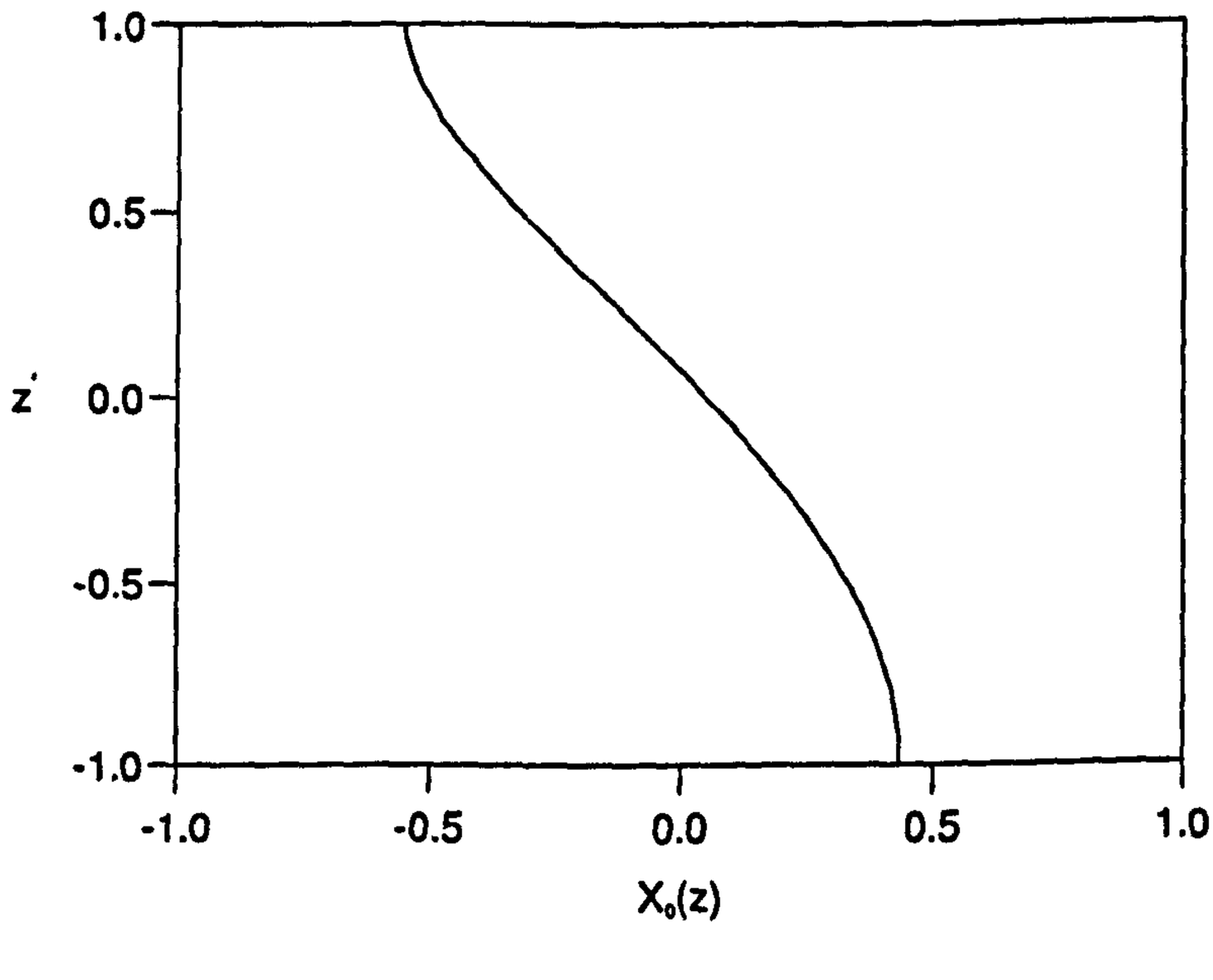

(b)

Figure 5.5: As in figure 5.2, but showing (a) $B_0(z)$, (b) $X_0(z)$.

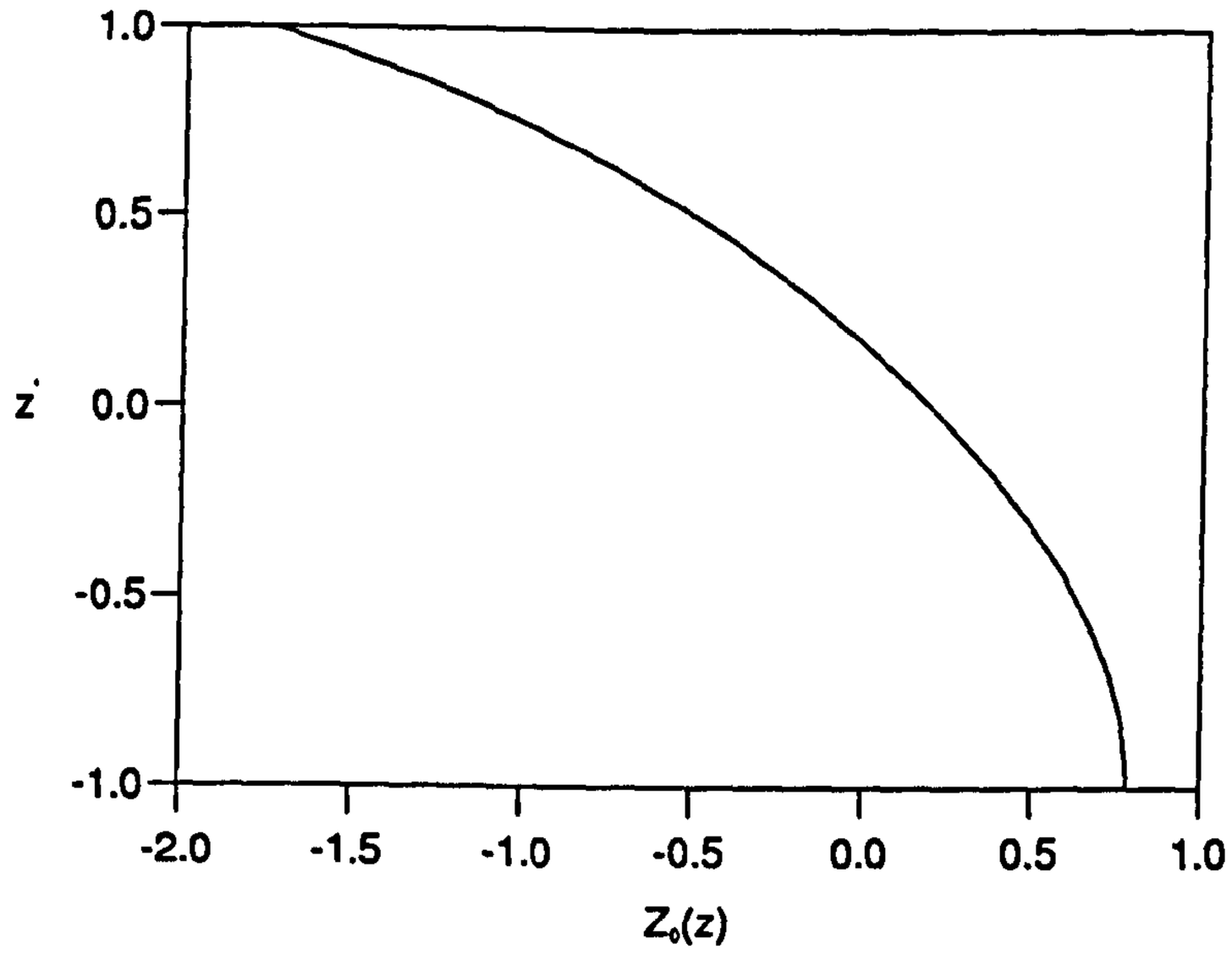

Figure 5.6: As in figure 5.2, but showing $Z_0(z)$.

The following convergence table is obtained:

N	H
1	0.5040877
3	0.4981831
5	0.5048673
7	0.5048670
9	0.5048671
11	0.5048671

Table 5.1

It can be seen that by taking a truncation of

$$N = 7, \tag{5.23}$$

the solution can be obtained to seven significant figures. This truncation gives ten Legendre polynomials in the z direction, which is accurate enough for most purposes. This truncation is adopted throughout the rest of this chapter.

Figure 5.1 shows a plot of H (as defined by (5.22)) against R, while figures 5.2, 5.3, 5.4, 5.5 and 5.6 show plots of T_0, U_{x0}, U_{y0}, W_0, B_{x0}, B_{y0}, B_0, X_0 and Z_0 (as defined by (5.26)) against z' at the point $R = 9.0$. As these quantities obey the condition (4.21), only the relevant real or imaginary part of each is shown. The numerical results compare excellently to the analytic results, proving the validity of the method.

5.4 Numerical Solution Of (5.10) And (5.11)

Equations (5.10), (5.11) and (5.12) are now solved using the Tau method. The perturbations are assumed to have the following spectral expansions

$$\mathbf{X}_r(z) = \begin{bmatrix} T_r(z) \\ W_r(z) \\ B_r(z) \\ X_r(z) \\ Z_r(z) \\ B_{xr}(z) \\ B_{yr}(z) \\ U_{xr}(z) \\ U_{yr}(z) \end{bmatrix} = \begin{bmatrix} \sum_{n=0}^{N+2} T_{rn} P_n(z') \\ \sum_{n=0}^{N+1} W_{rn} P_n(z') \\ \sum_{n=0}^{N+2} B_{rn} P_n(z') \\ \sum_{n=0}^{N+2} X_{rn} P_n(z') \\ \sum_{n=0}^{N} Z_{rn} P_n(z') \\ \sum_{n=0}^{N+1} B_{xrn} P_n(z') \\ \sum_{n=0}^{N+1} B_{yrn} P_n(z') \\ \sum_{n=0}^{N} U_{xrn} P_n(z') \\ \sum_{n=0}^{N} U_{yrn} P_n(z') \end{bmatrix}, \tag{5.24}$$

where $r = \pm 1$. The integer N is the truncation parameter, and is fixed by (5.23). The coefficients of the spectral expansions are complex constants. There are $2(9N + 18)$ spectral coefficients to determine from the perturbation equations. Substituting (5.24) and (5.18) into equations (5.10) and the boundary conditions (5.12) using the Tau method, the following linear equations for the spectral coefficients of $\mathbf{X}_{-1}$ are obtained

$$\frac{4(2n+1)}{\pi} \sum_{\substack{p=n+1 \\ p+n \text{ odd}}}^{N+1} W_{-1p} - \Lambda i m X_{-1n} = 0 \quad (0 \le n \le N), \tag{5.25a}$$

$$\frac{4(2n+1)}{\pi} \sum_{\substack{p=n+1 \\ p+n \text{ odd}}}^{N} Z_{-1p} + \Lambda i m \left\{ \frac{2(2n+1)}{\pi^2} \sum_{\substack{p=n+2 \\ p+n \text{ even}}}^{N+2} [p(p+1) - n(n+1)] B_{-1p} - k^2 B_{-1n} \right\}$$

$$+ R k^2 T_{-1n} = 0 \quad (0 \le n \le N-1), \tag{5.25b}$$

$$\frac{2(2n+1)}{\pi^2}\sum_{\substack{p=n+2\\ p+n\ \text{even}}}^{N+2}[p(p+1)-n(n+1)]B_{-1p}-k^2B_{-1n}-imW_{-1n}$$

$$+qimB^*_{0n}\mathcal{U}=q\lambda B_{-1n}\quad(0\le n\le N),\tag{5.25c}$$

$$\frac{2(2n+1)}{\pi^2}\sum_{\substack{p=n+2\\ p+n\ \text{even}}}^{N+2}[p(p+1)-n(n+1)]X_{-1p}-k^2X_{-1n}-imZ_{-1n}$$

$$-q\{-imX^*_{0n}+l^2B^*_{x0n}+lmB^*_{y0n}\}\mathcal{U}=q\lambda X_{-1n}\quad(0\le n\le N),\tag{5.25d}$$

$$\frac{2(2n+1)}{\pi^2}\sum_{\substack{p=n+2\\ p+n\ \text{even}}}^{N+2}[p(p+1)-n(n+1)]T_{-1p}-k^2T_{-1n}+W_{-1n}$$

$$+imT^*_{0n}\mathcal{U}=\lambda T_{-1n}\quad(0\le n\le N),\tag{5.25e}$$

$$k^2B_{x,-1n}-il\left\{\frac{2(2n+1)}{\pi}\sum_{\substack{p=n+1\\ p+n\ \text{odd}}}^{N+2}B_{-1p}\right\}+imX_{-1n}=0\quad(0\le n\le N+1),\tag{5.25f}$$

$$k^2B_{y,-1n}+im\left\{\frac{2(2n+1)}{\pi}\sum_{\substack{p=n+1\\ p+n\ \text{odd}}}^{N+2}B_{-1p}\right\}+ilX_{-1n}=0\quad(0\le n\le N+1),\tag{5.25g}$$

$$k^2U_{x,-1n}-il\left\{\frac{2(2n+1)}{\pi}\sum_{\substack{p=n+1\\ p+n\ \text{odd}}}^{N+1}W_{-1p}\right\}+imZ_{-1n}=0\quad(0\le n\le N),\tag{5.25h}$$

$$k^2U_{y,-1n}+im\left\{\frac{2(2n+1)}{\pi}\sum_{\substack{p=n+1\\ p+n\ \text{odd}}}^{N+1}W_{-1p}\right\}+ilZ_{-1n}=0\quad(0\le n\le N),\tag{5.25i}$$

$$\sum_{p=0}^{N+1}(-1)^p W_{-1p} = 0, \tag{5.25j}$$

$$\sum_{p=0}^{N+1} W_{-1p} = \frac{-im\mathcal{U}}{2}, \tag{5.33k}$$

$$\sum_{p=0}^{N+2}(-1)^p T_{-1p} = 0, \tag{5.25l}$$

$$\sum_{p=0}^{N+2} T_{-1p} = 0, \tag{5.25m}$$

$$\sum_{p=0}^{N+2}(-1)^p B_{-1p} = 0, \tag{5.25n}$$

$$\sum_{p=0}^{N+2} B_{-1p} = 0, \tag{5.25o}$$

$$\sum_{p=0}^{N+2}\frac{1}{2}(-1)^{p+1}p(p+1)X_{-1p} = 0, \tag{5.25p}$$

$$\sum_{p=0}^{N+2}\frac{1}{2}p(p+1)X_{-1p} = 0. \tag{5.25q}$$

The equations for $\mathbf{X}_1$ are given by

$$\frac{4(2n+1)}{\pi}\sum_{p=n+1}^{N+1} W_{1p} + \Lambda imX_{1n} = 0 \quad (0 \le n \le N), \tag{5.26a}$$
$$p+n \text{ odd}$$

$$\frac{4(2n+1)}{\pi}\sum_{\substack{p=n+1\\ p+n \text{ odd}}}^{N} Z_{1p} - \Lambda im\left\{\frac{2(2n+1)}{\pi^2}\sum_{\substack{p=n+2\\ p+n \text{ even}}}^{N+2}[p(p+1)-n(n+1)]B_{1p} - k^2 B_{1n}\right\}$$

$$+Rk^2 T_{1n} = 0 \quad (0 \le n \le N-1), \tag{5.26b}$$

$$\frac{2(2n+1)}{\pi^2}\sum_{\substack{p=n+2\\ p+n\ \text{even}}}^{N+2}[p(p+1)-n(n+1)]B_{1p}-k^2B_{1n}+imW_{1n}$$

$$-qimB_{0n}\mathcal{U}=q\lambda B_{1n}\quad(0\le n\le N),\tag{5.26c}$$

$$\frac{2(2n+1)}{\pi^2}\sum_{\substack{p=n+2\\ p+n\ \text{even}}}^{N+2}[p(p+1)-n(n+1)]X_{1p}-k^2X_{1n}+imZ_{1n}$$

$$-q\{imX_{0n}+l^2B_{x0n}-lmB_{y0n}\}\mathcal{U}=q\lambda X_{1n}\quad(0\le n\le N),\tag{5.26d}$$

$$\frac{2(2n+1)}{\pi^2}\sum_{\substack{p=n+2\\ p+n\ \text{even}}}^{N+2}[p(p+1)-n(n+1)]T_{1p}-k^2T_{1n}+W_{1n}$$

$$-imT_{0n}\mathcal{U}=\lambda T_{1n}\quad(0\le n\le N),\tag{5.26e}$$

$$k^2B_{x,1n}-il\left\{\frac{2(2n+1)}{\pi}\sum_{\substack{p=n+1\\ p+n\ \text{odd}}}^{N+2}B_{1p}\right\}-imX_{1n}=0\quad(0\le n\le N+1),\tag{5.26f}$$

$$k^2B_{y,1n}-im\left\{\frac{2(2n+1)}{\pi}\sum_{\substack{p=n+1\\ p+n\ \text{odd}}}^{N+2}B_{1p}\right\}+ilX_{1n}=0\quad(0\le n\le N+1),\tag{5.26g}$$

$$k^2U_{x,1n}-il\left\{\frac{2(2n+1)}{\pi}\sum_{\substack{p=n+1\\ p+n\ \text{odd}}}^{N+1}W_{1p}\right\}-imZ_{1n}=0\quad(0\le n\le N),\tag{5.26h}$$

$$k^2U_{y,1n}-im\left\{\frac{2(2n+1)}{\pi}\sum_{\substack{p=n+1\\ p+n\ \text{odd}}}^{N+1}W_{1p}\right\}+ilZ_{1n}=0\quad(0\le n\le N),\tag{5.26i}$$

$$\sum_{p=0}^{N+1}(-1)^p W_{1p} = 0, \tag{5.26j}$$

$$\sum_{p=0}^{N+1} W_{1p} = \frac{im\mathcal{U}}{2}, \tag{5.26k}$$

$$\sum_{p=0}^{N+2}(-1)^p T_{1p} = 0, \tag{5.26l}$$

$$\sum_{p=0}^{N+2} T_{1p} = 0, \tag{5.26m}$$

$$\sum_{p=0}^{N+2}(-1)^p B_{1p} = 0, \tag{5.26n}$$

$$\sum_{p=0}^{N+2} B_{1p} = 0, \tag{5.26o}$$

$$\sum_{p=0}^{N+2}\frac{1}{2}(-1)^{p+1}p(p+1)X_{1p} = 0, \tag{5.26p}$$

$$\sum_{p=0}^{N+2}\frac{1}{2}p(p+1)X_{1p} = 0. \tag{5.26q}$$

Equations (5.25) and (5.26) define $2(9N+18)$ complex, linear algebraic equations in the $2(9N+18)$ complex spectral coefficients. It now just remains to evaluate equation (5.11) for the coefficient $\mathcal{U}$ of the geostrophic flow using the Tau method. Using the orthogonality condition (5.15) this equation becomes

$$\mathcal{U} - \frac{\Gamma i l \Lambda q}{2}\sum_{n=0}^{N+1}\frac{1}{2n+1}\left\{B^*_{x0n}B_{y1n} + B_{x0n}B_{y,-1n} + B_{x,-1n}B_{y0n} + B_{x1n}B^*_{y0n}\right\} = 0. \tag{5.27}$$

Defining $\mathcal{U}$ as an unknown, and combining (5.25), (5.26) and (5.27), a system of $18N+37$ complex, linear algebraic equations in $18N+37$ complex unknowns is

obtained. In matrix notation, this system takes the form of a generalised eigenvalue problem,

$$\mathbf{L}_p\mathbf{Y}_p = \lambda\mathbf{R}\mathbf{Y}_p, \tag{5.28}$$

where $\mathbf{L}_p$ and $\mathbf{R}_p$ are complex matrices of size $(18N+37)\times(18N+37)$ and $\mathbf{Y}_p$ is the $(18N+37)\times 1$ vector of unknowns. If $\mathbf{Y}_p$ is partitioned as follows,

$$\mathbf{Y}_p = \begin{bmatrix}\mathbf{Y}_{pT}\\ \mathbf{Y}_{pB}\end{bmatrix},$$

where $\mathbf{Y}_{pT}$ is a $(6N+6)\times 1$ vector of unknowns defined by

$$\mathbf{Y}_{pT}^T = \Big[T_{-10}\,T_{-11}...T_{-1N}\,B_{-10}\,B_{-11}...B_{-1N}\,X_{-10}\,X_{-11}...X_{-1N}$$
$$T_{10}\,T_{11}...T_{1N}\,B_{10}\,B_{11}...B_{1N}\,X_{10}\,X_{11}...X_{1N}\Big], \tag{5.29}$$

and $\mathbf{Y}_{pB}$ is a $(12N+31)\times 1$ vector containing the remaining unknowns, then (5.28) takes the form

$$\begin{bmatrix}\mathbf{L}_{11} & \mathbf{L}_{12}\\ \mathbf{L}_{21} & \mathbf{L}_{22}\end{bmatrix}\begin{bmatrix}\mathbf{Y}_{pT}\\ \mathbf{Y}_{pB}\end{bmatrix} = \lambda\begin{bmatrix}\mathbf{I}_{6N+6} & 0\\ 0 & 0\end{bmatrix}\begin{bmatrix}\mathbf{Y}_{pT}\\ \mathbf{Y}_{pB}\end{bmatrix},$$

where $\mathbf{L}_{11}$ is a matrix of size $(6N+6)\times(6N+6)$, $\mathbf{L}_{12}$ is a matrix of size $(6N+6)\times(12N+31)$, $\mathbf{L}_{21}$ is a matrix of size $(12N+31)\times(6N+6)$ and $\mathbf{L}_{22}$ is a matrix of size $(12N+31)\times(12N+31)$. $\mathbf{I}_{6N+6}$ denotes the $(6N+6)\times(6N+6)$ identity matrix. Therefore, the equations

$$\mathbf{L}_{11}\mathbf{Y}_{pT} + \mathbf{L}_{12}\mathbf{Y}_{pB} = \lambda\mathbf{Y}_{pT},$$

$$\mathbf{L}_{21}\mathbf{Y}_{pT} + \mathbf{L}_{22}\mathbf{Y}_{pB} = 0,$$

are obtained. These can be rearranged to give the matrix equations

$$[\mathbf{L}_{11} - \mathbf{L}_{12}\mathbf{L}_{22}^{-1}\mathbf{L}_{21}]\mathbf{Y}_{pT} = \lambda \mathbf{Y}_{pT}, \tag{5.30a}$$

$$\mathbf{Y}_{pB} = -\mathbf{L}_{22}^{-1}\mathbf{L}_{21}\mathbf{Y}_{pT}, \tag{5.30b}$$

which can be solved successively. (5.30) is an equivalent system to (5.28). Now, (5.30a) says that $\mathbf{Y}_{pT}$ is the eigenvector and λ is the eigenvalue of the $(6N+6) \times (6N+6)$ complex matrix defined by

$$\mathbf{M} = \mathbf{L}_{11} - \mathbf{L}_{12}\mathbf{L}_{22}^{-1}\mathbf{L}_{21}. \tag{5.31}$$

The coefficients of the matrix M depend on the values of Λ, q, l, m, $\mathbf{Y}_0$, Γ and R, and values must be assigned to these parameters before the problem can be solved. As usual, only the cases

$$\Lambda = 4.0, \quad q = 0.1, \quad 1.0, \quad \text{and} \quad 10.0,$$

will be considered. The wavenumbers l and m define the lengthscales in the x and y directions on which the convection takes place. They are assumed to take the values

$$l = \sqrt{2 - \frac{\sqrt{3}}{2}}, \quad m = \sqrt{\frac{\sqrt{3}}{2}}. \tag{5.32}$$

These are the critical wavenumbers associated with a steady oblique convection roll in a standard plane layer, when $\Lambda = 4$. Since

$$l \approx m \approx 1,$$

these values ensure that the periodic box in which the convection takes place has an aspect ratio of about 1. This is appropriate for modelling spherical geometry. The values of l and m also ensure that the two oblique rolls defined by (5.7) and (5.8) are orientated at angles of about $\pm\frac{\pi}{4}$ to the applied magnetic field. This avoids any limiting cases where (for instance) the rolls are nearly parallel (small l) or perpendicular (small m) to the forced transverse roll in the layer.

Finally, ranges of values of R and Γ are chosen. For each required value of R and Γ, equations (5.20) are solved for $\mathbf{Y}_0$ using the prescribed parameter values. Then, the matrix M is set up, and NAG routine F02AKF is employed to find the $6N+6$ eigenvalues λ_j and eigenvectors $\mathbf{Y}_{pTj}$ of M. This routine works by first finding a transformation that converts M to Hessenberg form, M_H. Then, an LR decomposition of M_H is used to find the eigenvalues and eigenvectors of M_H. These are then mapped to the eigenvalues and eigenvectors of M using the inverse transformation. A simple matrix multiplication routine then gives $\mathbf{Y}_{pBj}$ from $\mathbf{Y}_{pTj}$. In this way, the $6N+6$ eigenvalues λ_j and eigenvectors $\mathbf{Y}_{pj}$ of (5.28) are obtained for each required value of R and Γ.

5.4.1 The Stability Criteria

The following definitions are made

$$s_j = RE(\lambda_j), \quad j = 1, 2, ..., (6N+6), \tag{5.33a}$$

$$\omega_j = IM(\lambda_j), \quad j = 1, 2, ..., (6N+6). \tag{5.33b}$$

Each eigenvector $\mathbf{Y}_{pj}$ gives a possible z-structure for the perturbations. Each s_j represents the growth rate, and ω_j the frequency, of the perturbations whose z-structures are given by the eigenvector $\mathbf{Y}_{pj}$. The stability characteristics of these perturbations are found by looking at the s_j and the ω_j.

Now, the s_j can be ordered so that

$$s_1 > s_2 > s_3 > ..... > s_{(6N+6)}. \tag{5.34}$$

With Λ, q, l and m fixed, the growth rates only depend upon the values taken by Γ and R. Hence

$$s_j = s_j(\Gamma, R) \quad \forall j. \tag{5.35}$$

It transpires that the stability of the basic state depends upon the sign of s_1, the largest growth rate. To see this, note that if

$$s_1(\Gamma, R) < 0,$$

then the basic state is stable, since (5.34) then gives

$$s_j(\Gamma, R) < 0 \quad \forall j.$$

Hence, all the possible perturbations are exponentially decaying. On the other hand, if

$$s_1(\Gamma, R) > 0,$$

then the basic state is unstable, since then the perturbations whose z-structures are given by $\mathbf{Y}_{p1}$ are exponentially growing. The point at which the basic state *first* loses stability is defined by the condition that

$$s_1(\Gamma, R) = 0.$$

This in turn defines a relation of the form

$$R = R_1(\Gamma), \tag{5.36}$$

which, for each value of the bump parameter Γ, gives the critical Rayleigh number at which the basic state first loses stability to the perturbations whose z-structures are given by the eigenvector $\mathbf{Y}_{p1}$. These perturbations will be called the most unstable perturbations.

The value of

$$\omega_1 = \omega_1(\Gamma, R),$$

at $R = R_1(\Gamma)$ says how the basic state loses stability. If

$$\omega(\Gamma, R_1(\Gamma)) = 0,$$

then the basic state loses stability through the exchange of stabilities. However, if

$$\omega(\Gamma, R_1(\Gamma)) \neq 0,$$

the the mechanism is overstability, and the frequency of the perturbations at criticality is given by $\omega_1(\Gamma, R_1(\Gamma))$.

The stability criteria for each of the other possible perturbations that arise can be derived by analogy with those for the most unstable perturbations.

5.5 Results

In this section, the stability characteristics of the most unstable perturbations, for the chosen parameter values, are described. These characteristics define where and how the basic state first loses stability for the given parameter values. For comparison, the stability characteristics of the perturbations whose z-structures are given by $\mathbf{Y}_{p2}$ are also described. These perturbations have the second largest growth rate, s_2, and will be called the second most unstable perturbations.

5.5.1 The Most Unstable Perturbations

This is the preferred mode of instability for the basic state. It consists of a double oblique roll (i.e. a linear combination of a (+)-roll and a (-)-roll in the notation of chapter 3). These two rolls align themselves with the transverse roll forced by the bumps in such a way that Taylors constraint is satisfied at $O(\delta)$, so the solution satisfies

$$\frac{\partial}{\partial x}\left\{\frac{m}{2\pi^2}\int_0^{\frac{2\pi}{m}}\int_0^{\pi}(b_{x0}b_{yp}+b_{xp}b_{y0})dzdy\right\}=0. \tag{5.37}$$

Hence, the perturbations do not accelerate a geostrophic flow when they interact with the basic state, so $V_p = 0$. A consequence of this surprising result is that the stability characteristics of these perturbations are independent of the values taken by Γ and q. The critical Rayleigh numbers at which the basic state loses stability to these perturbations, which are defined by

$$R = R_1(\Gamma), \tag{5.38}$$

turn out to be the same, no matter what value of Γ is chosen. In fact, the basic state loses stability to these perturbations once R exceeds

$$R_1 = 10.39230485 = 6\sqrt{3}\,,$$

irrespective of Γ. A graph of (5.38) against Γ is a straight line in the (Γ, q) plane (this is shown in figure 5.7). It turns out that the frequency associated with these perturbations satisfies

$$\omega_1(\Gamma, R_1(\Gamma)) = 0.$$

Again, this is irrespective of the value of Γ. Hence, the basic state loses stability to these perturbations through the exchange of stabilities mechanism (at least, for the parameter values chosen). Figure 5.8 shows a plot of s_1 and ω_1 against R.

In figures 5.9, 5.10, 5.11, 5.12 and 5.13 the z-structure of the perturbations are plotted against z', when $R = R_1$. These figures show that the unknowns adopt simple sinusoidal profiles at criticality. The solutions can adopt such simple z-structures since with no geostrophic flow forced by the interaction of the perturbations with the basic state, there is no forcing on the perturbations, and the boundary conditions on the perturbations become homogeneous. Simple, homogeneous boundary conditions can easily be accomodated by sinusoidal profiles. Note that the unknowns obey the conditions

$$T_r = -T_r^*,$$

$$U_{xr} = U_{x0}^*,$$

$$U_{yr} = U_{yr}^*,$$

$$W_r = -W_0^*,$$

$$B_{xr} = -B_{xr}^*, \tag{5.39}$$

$$B_{yr} = -B_{yr}^*,$$

$$B_r = B_r^*,$$

$$X_r = X_r^*,$$

$$Z_r = -Z_r^*,$$

where $r = \pm 1$. Hence, only the relevant real or imaginary parts of each unknown are plotted.

The stability characteristics of these perturbations are identical to the stability results obtained by Roberts and Stewartson (1974) for steady single or double oblique roll solutions in a standard plane layer, with one significant difference - here only double roll solutions are observed. To explain this, recall from Chapter 3 that in the standard plane layer, there was no relation which linked the (+)-roll to the (-)-roll in the linear case. However, here, the rolls can generate a mean Maxwell stress by interacting with the basic state. The equation for the perturbation geostrophic flow provides a linear relation between the (+)-roll and the (-)-roll. In order to make this geostrophic flow vanish, a positive (or negative) contribution to the mean Maxwell stress from one roll interacting with the basic state must be cancelled by a negative (or positive) contribution from the other rolls interaction with the basic state. This cancellation could not occur if one of the rolls were absent. Hence, both types of oblique roll are forced.

5.5.2 The Second Most Unstable Perturbations

When the z-structures of the perturbations are given by $\mathbf{Y}_{p2}$, their stability characteristics change quite drastically. Again, the perturbations consist of a double oblique roll solution. Now, however, these rolls interact with the transverse roll forced by the bumps to accelerate a geostrophic flow of the form

$$V_p = \mathcal{U} \exp(ilx) + c.c.,$$

in the layer. Consequently, the stability characteristics of these perturbations are no longer independent of Γ or q.

The critical Rayleigh numbers at which the basic state loses stability to these perturbations are defined by a relation of the form

$$s_2(\Gamma, R) = 0,$$

where s_2 is the second largest growth rate. This relation yields

$$R = R_2(\Gamma), \tag{5.40}$$

which for each value of Γ gives the critical Rayleigh number at which the basic state loses stability to these perturbations. (5.40) defines curves in the (Γ, R) plane. These curves are plotted for the three values of q chosen in figures 5.14, 5.15 and 5.16. It transpires that

$$\omega_2(\Gamma, R_2(\Gamma)) = 0,$$

for each value of Γ (where ω_2 is the frequency associated with these perturbations). Hence, the basic state loses stability to these perturbations through the exchange of stabilities (again, this is only for the parameter values examined).

The s-shape of these marginal stability curves may be explained by examining figure 5.17, which shows a plot of s_2 and ω_2 against R, for the cases $\Gamma = 0.05$, $\Gamma = 0.2$, $\Gamma = 0.35$ when $q = 0.1$. The s_2 curve consists of two branches: the first branch exists for

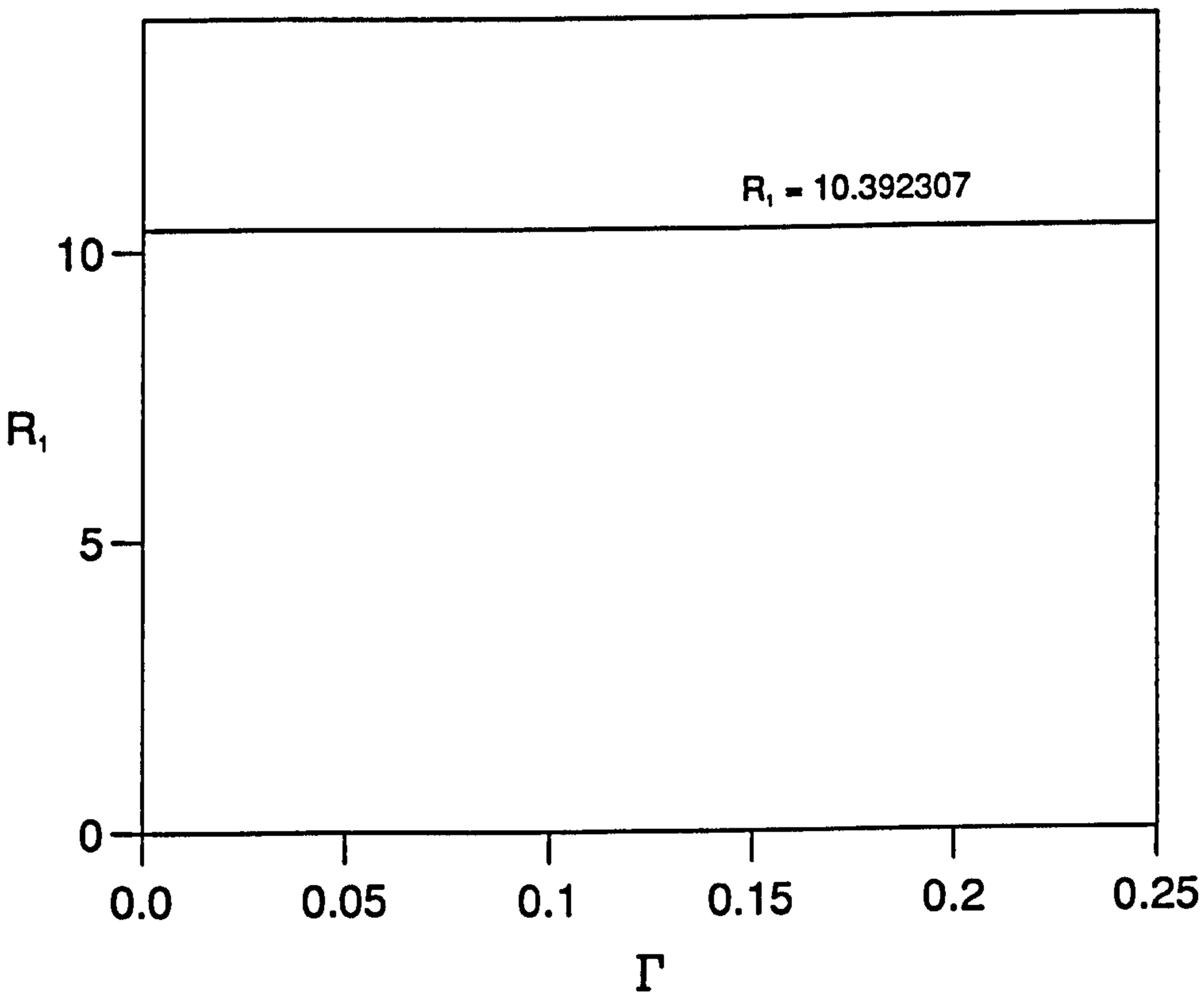

Figure 5.7: A plot of $R_1(\Gamma)$ against Γ.

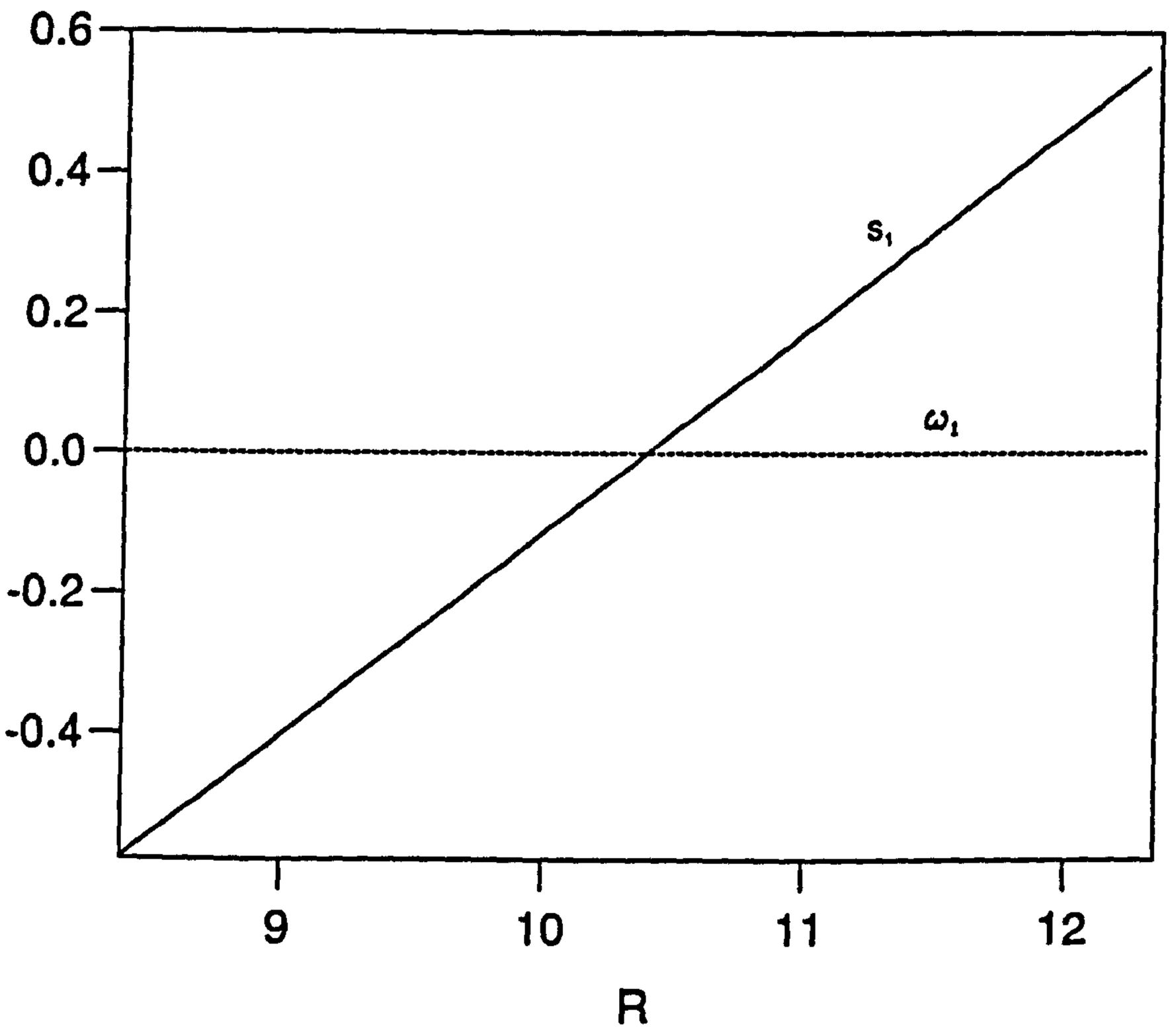

Figure 5.8: A plot of s_1 and ω_1 against R.

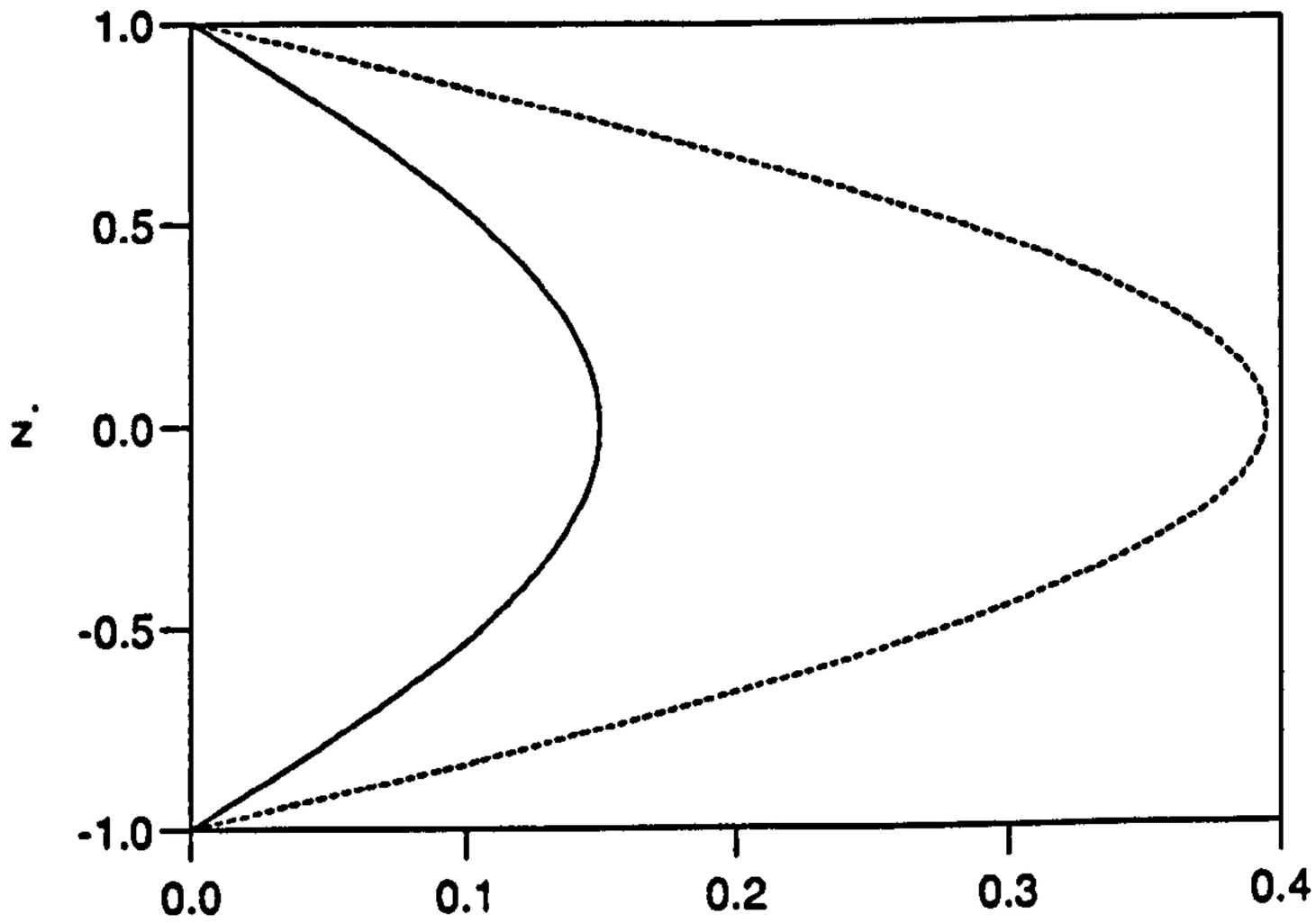

(a)

(b)

Figure 5.9: Plots of (a) $T_{-1}(z)$ (——), $T_1(z)$ (- - -) (b) $U_{z,-1}(z)$ (——), $U_{z,1}(z)$ (- - -) against z' at the point $R = R_1$.

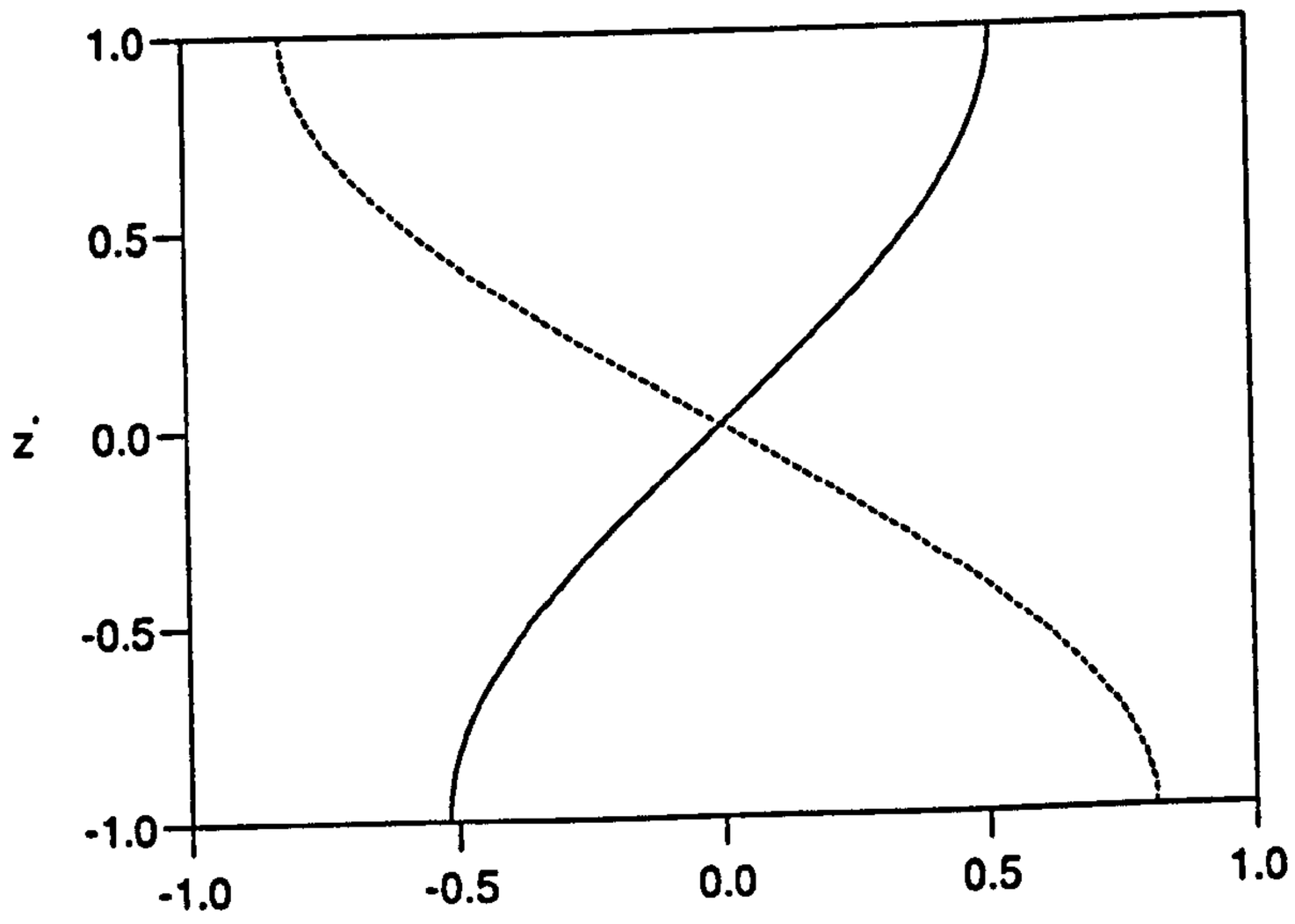

(a)

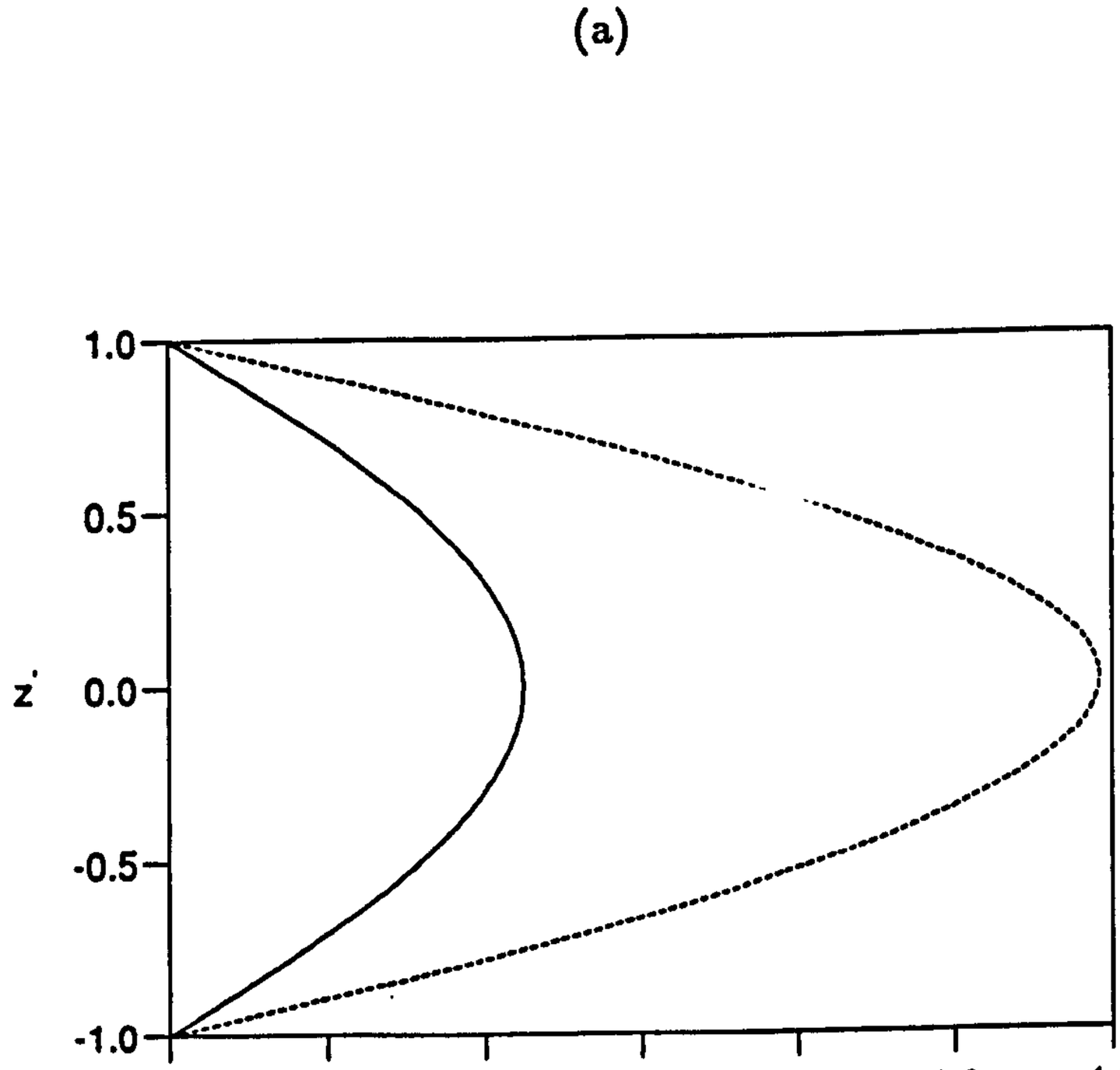

(b)

Figure 5.10: As in figure 5.9, but showing (a) $U_{y,-1}(z)$ (——), $U_{y1}(z)$ (- - -), (b) $W_{-1}(z)$ (——), $W_1(z)$ (- - -).

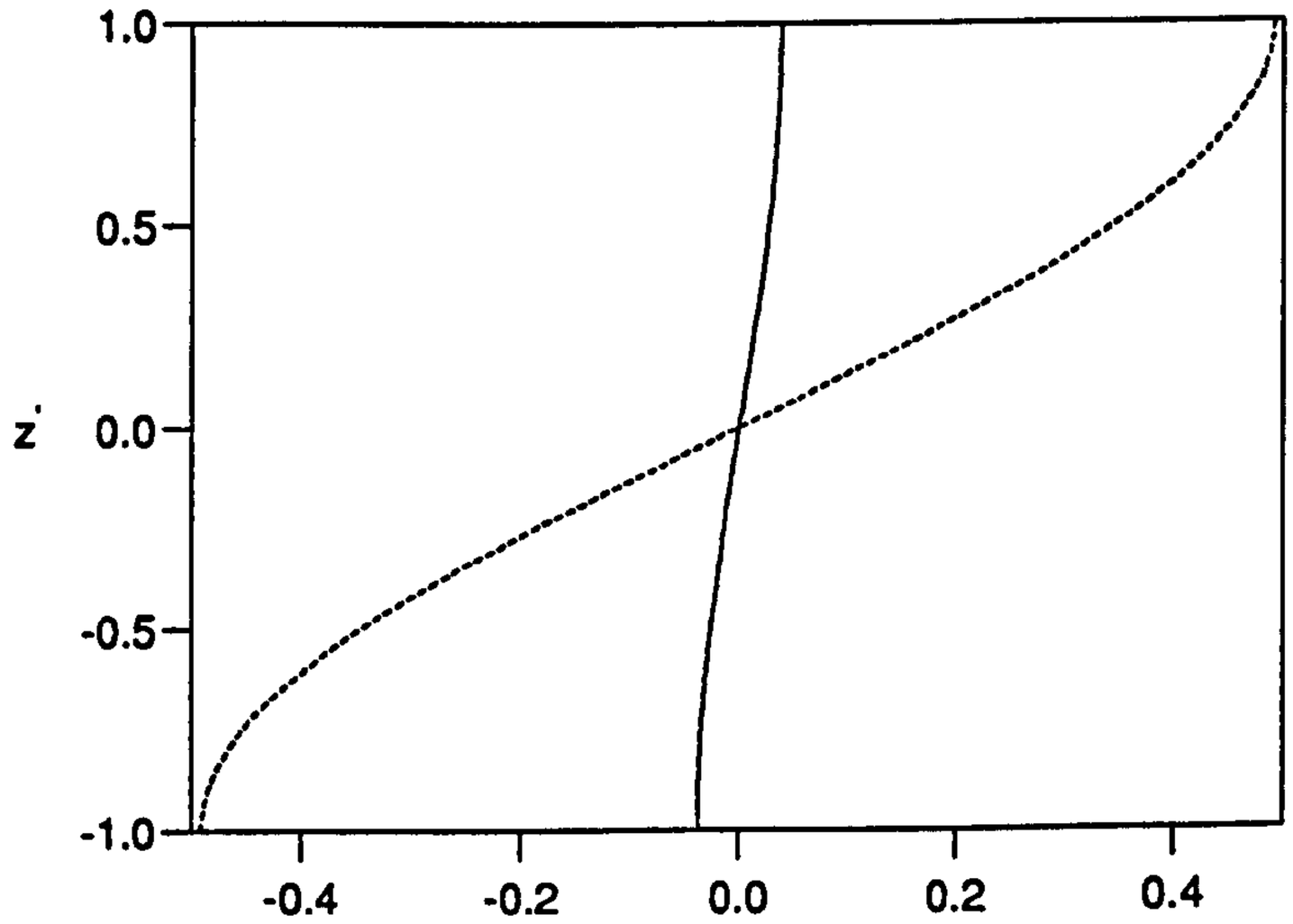

(a)

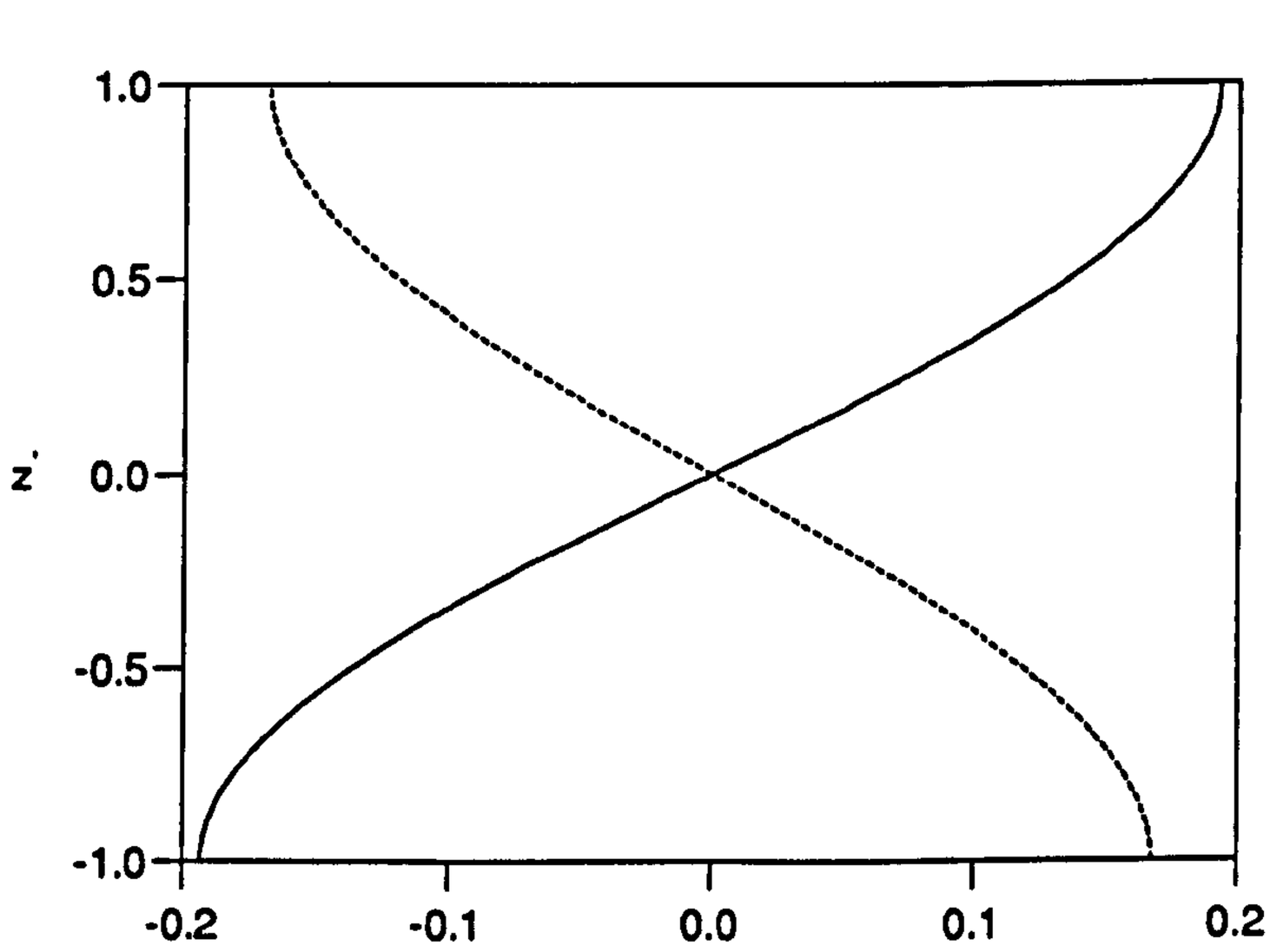

(b)

Figure 5.11: As in figure 5.9, but showing (a) $B_{x,-1}(z)$ (——), $B_{x1}(z)$ (- - -), (b) $B_{y,-1}(z)$ (——), $B_{y1}(z)$ (- - -).

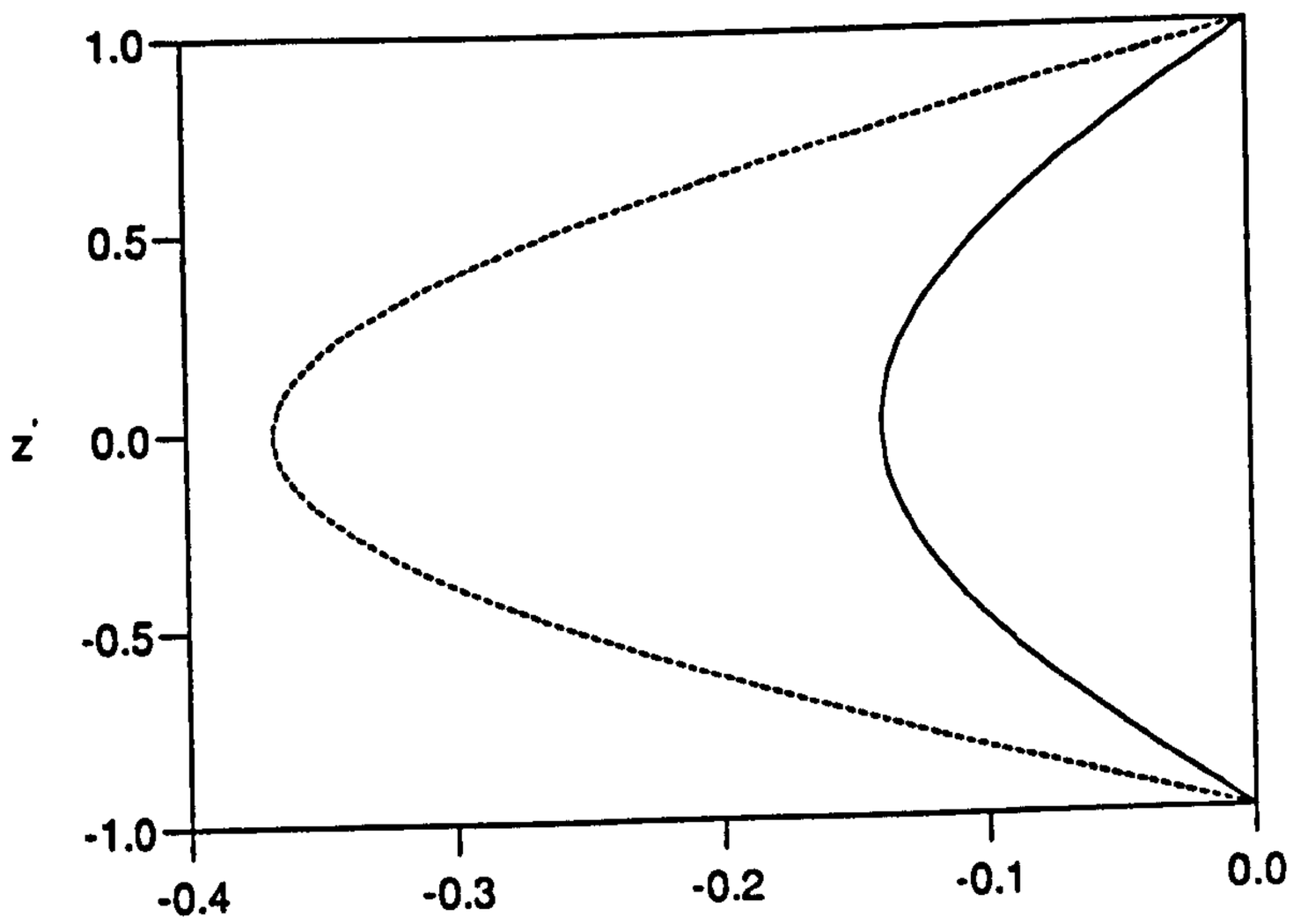

(a)

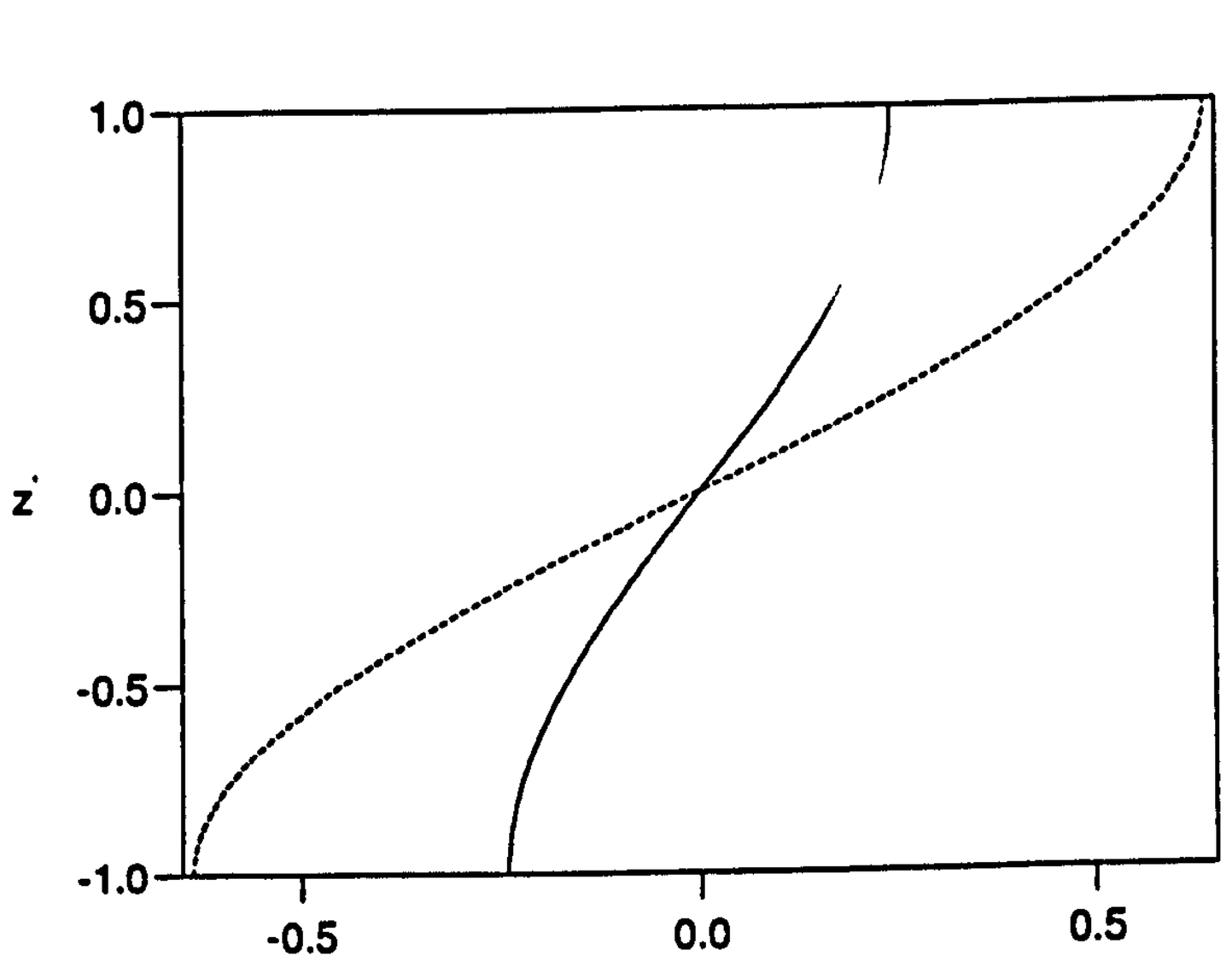

(b)

Figure 5.12: As in figure 5.9, but showing (a) $B_{-1}(z)$ (——), $B_1(z)$ (- - -), (b) $X_{-1}(z)$ (——), $X_1(z)$ (- - -).

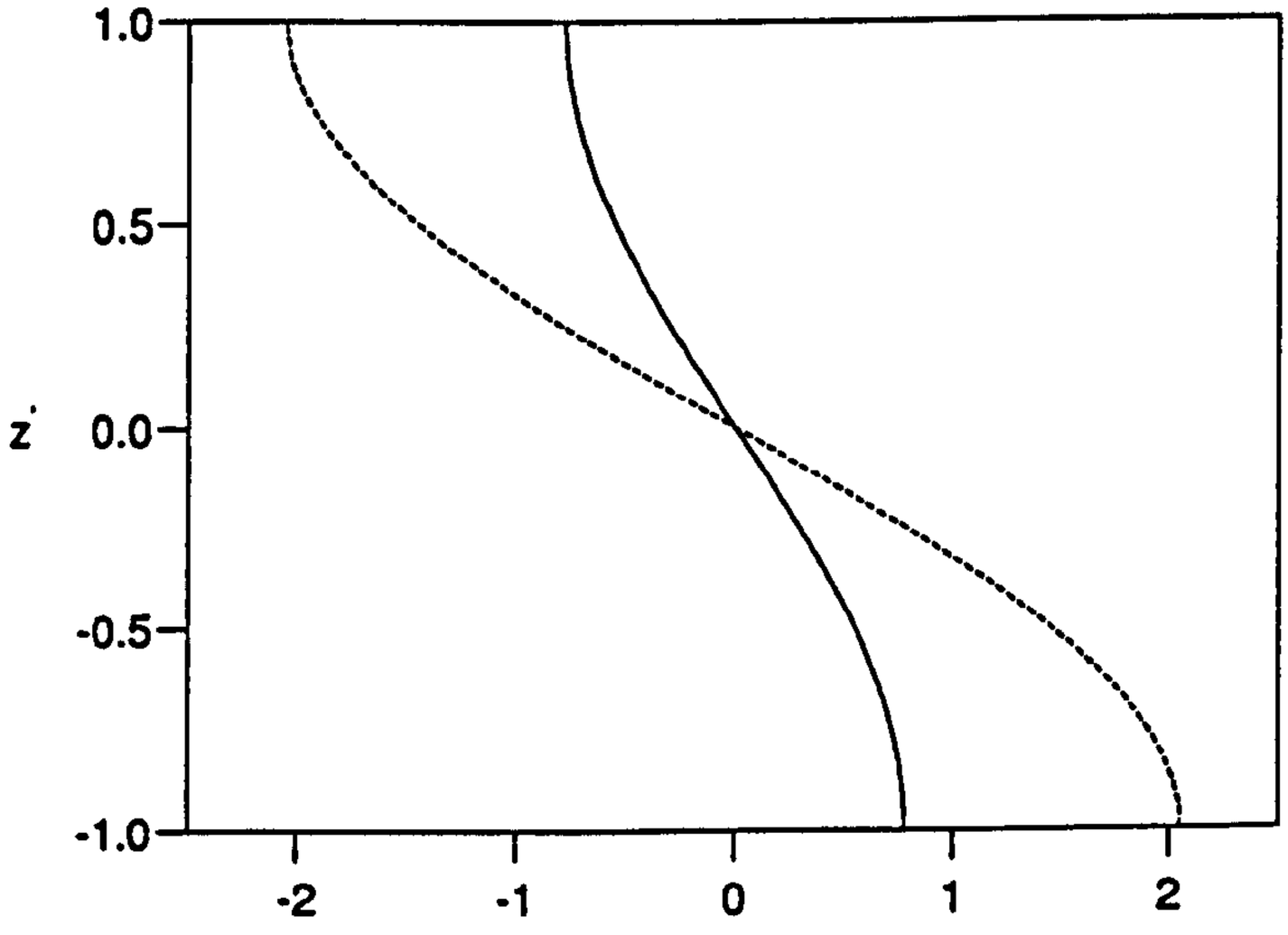

Figure 5.13: As in figure 5.9, but showing $Z_{-1}(z)$ (——), $Z_1(z)$ (- - -).

$$R < R_s,$$

(where R_s is the value of the Rayleigh number at which the basic state is singular, as defined in Chapter 4) while the second branch exists for

$$R > R_s.$$

The points where the s_2 curve crosses the R axis define the critical Rayleigh numbers for these perturbations. Multiple critical Rayleigh numbers arise because s_2 satisfies

$$s_2 \to -\infty \quad \text{as} \quad R \to R_s^{\pm}.$$

This says that the basic state is stable to these perturbations in the region of it's singularity. However, if the s_2 curve crosses the R axis below R_s (i.e. on the first branch), then it must do so again to satisfy this condition. Since the second branch always crosses the R axis, multiple critical Rayleigh numbers are obtained for those values of Γ at which the first branch can cross the R axis. As always, however, it is the perturbations with the smallest associated critical Rayleigh numbers that will be preferred at a given value of Γ.

Note also from figure 5.14, 5.15 and 5.16 that

$$R_2(\Gamma) \to \infty \quad \text{as} \quad \Gamma \to \infty,$$

so increasing the bumpsize parameter makes the basic state more stable to these perturbations. This may be traced to the fact that larger values of Γ increase the strength of the geostrophic flow. This increases the shear generated by V_p, and since shear suppresses convection (Fearn and Proctor 1983b; Fearn 1989) this leads to an increase in the critical Rayleigh number.

In figures 5.18, 5.19, 5.20, 5.21 and 5.22 the z-structure of these perturbations are plotted against z', when $\Gamma = 0.1$, $R = R_2(0.1)$ and $q = 1.0$. These perturbations also obey (5.39), so only the relevant real or imaginary part of each is plotted. Figure 5.23 shows the geostrophic flow profile set up by the interaction of the

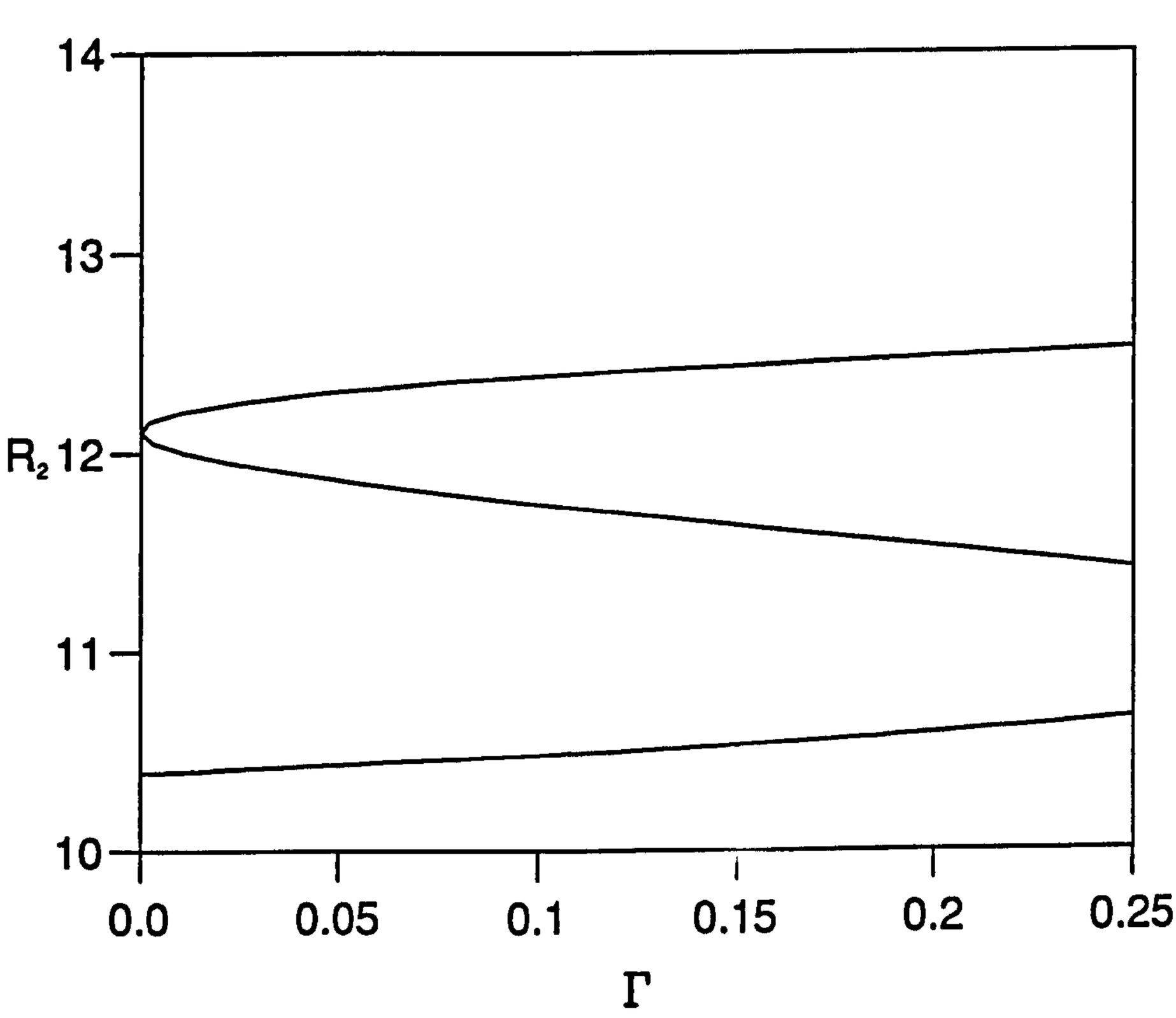

Figure 5.14: A plot of $R_2(\Gamma)$ against Γ in the case $q = 0.1$.

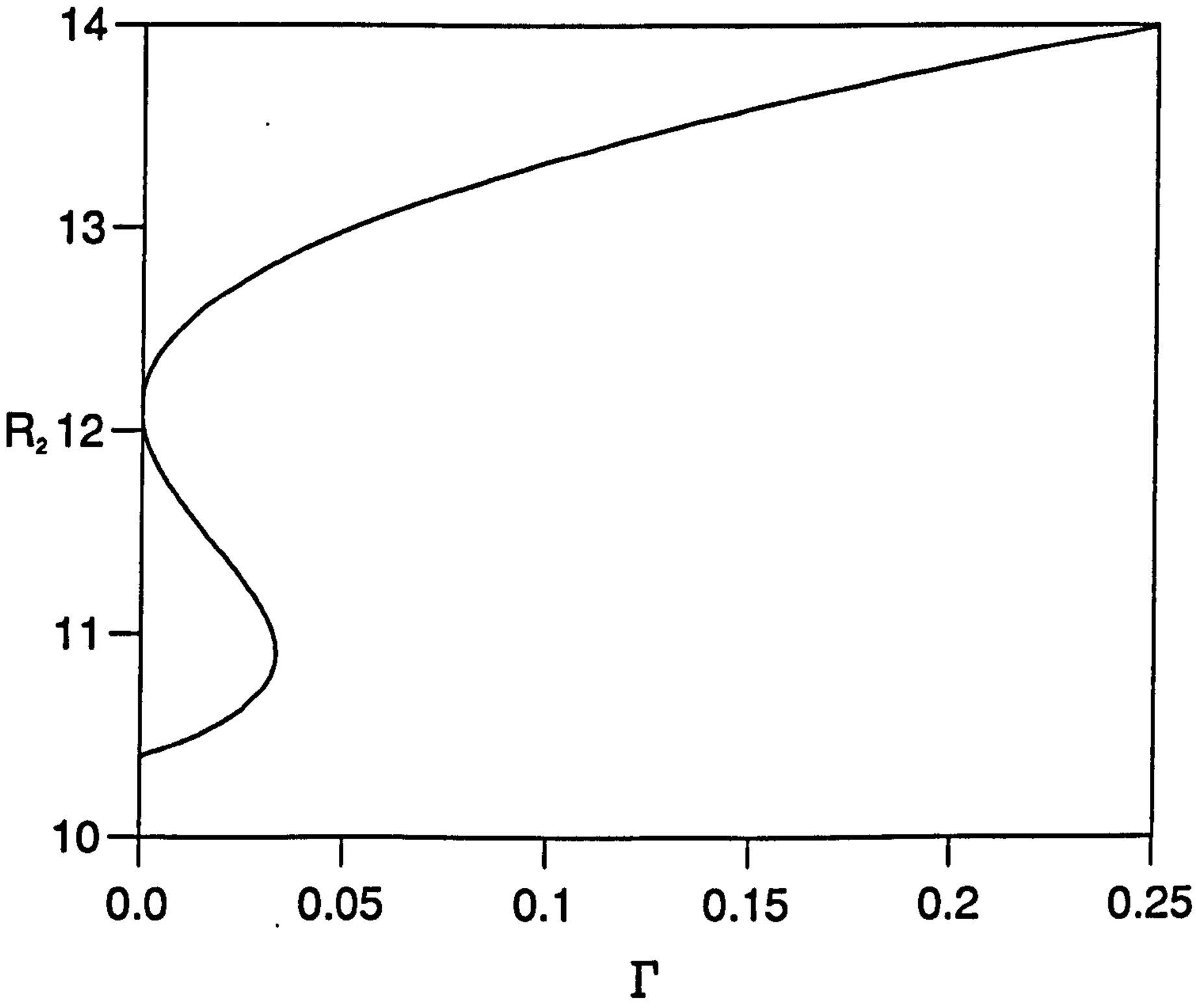

Figure 5.15: A plot of $R_2(\Gamma)$ against Γ in the case $q = 1.0$.

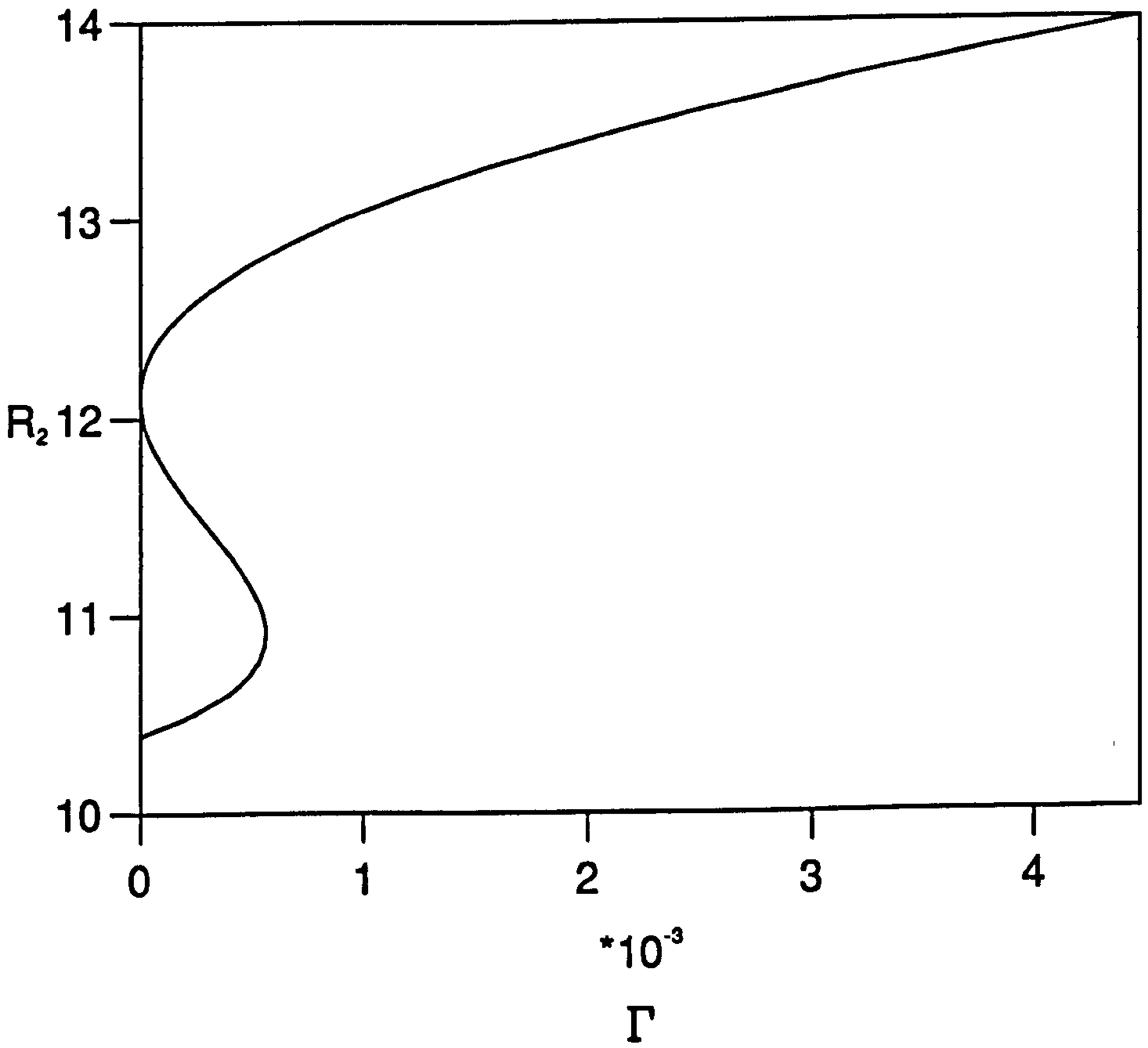

Figure 5.16: A plot of $R_2(\Gamma)$ against Γ in the case $q = 10.0$.

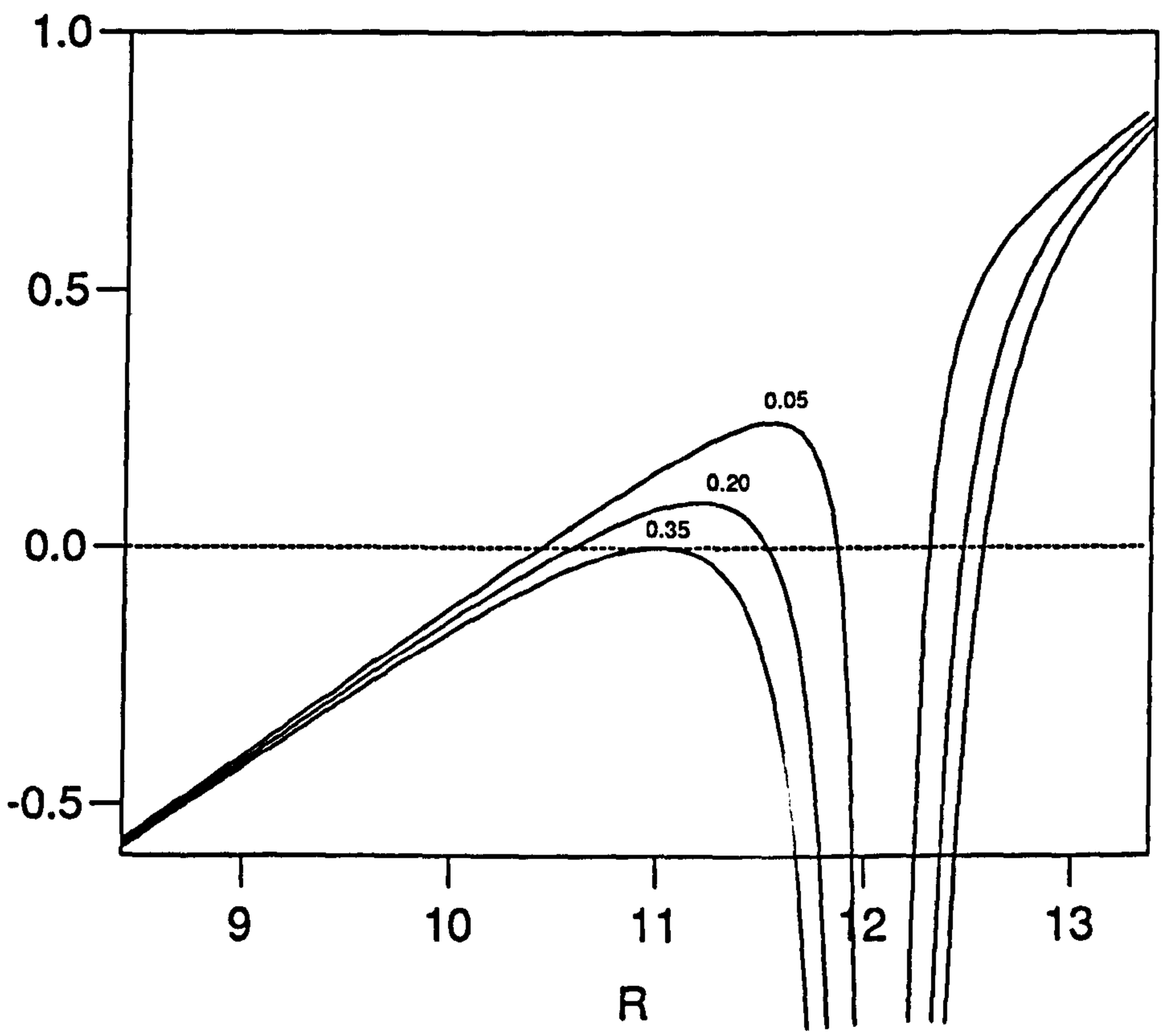

Figure 5.17: A plot of s_2 (——) and ω_2 (- - -) against R for the cases $\Gamma = 0.05, 0.2, 0.35$ when $q = 0.1$.

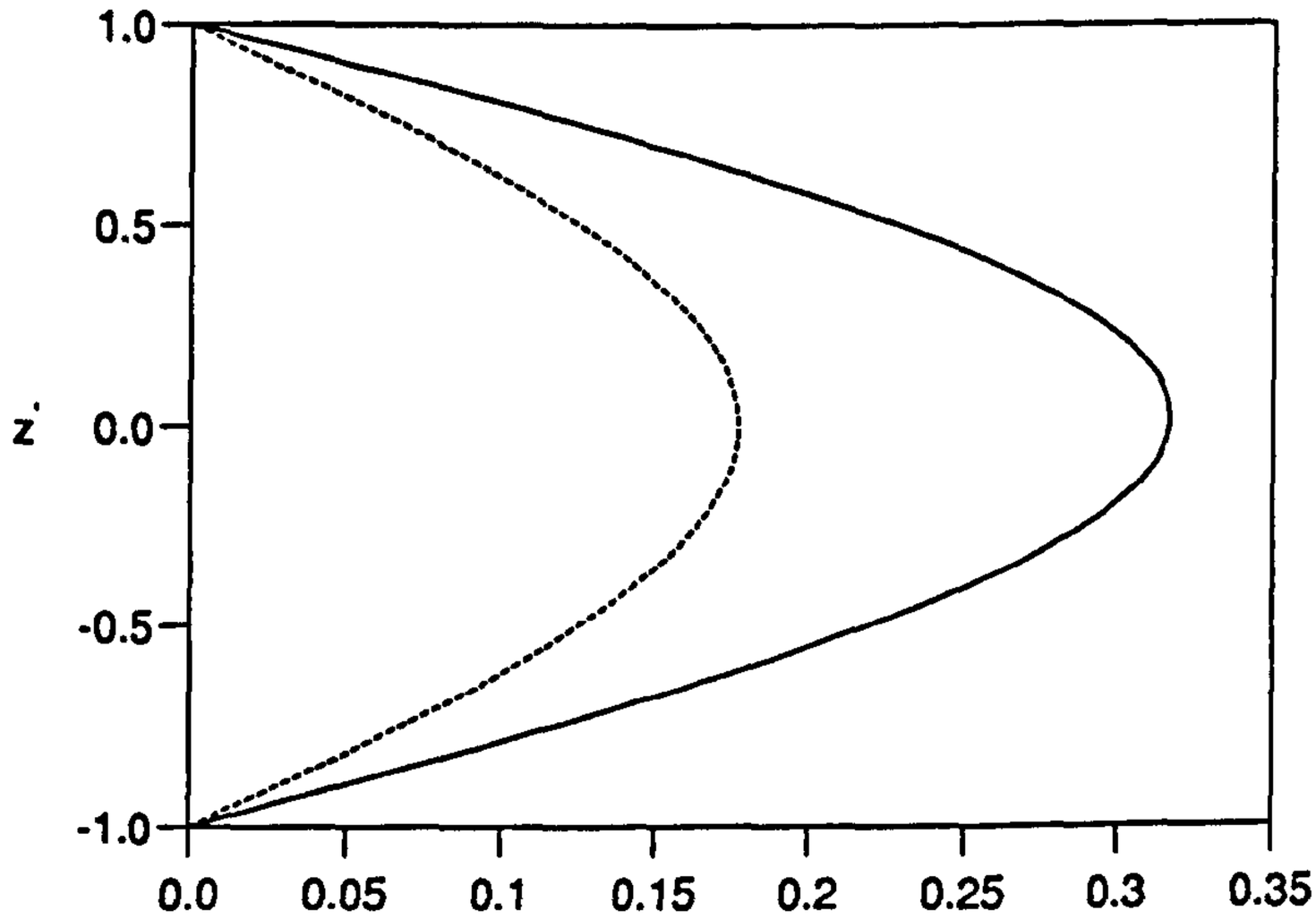

(a)

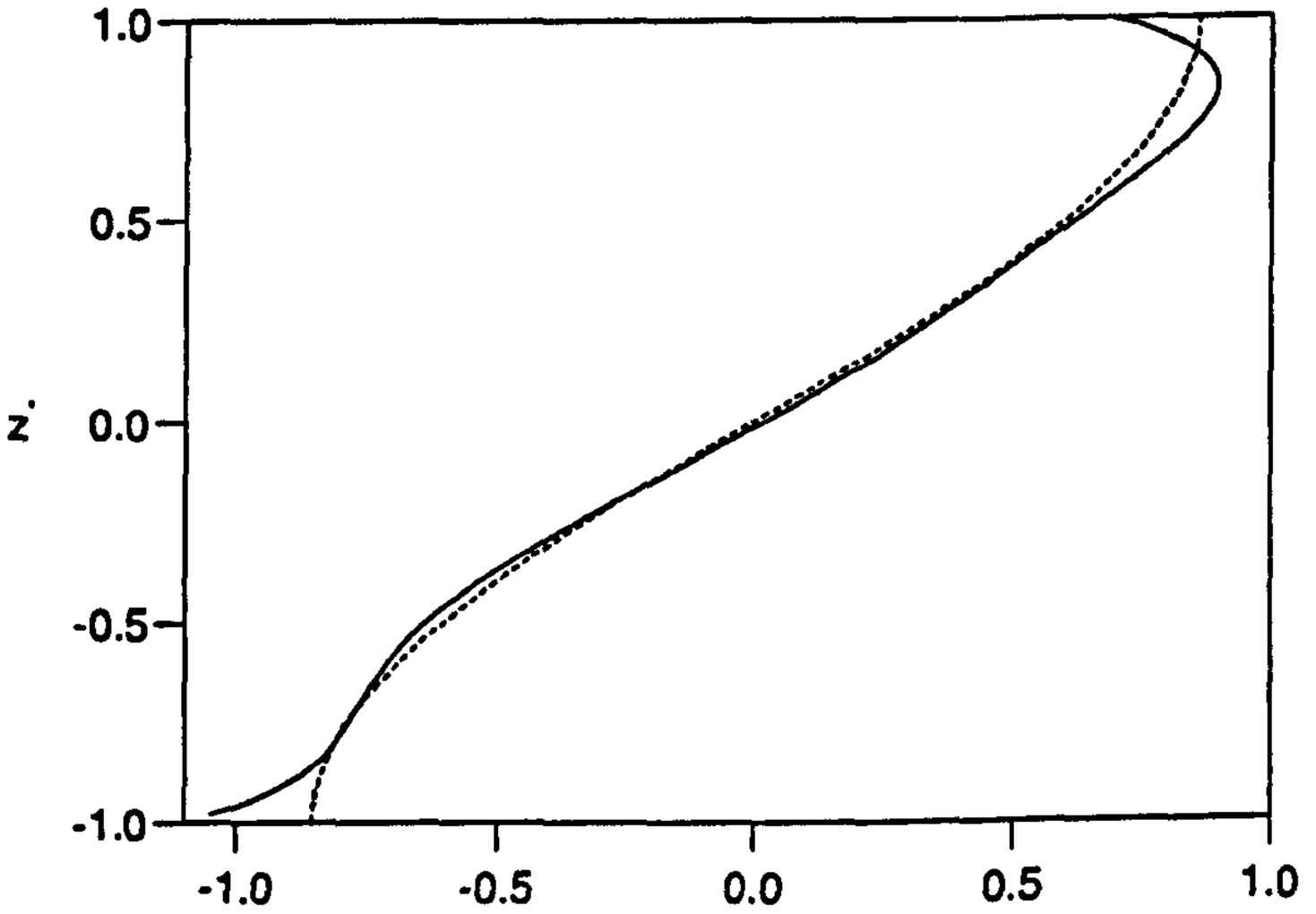

(b)

Figure 5.18: Plots of (a) $T_{-1}(z)$ (——), $T_1(z)$ (- - -) (b) $U_{x,-1}(z)$ (——), $U_{x,1}(z)$ (- - -) against z' at the point $R = R_2(0.1)$, for the case $q = 1.0$, $\Gamma = 0.1$.

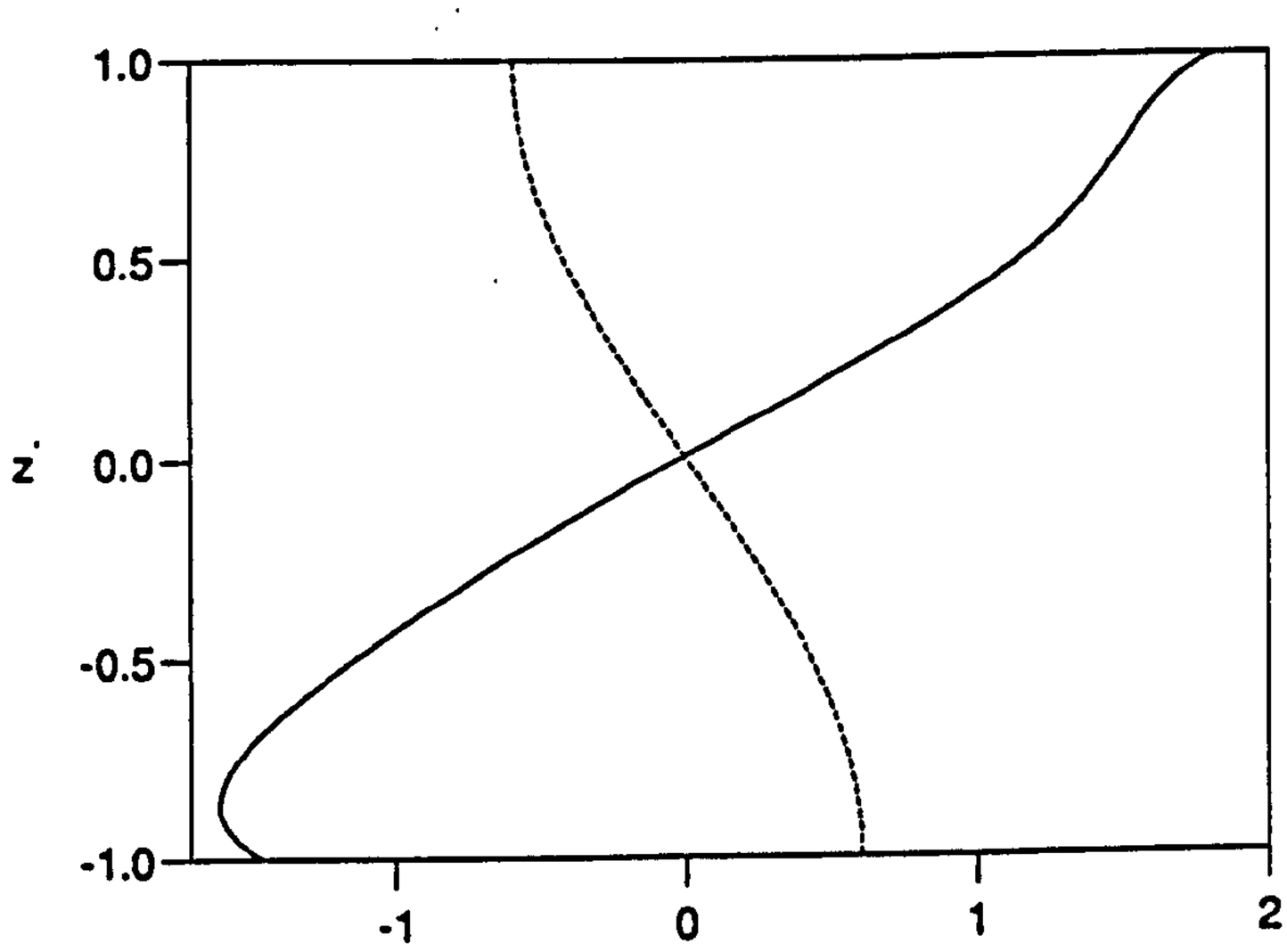

(a)

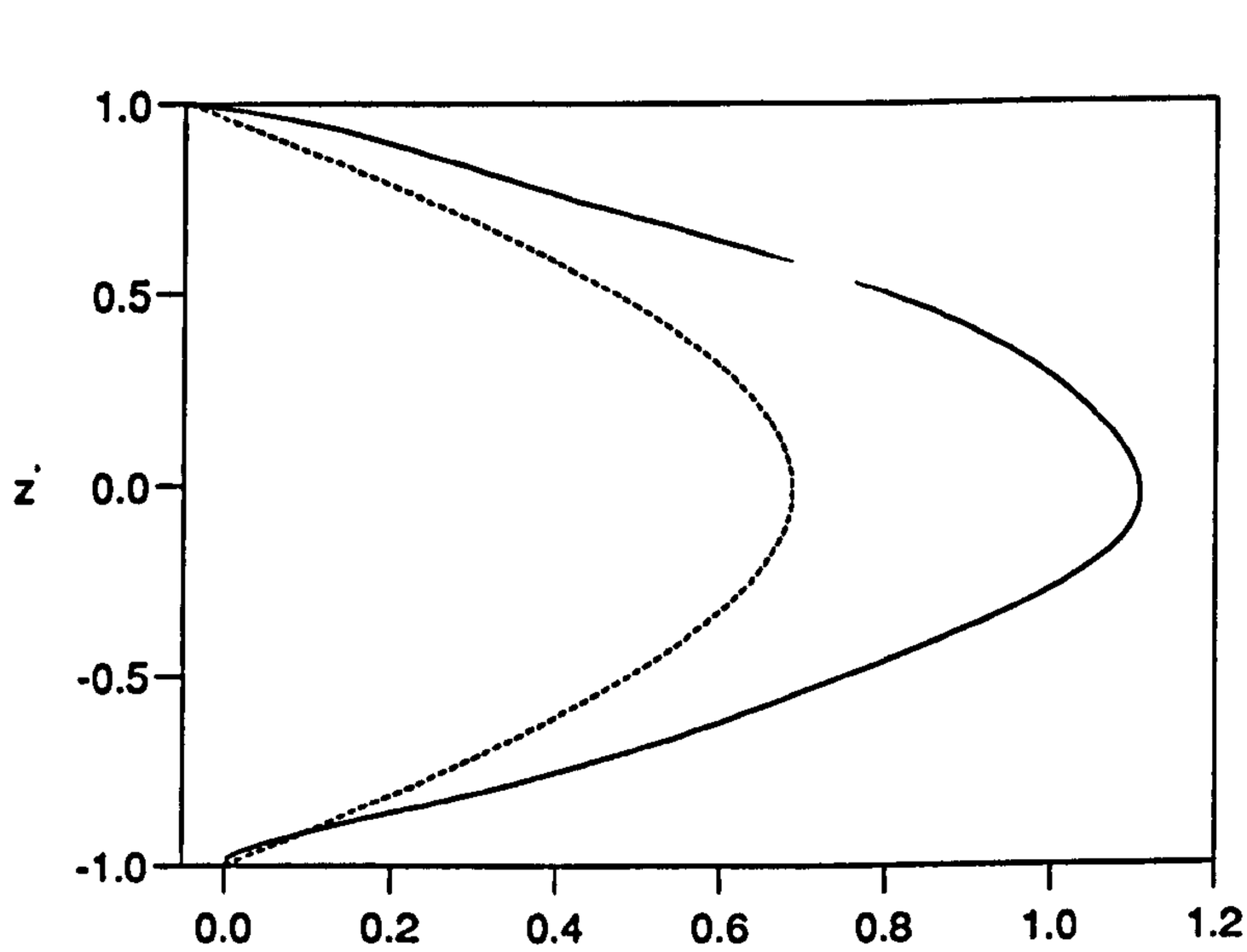

(b)

Figure 5.19: As in figure 5.18, but showing (a) $U_{y,-1}(z)$ (——), $U_{y1}(z)$ (- - -), (b) $W_{-1}(z)$ (——), $W_1(z)$ (- - -).

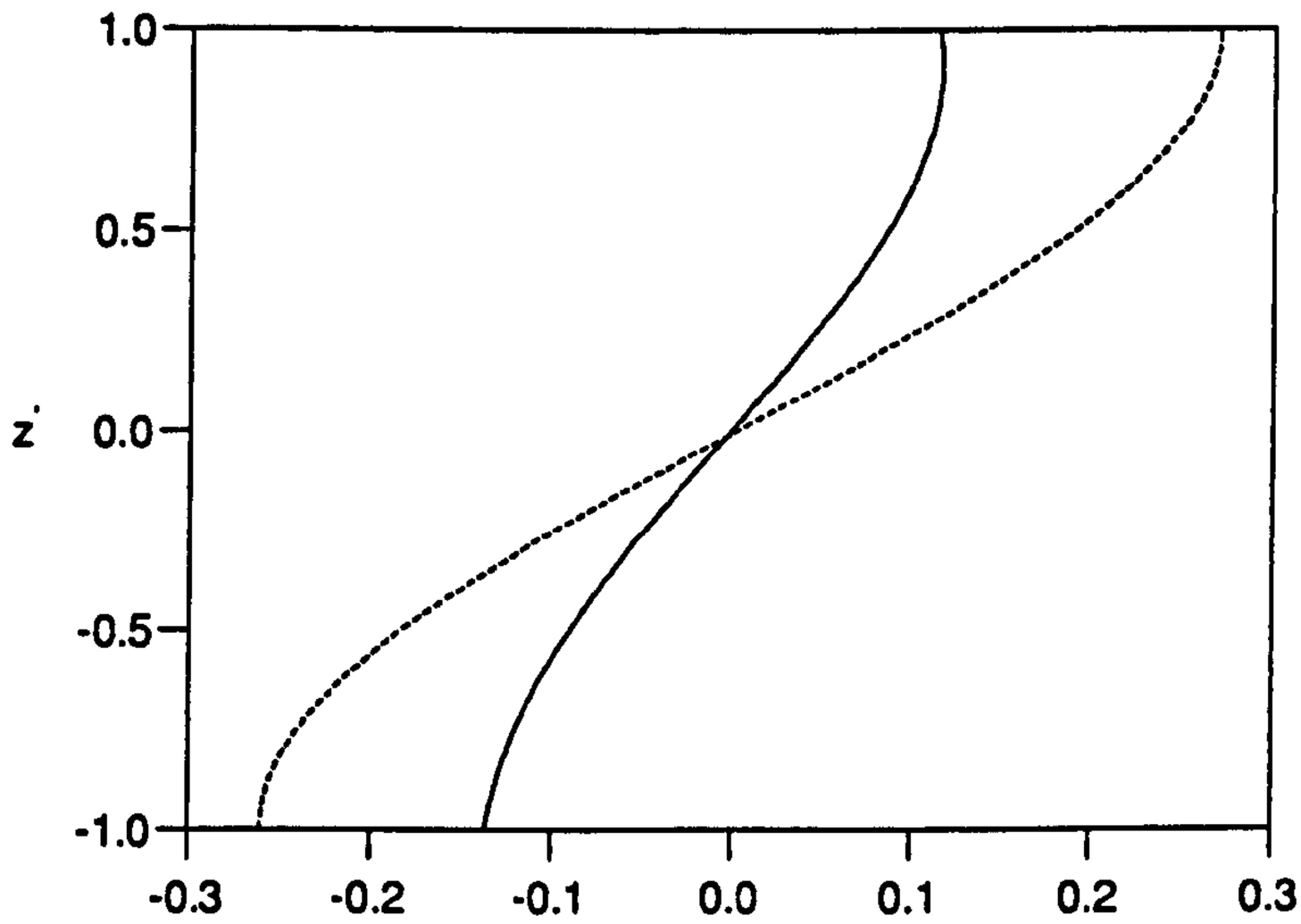

(a)

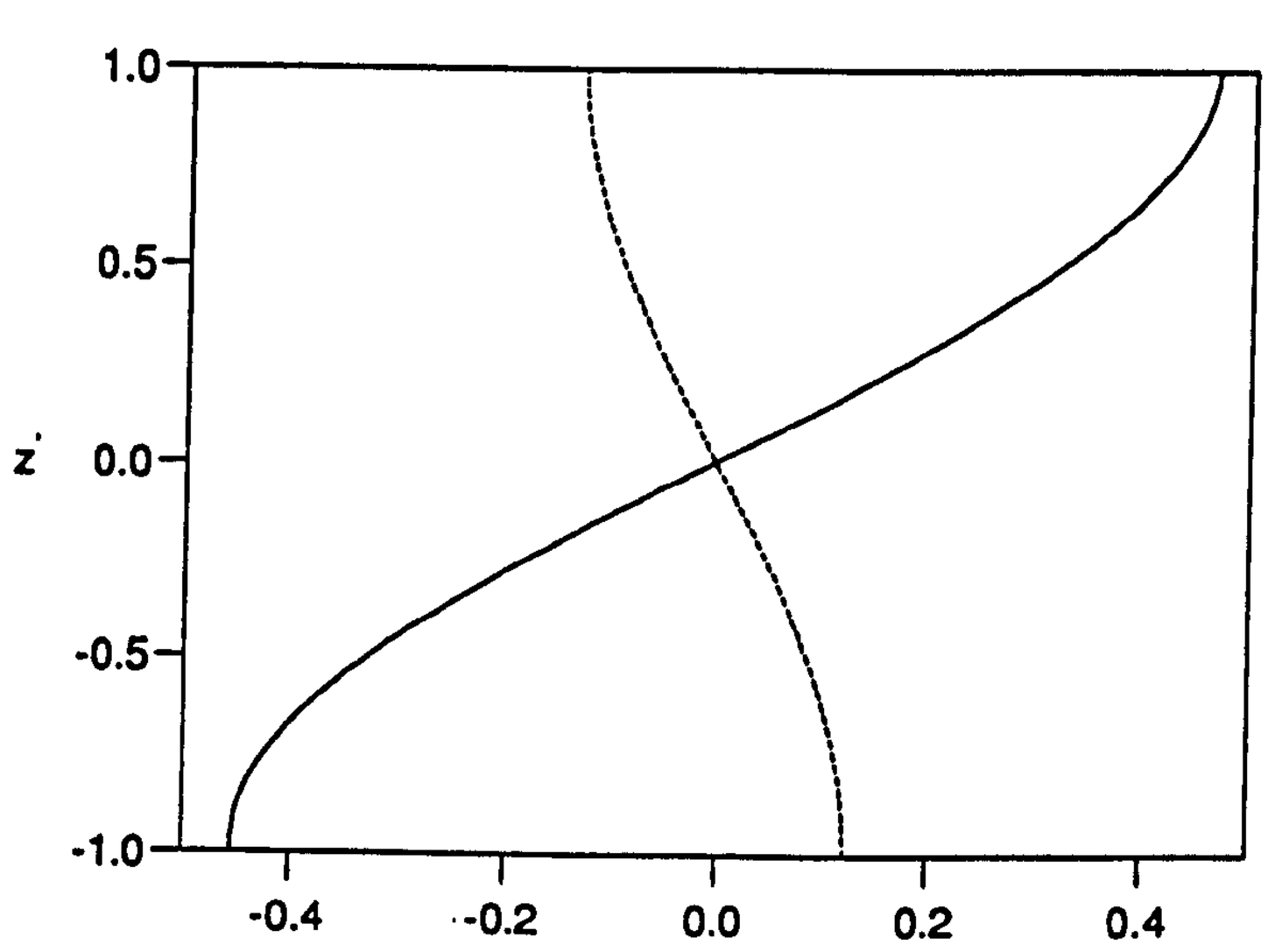

(b)

Figure 5.20: As in figure 5.18, but showing (a) $B_{x,-1}(z)$ (——), $B_{x1}(z)$ (- - -), (b) $B_{y,-1}(z)$ (——), $B_{y1}(z)$ (- - -).

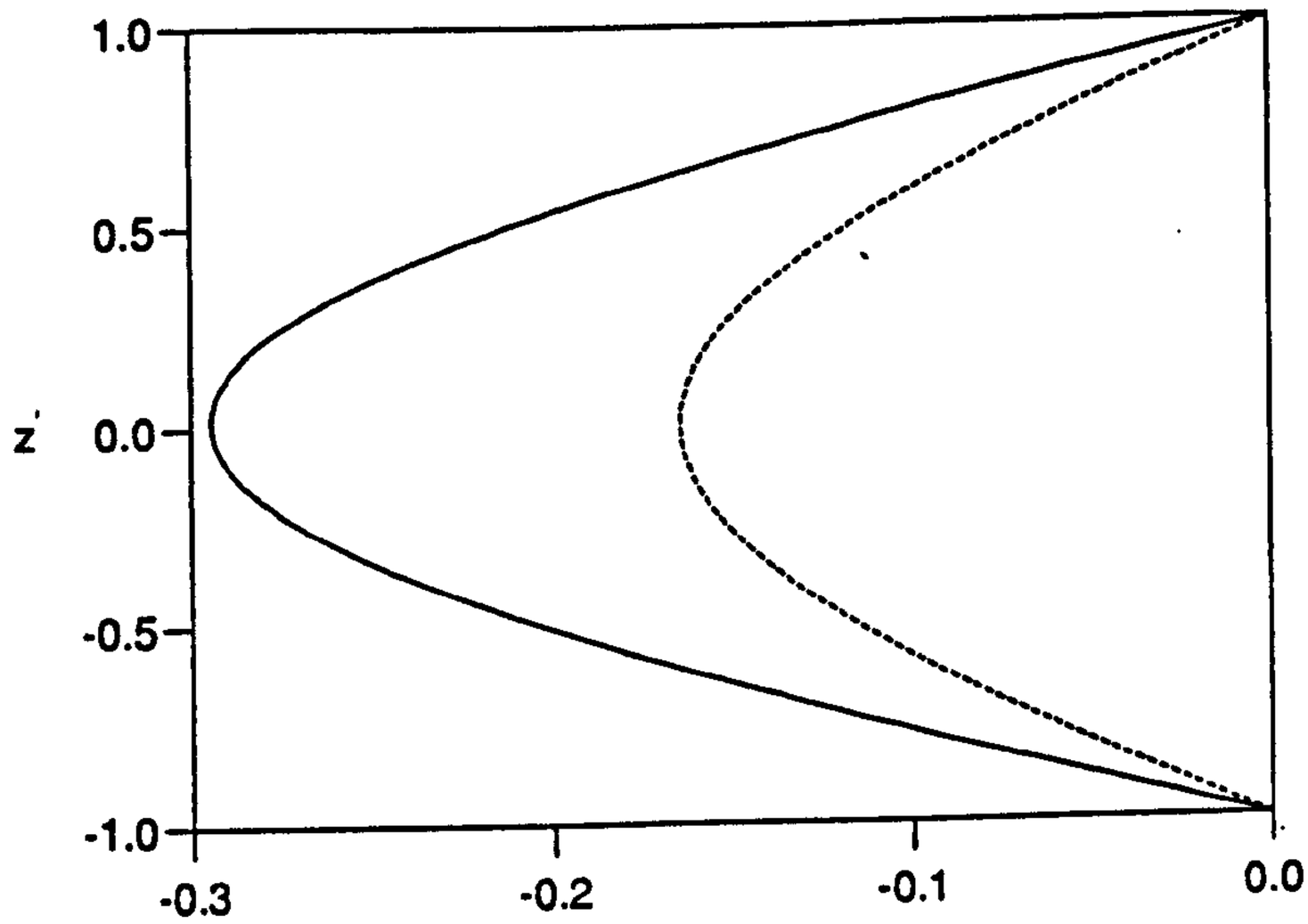

(a)

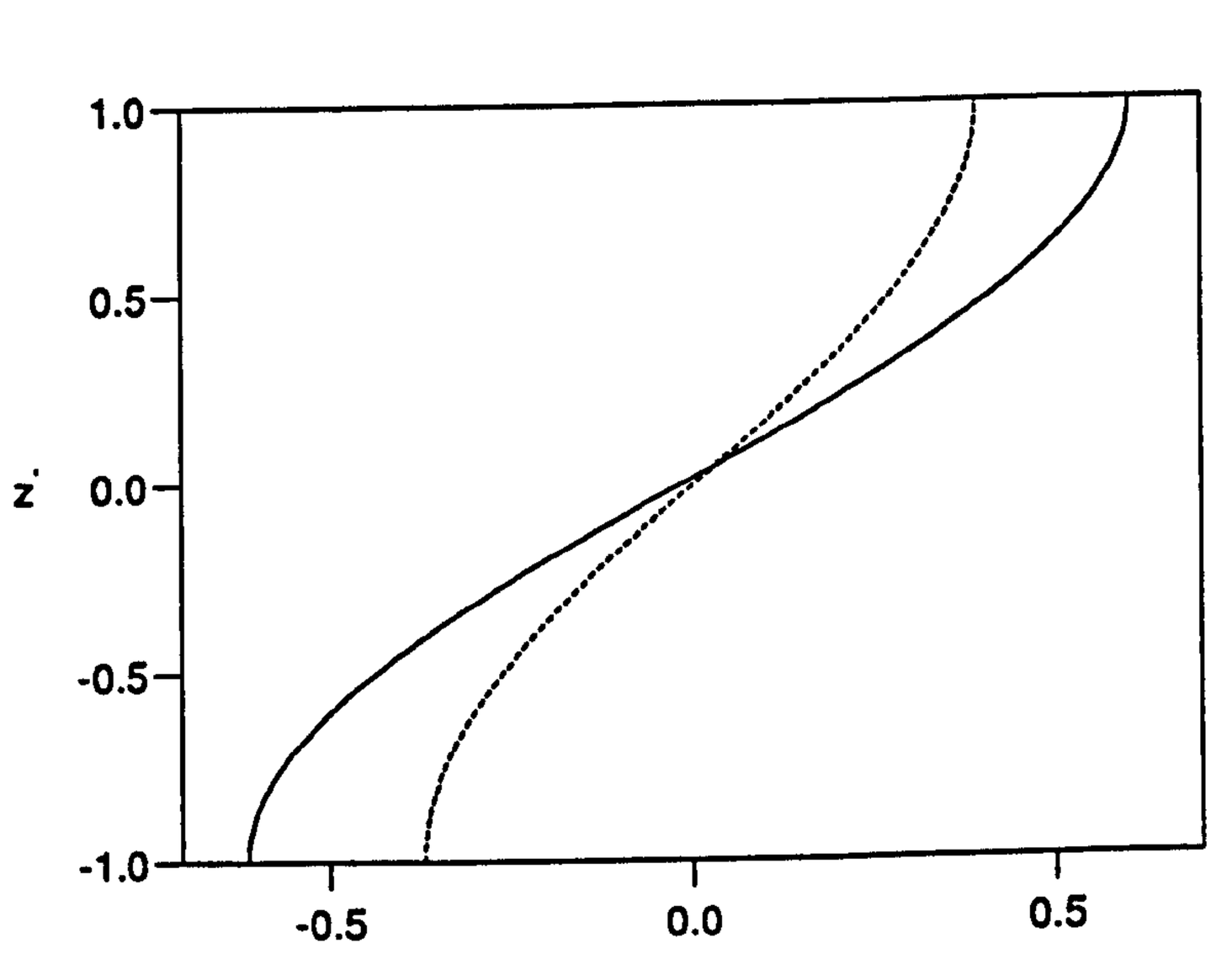

(b)

Figure 5.21: As in figure 5.18, but showing (a) $B_{-1}(z)$ (——), $B_1(z)$ (- - -), (b) $X_{-1}(z)$ (——), $X_1(z)$ (- - -).

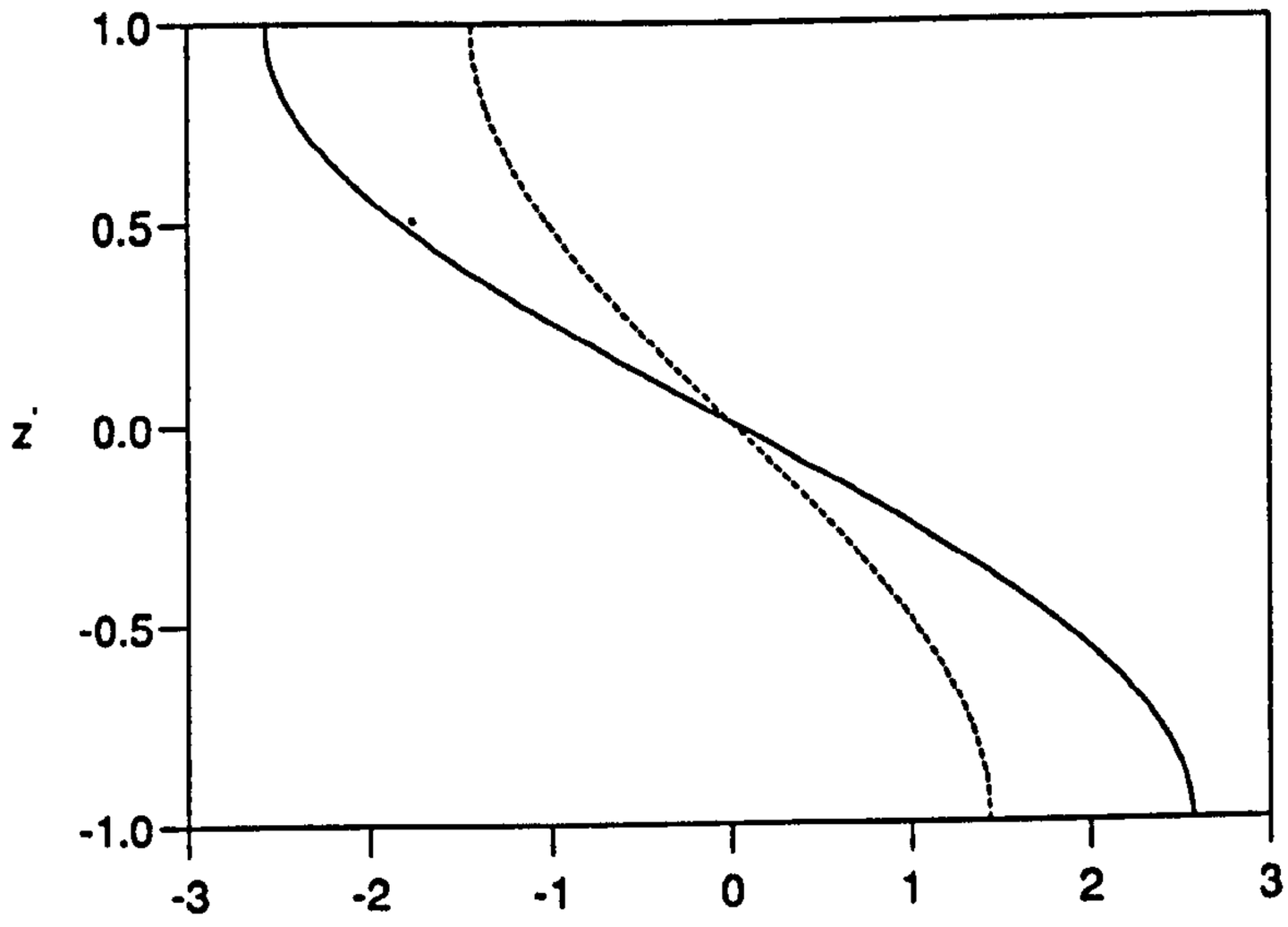

Figure 5.22: As in figure 5.18, but showing $Z_{-1}(z)$ (——), $Z_1(z)$ (- - -).

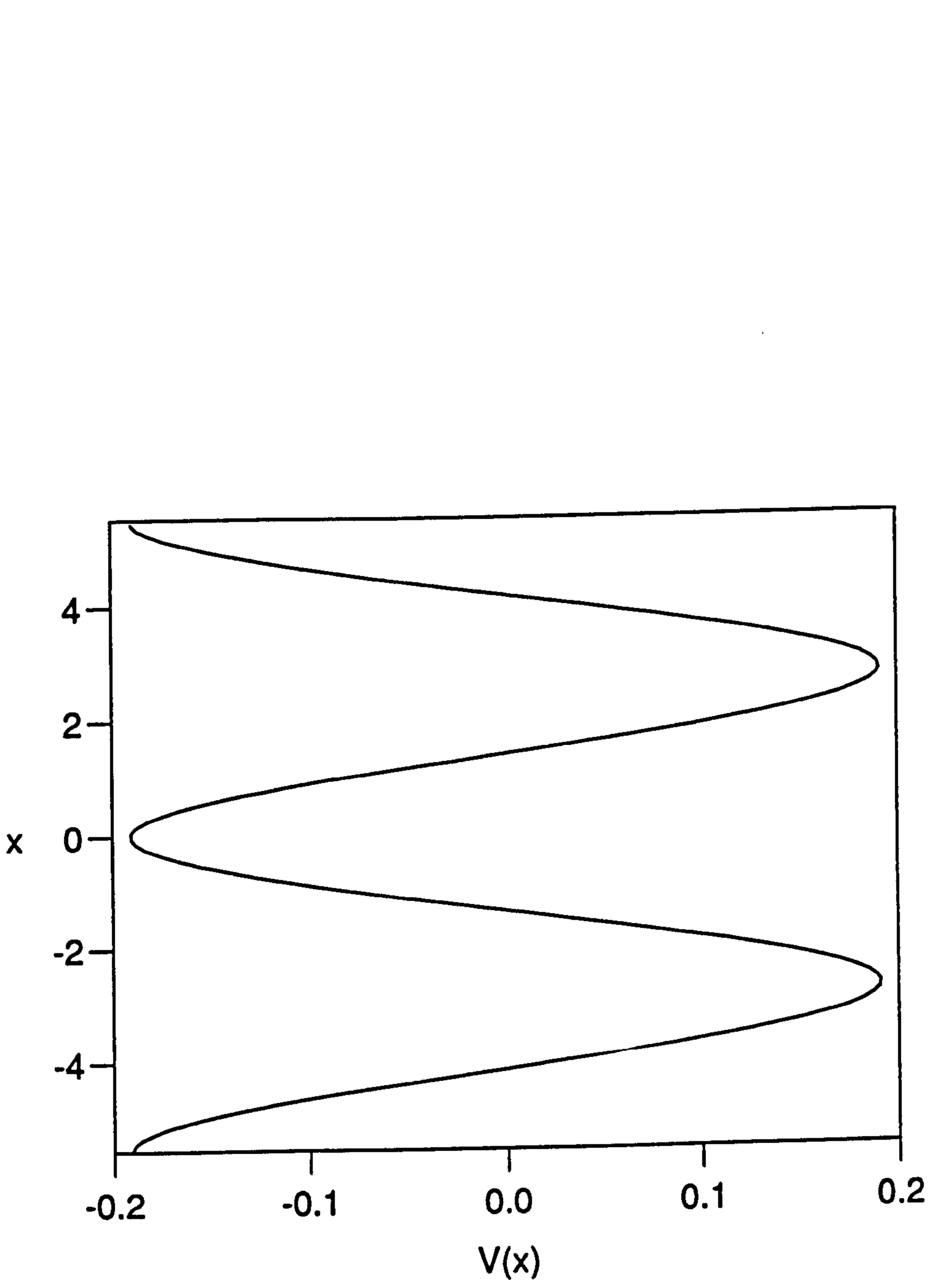

Figure 5.23: $V(x)$ against x at $R = R_2(0.1)$, $\Gamma = 0.1$, $q = 0.1$.

perturbations with the basic state. The presence of a non-zero geostrophic flow means that the perturbations are inhomogeneously forced by the interaction of this flow with the bumps. These inhomogeneities forbid the perturbations from adopting simple sinusoidal profiles. The z-structures of these perturbations are more complicated than those of the most unstable perturbations, and this explains why these perturbations have a larger critical Rayleigh number associated with them: it takes more energy to excite a complicated z-structure.

5.5.3 The Behaviour As $\Gamma \to 0$

Examination of figures 5.14, 5.15 and 5.16 reveals that

$$R_2 \to 6\sqrt{3} = R_1 \quad \text{as} \quad \Gamma \to 0.$$

This occurs because in this limit, the effects of the geostrophic flow upon the second most unstable perturbations vanish, since

$$V_p \to 0 \quad \text{as} \quad \Gamma \to 0.$$

The reduced effect of V_p allows the second most unstable perturbations to adopt simpler z structures, while the reduced shear allows the convection to occur more easily, leading to a smaller critical Rayleigh number for these perturbations.

For small, finite Γ, the two sets of perturbations remain distinct, the most unstable perturbations being the preferred mode of instability. However, when Γ becomes zero, do the two types of perturbations coalesce to form a single, unique mode of instability? Or do they remain two distinct modes of instability, having a common critical Rayleigh number (as in the case of single and double oblique roll solutions in the standard plane layer).

It transpires that that this question does not arise at all for this problem, since Γ must remain finite and non-zero to have a solution of this problem. To see this, recall (from the definition of Γ) that

$$\Gamma = 0 \Rightarrow \gamma = 0,$$

and so zero Γ corresponds to the no bump case. But, the convective motions described here are all topographically forced, i.e. they are forced by the bumps. So, as $\Gamma \rightarrow 0$, this forcing vanishes, and the convective motions evaporate. In the no bump limit, the solution (2.24) that is being examined collapses back onto the hydrostatic conduction solution. Therefore, the solutions considered here are only valid for non-zero values of Γ.

5.6 A Check On The Numerics

To check the linear stability results quoted in the previous section, the perturbation equations were solved in the limit of small but finite Γ, i.e. for those values of Γ which satisfy

$$0 < \Gamma \ll 1. \tag{5.41}$$

The exact details of the calculation are given in Appendix B, but the main results will be discussed here.

The equations yield an analytic solution for the perturbations which takes the form of a double oblique roll,

$$\mathbf{X}_P = \{a_1 \mathbf{X}_{-1RS}(z)\} \exp(ilx - imy + i\omega_{c0}t) + \{-a_2 \mathbf{X}_{1RS}(z)\} \exp(ilx + imy + i\omega_{c0}t) + c.c., \tag{5.42}$$

where the complex constants a_1 and a_2 are defined by (B.25) and $\mathbf{X}_{\pm 1RS}(z)$ are the Roberts and Stewartson (+) and (-) oblique roll solutions defined in chapter 3. These perturbations interact with the basic state in such a way that no geostrophic flow is accelerated, so

$$V_p = 0. \tag{5.43}$$

The fact that no geostrophic flow is accelerated means that this solution is independent of Γ. That is, the solution is valid for *all* non zero values of Γ, not just for those values which satisfy (5.41).

The values of R_c and ω_c at which this solution exists are defined by (B.19) and (B.20), namely

$$\omega_{c0}^2 = 0,$$

$$R_{c0} = \frac{4(1+k^2)^2}{\Lambda m^2 k^2} + \frac{\Lambda m^2 (1+k^2)}{k^2},$$

for the exchange of stabilities case, and

$$\omega_{c0}^2 = \frac{(q-1)\Lambda^2 m^4 (1+k^2) - 4(q+1)^2(1+k^2)^2}{4q^2(1+q)^2},$$

$$R_{c0} = \frac{2}{q}\left\{\frac{4(1+q)(1+k^2)^2}{\Lambda m^2 k^2} + \frac{\Lambda m^2(1+k^2)}{k^2(1+q)}\right\}.$$

for the overstable case. These stability results are identical to those obtained by Roberts and Stewartson (1974), and quoted in chapter 3, for the stability of the hydrostatic conduction solution to perturbation by oblique convection rolls in the standard plane layer. Hence, all the stability results of chapter 3 are applicable here for the solution (5.42) and (5.43).

Hence, quoting from chapter 3, the basic state (i.e. the transverse roll forced by the bumps) loses stability to the perturbations (5.42) through the exchange of stabilites once R exceeds

$$R_c = 6\sqrt{3},$$

the critical wavenumbers being given by

$$l_c^2 = 2 - \frac{2\sqrt{3}}{\Lambda}, \quad m_c^2 = \frac{2\sqrt{3}}{\Lambda}.$$

It loses stability to (5.42) through overstability once R exceeds

$$R_c = \frac{12\sqrt{3}}{q},$$

the frequency of the perturbations being given by

$$\omega_c = \frac{9(q^2-2)}{q^2},$$

and the critical wavenumbers for this case being

$$l_c^2 = 2 - \frac{2\sqrt{3}}{\Lambda}(1+q), \quad m_c^2 = \frac{2\sqrt{3}}{\Lambda}(1+q).$$

The exchange of stabilities is preferred in the region

$$q < 2, \quad \Lambda > \sqrt{3} \quad \text{and} \quad q > 2, \quad \sqrt{3} < \Lambda \leq \sqrt{3}(1+q),$$

while overstability is preferred in the region

$$q > 2, \quad \Lambda \geq \sqrt{3}(1+q).$$

These oblique perturbations do not exist in the region

$$\Lambda \leq \sqrt{3}.$$

This is because oblique convection rolls are not supported by weak magnetic fields. As Λ is decreased towards $\sqrt{3}$, the axis of the oblique rolls become parallel to that of the transverse roll forced by the bumps, and hence, do not perturb it. For this reason, the basic state is stable to perturbation by oblique rolls for weak magnetic fields. These stability results are shown in figure 5.24.

These results can be used to check the results obtained numerically in the previous section. To do this, recall that the most unstable perturbations determined numerically (i.e. the perturbations whose z-structures were given by $\mathbf{Y}_{p1}$) have the same characteristics as the solution (5.42) determined in Appendix B. They have simple sinusoidal z-structures, obey Taylor's constraint (i.e. accelerate no geostrophic flow through interaction with the basic state) and have the same stability characteristics as the Roberts and Stewartson oblique roll solutions in the standard plane layer. Therefore, (5.42) is the analytic form of the most unstable

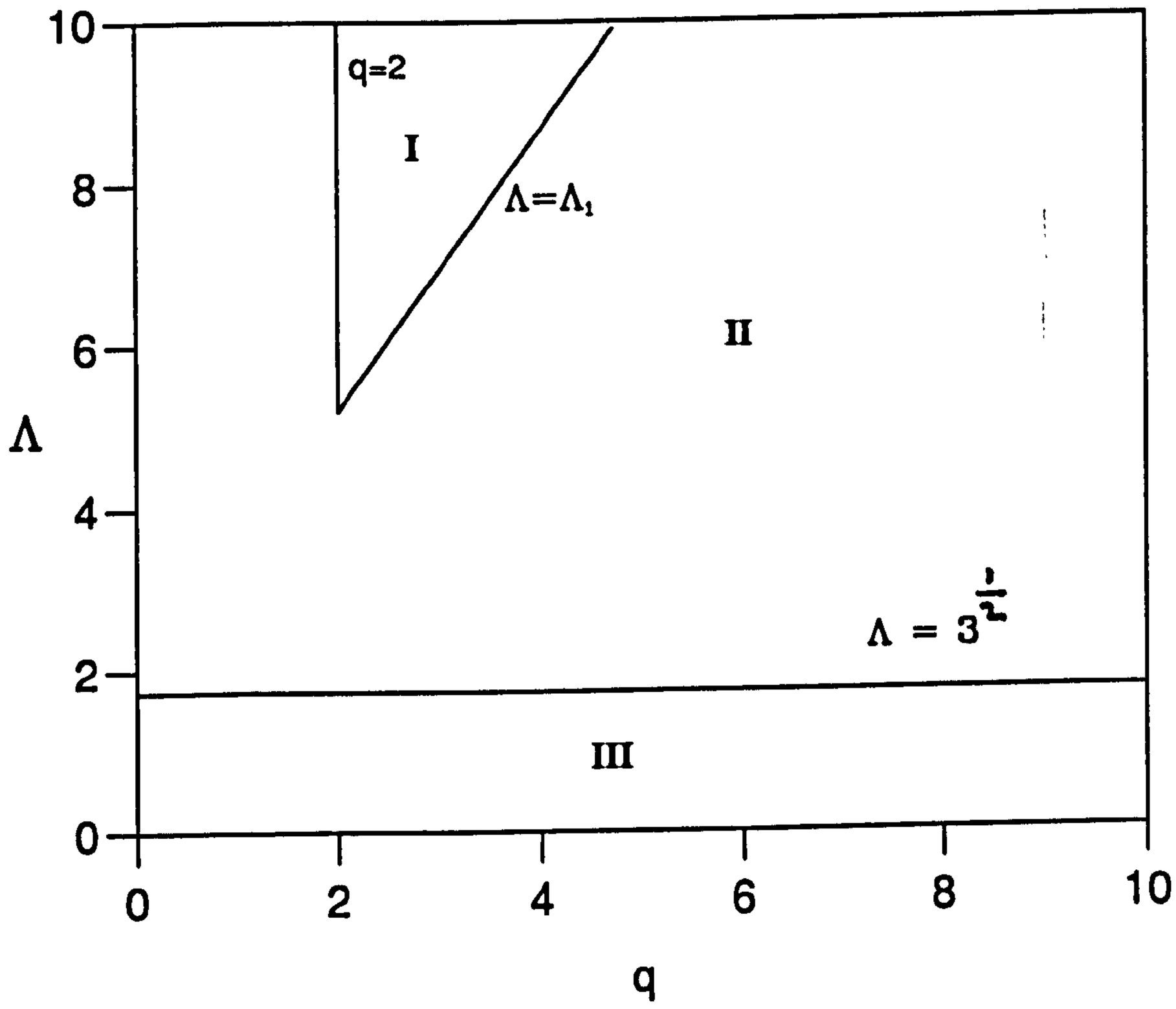

Figure 5.24: The regions of the (q, Λ) plane where the basic state loses stability to the perturbations through overstability (region I) or through the exchange of stabilities (region II). The perturbations do not exist in region III, so the basic state is stable there.

perturbations found previously. To check the numerics, therfore, the numerical results obtained previously will be compared to these analytic results at the point

$$\Lambda = 4.$$

As the stability results indicate that the exchange of stabilities is valid at this value of Λ, the critical wavenumbers are given by

$$l^2 = 2 - \frac{\sqrt{3}}{2}, \quad m^2 = \frac{\sqrt{3}}{2}. \tag{5.44}$$

This justifies a postiori the choice (5.32) made for l and m, since it has been shown that these are in fact the critical values for this stability problem. At this value of Λ, a_1 and a_2 take the values

$$a_1 = ql\Big\{(\sqrt{3}l - m)I_2^* - (\sqrt{3}m + l)I_1^*\Big\}, \tag{5.45a}$$

$$a_2 = ql\Big\{(\sqrt{3}l + m)I_2 - (l - \sqrt{3}m)I_1\Big\}, \tag{5.45b}$$

where the integrals I_1 and I_2 are defined by (B.26). Figure 5.25 shows a plot of $|a_1|^2$ and $|a_2|^2$ against q for $\Lambda = 4$.

Now, from the definitions of $\mathbf{X}_{\pm 1RS}$,

$$T_{-1} = a_1 \sin(z), \quad T_1 = -a_2 \sin(z).$$

Using this, it can be shown that

$$\frac{|a_1|^2}{|a_2|^2} = \frac{\int_0^\pi T_{-1}T_{-1}^* dz}{\int_0^\pi T_1 T_1^* dz}. \tag{5.46}$$

The quantity on the left hand side of (5.46) is plotted against q in figure 5.26(a).

The spectral approximations to $T_{\pm 1}$ are given by

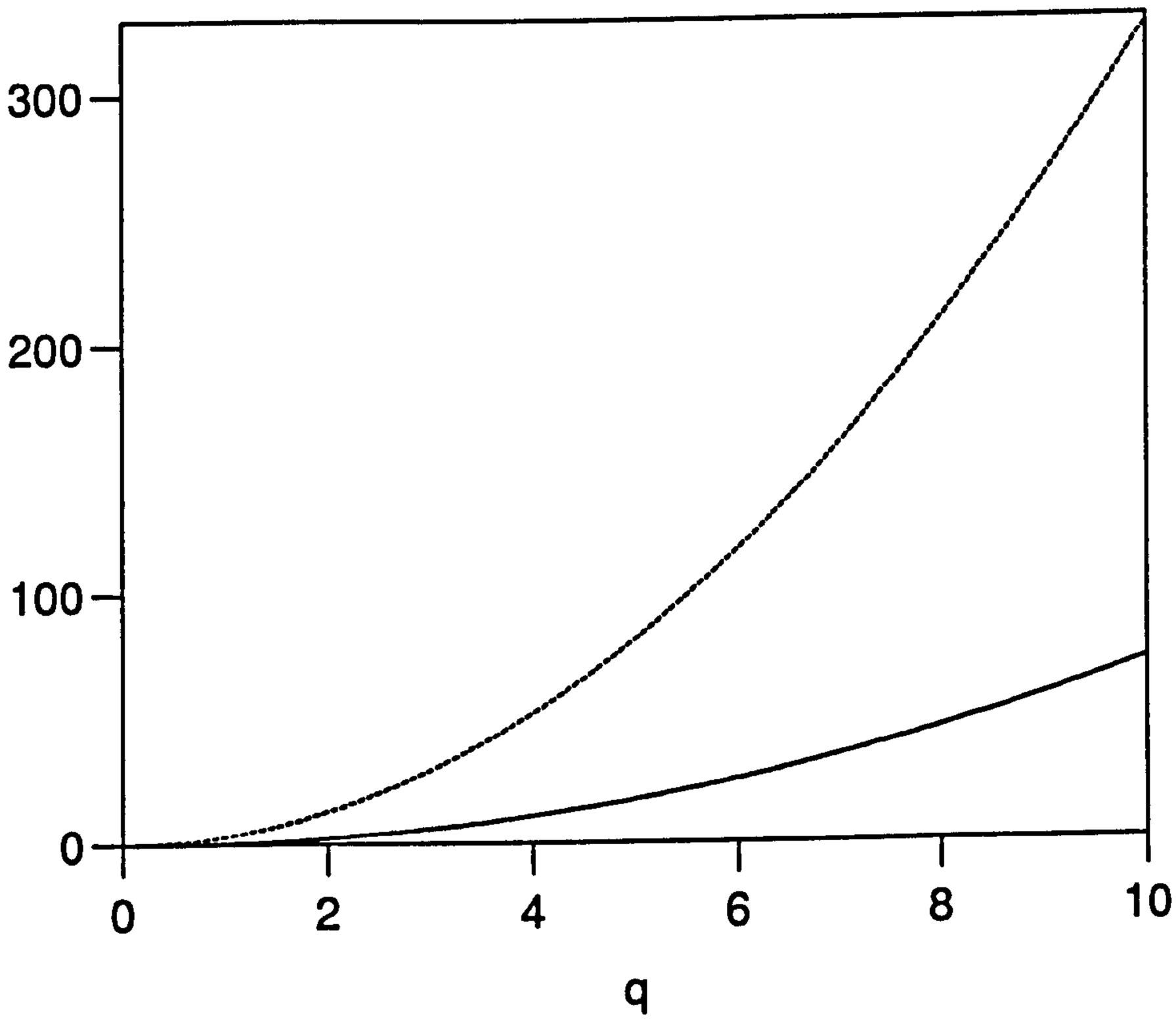

Figure 5.25: A plot of $|a_1|^2$ (—) and $|a_2|^2$ (- - -) against q for the case $\Lambda = 4$.

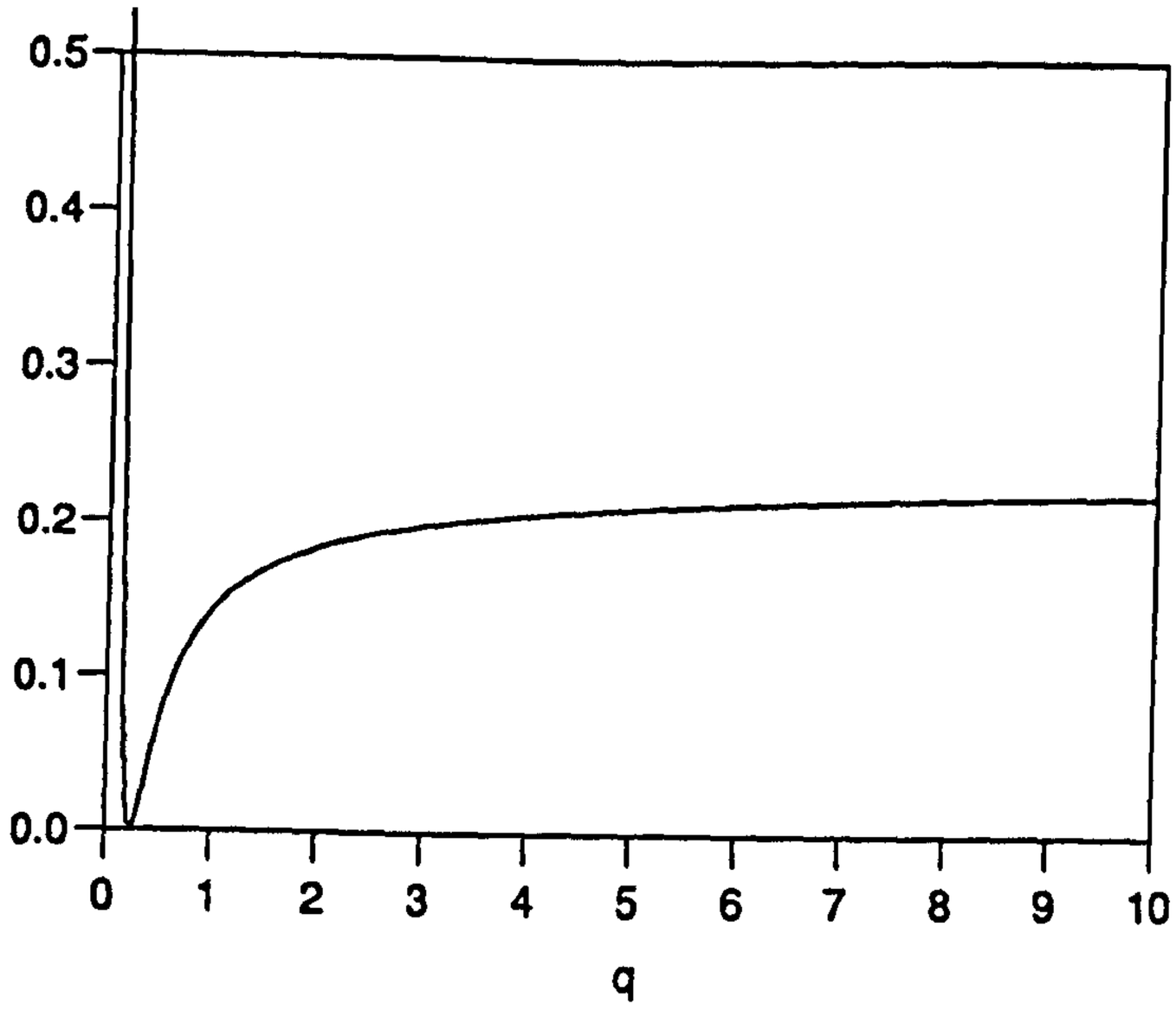

(a)

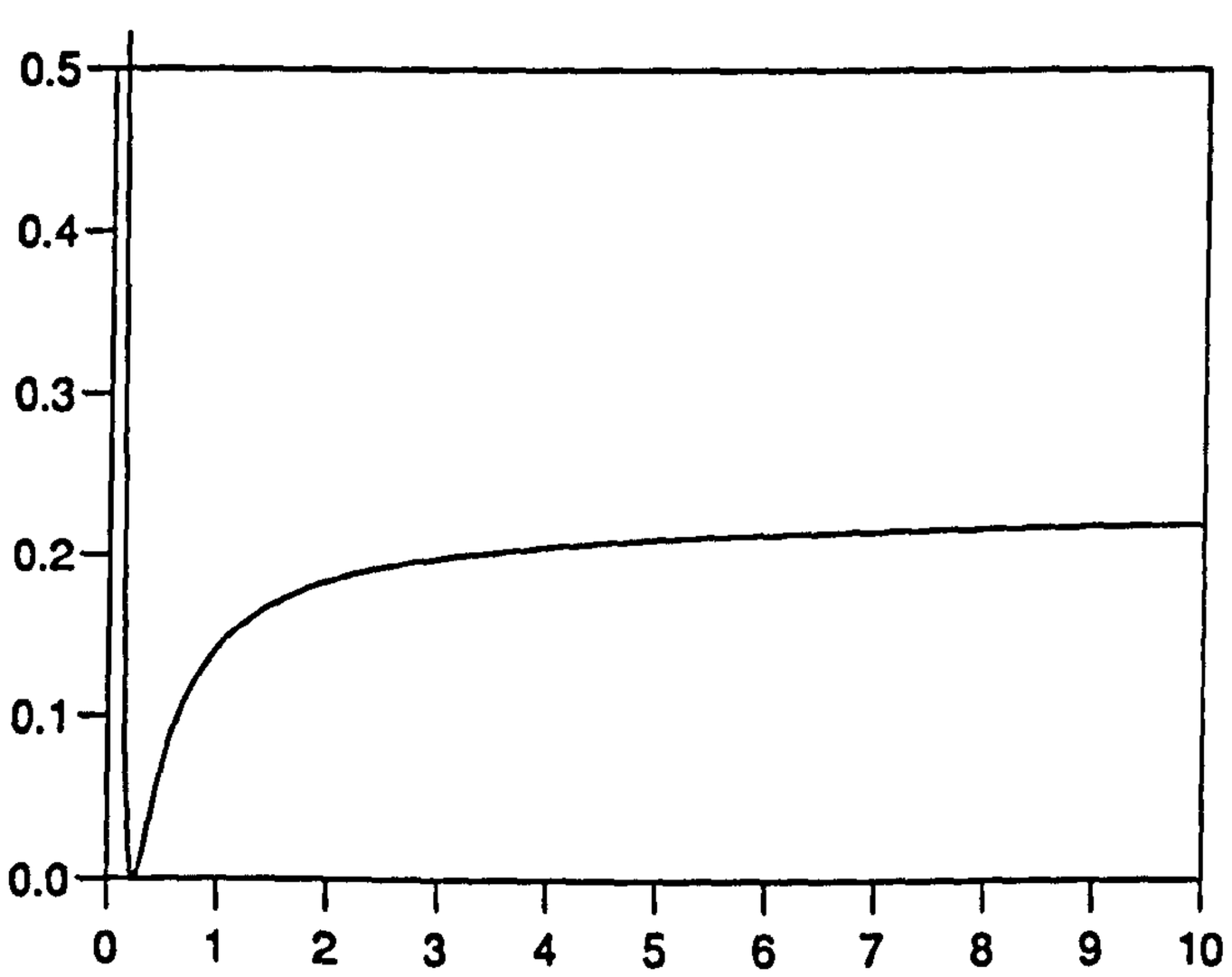

(b)

Figure 5.26: These graphs show plots of the ratio $\frac{\int_0^\pi T_{-1}T_{-1}^* dx}{\int_0^\pi T_1 T_1^* dx}$ against q, using (a) the analytic results, (b) the numerical results.

$$T_{\pm 1} = \sum_{n=0}^{N+2} T_{\pm 1n} P_n(z'),$$

where $N = 7$, P_n is the n^{th} Legendre polynomial and z' is defined by (5.14). The constants $T_{\pm 1n}$ are obtained from the eigenvector $\mathbf{Y}_{p1}$, obtained numerically. Using the orthogonality condition that holds for Legendre polynomials, it can be shown that

$$\frac{\sum_{n=0}^{N+2} \frac{|T_{-1n}|^2}{2n+1}}{\sum_{m=0}^{N+2} \frac{|T_{1m}|^2}{2m+1}} = \frac{\int_0^\pi T_{-1} T_{-1}^* dz}{\int_0^\pi T_1 T_1^* dz}. \tag{5.47}$$

The quantity on the left hand side of (5.47) is plotted against q in figure 5.26(b).

The results (5.46) and (5.47) indicate that the two curves should be identical, and this is borne out by the graphs in figure 5.26. This confirms that (5.42) is the analytic form of the most unstable perturbations obtained numerically in chapter 5. Hence, the stability characteristics of these perturbations have been determined for all values of Λ and q.

Now, the second eigensolution of (B.64) yields another solution of the perturbation equations, which again takes the form of a double oblique roll

$$\mathbf{X}_P = \{a_3 \mathbf{X}_{-1RS}(z) + \Gamma \mathbf{X}_{-11}(z) + ...\} \exp(ilx - imy) +$$

$$\{a_4 \mathbf{X}_{1RS}(z) + \Gamma \mathbf{X}_{11}(z) + ...\} \exp(ilx + imy) + c.c., \tag{5.48}$$

where a_3 and a_4 are defined by (B.78), $\mathbf{X}_{\pm 1RS}$ are the Roberts and Stewartson (+) and (-) oblique roll solutions, and $\mathbf{X}_{\pm 11}$ are the solutions of the $n = 1$ system of equations derived in Appendix B using the second eigensolution of (B.64). These perturbations interact with the basic state to accelerate a geostrophic flow of the form

$$V_p = \{\Gamma \mathcal{U}_1 + ...\} \exp(ilx) + c.c..$$

where

$$\mathcal{U}_1 = a_1 a_4 + a_2 a_3. \tag{5.49}$$

This solution has a much more complicated z-structure than the previous case considered. It is the presence of the geostrophic flow V_p which necessitates the complicated z-structure of this solution. This solution is dependent upon the value of Γ, and is only valid in the limit (5.41).

The critical Rayleigh number associated with this solution is given by

$$R_c = 6\sqrt{3} + \Gamma R_{c1} + ... \tag{5.50a}$$

where

$$R_{c1} = a_1 a_4 + a_3 a_2. \tag{5.50b}$$

Figure 5.27 shows a plot of R_{c1} against q. This graph indicates that R_{c1} is positive for each value of q. Hence,

$$R_c > 6\sqrt{3},$$

so this solution has a larger critical Rayleigh number associated with it. This is to be expected, since the shear generated by V_p suppresses convection, and makes this solution more difficult to excite. The basic state loses stability to this solution through the exchange of stabilities, since

$$\omega_c = 0 \quad \text{to} \quad O(\Gamma^2).$$

Recall that the second most unstable perturbations (i.e. the perturbations whose z-structures are given by $\mathbf{Y}_{p2}$) have the same characteristics as this solution. Consequently, this solution is the analytic form of the second most unstable perturbations. To show this, the approximation (5.50) to the critical Rayleigh number of this solution must be compared to the numerically calculated critical Rayleigh numbers associated with the second most unstable perturbations. These are given by

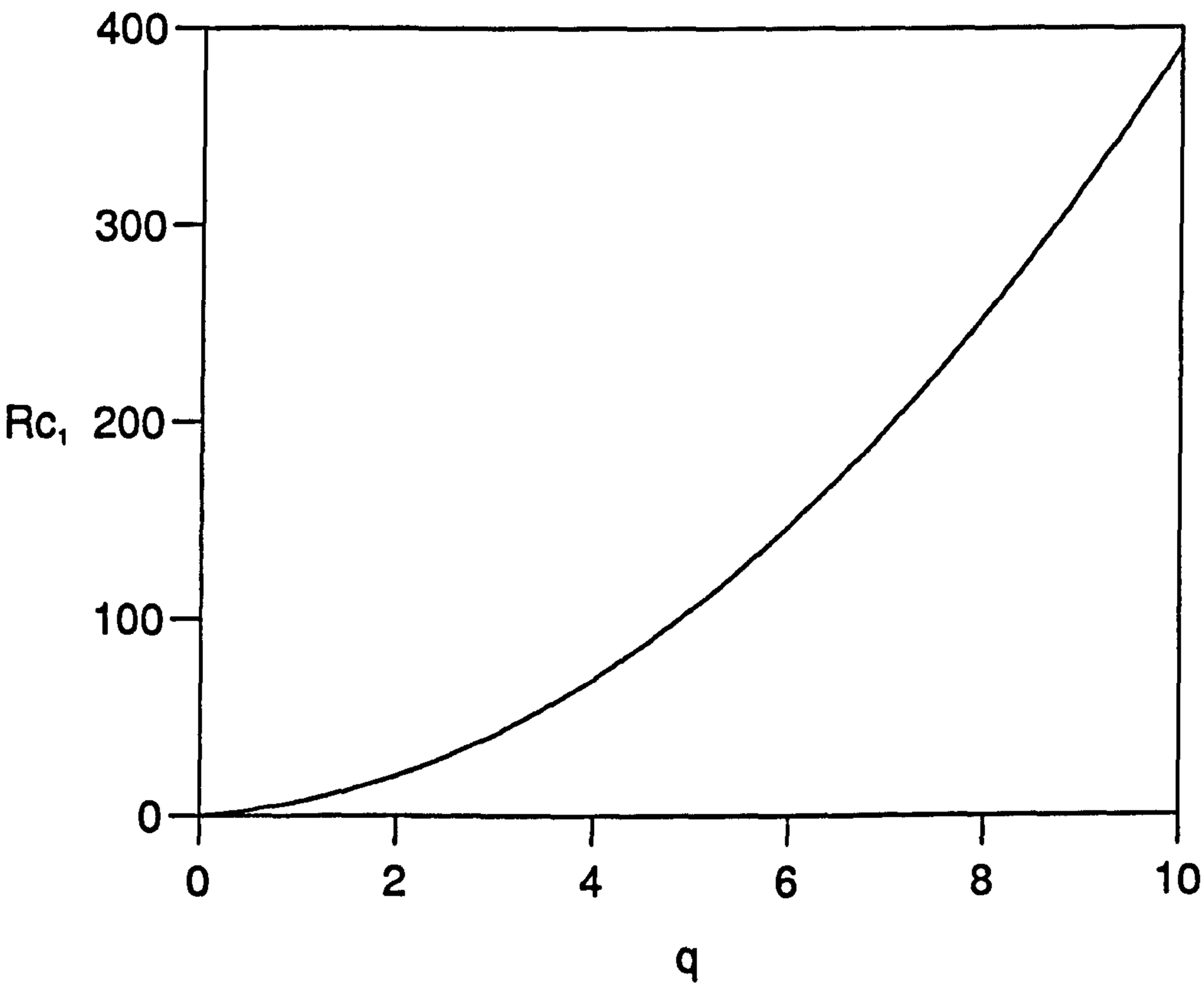

Figure 5.27: A plot of R_{c1} against q when $\Lambda = 4$.

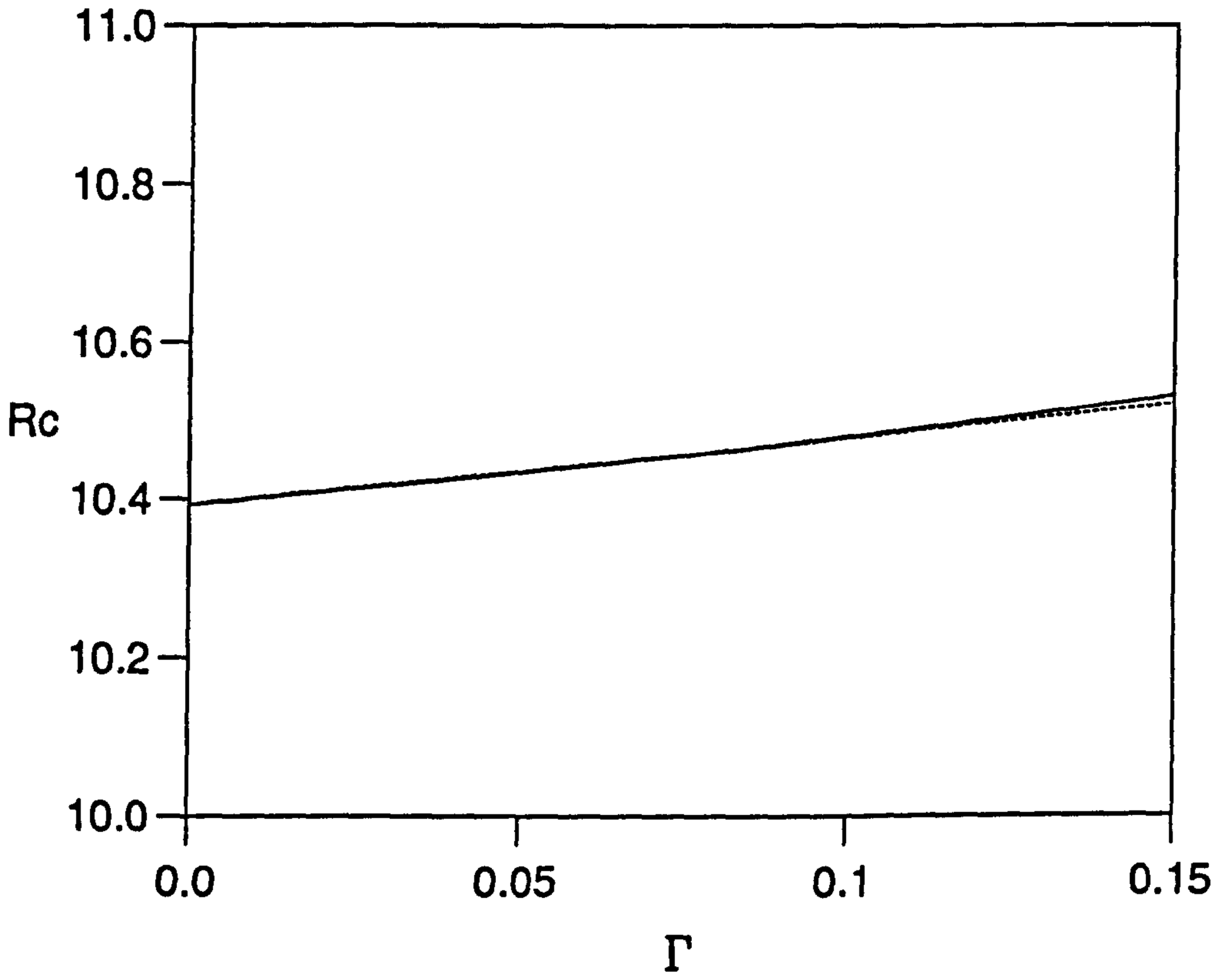

Figure 5.28: A plot of $R = R_2(\Gamma)$ (——) and $R = 6\sqrt{3} + \Gamma R_{c1}$ (- - -) against Γ for the case $q = 0.1$, $\Lambda = 4$.

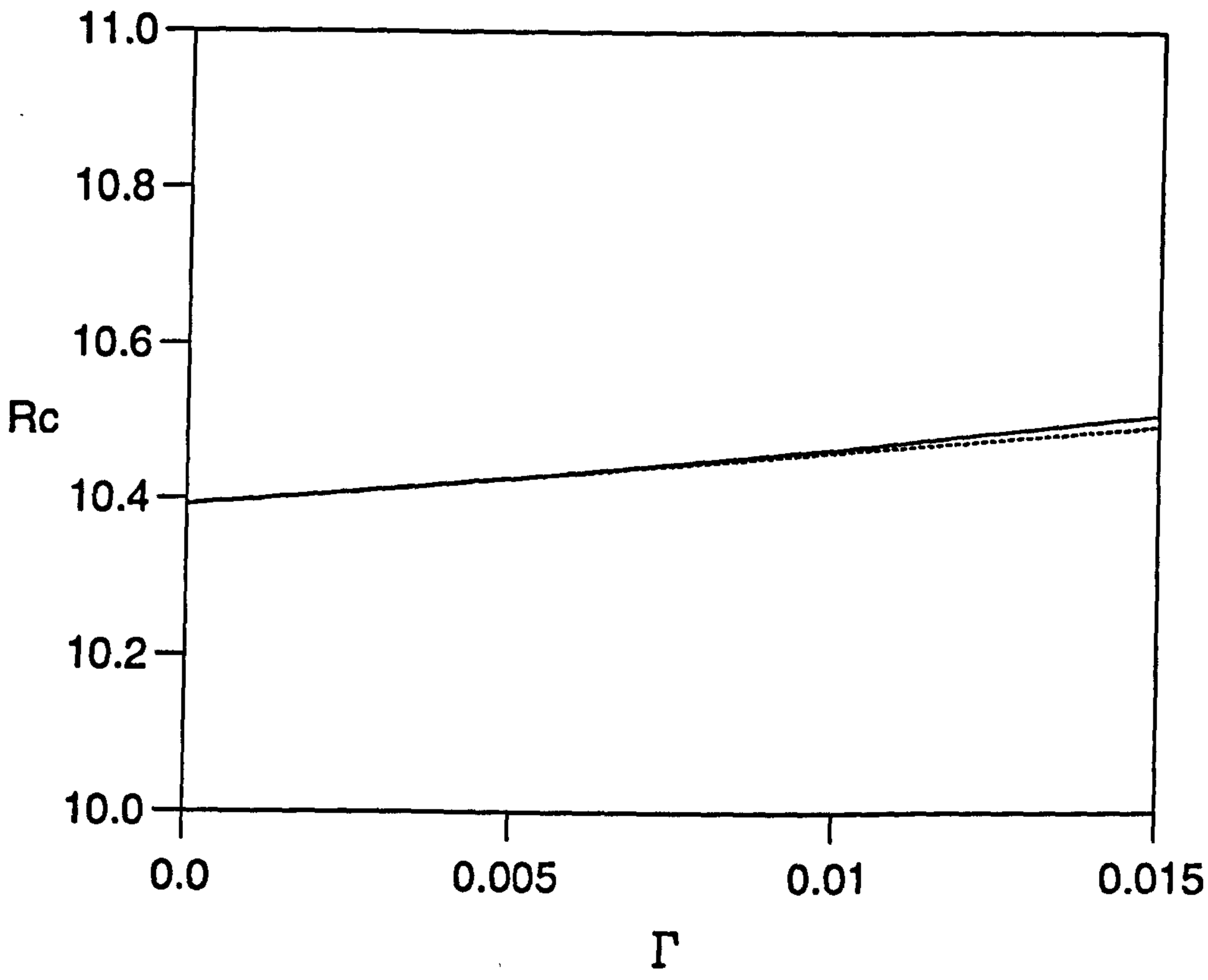

Figure 5.29: As in figure 5.28, but for $q = 1.0$.

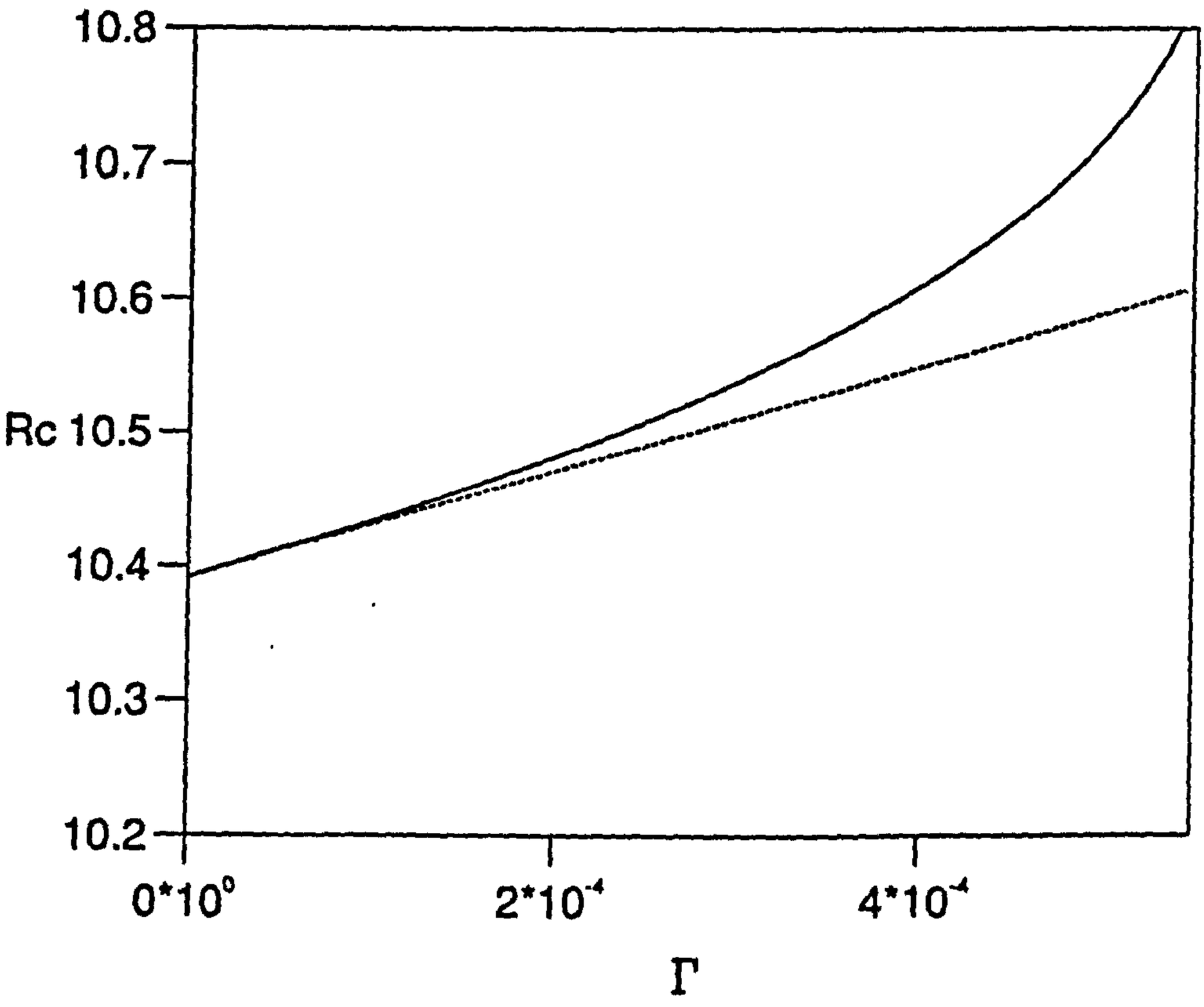

Figure 5.30: As in figure 5.28, but for $q = 10.0$.

$$R = R_2(\Gamma). \tag{5.51}$$

It is expected that (5.50) will be a linear approximation to these curves close to the $\Gamma = 0$ axis. Figures 5.28, 5.29 and 5.30 show plots of (5.50) and (5.51) close to the $\Gamma = 0$ axis for the cases

$$q = 0.1, \quad 1.0, \quad 10.0.$$

The figures show that (5.50) is indeed a linear approximation to the exact, numerically calculated critical Rayleigh numbers for the second most unstable mode, provided that Γ is small. This confirms that the solution (5.48) is the analytic form of the second most unstable linear perturbations for small values of Γ. These results confirm the accuracy of the numerical method used in chapter 5.

Chapter VI

The Nonlinear Regime

6.1 The Nonlinear Equations

To investigate the nonlinear regime that develops from the linear solutions found in chapter 5, the nonlinear terms neglected in the linear problem are restored to the governing equations. This has two main consequences. Firstly, these nonlinear terms lead to the formation of new harmonics in the x and y directions. The interaction of these new harmonics with each other produces the nonlinear behaviour that is investigated here. Secondly, Taylor's constraint is not in general satisfied in the nonlinear regime. The Maxwell stress generated by the nonlinear solutions leads to the acceleration of a geostrophic flow though Ekman suction at the boundaries. Because the shear generated by this flow is responsible for equilibrating the amplitude of the solutions, they are called Ekman solutions. The importance of these Ekman solutions lies in the fact that they may evolve in such a way that Taylor's constraint becomes satisfied. Of key importance is finding whether this occurs, and if so, how Taylor's constraint comes to be satisfied.

For geophysical values of q, namely

$$q \ll 1,$$

the results of chapter 5 indicate that the exchange of stabilities is the preferred mechanism of instability. For these values of q therefore, the nonlinear regime that develops from the linear solutions will be steady. For this reason, the oscillatory case will not be considered, since it is not relevant to the Earth's interior.

Hence, solutions of the following equations are required

$$2\frac{\partial w}{\partial z} + \Lambda\frac{\partial \xi}{\partial y} = 0, \tag{6.1a}$$

$$2\frac{\partial \zeta}{\partial z} - \Lambda\frac{\partial}{\partial y}(\nabla^2 b) - R\nabla_H^2\theta = 0, \tag{6.1b}$$

$$2V = \Gamma\Lambda q\frac{\partial}{\partial x}\Big[\frac{m}{2\pi^2}\int_0^{\frac{2\pi}{m}}\int_0^{\pi}(b_x b_y)dzdy\Big], \tag{6.1c}$$

$$qV\frac{\partial b}{\partial y} = \frac{\partial w}{\partial y} + \nabla^2 b, \tag{6.1d}$$

$$qV\frac{\partial \xi}{\partial y} = \frac{\partial \zeta}{\partial y} + \nabla^2\xi + q\Big(b_x\frac{d^2V}{dx^2} - \frac{dV}{dx}\Big(\frac{\partial b_y}{\partial y} - \frac{\partial b_x}{\partial x}\Big)\Big), \tag{6.1e}$$

$$V\frac{\partial \theta}{\partial y} = w + \nabla^2\theta, \tag{6.1f}$$

$$\nabla_H^2 b_x = -\frac{\partial^2 b}{\partial x\partial z} - \frac{\partial \xi}{\partial y}, \tag{6.1g}$$

$$\nabla_H^2 b_y = -\frac{\partial^2 b}{\partial y\partial z} + \frac{\partial \xi}{\partial x}, \tag{6.1h}$$

$$\nabla_H^2 u_x = -\frac{\partial^2 w}{\partial x\partial z} - \frac{\partial \zeta}{\partial y}, \tag{4.2i}$$

$$\nabla_H^2 u_y = -\frac{\partial^2 w}{\partial y\partial z} + \frac{\partial \zeta}{\partial x}. \tag{6.1j}$$

These are the nonlinear, time-independent equations governing the system. They are to be solved subject to the usual boundary conditions,

$$w = b = \frac{\partial \xi}{\partial z} = \theta = 0 \quad \text{on} \quad z = 0, \tag{6.2a}$$

$$w + mV\sin(my) = b + \frac{m}{q}\sin(my) = \frac{\partial \xi}{\partial z} = \theta - \cos(my) = 0 \quad \text{on} \quad z = \pi. \tag{6.2b}$$

The solutions of (6.1) and (6.2) are assumed to take the form

$$\mathbf{X} = \sum_{n=-\infty}^{\infty} \mathbf{X}_n(z)\exp(inlx + imy) + c.c., \tag{6.3a}$$

$$V = \sum_{n=-\infty}^{\infty} V_n \exp(inlx) + c.c., \tag{6.3b}$$

where

$$\mathbf{X}_n^T(z) = \Big[T_n(z) \quad W_n(z) \quad B_n(z) \quad X_n(z) \quad Z_n(z)$$

$$B_{xn}(z) \quad B_{yn}(z) \quad U_{xn}(z) \quad U_{yn}(z) \Big], \tag{6.4}$$

represents the z-structure of the n^{th} harmonic, and the V_n are complex constants. It can be seen from (6.3) that the nonlinear terms only create new harmonics in the x direction. This occurs because the nonlinear terms in the governing equations are those associated with the geostrophic flow, V. The y average in the mean Maxwell stress,

$$M = \frac{m}{2\pi^2}\int_0^{\frac{2\pi}{m}}\int_0^{\pi} B_x B_y dz dy,$$

(which is used to determine V) has the effect of removing any new harmonics created in the y direction. However, any new harmonics created in the x direction

will be retained. Since the product of V with any other quantity can therefore only create x harmonics, there are no new y harmonics introduced into the problem

Substituting (6.3) into (6.1), equations are obtained for the z structure of the n^{th} harmonic and the n^{th} coefficient of V. They are given by

$$2DW_n + \Lambda imX_n = 0, \tag{6.5a}$$

$$2DZ_n - \Lambda im(D^2 - k_n^2)B_n + Rk_n^2 T_n = 0, \tag{6.5b}$$

$$2V_n = \Gamma\Lambda qinl \sum_{p=-\infty}^{\infty} \left\{ \frac{1}{\pi} \int_0^{\pi} (B_{xp} B^*_{y,p-n}) dz \right\}, \tag{6.5c}$$

$$(D^2 - k_n^2)B_n + imW_n = \sum_{p=-\infty}^{\infty} qim(V_p + V^*_{-p})B_{n-p}, \tag{6.5d}$$

$$(D^2 - k_n^2)X_n + imZ_n = \sum_{p=-\infty}^{\infty} q(V_p + V^*_{-p})\Big[imX_{n-p} + pnl^2 B_{x,n-p} - plmB_{y,n-p}\Big], \tag{6.5e}$$

$$(D^2 - k_n^2)T_n + W_n = \sum_{p=-\infty}^{\infty} im(V_p + V^*_{-p})T_{n-p}, \tag{6.5f}$$

$$k_n^2 B_{xn} = inlDB_n + imX_n, \tag{6.5g}$$

$$k_n^2 B_{yn} = imDB_n - inlX_n, \tag{6.5h}$$

$$k_n^2 U_{xn} = inlDW_n + imZ_n, \tag{6.5i}$$

$$k_n^2 U_{yn} = imDW_n - inlZ_n, \tag{6.5j}$$

where $D = \frac{d}{dz}$ and

$$k_n^2 = n^2 l^2 + m^2.$$

Substituting (6.3) into (6.2), the boundary conditions become

$$W_n = B_n = DX_n = T_n = 0 \quad \text{on} \quad z = 0, \tag{6.6a}$$

$$W_n - \frac{im}{2}(V_n + V_{-n}^*)\{1 - \delta_{0n}\} = B_n - \frac{im}{2q}\delta_{0n} = DX_n = T_n - \frac{1}{2}\delta_{0n} = 0 \quad \text{on} \quad z = \pi, \tag{6.6b}$$

where δ_{nm} is the Kronecker delta. The form of the boundary conditions on the top boundary is indicative of the fact that different effects are forcing different harmonics. It is the interaction of the geostrophic flow V with the bumps that forces the oblique ($n \neq 0$) harmonics, while the distortion of the isotherms and vertical magnetic field by the bumps forces the transverse ($n = 0$) harmonic.

6.2 Non-Uniqueness Of Solution

Equations (6.5) and (6.6) are invariant under the transformation

$$x \longrightarrow x + \frac{\Delta}{l}, \tag{6.7}$$

where Δ is a real constant. This reflects the fact that the layer is invariant under translation in the x direction. Because of this, solutions of (6.5) and (6.6) are not unique. If

$$\mathrm{X} = \sum_{n=-\infty}^{\infty} \mathrm{X}_n(z) \exp(inlx + imy) + c.c.,$$

$$V = \sum_{n=-\infty}^{\infty} V_n \exp(inlx) + c.c.,$$

is a solution of (6.5) and (6.6), then so is

$$\mathbf{X}_\Delta = \sum_{n=-\infty}^{\infty} \left\{ \exp(in\Delta)\mathbf{X}_n(z) \right\} \exp(inlx + imy) + c.c.,$$

$$V_\Delta = \sum_{n=-\infty}^{\infty} \left\{ \exp(in\Delta)V_n \right\} \exp(inlx) + c.c..$$

To obtain unique solutions, the arbitrary phase Δ must be fixed. This is done as follows.

Recall that the z-structure of the basic state obeys the conditions (4.21), namely

$$T_0 = T_0^*,$$

$$U_{x0} = -U_{x0}^*,$$

$$U_{y0} = -U_{y0}^*,$$

$$W_0 = W_0^*,$$

$$B_{x0} = B_{x0}^*$$

$$B_{y0} = B_{y0}^*,$$

$$B_0 = -B_0^*,$$

$$X_0 = -X_0^*,$$

$$Z_0 = Z_0^*.$$

Since the arbitrary phase does not effect the transverse ($n = 0$) harmonic, it can be assumed that the transverse harmonic continues to obey (4.21) in the nonlinear regime. However, by imposing (4.21) on the transverse harmonic, it transpires that the coefficients of the nonlinear harmonics obey the following conditions.

$$T_n = \begin{cases} T_n^* & \text{n even,} \\ \\ -T_n^* & \text{n odd,} \end{cases} \tag{6.8a}$$

$$U_{xn} = \begin{cases} -U_{xn}^* & \text{n odd,} \\ \\ U_{xn}^* & \text{n even,} \end{cases} \tag{6.8b}$$

$$U_{yn} = \begin{cases} -U_{yn}^* & \text{n odd,} \\ \\ U_{yn}^* & \text{n even,} \end{cases} \tag{6.8c}$$

$$W_n = \begin{cases} W_n^* & \text{n even,} \\ \\ -W_n^* & \text{n odd,} \end{cases} \tag{6.8d}$$

$$B_{xn} = \begin{cases} B_{xn}^* & \text{n even,} \\ \\ -B_{xn}^* & \text{n odd,} \end{cases} \tag{6.8e}$$

$$B_{yn} = \begin{cases} B_{yn}^* & \text{n even,} \\ \\ -B_{yn}^* & \text{n odd,} \end{cases} \tag{6.8f}$$

$$B_n = \begin{cases} -B_n^* & \text{n odd,} \\ \\ B_n^* & \text{n even,} \end{cases} \tag{6.8g}$$

$$X_n = \begin{cases} -X_n^* & \text{n odd,} \\ \\ X_n^* & \text{n even,} \end{cases} \tag{6.8h}$$

$$Z_n = \begin{cases} Z_n^* & \text{n even,} \\ \\ -Z_n^* & \text{n odd.} \end{cases} \tag{6.8i}$$

That is, each unknown is either purely real or purely imaginary, depending on the value of n. (Note that (6.8) is also consistent with the conditions (5.47) obeyed by the perturbations found in chapter 5). By imposing (6.8) on the nonlinear solutions, the arbitrary phase the x direction will be fixed, and unique solutions will be obtained.

6.3 The Method Of Solution

The equations for the z structure of the nonlinear solutions form an infinite set of coupled nonlinear ODE's. To solve the system numerically, it is necessary to truncate the solutions in such a way that a finite number of equations is obtained. This is done by approximating the infinite series (6.3) that define the exact solutions by finite series of the form

$$\mathbf{X} = \sum_{n=-N}^{N} \mathbf{X}_n(z) \exp(inlx + imy) + c.c., \tag{6.9a}$$

$$V = \sum_{n=-N}^{N} V_n \exp(inlx) + c.c., \tag{6.9b}$$

where N is a positive integer. Under the approximation (6.9), only the $2N+1$ harmonics

$$\mathbf{X}_n(z), \quad n \in \{-N, -N+1, ..., N-1, N\},$$

and the $2N+1$ coefficients

$$V_n, \quad n \in \{-N, -N+1, ..., N-1, N\},$$

need to be determined. This is done by solving $2N+1$ sets of coupled ODE's (one set for each $n \in \{-N, -N+1, ..., N-1, N\}$) of the form

$$2DW_n + \Lambda imX_n = 0, \tag{6.10a}$$

$$2DZ_n - \Lambda im(D^2 - k_n^2)B_n + Rk_n^2 T_n = 0, \tag{6.10b}$$

$$2V_n = \Gamma\Lambda qinl \sum_{\substack{p=-N \\ |p-n|\leq N}}^{N} \left\{ \frac{1}{\pi} \int_0^{\pi} (B_{xp} B^*_{y,p-n}) dz \right\}, \tag{6.10c}$$

$$(D^2 - k_n^2)B_n + imW_n = \sum_{\substack{p=-N \\ |p-n|\leq N}}^{N} qim(V_p + V^*_{-p})B_{n-p}, \tag{6.10d}$$

$$(D^2 - k_n^2)X_n + imZ_n = \sum_{\substack{p=-N \\ |p-n|\leq N}}^{N} q(V_p + V^*_{-p}) \Big[imX_{n-p} + pnl^2 B_{x,n-p} - plmB_{y,n-p} \Big], \tag{6.10e}$$

$$(D^2 - k_n^2)T_n + W_n = \sum_{\substack{p=-N \\ |p-n|\leq N}}^{N} im(V_p + V^*_{-p})T_{n-p}, \tag{6.10f}$$

$$k_n^2 B_{xn} = inlDB_n + imX_n, \tag{6.10g}$$

$$k_n^2 B_{yn} = imDB_n - inlX_n, \tag{6.10h}$$

$$k_n^2 U_{xn} = inlDW_n + imZ_n, \tag{6.10i}$$

$$k_n^2 U_{yn} = imDW_n - inlZ_n. \tag{6.10j}$$

The boundary conditions applied for each value of n are given by

$$W_n = B_n = DX_n = T_n = 0 \quad \text{on} \quad z = 0, \tag{6.11a}$$

$$W_n - \frac{im}{2}(V_n + V_{-n}^*)\{1 - \delta_{0n}\} = B_n - \frac{im}{2q}\delta_{0n} = DX_n = T_n - \frac{1}{2}\delta_{0n} = 0 \quad \text{on} \quad z = \pi. \tag{6.11b}$$

The solution of (6.10) and (6.11) will tend to the solution of the exact problem in the limit $N \to \infty$. Therefore, provided N is made large enough, (6.9) will be a good approximation to the exact solution.

Equations (6.10) and (6.11) can be solved numerically since they constitute a finite system of equations. This is done using the Tau method in the usual manner. The harmonics to be determined are assumed to have the following spectral expansions

$$\mathbf{X}_n(z) = \begin{bmatrix} T_n(z) \\ W_n(z) \\ B_n(z) \\ X_n(z) \\ Z_n(z) \\ B_{xn}(z) \\ B_{yn}(z) \\ U_{xn}(z) \\ U_{yn}(z) \end{bmatrix} = \begin{bmatrix} \sum_{r=0}^{M+2} T_{nr} P_r(z') \\ \sum_{r=0}^{M+1} W_{nr} P_r(z') \\ \sum_{r=0}^{M+2} B_{nr} P_r(z') \\ \sum_{r=0}^{M+2} X_{nr} P_r(z') \\ \sum_{r=0}^{M} Z_{nr} P_r(z') \\ \sum_{r=0}^{M+1} B_{xnr} P_r(z') \\ \sum_{r=0}^{M+1} B_{ynr} P_r(z') \\ \sum_{r=0}^{M} U_{xnr} P_r(z') \\ \sum_{r=0}^{M} U_{ynr} P_r(z') \end{bmatrix}, \tag{6.12}$$

where M is a positive integer, and the spectral coefficients are complex constants. There are $9M + 18$ spectral coefficients to determine for each n. This gives a total of $(2N + 1)(9M + 18)$ spectral coefficients. Including the $2N + 1$ complex coefficients in the expansion for V, there are $(2N+1)(9M+19)$ complex unknowns to determine.

(6.12) is substituted into (6.10) and (6.11) using the Tau method, and the following algebraic equations for the spectral coefficients of the n^{th} harmonic and the n^{th} coefficient of the expansion of V are obtained

$$\frac{4(2r+1)}{\pi} \sum_{\substack{p=r+1 \\ p+r \text{ odd}}}^{M+1} W_{np} + \Lambda im X_{nr} = 0 \quad (0 \le r \le M), \tag{6.13a}$$

$$\frac{4(2r+1)}{\pi} \sum_{\substack{p=r+1 \\ p+r \text{ odd}}}^{M} Z_{np} - \Lambda im\left\{\frac{2(2r+1)}{\pi^2} \sum_{\substack{p=r+2 \\ p+r \text{ even}}}^{M+2} [p(p+1) - r(r+1)]B_{np} - k_n^2 B_{nr}\right\}$$

$$+ Rk_n^2 T_{nr} = 0 \quad (0 \le r \le M-1), \tag{6.13b}$$

$$\frac{2(2r+1)}{\pi^2} \sum_{\substack{p=r+2 \\ p+r \text{ even}}}^{M+2} [p(p+1) - r(r+1)]B_{np} - k_n^2 B_{nr} + imW_{nr}$$

$$= \sum_{\substack{s=-N \\ |s-n| \le N}}^{N} qim(V_s + V_{-s}^*)B_{(n-s)r} \quad (0 \le r \le M), \tag{6.13c}$$

$$\frac{2(2r+1)}{\pi^2} \sum_{\substack{p=r+2 \\ p+r \text{ even}}}^{M+2} [p(p+1) - r(r+1)]X_{np} - k_n^2 X_{nr} + imZ_{nr} =$$

$$\sum_{\substack{s=-N \\ |s-n| \le N}}^{N} q(V_s + V_{-s}^*)\Big[imX_{(s-n)r}$$

$$+ snl^2 B_{x,(s-n)r} - slmB_{y,(s-n)r}\Big] \quad (0 \le r \le M), \tag{6.13d}$$

$$\frac{2(2r+1)}{\pi^2}\sum_{\substack{p=r+2\\ p+r\ \text{even}}}^{M+2}[p(p+1)-r(r+1)]T_{np}-k_n^2T_{nr}+W_{nr}$$

$$=\sum_{\substack{s=-N\\ |s-n|\le N}}^{N} im(V_s+V_{-s}^*)T_{(n-s)r}\quad(0\le r\le M),\tag{6.13e}$$

$$k_n^2B_{x,nr}=inl\left\{\frac{2(2r+1)}{\pi}\sum_{\substack{p=r+1\\ p+r\ \text{odd}}}^{M+2}B_{np}\right\}+imX_{nr}\quad(0\le r\le M+1),\tag{6.13f}$$

$$k_n^2B_{y,nr}=im\left\{\frac{2(2r+1)}{\pi}\sum_{\substack{p=r+1\\ p+r\ \text{odd}}}^{M+2}B_{np}\right\}-inlX_{nr}\quad(0\le r\le M+1),\tag{6.13g}$$

$$k_n^2U_{x,nr}=inl\left\{\frac{2(2r+1)}{\pi}\sum_{\substack{p=r+1\\ p+r\ \text{odd}}}^{M+1}W_{np}\right\}+imZ_{nr}\quad(0\le r\le M),\tag{6.13h}$$

$$k_n^2U_{y,nr}=im\left\{\frac{2(2r+1)}{\pi}\sum_{\substack{p=r+1\\ p+r\ \text{odd}}}^{M+1}W_{np}\right\}-inlZ_{nr}\quad(0\le r\le M),\tag{6.13i}$$

$$2V_n=\Gamma\Lambda qinl\sum_{\substack{s=-N\\ |s-n|\le N}}^{N}\left\{\sum_{p=0}^{M+1}\frac{B_{x,sp}B_{y,(s-n)p}^*}{2p+1}\right\},\tag{6.13j}$$

$$\sum_{p=0}^{M+1}(-1)^pW_{1p}=0,\tag{6.13k}$$

$$\sum_{p=0}^{M+1}W_{np}=\frac{im(V_n+V_{-n}^*)}{2}(1-\delta_{0n}),\tag{6.13l}$$

$$\sum_{p=0}^{M+2}(-1)^p T_{np} = 0, \tag{6.13m}$$

$$\sum_{p=0}^{M+2} T_{np} = \frac{1}{2}\delta_{0n}, \tag{6.13n}$$

$$\sum_{p=0}^{M+2}(-1)^p B_{np} = 0, \tag{6.13o}$$

$$\sum_{p=0}^{M+2} B_{np} = \frac{im}{2q}\delta_{0n}, \tag{6.13p}$$

$$\sum_{p=0}^{M+2}(-1)^{p+1} p(p+1) X_{np} = 0, \tag{6.13q}$$

$$\sum_{p=0}^{M+2} p(p+1) X_{np} = 0. \tag{6.13r}$$

(6.13) defines $9M+19$ algebraic equations for each value of n. Therefore, a total of $(2N+1)(9M+19)$ complex algebraic equations in the $(2N+1)(9M+19)$ complex unknowns is obtained. This corresponds to a system of $2(2N+1)(9M+19)$ real equations in $2(2N+1)(9M+19)$ real unknowns.

However, applying (6.8) to eliminate the arbitrary phase in the x direction, it can be seen that exactly half of these unknowns are trivially zero, since each coefficient is either purely real (no imaginary part) or purely imaginary (no real part). Setting the relevant real or imaginary parts of each coefficient to zero to satisfy (6.8) leaves a system of $(2N+1)(9M+19)$ real algebraic equations in $(2N+1)(9M+19)$ real unknowns. These nonzero unknowns are all that are necessary to define the coefficients of the expansions of each harmonic and the coefficients of the geostrophic flow.

The algebraic equations for the coefficients of the expansions are solved using NAG routine C05NCF. To use this routine, it is necessary to input an initial guess for the values of the unknowns. The routine then uses a modification of the Powell hybrid method to find the exact solution from this guess. The correction

to the guessed solution at each iteration is found from a convex combination of the Newton-Raphson and scaled gradient directions. Under reasonable conditions, this ensures global convergence for solutions far from the exact solution and fast convergence rates. In practice however, it is necessary for the guess to be close to the exact solution in order for the routine to converge.

6.3.1 Parameter Values

In order to solve the equations, values must be assigned to the parameters of the problem, namely Λ, q, l, m, Γ and R.

The case

$$\Lambda = 4, \quad q = 1.0, \tag{6.14}$$

will be used exhaustively to discuss the results. Although the value of q lies outside the geophysical limit, it does lie in the region of the (q, Λ) plane where the exchange of stabilities is the preferred mechanism of instability, so the results will be applicable to the core. The value of q is also large enough to avoid any of the numerical problems associated will small values of q. The wavenumbers l and m are chosen to be the critical wavenumbers derived in chapter 5. That is, they are taken to be

$$l = \sqrt{2 - \frac{\sqrt{3}}{2}}, \quad m = \sqrt{\frac{\sqrt{3}}{2}}. \tag{6.15}$$

Three values of Γ are chosen, namely

$$\Gamma = 0.1, \quad 1.0, \quad \text{and} \quad 10.0. \tag{6.16}$$

This ensures that a large range of values of Γ is covered. Finally, the equations are solved over a range of values of the driving parameter R.

6.3.2 Finding Nonlinear Solutions

To find nonlinear solutions, an initial guess at the solution of equations (6.13) is required. To obtain this guess, consider the solutions of the linear stability problem

described in chapter 5. For the parameter values considered, the solutions of the linear stability problem have the form

$$\mathbf{X} = \delta \mathbf{X}^*_{-1}(z)\exp(-ilx + imy) + \mathbf{X}_0(z)\exp(imy)$$
$$+\delta \mathbf{X}_1(z)\exp(ilx + imy) + c.c., \qquad (6.17)$$

where δ is an arbitrary parameter, which in chapter 5 defined the size of the perturbations, and was there assumed to be small. Associated with (6.17) is a critical Rayleigh number R_c, at which the basic state loses stability to the linear perturbations.

Now, (6.17) can be written more compactly in the form

$$\mathbf{X} = \sum_{n=-1}^{1} \left\{ \delta^{|n|} \hat{\mathbf{X}}_n(z) \right\} \exp(inlx + imy) + c.c., \qquad (6.18)$$

where

$$\hat{\mathbf{X}}_{-1}(z) = \mathbf{X}^*_{-1}(z), \quad \hat{\mathbf{X}}_0(z) = \mathbf{X}_0(z), \quad \hat{\mathbf{X}}_1(z) = \mathbf{X}_1(z).$$

Recall from chapter 5 that the $\hat{\mathbf{X}}_n(z)$ are determined numerically using the Tau method, based on a truncation in the z direction of

$$M = 7.$$

This numerical solution for the z structure of (6.18) will be used as an initial guess for the solution of the $N = 2$, $M = 7$ nonlinear equations at values of R just greater than (or just less than) R_c, the critical Rayleigh number associated with (6.18).

However, in addition to the desired $N = 2$, $M = 7$ nonlinear solution is the solution given by

$$\mathbf{X} = \mathbf{X}_0(z)\exp(imy) + c.c., \quad V = 0, \qquad (6.19)$$

where $\mathbf{X}_0(z)$ is the solution of equations (4.6). This solution defines the basic state at R. To prevent the NAG routine from taking the initial guess onto the basic state, the parameter δ is varied until convergence to the required $N = 2$, $M = 7$ nonlinear solution is found. This nonlinear solution can then be used as a guess for solutions at higher values of N and M.

6.3.3 Truncation Analysis

It is necessary to find values for N and M so that the nonlinear solution is converged, i.e. so that any increase in N or M has no effect upon the solution. Now, it transires that the value chosen for M in the linear problem, namely

$$M = 7, \tag{6.20}$$

is also a valid choice for the nonlinear problem. Increasing M to eight has no effect upon the following truncation analysis. To find how many harmonics are needed to achieve convergence, the meansquare value of the geostrophic flow,

$$< V^2 >= \frac{l}{2\pi} \int_0^{\frac{2\pi}{l}} V^2 dx,$$

is computed at a fixed value of the Rayleigh number. Using (6.9b) and performing the integration, it turns out that

$$< V^2 >= \sum_{n=-N}^{N} |V_n + V_{-n}^*|^2. \tag{6.21}$$

This quantity is calcuated for various N at the point

$$R = 11.051,$$

and the following convergence table is obtained

N	$< V^2 >$
2	0.4687013
3	0.3784930
4	0.3792582
5	0.3752553
6	0.3743778
7	0.3743484
8	0.3743424
9	0.3743413

Table 6.1

This table shows that the solution does indeed converge as N is increased. It was decided to choose a truncation of

$$N = 6, \tag{6.22}$$

since this gives an accuracy of 5sf, which is precise enough for most purposes. This truncation gives thirteen harmonics in the x direction and requires the solution of 1088 nonlinear, algebraic equations in 1088 unknowns.

6.4 The Results

The amplitude of the nonlinear solutions will be defined by two quantities. The first of these is the meansquare heatflux generated by the nonlinear solution on the bottom boundary. This is defined as usual by

$$H = \frac{ml}{4\pi^2} \int_0^{\frac{2\pi}{l}} \int_0^{\frac{2\pi}{m}} \mathcal{F}(x, y, 0)^2 dy dx,$$

where $\mathcal{F}$ is the heatflux,

$$\mathcal{F} = \frac{\partial \theta}{\partial z} = \sum_{n=-N}^{N} DT_n(z) \exp(inlx + imy) + c.c..$$

Performing the relevant integrations it turns out that

$$H = \frac{2}{\pi^2} \sum_{n=-N}^{N} \left| \sum_{p=0}^{M+2} (-1)^{p+1} p(p+1) T_{np} \right|^2. \tag{6.23}$$

The second quantity used to define the amplitude of the nonlinear solution is the meansquare value of the geostrophic flow V, and is given by

$$< V^2 >= \sum_{n=-N}^{N} |V_n + V_{-n}^*|^2. \tag{6.24}$$

H and $< V^2 >$ will be plotted against the Rayleigh number, for each solution found. The results for the three values of Γ considered will be discussed seperately.

6.4.1 The Case $\Gamma = 0.1$

Figure 6.1 shows the bifurcation structure of the nonlinear solutions when $\Gamma = 0.1$. It is a plot of H over the complete range of R considered in this case. The dashed curve (- - -) represents the basic state. It is the meansquare heatflux generated at the bottom boundary by the transverse roll forced by the bumps (as computed in chapter 4). All the other curves in this figure represent nonlinear solutions.

The solid curve (——) represents the nonlinear evolution of the most unstable linear solution found in chapter 5. Figure 6.2(a) shows an enlargement of figure 6.1 close to the bifurcation point of this solution, while figure 6.2(b) shows the amplitude of the geostrophic flow associated with the solution. The bifurcation is subcritical, and occurs at the point $R_c^{(1)} = 10.3923$, (which is the critical Rayleigh number associated with the underlying linear solution). Because the bifurcation is subcritical, the solution exists for values of R less than those predicted by linear stability theory. In fact, the solution exists for $10.3053 \leq R \leq 10.3923$. For each value of R on this range, two solutions exist, one with a higher value of H than the other. The larger amplitude solutions constitute the upper branch of the graph. Figure 6.2(a) shows that as R in increased from $R = 10.3053$, the amplitude of the solution on the upper branch diverges, becoming infinite at the point $R_T^{(1)} = 10.3923$. Figures 6.2(b) and 6.3 (which show plots of $< V^2 >$ against R and H respectively) show how the amplitude of the geostrophic flow adjusts as the solution becomes unbounded. Together, they imply that

$$< V^2 > \rightarrow 0 \quad \text{as} \quad R \uparrow R_T^{(1)}.$$

This is the Malkus-Proctor scenario (Malkus and Proctor 1975). The geostrophic flow adjusts it's amplitude in such a way that it's influence on the magnetic field through the induction equation can enable the field to satisfy Taylor's constraint. In this case, it adjusts it's amplitude to zero as $R \uparrow R_T^{(1)}$ (see figure 6.2(b)). Because V is zero at $R = R_T^{(1)}$, the condition

$$\frac{\partial}{\partial x}\left[\frac{m}{2\pi^2}\int_0^{\frac{2\pi}{m}}\int_0^{\pi}(b_x b_y)dzdy\right] = 0 \quad \text{at} \quad R = R_T^{(1)},$$

is (trivially) satisfied, and so a Taylor state exists at $R = R_T^{(1)}$. The amplitude of the nonlinear solution becomes unbounded as the Taylor state is approached because the shear which equilibrates the solution vanishes with the geostrophic flow, and there is then nothing to control the amplitude of the solution, which increases without bound.

This solution is a Type I Ekman solution, as defined by Soward and Jones (1983). Solutions exhibiting this behaviour have been observed in various models of kinematic dynamos incorporating a geostrophic nonlinearity (see for example Ierley 1985; Hollerbach and Ierley 1991; Barenghi and Jones 1991 for the α^2 case, and Abdel-Aziz and Jones 1988 for the $\alpha\omega$ case).

The Taylor state at $R = R_T^{(1)}$ is itself interesting. As $R \uparrow R_T^{(1)}$, the amplitude of the +1 harmonic begins to diverge to infinity, while the amplitudes of the other oblique harmonics all decay to zero. The Taylor state consists of a large amplitude (+)-roll (in the notation of chapter 3), together with the finite amplitude transverse roll forced by the bumps. They are aligned in such a way that that Taylor's constraint is satisfied. This Taylor solution can be identified with the single (+)-roll Taylor solution obtained by Roberts and Stewartson (1974).

The dotted curve (.....) on figure 6.1 shows the nonlinear evolution of the second most unstable linear solution found in chapter 5 (i.e. the solution with the second largest growth rate). This solution is shown more clearly in figure 6.5. It consists of three branches: a lower branch (labelled a), an upper branch (labelled b) and a middle branch (labelled c). Figure 6.6 is a plot of the geostrophic flow amplitudes associated with each branch close to the points where branches b and c bifurcate off branch a.

Figure 6.7(a) shows an enlargement of figure 6.1 in the region of the bifurcation of branch a off the basic state, while figure 6.7(b) shows the geostrophic flow amplitude associated with branch a. The bifurcation of branch a is subcritical, and occurs at $R_c^{(2)} = 13.3230$, (which is the critical Rayleigh number associated with the underlying linear solution), and the solution again exists for values of R less than those predicted by linear stability theory.

As R is decreased from $R_c^{(2)}$, the amplitude of V adjusts it's value in such a way that this solution evolves towards a Taylor state at $R_T^{(2)} = 10.3923$. It does this exactly as previously: the amplitude of V decays to zero, removing the shear which equilibrates the solution, and therby allowing the amplitude of the solution to diverge to infinity. However, as V is zero at $R = R_T^{(2)}$, Taylor's constraint is satisfied, so the solution satisfies

$$\frac{\partial}{\partial x}\left[\frac{m}{2\pi^2}\int_0^{\frac{2\pi}{m}}\int_0^{\pi}(b_x b_y)dzdy\right] = 0 \quad \text{at} \quad R = R_T^{(2)}.$$

The Taylor state for this solution is different to the Taylor state found in the previous case, even though both Taylor states exist at the same value of R. In this case, as $R \downarrow R_T^{(2)}$, it is the amplitude of the -1 harmonic that diverges to infinity, while the amplitudes of the other oblique harmonics all decay to zero. This Taylor state therefore consists of a large amplitude (-)-roll, together with the finite amplitude transverse roll forced by the bumps, aligned so that Taylor's constraint is satisfied. It is the analogue of the other single roll Taylor solution (the (-)-roll Taylor solution) found by Roberts and Stewartson (1974).

Figure 6.9(a) is an enlargement of figure 6.1 in the region of the bifurcation of branch b off branch a, while figure 6.9(b) shows the amplitude of the geostrophic flow associated with branch b. The bifurcation occurs at $R_c^{(3)} = 10.4388$ (see figure 6.6). At this point, the solution is still in an Ekman state, although it is close to the Taylor state on branch a. The solutions on branch b appear to evolve to another, different Taylor state at the point $R_T^{(3)} = 10.8698$. The Malkus-Proctor mechanism allows the geostrophic flow to adjust so that it's influence on the magnetic field is precisely that which enables Taylor's constraint to be met. In order to do this, the geostrophic flow adjusts its amplitude so that

$$< V^2 > \rightarrow O(1),$$

as the Taylor state is approached, i.e. there is still a finite geostrophic flow in the Taylor state. In the Taylor state, V is determined implicitly by the requirement that it's effect on the magnetic field be precisely that which is needed to satisfy Taylor's constraint: it is no longer determined through Ekman suction. Malkus and Proctor (1975) call a V thus determined an eigenflow. As the eigenflow gets selected by the solution, and Taylor's constraint becomes satisfied, the nonlinearity of the problem (the Taylor integral) vanishes. Once this occurs, the amplitude of the nonlinear solution can no longer be determined, and the solution becomes unbounded.

However, despite the fact that the amplitude of the solutions on branch b are diverging to infinity, it is not clear whether the geostrophic flow is becoming an eigenflow - the amplitude is clearly continuing to grow as the amplitude of the solutions on branch b diverge (see figure 6.9(b) for details). Therefore, it is not possible to say with any certainty whether this is a Taylor state, or whether the solution is not fully converged on branch b. Given that the solutions on branch b are already of quite large amplitude, it seems that the latter is probably the case. It could probably be shown that this is indeed a Taylor state, and that an eigenflow is being selected, by increasing the truncation of the solution on branch b. However, this was not done, as the computing power necessary to do this was not available. Hence, we treat the solutions on branch b with caution, as it seems likely that the solution is not fully converged there.

Figure 6.10(a) shows an enlargement of figure 6.1 in the region where the final branch of this solution lies. This is branch c. The geostrophic flow amplitude associated with branch c is shown in figure 6.10(b). Branch c bifurcates off branch a at the point $R_c^{(4)} = 10.4744$ (see figure 6.6). No Taylor solutions were found on branch c. As R is increased from $R_c^{(4)}$, the solutions on branch c remain in an Ekman state, their amplitudes controlled by the shear generated by the geostrophic flow. Branch c comes to an end at the point $R_c^{(5)} = 18.9771$, where it bifurcates onto the last nonlinear solution considered, which is shown as the double dashed (– –) curve in figure 6.1. Figures 6.11(a) and 6.11(b) show how branch c bifurcates onto this solution.

The nature of the bifurcation may be understood as follows. As $R \uparrow R_c^{(5)}$, the amplitudes of the harmonics of the solutions on branch c that are not of the form

$$\exp(3inlx + imy),$$

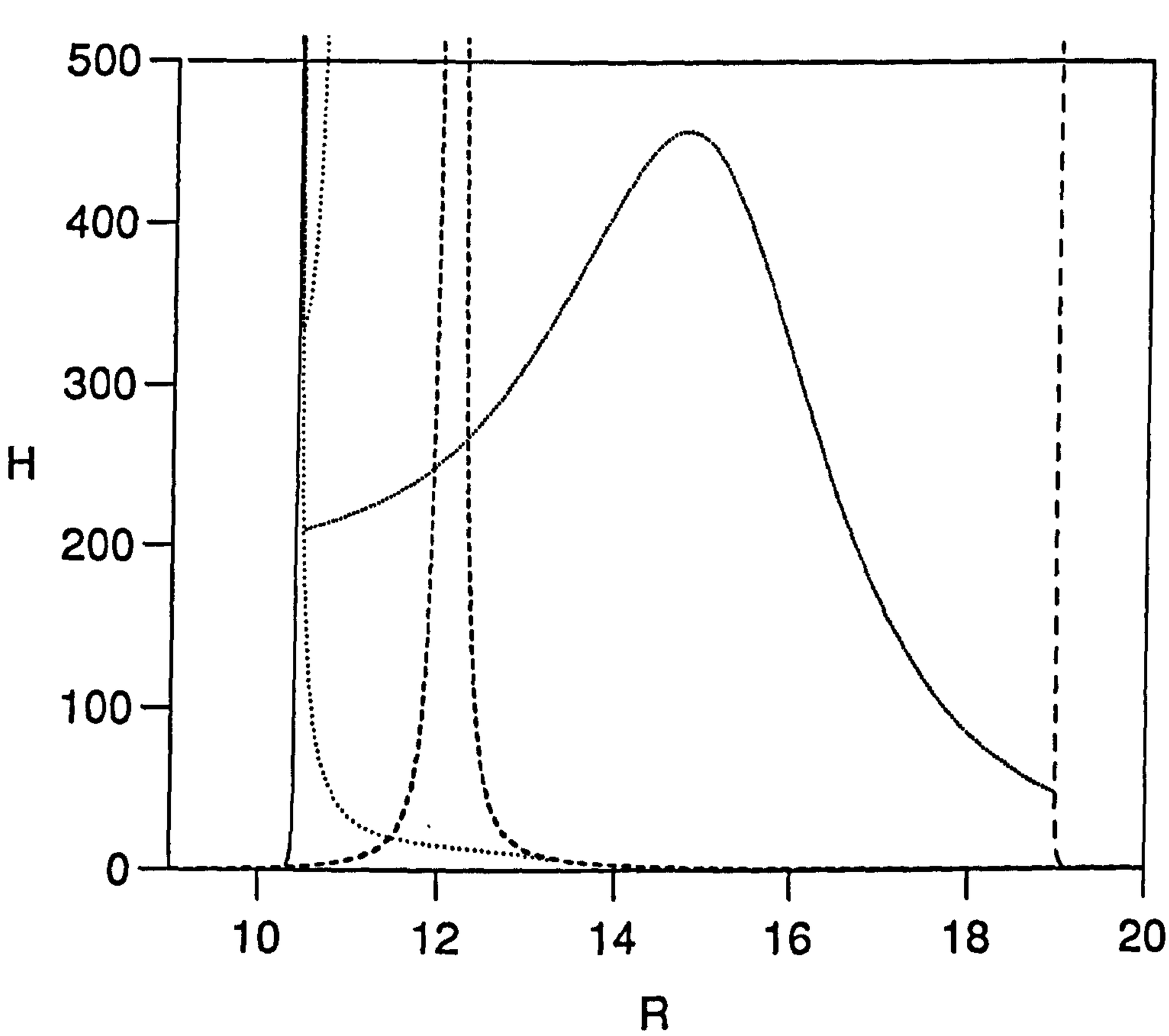

Figure 6.1: The bifurcation structure of the nonlinear solutions for the case $\Gamma = 0.1$. The curve (- - -) is the basic state, while all the other curves represent nonlinear solutions.

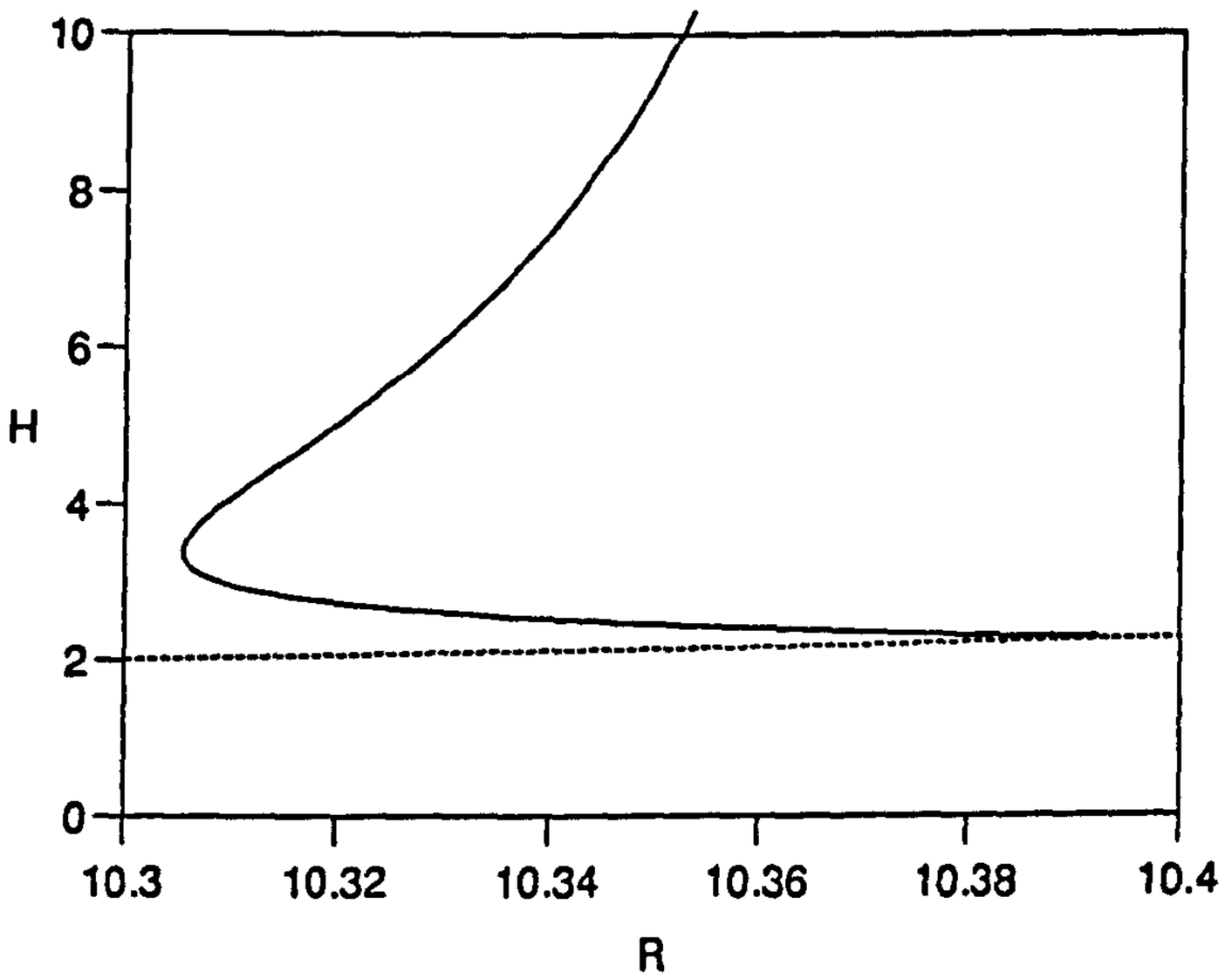

(a)

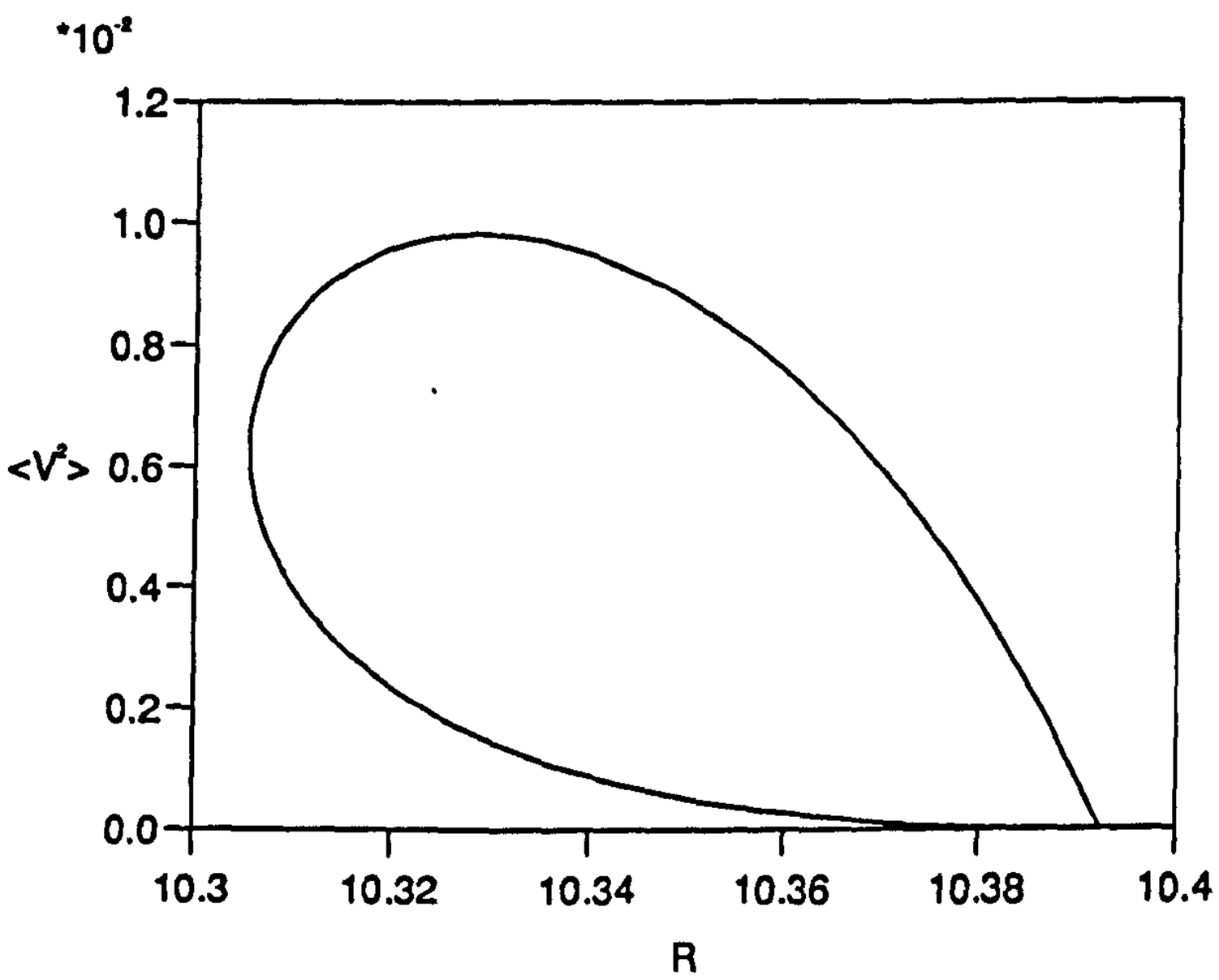

(b)

Figure 6.2: The nonlinear evolution of the most unstable linear solution when $\Gamma = 0.1$.
(a) H against R for the basic state (- - -) and this solution (——).
(b) $< V^2 >$ against R for this solution.

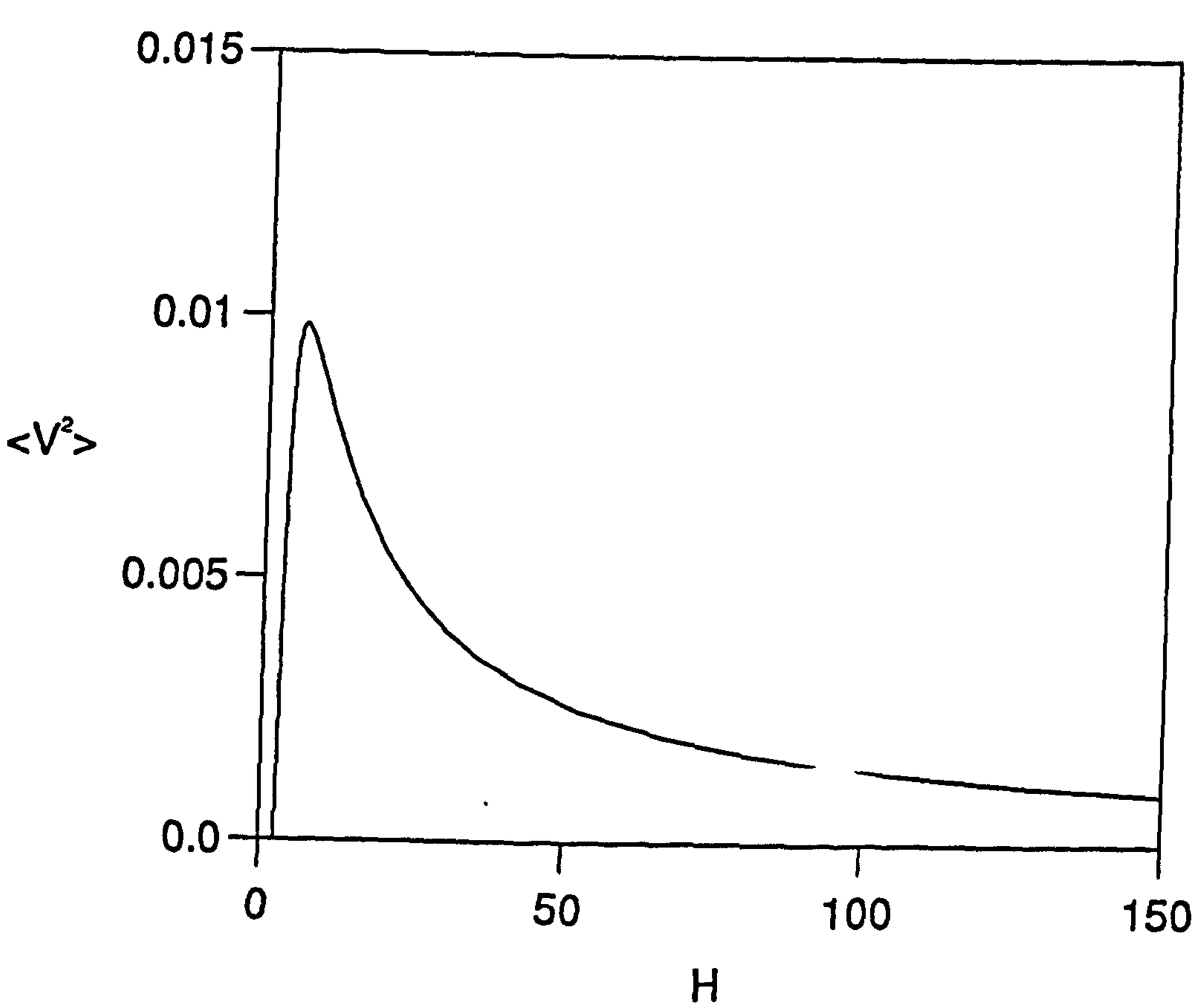

Figure 6.3: A plot of $< V^2 >$ against H for the first nonlinear solution when $\Gamma = 0.1$.

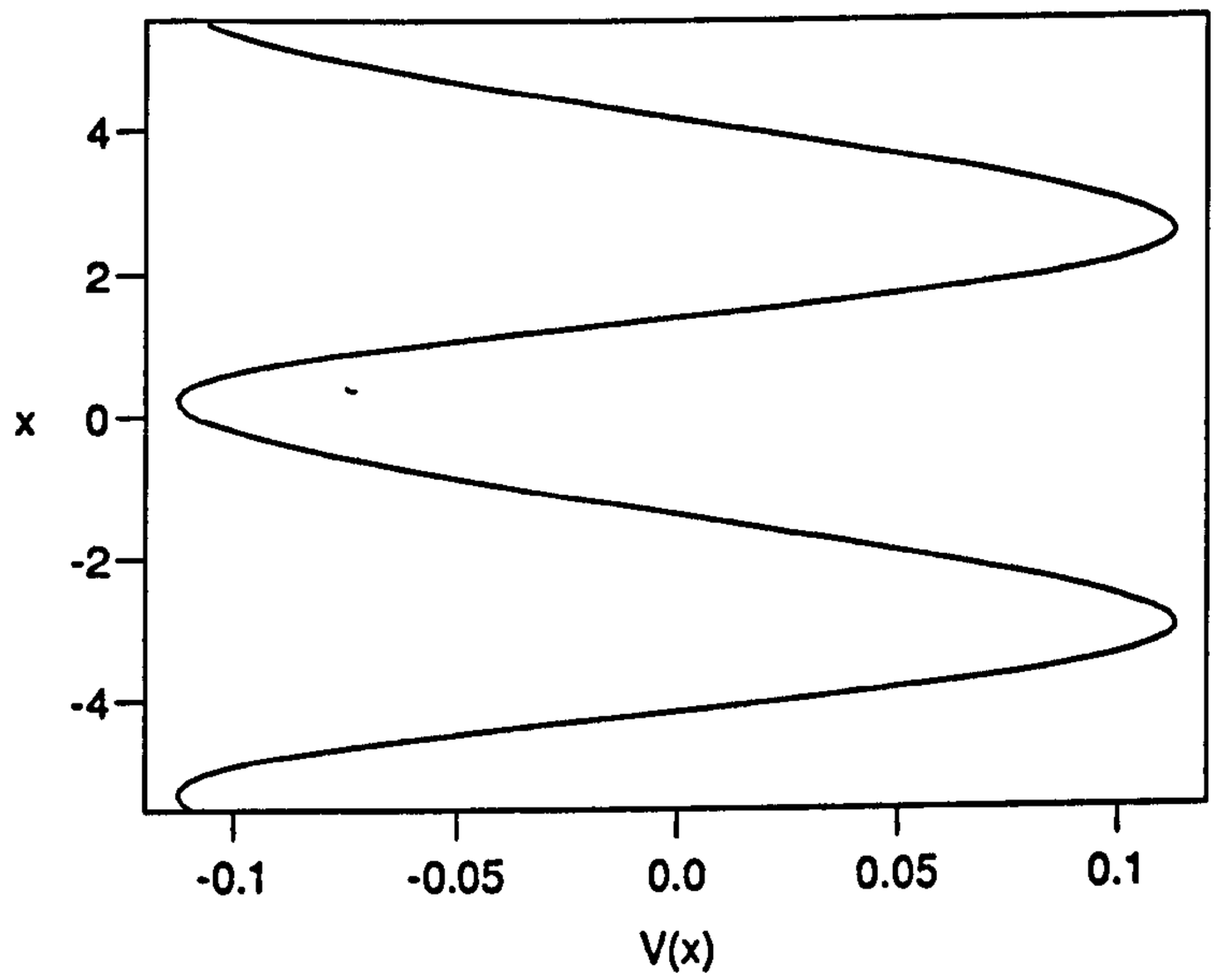

(a)

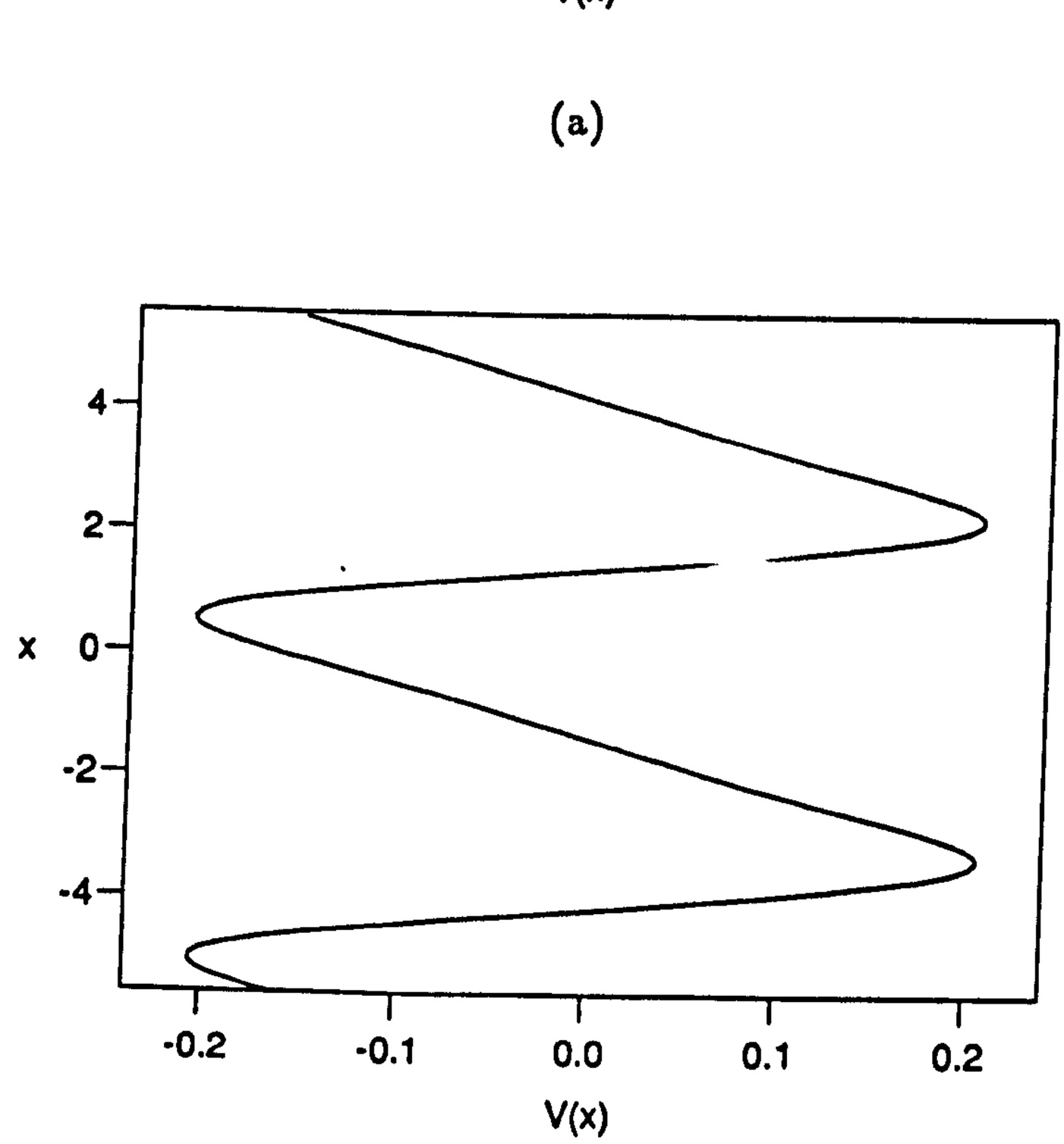

(b)

Figure 6.4: Geostrophic flow profiles for the first nonlinear solution for $\Gamma = 0.1$ when (a) $R = 10.3823$ and, (b) $R = 10.3458$, on the upper branch of the solution.

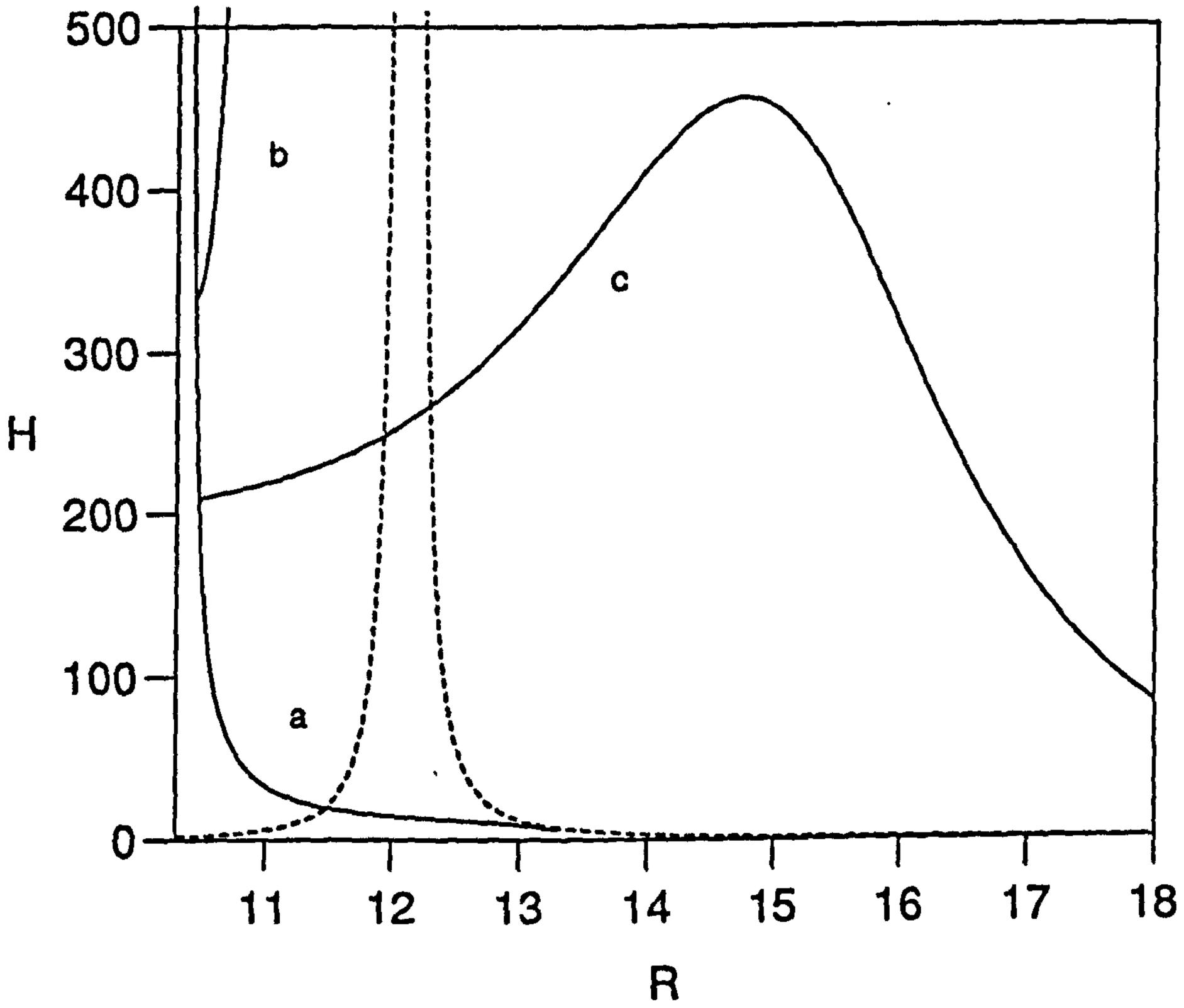

Figure 6.5: The nonlinear evolution of the second most unstable linear solution when $\Gamma = 0.1$. H against R for the basic state (- - -) and this solution (——).

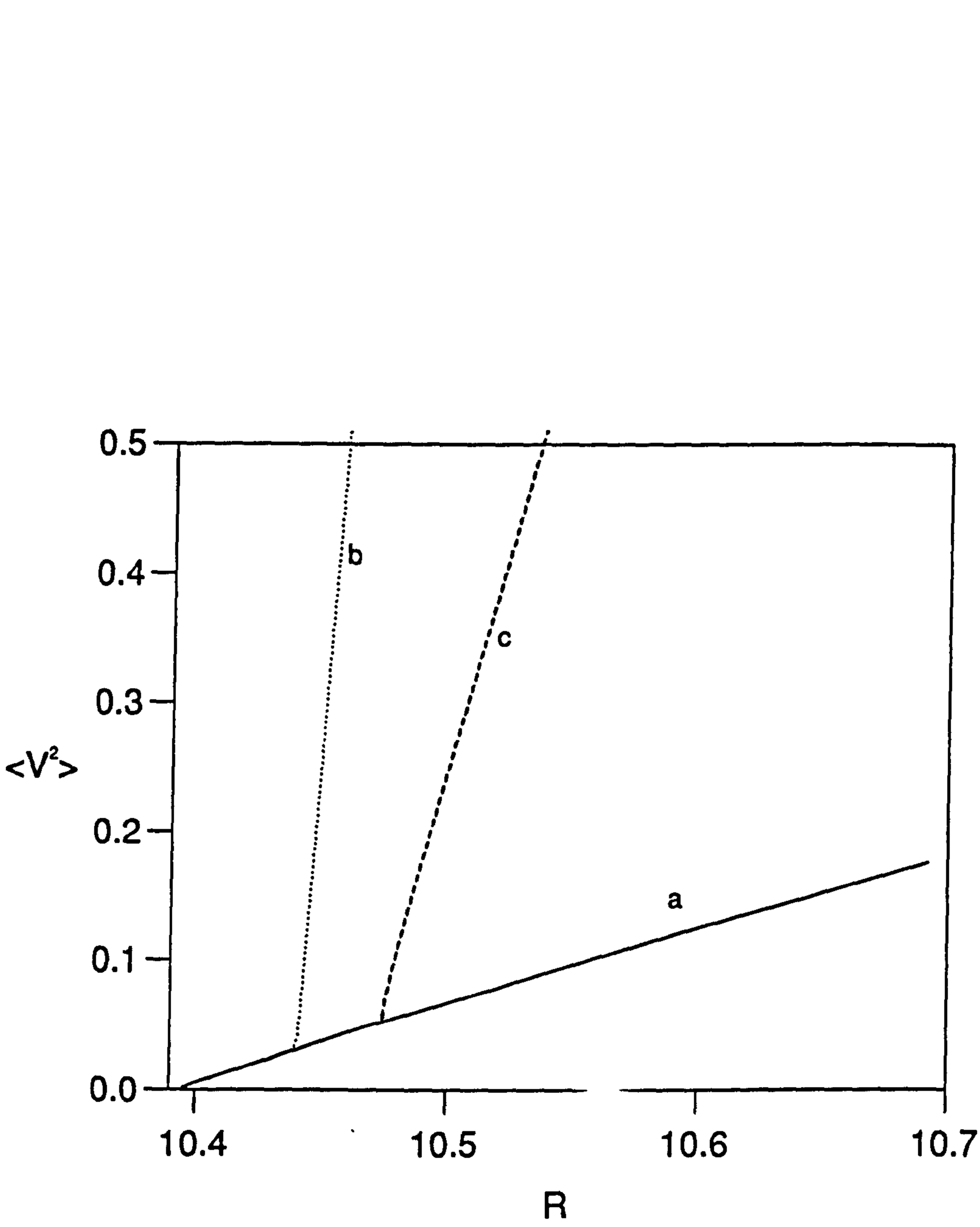

Figure 6.6: The bifurcation of branches b and c off branch a when $\Gamma = 0.1$.

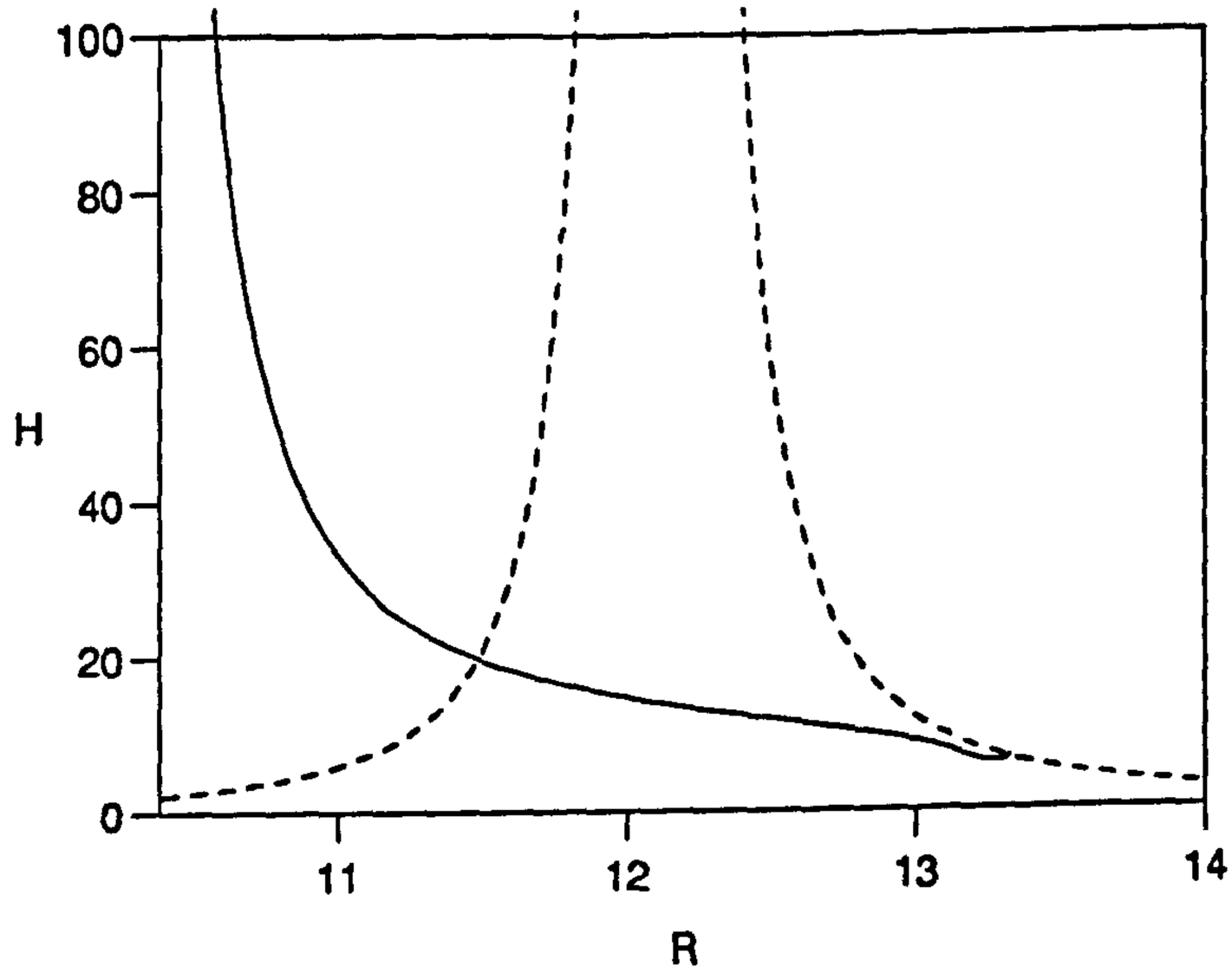

(a)

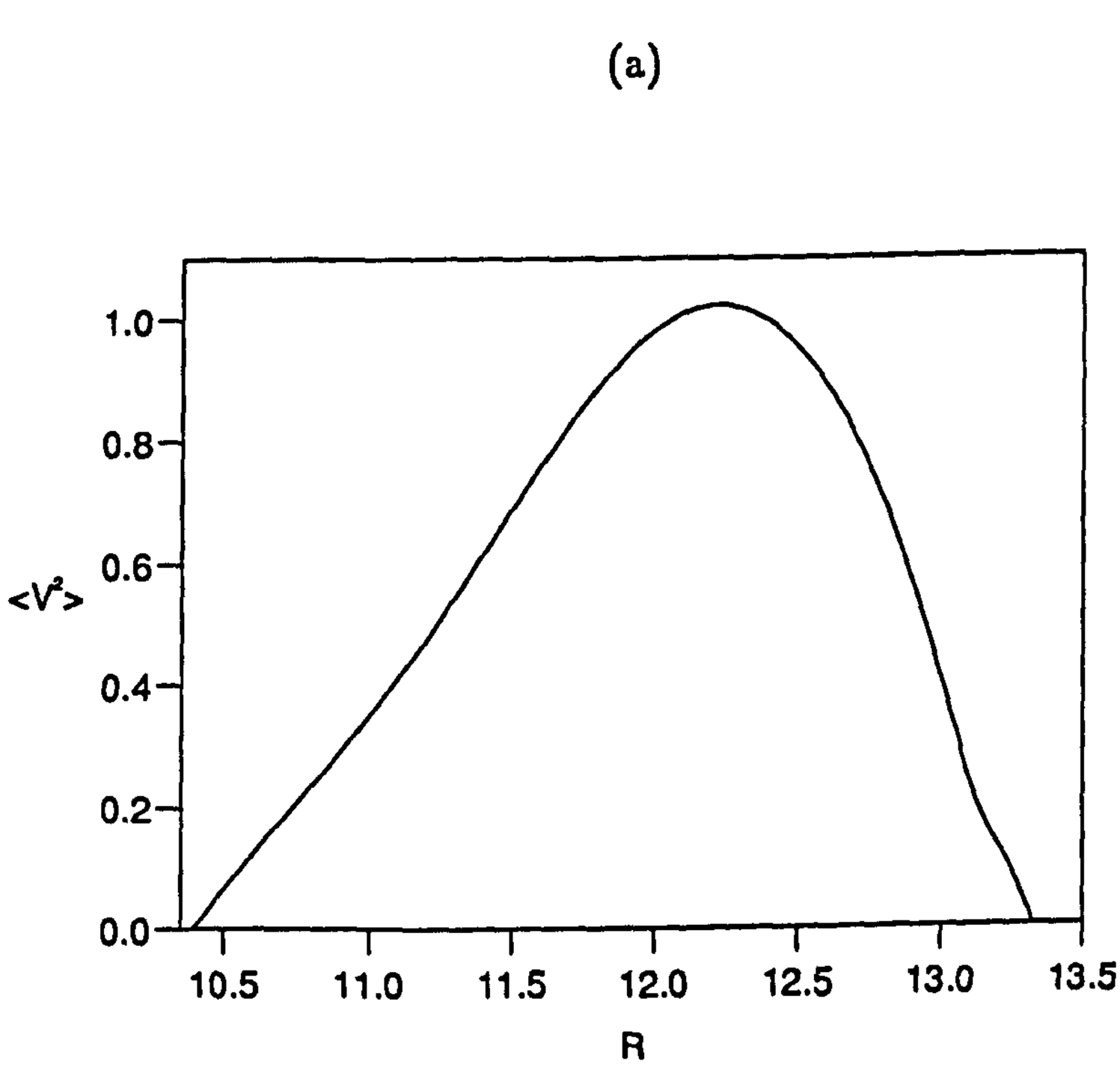

(b)

Figure 6.7: An enlargement of branch a of the second nonlinear solution when $\Gamma = 0.1$.
(a) H against R for the basic state (- - -) and branch a (——).
(b) $< V^2 >$ against R for branch a.

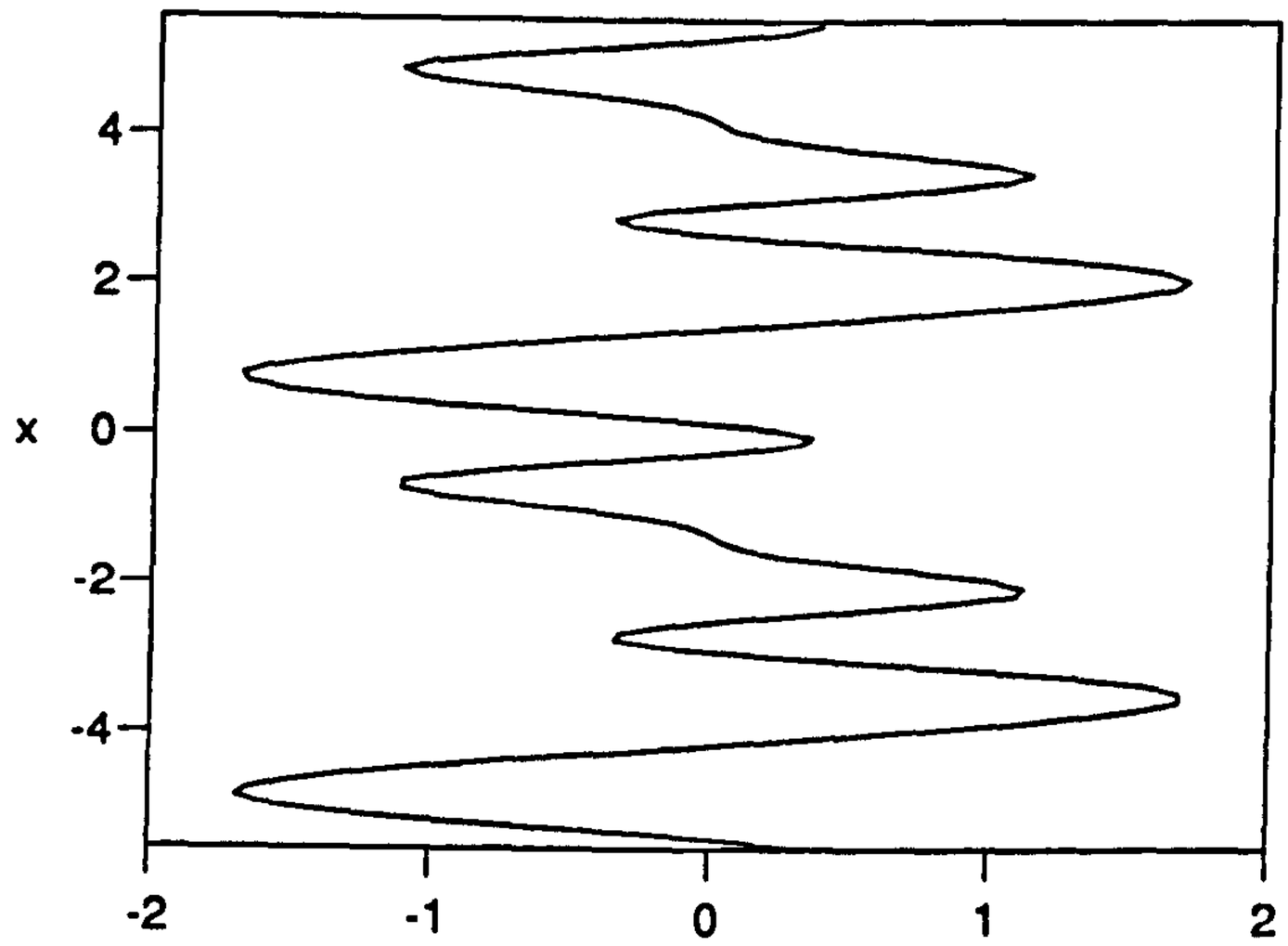

(a)

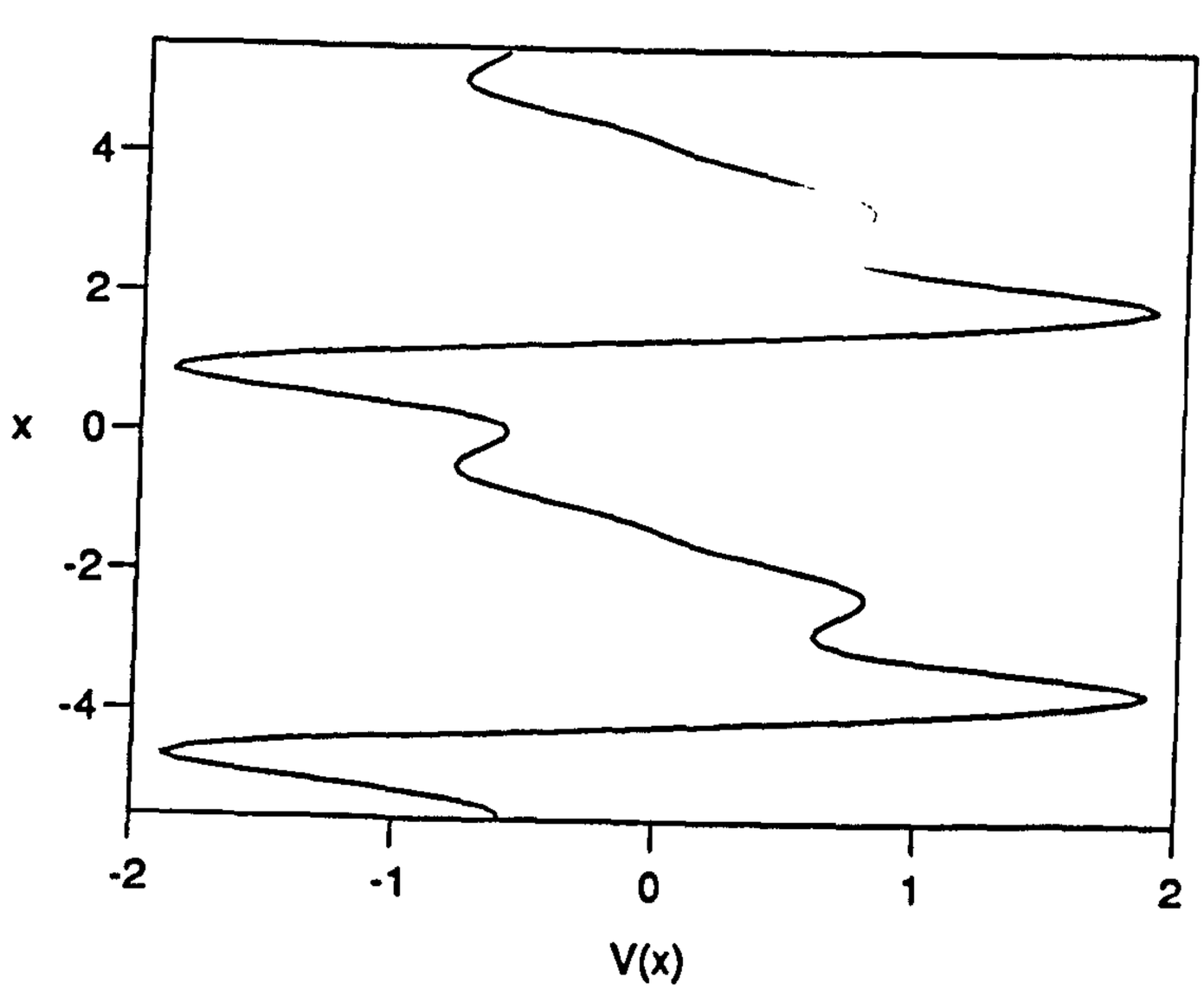

(b)

Figure 6.8: Geostrophic flow profiles for branch a for $\Gamma = 0.1$.
(a) $R = 12.9923$ and, (b) $R = 11.2173$.

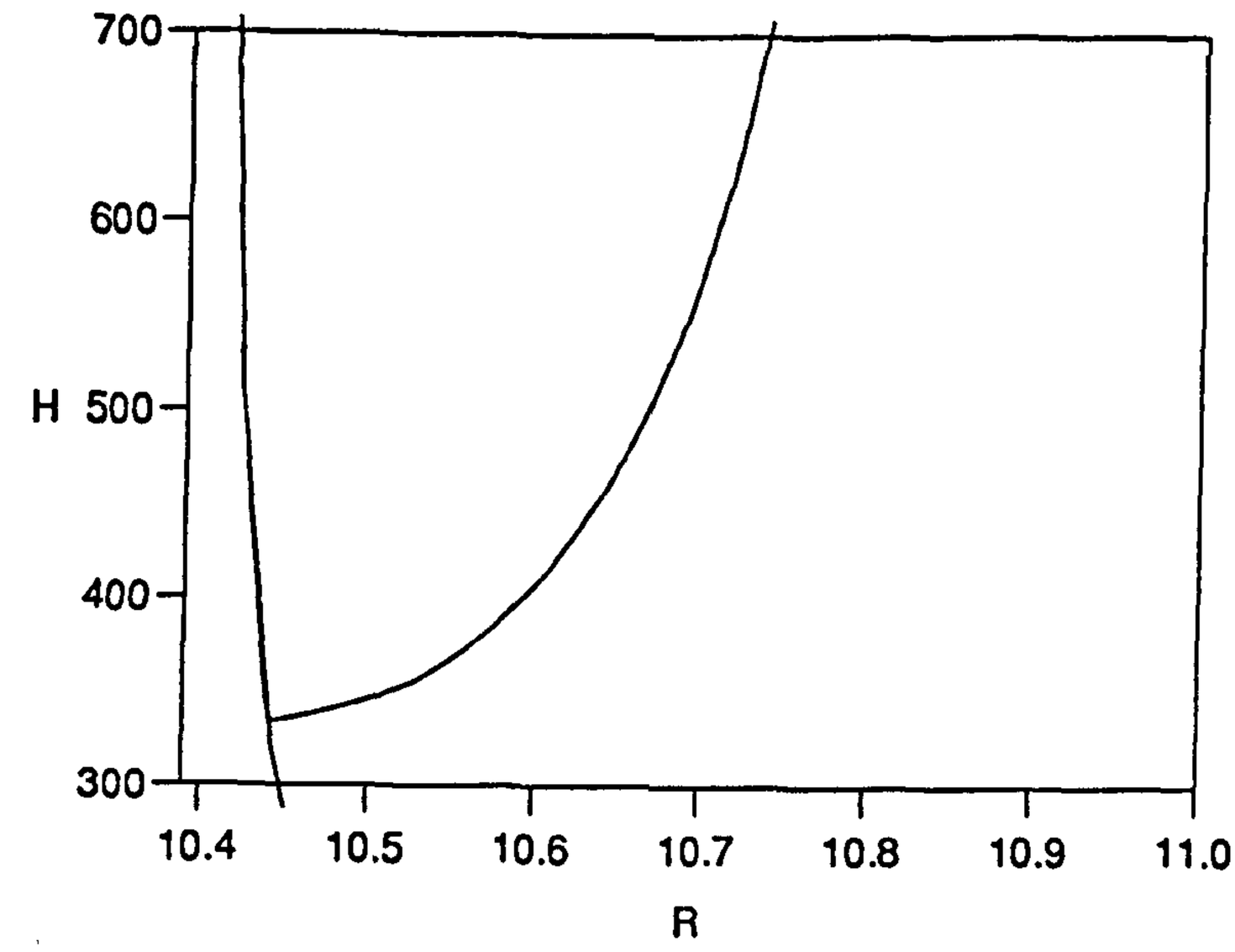

(a)

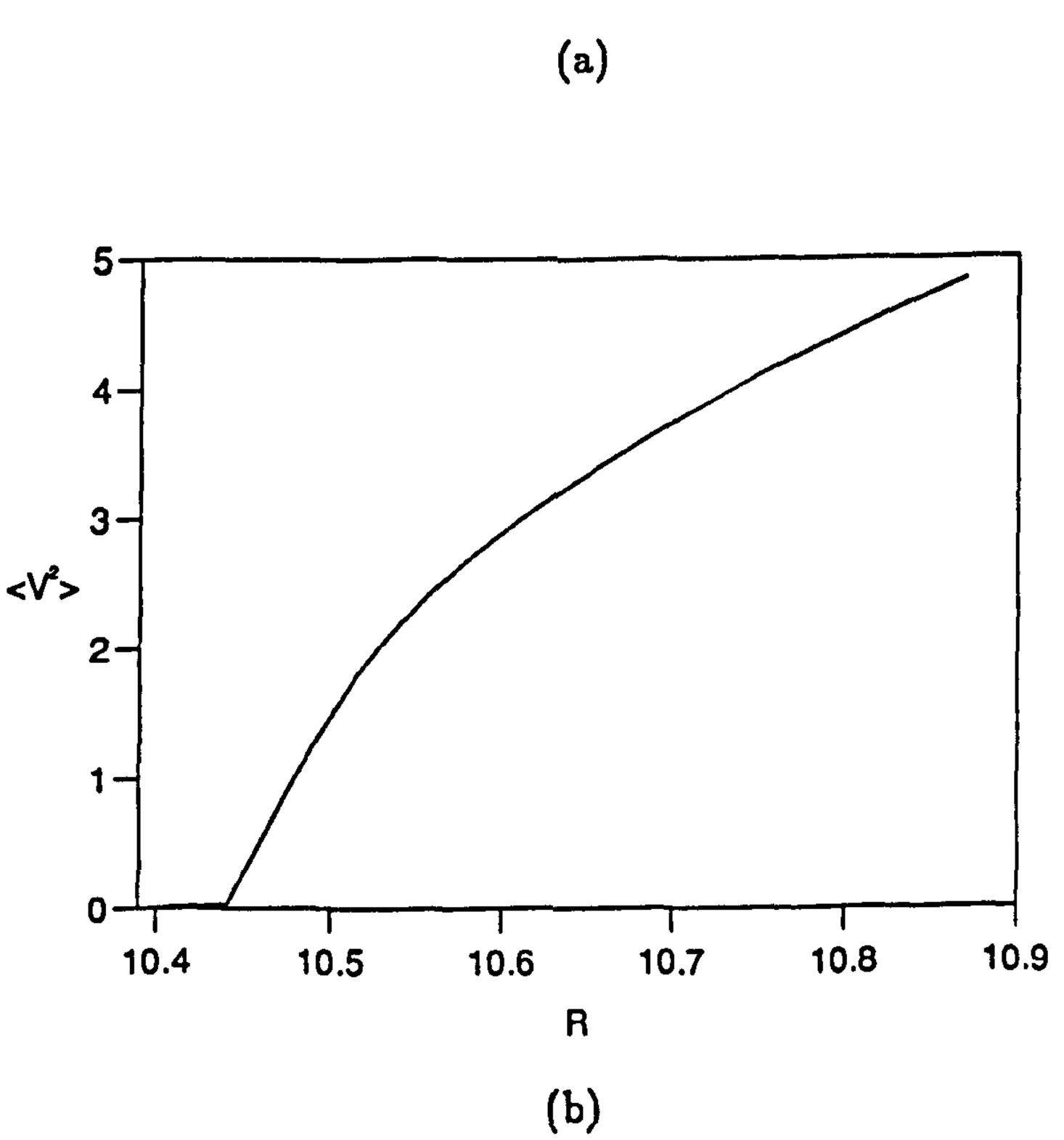

(b)

Figure 6.9: An enlargement of branch b of the second nonlinear solution when $\Gamma = 0.1$.
(a) H against R for branch b.
(b) $< V^2 >$ against R for branch b.

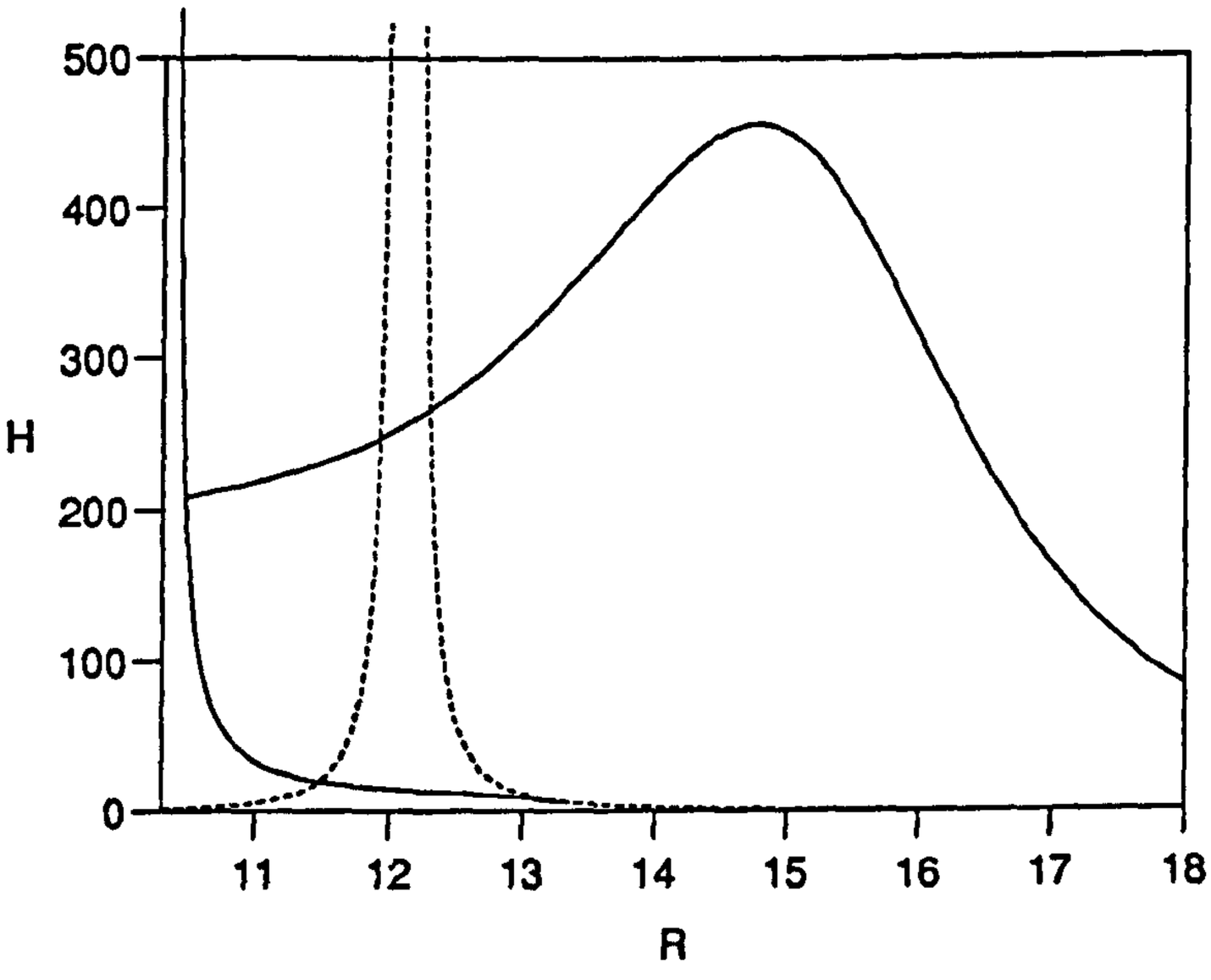

(a)

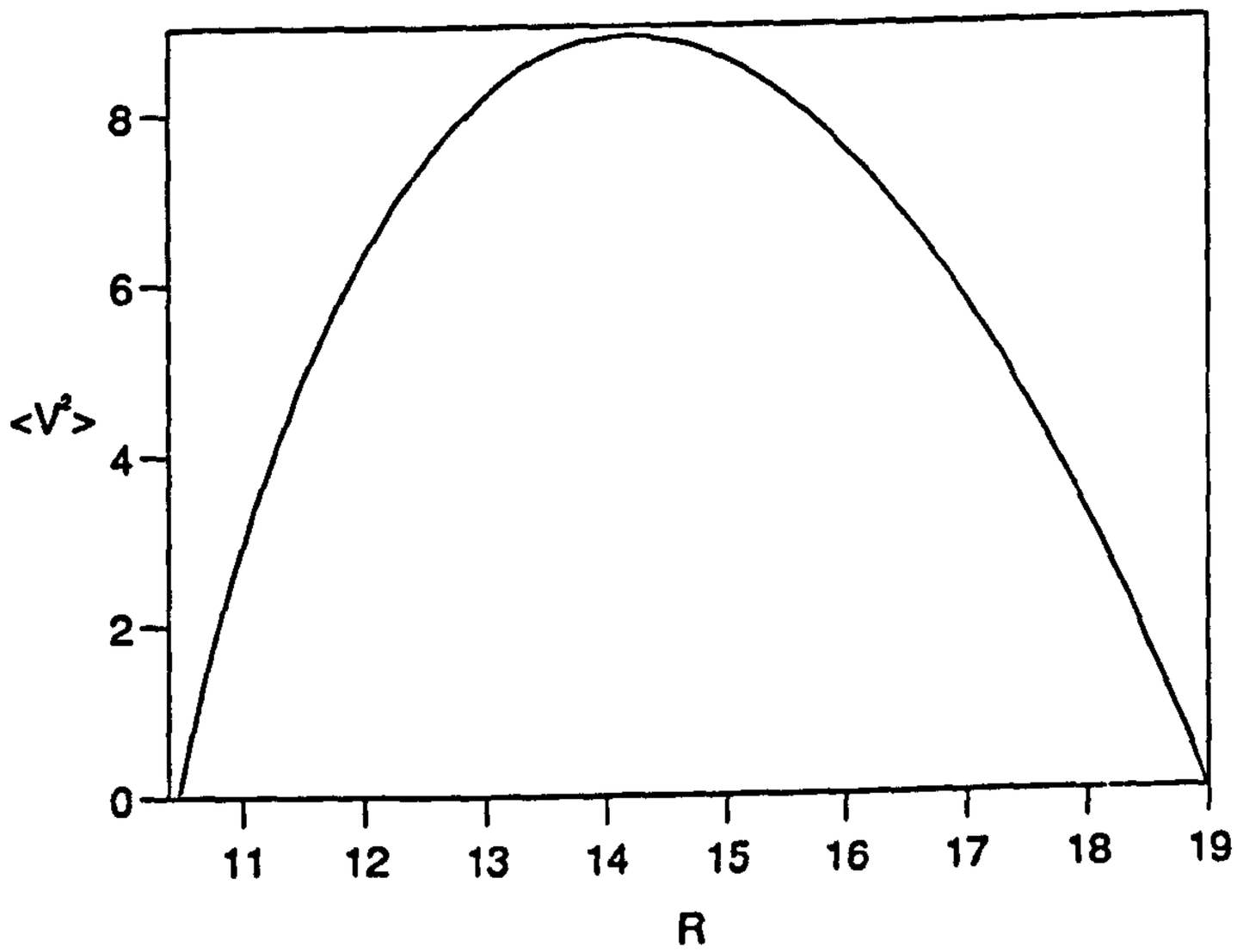

(b)

Figure 6.10: An enlargement of branch c of the second nonlinear solution when $\Gamma = 0.1$.
(a) H against R for the basic state (- - -) and branch c (——).
(b) $< V^2 >$ against R for branch c.

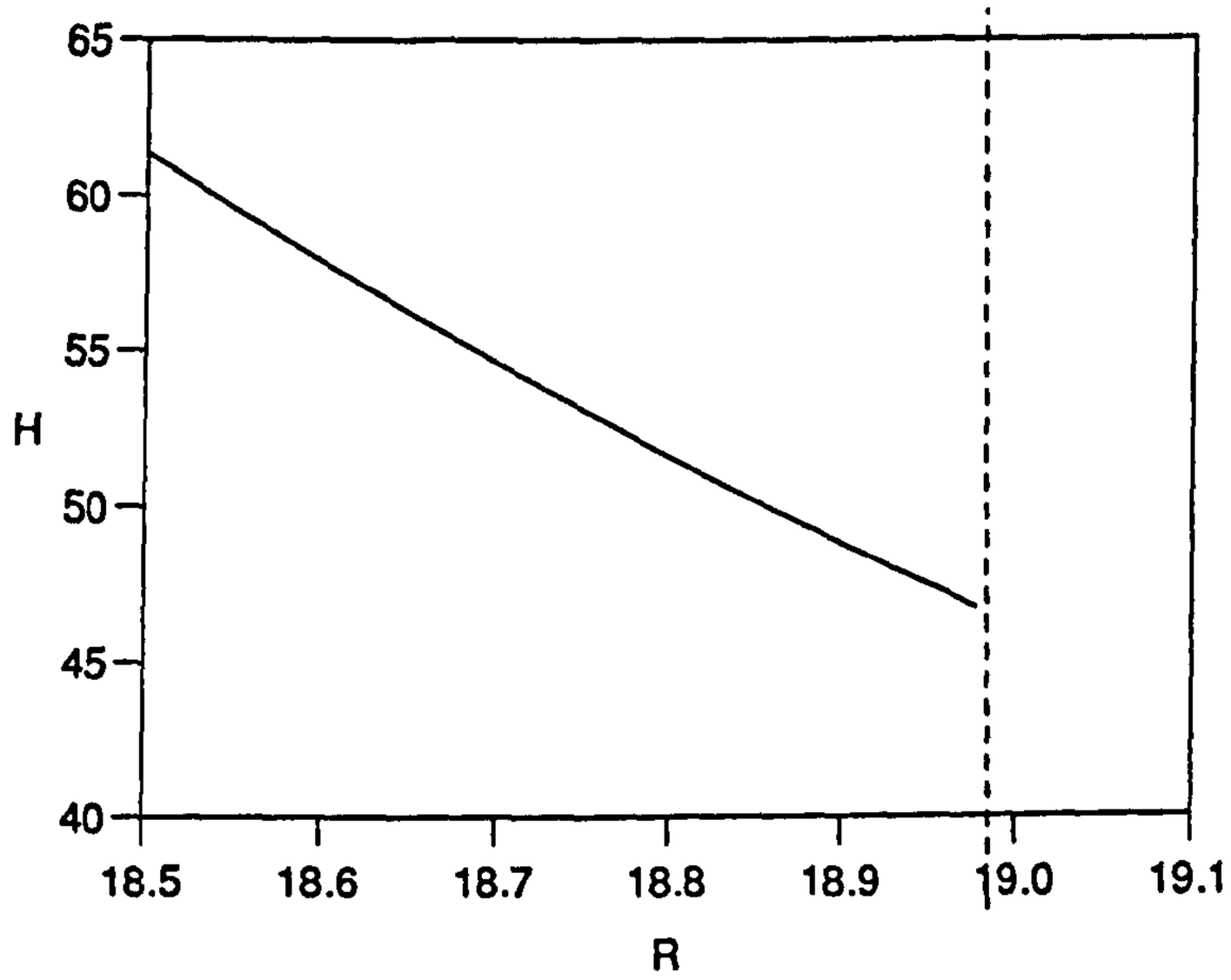

(a)

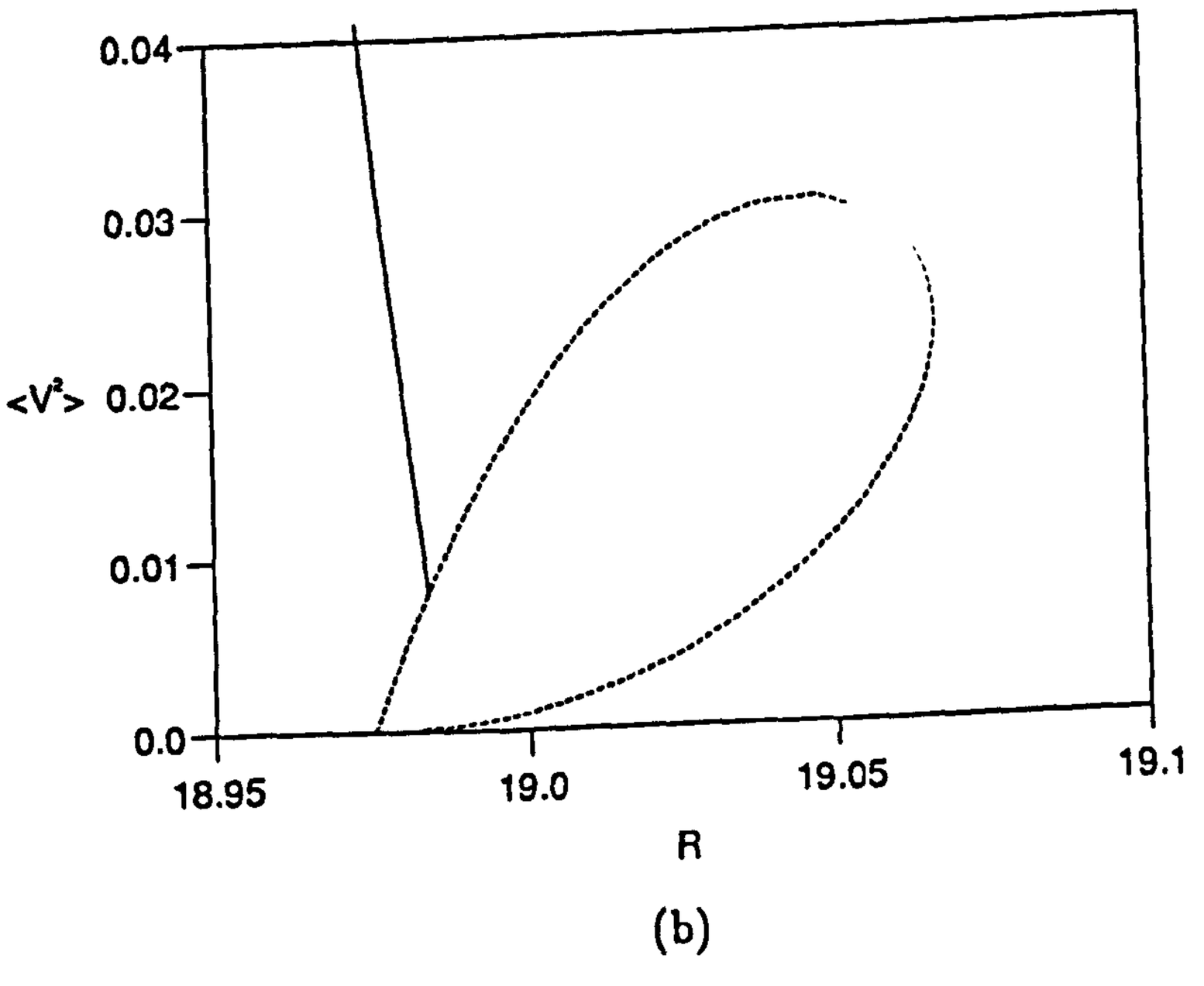

(b)

Figure 6.11: The bifurcation of branch c onto the solution (6.25) when $\Gamma = 0.1$.
(a) The curve (——) is branch c, while (– –) is (6.25).
(b) as in (a) but showing $< V^2 >$.

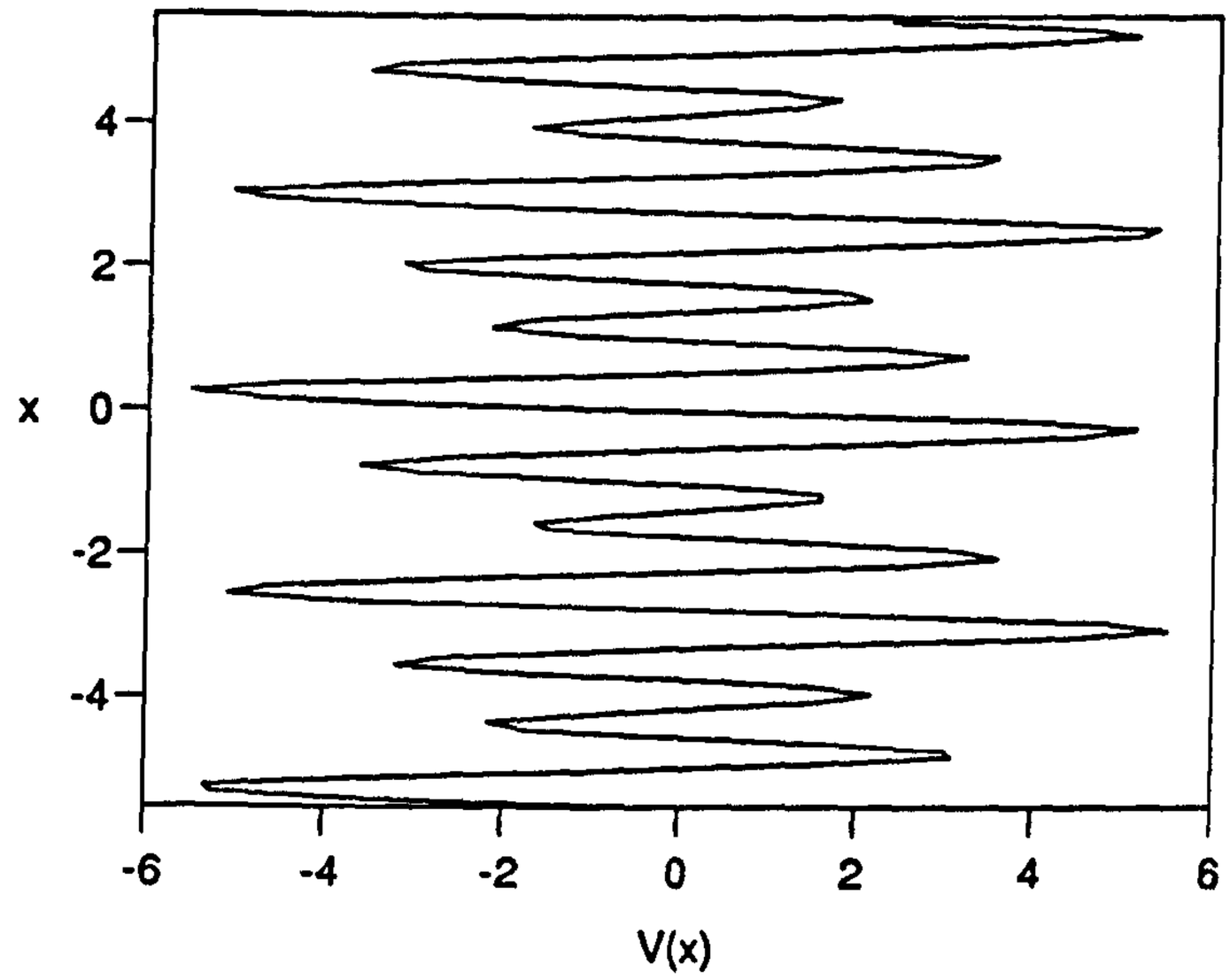

(a)

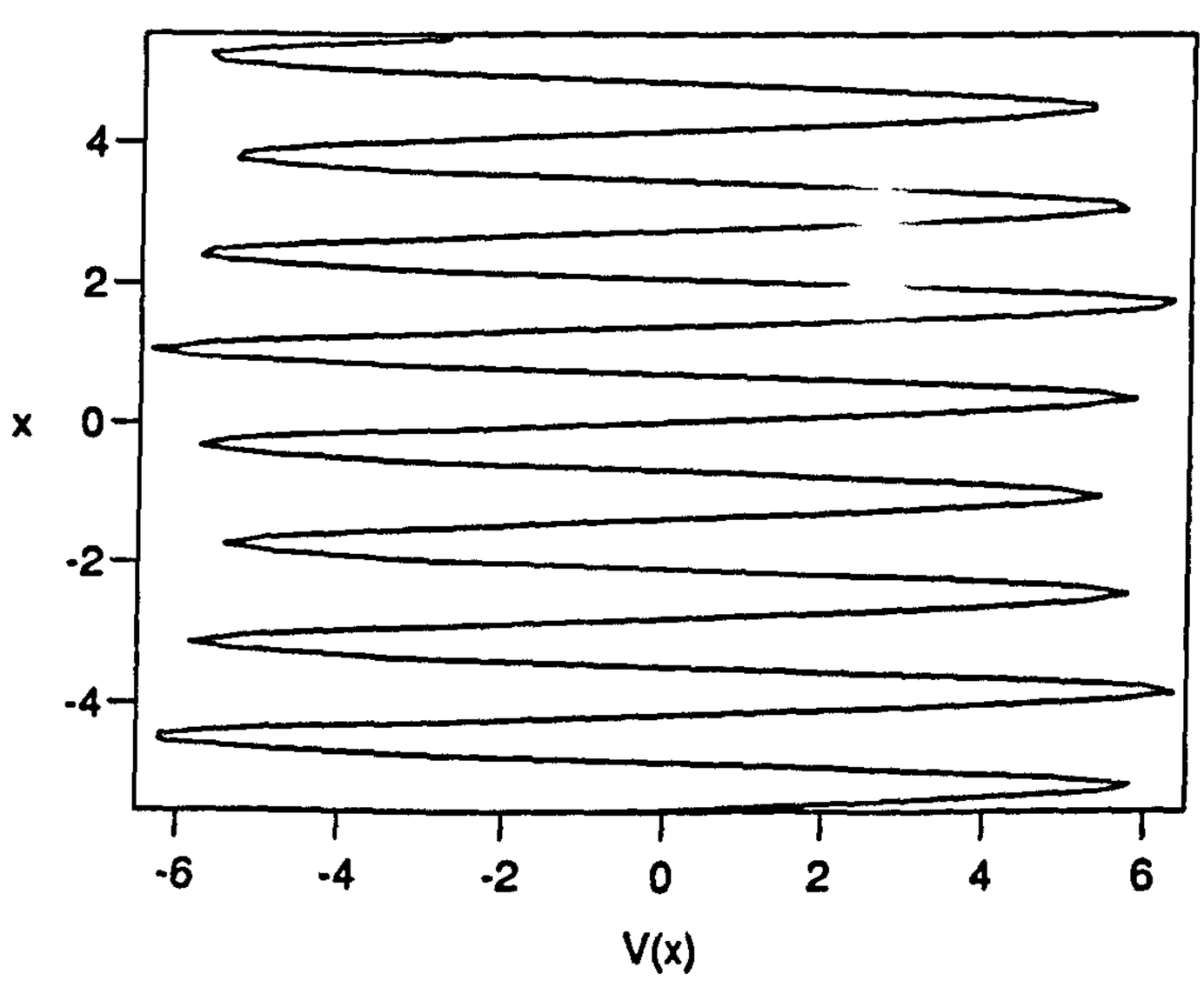

(b)

Figure 6.12: (a) Geostrophic flow profile for branch b at the point $R = 10.7299$ when $\Gamma = 0.1$ (b) Geostrophic flow profile for branch c at the point $R = 14.9926$ when $\Gamma = 0.1$.

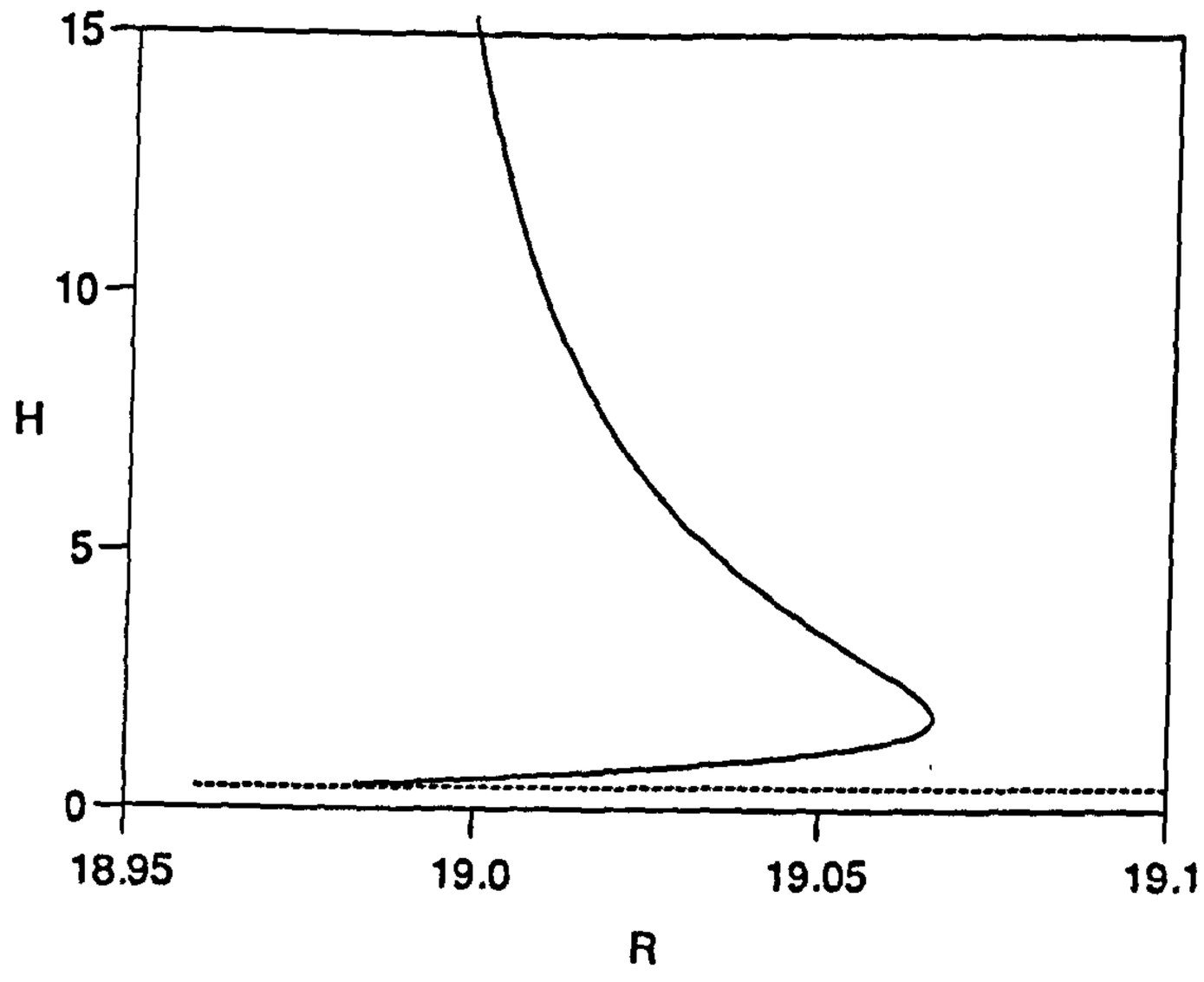

(a)

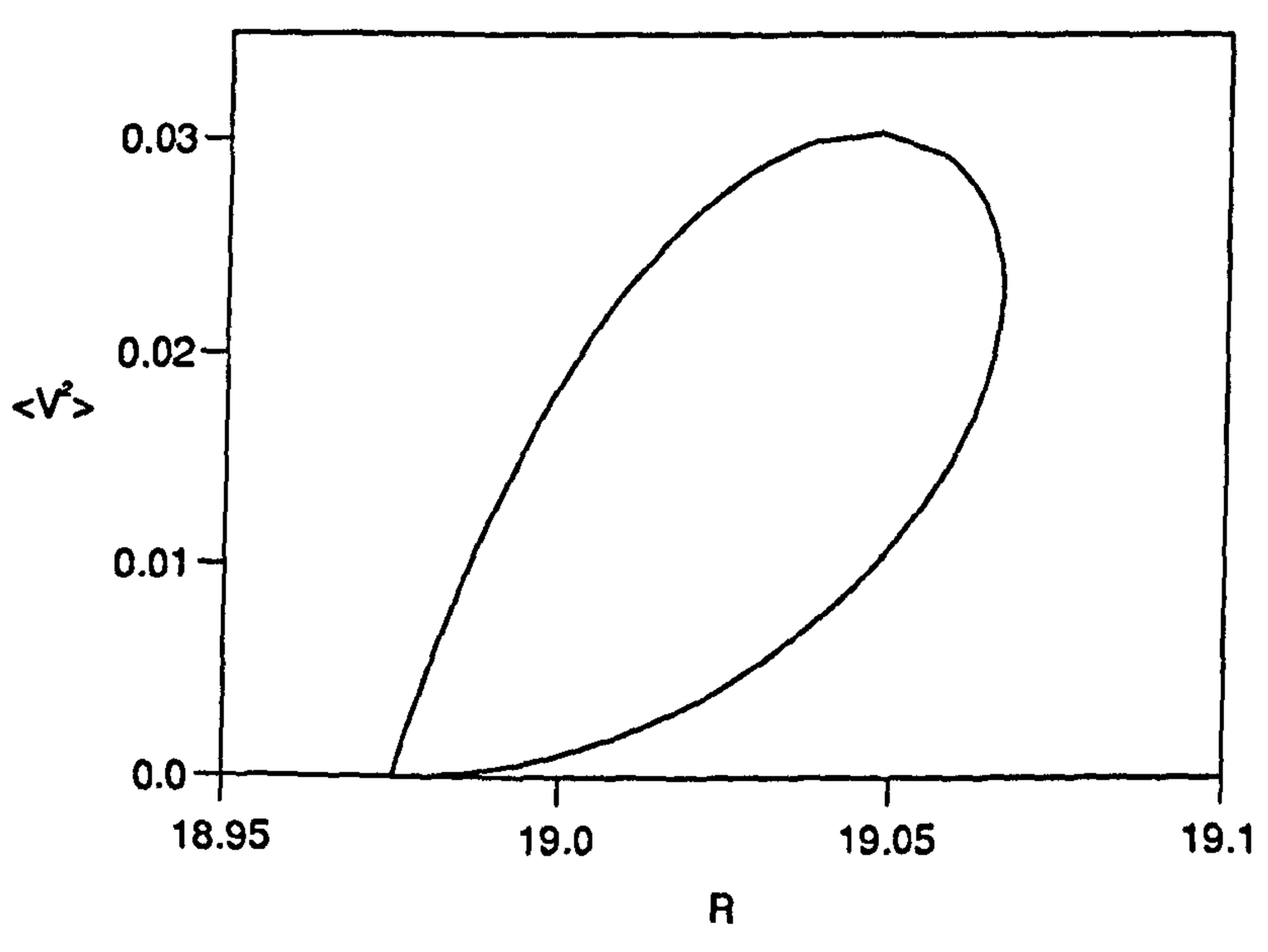

(b)

Figure 6.13: The nonlinear evolution of the solution (6.25) when $\Gamma = 0.1$.
(a) H against R for the basic state (- - -) and this solution (——).
(b) $< V^2 >$ against R for this solution.

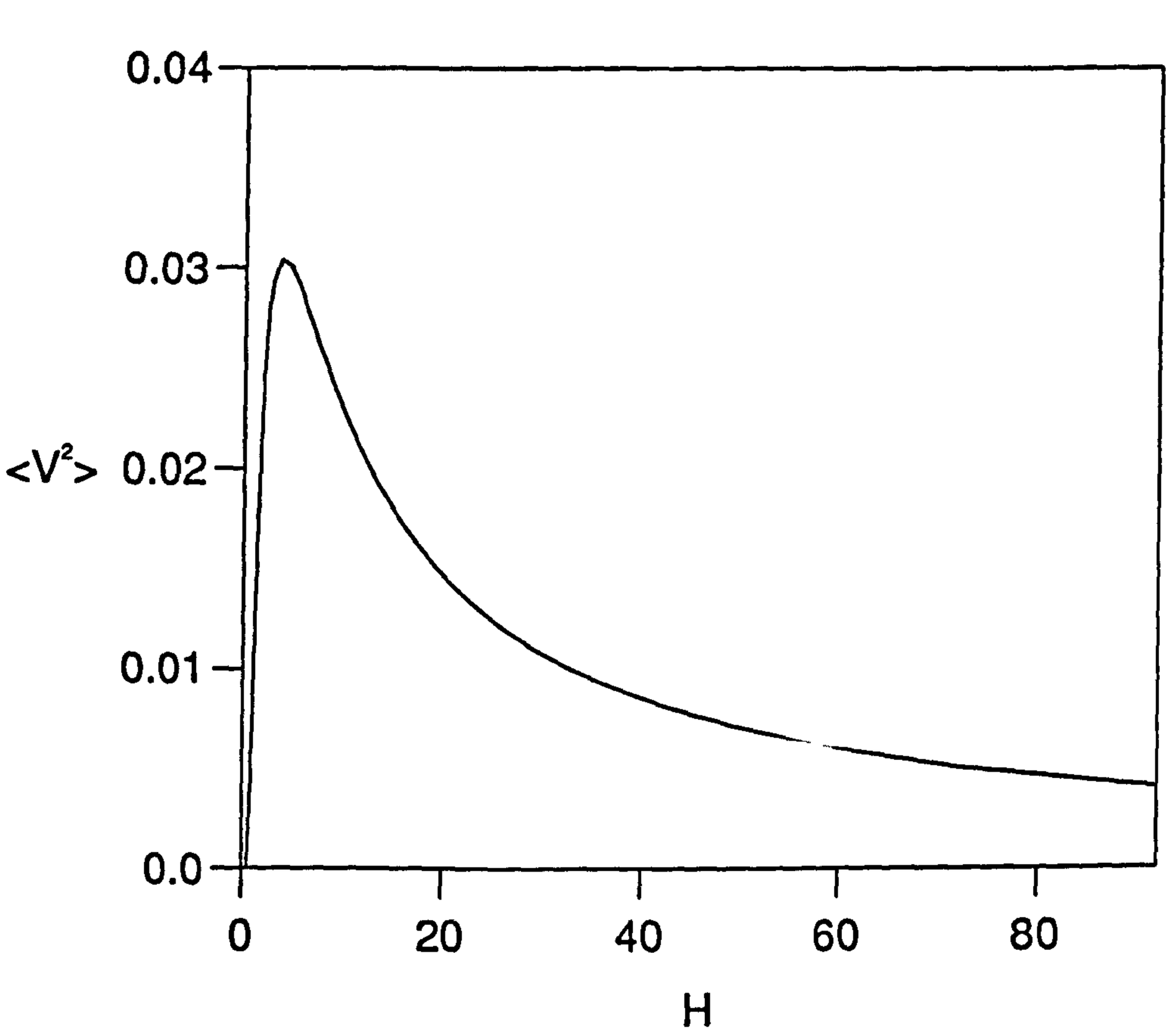

Figure 6.14: A plot of $< V^2 >$ against H for the solution (6.25) when $\Gamma = 0.1$.

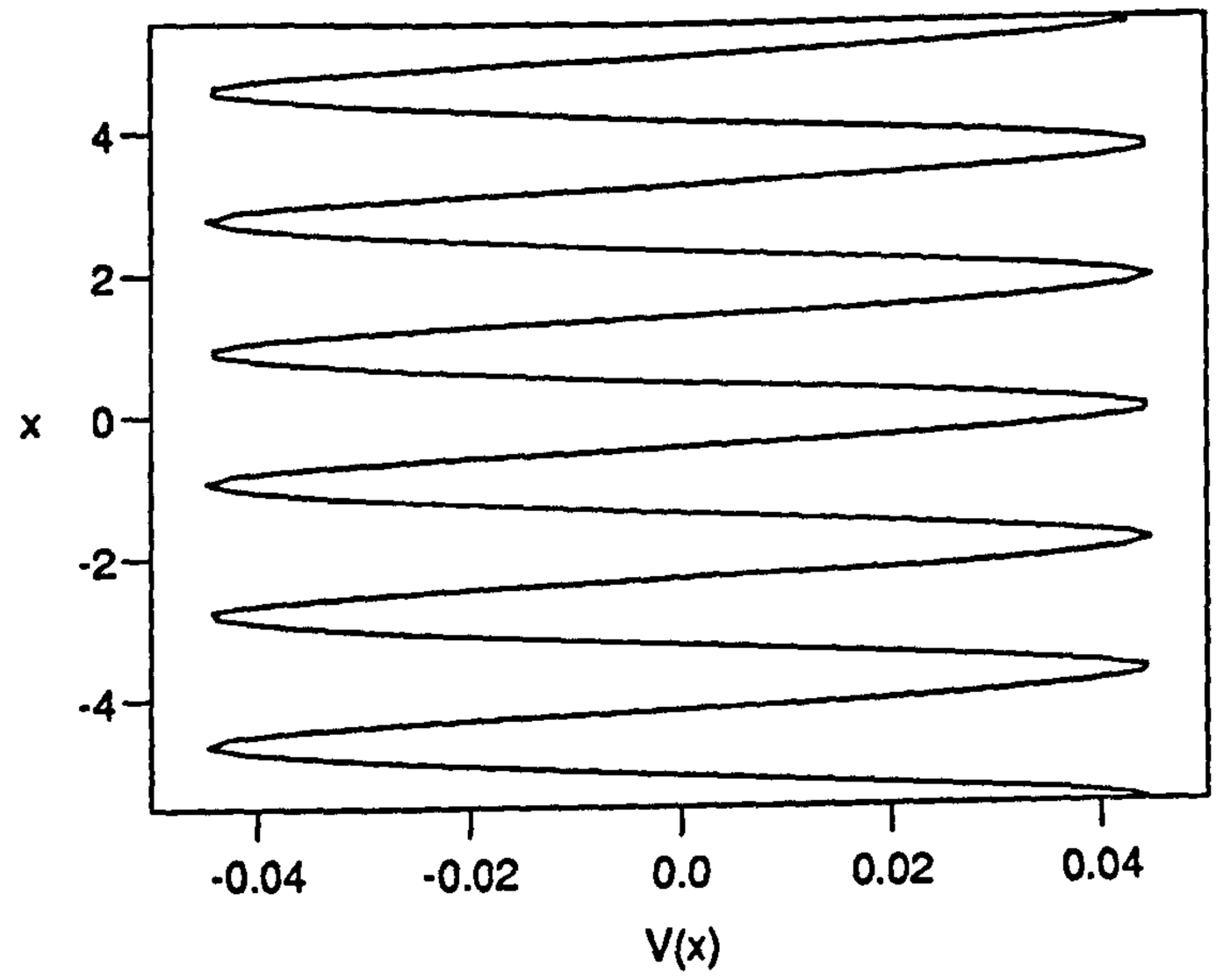

(a)

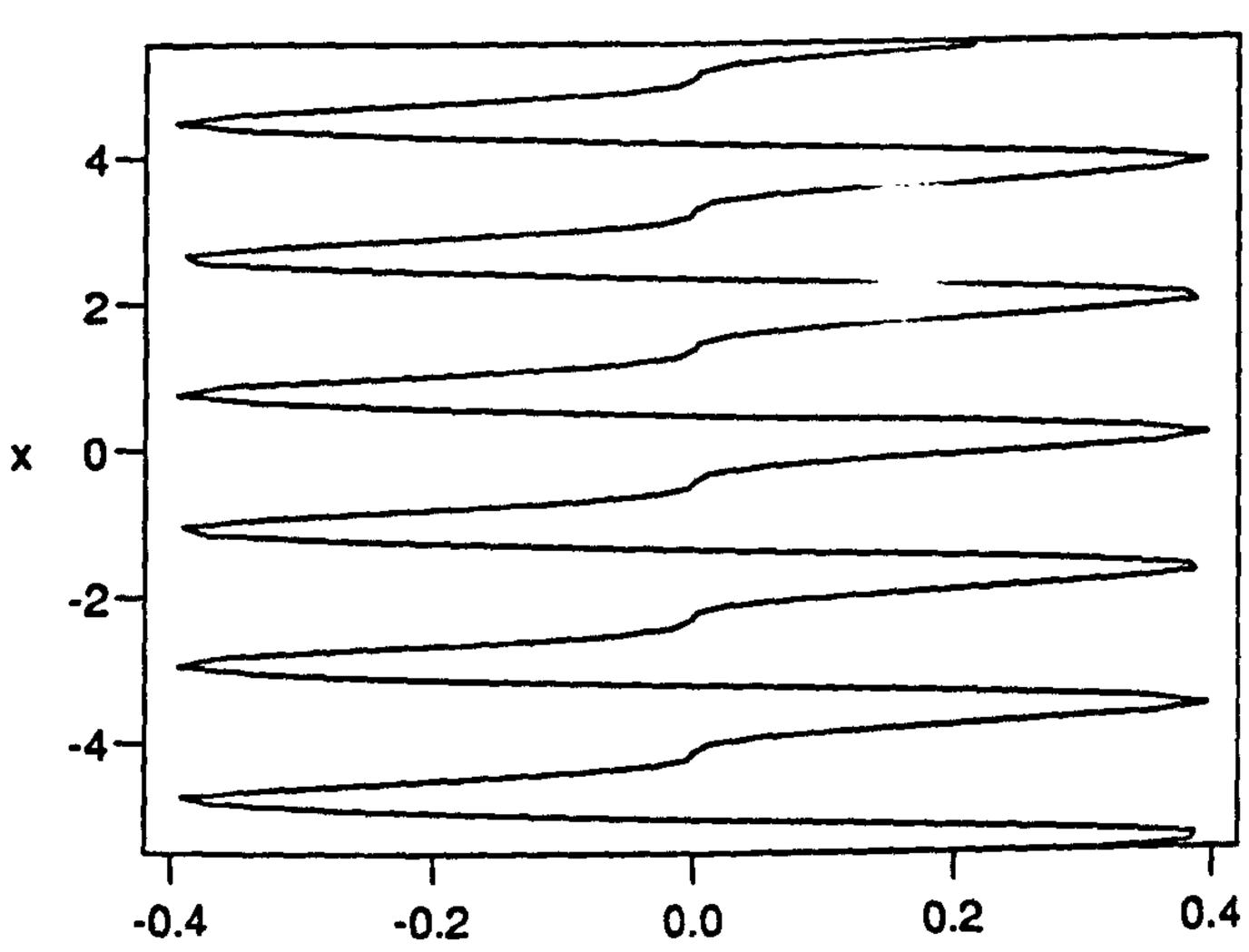

(b)

Figure 6.15: Geostrophic flow profiles for the solution (6.25) for $\Gamma = 0.1$ when (a) $R = 18.9756$ and, (b) $R = 19.0675$, on the upper branch of the solution.

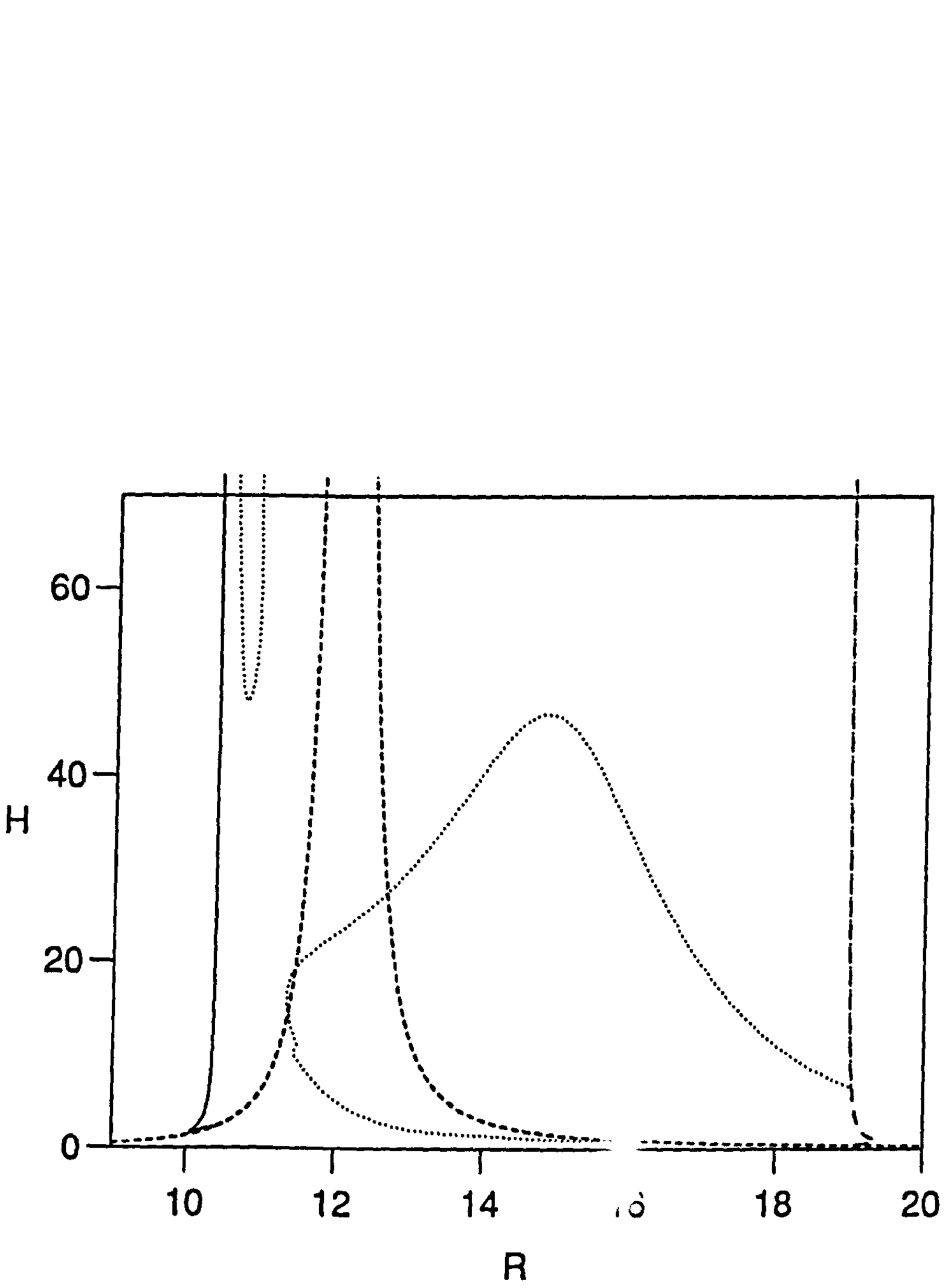

Figure 6.16: The bifurcation structure of the nonlinear solutions for the case $\Gamma = 1.0$. The curve (- - -) is the basic state, while all the other curves represent nonlinear solutions.

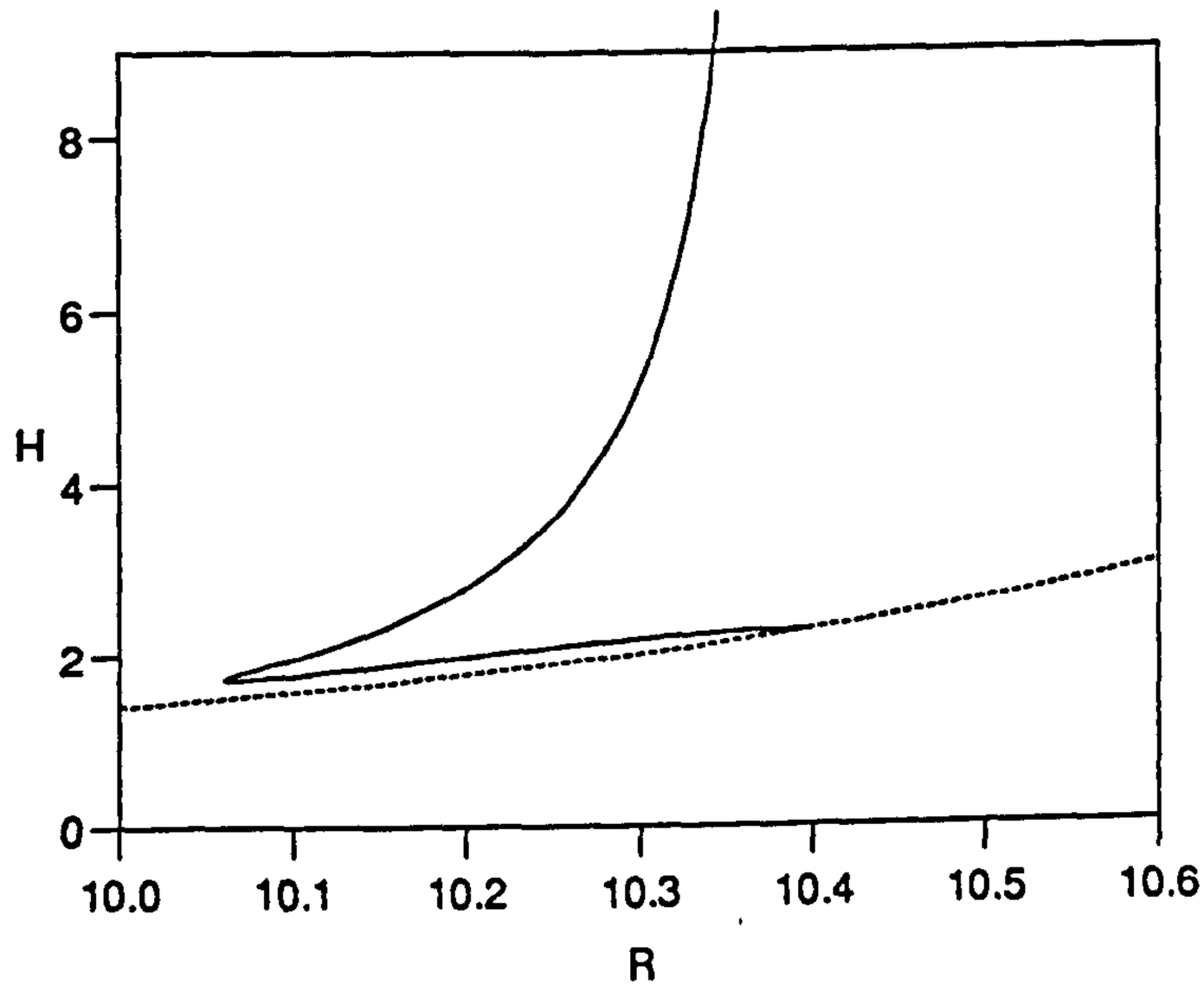

(a)

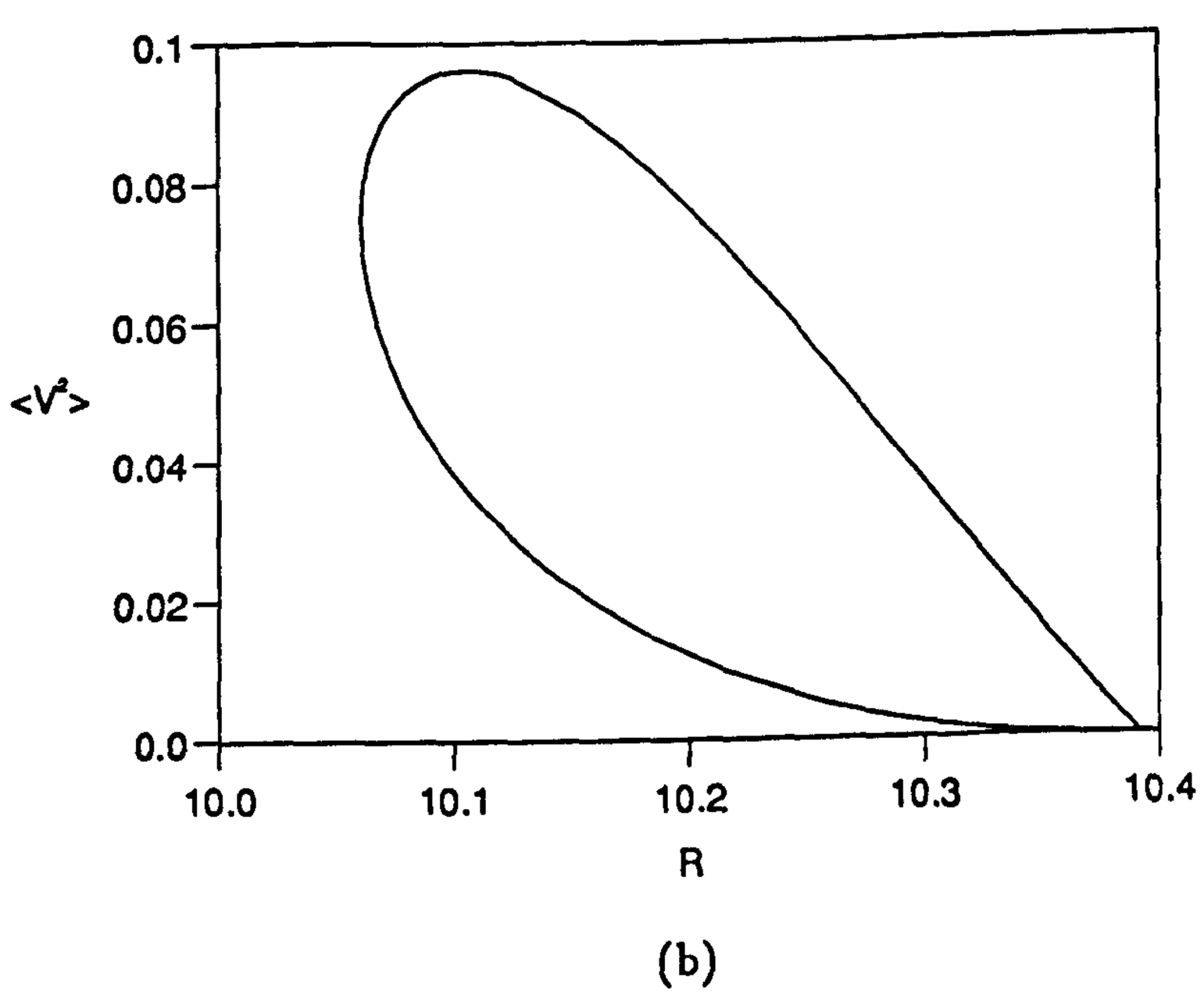

(b)

Figure 6.17: The nonlinear evolution of the most unstable linear solution when $\Gamma = 1.0$.
(a) H against R for the basic state (- - -) and this solution (——).
(b) $< V^2 >$ against R for this solution.

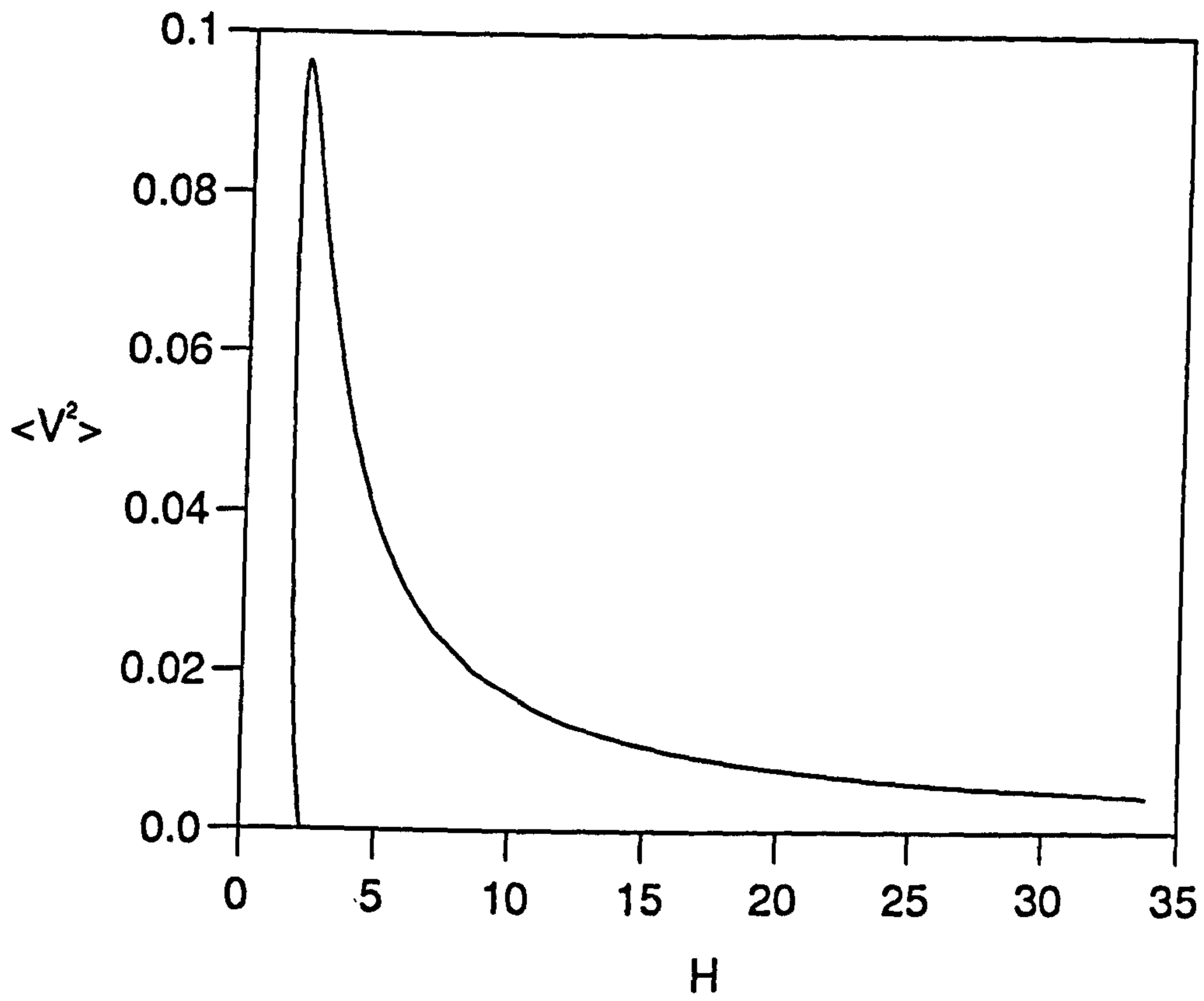

Figure 6.18: A plot of $< V^2 >$ against H for the first nonlinear solution when $\Gamma = 1.0$.

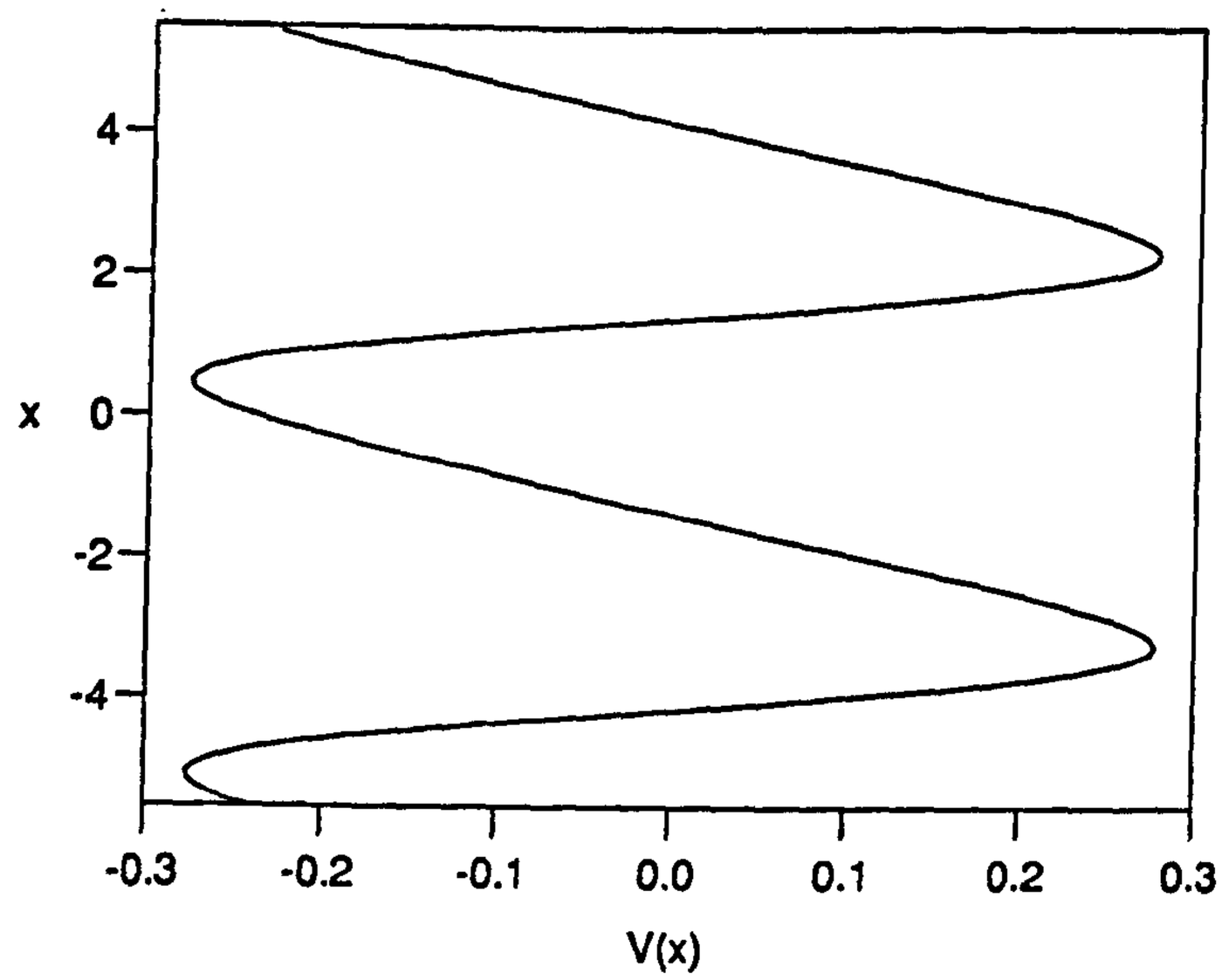

(a)

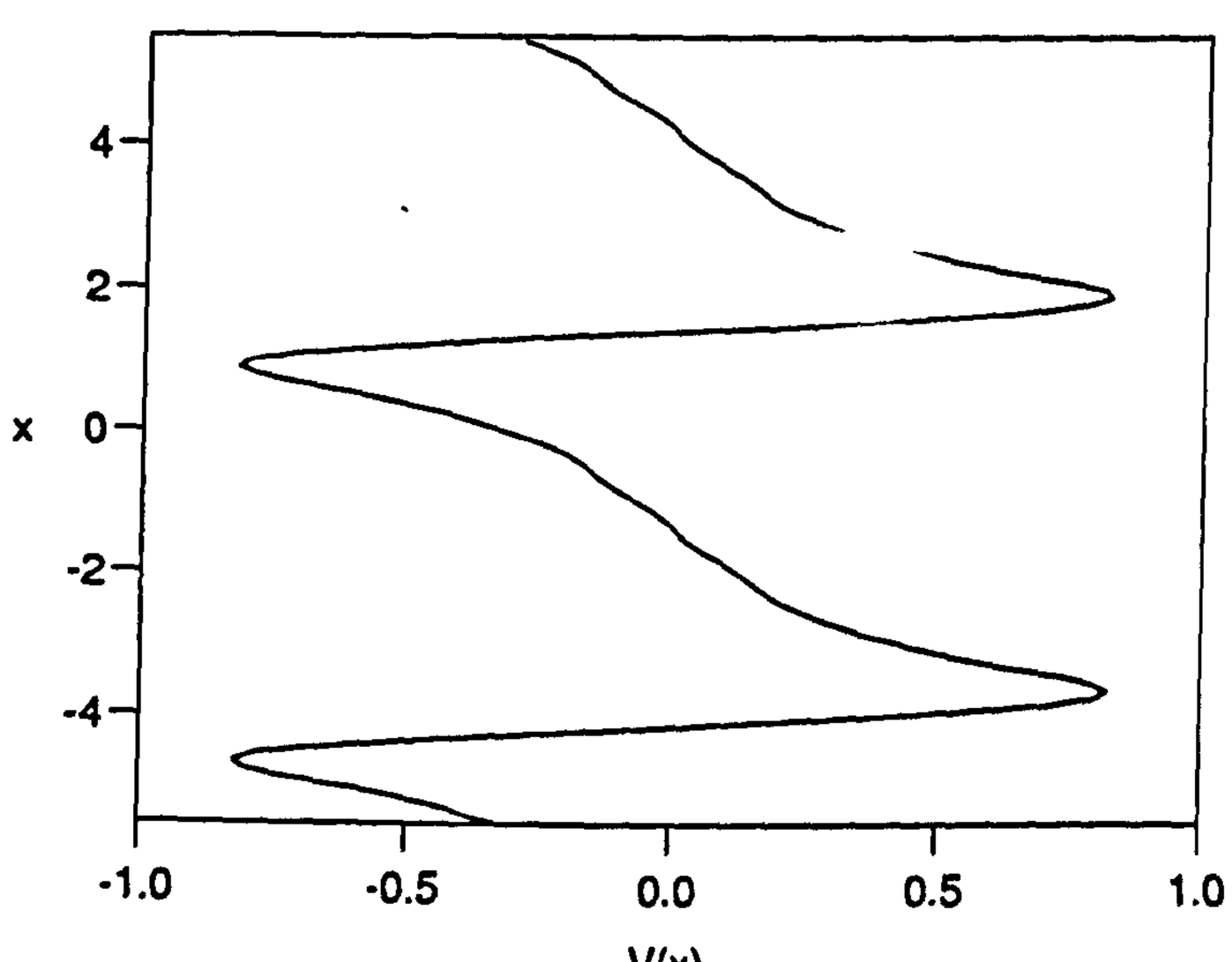

(b)

Figure 6.19: Geostrophic flow profiles for the first nonlinear solution for $\Gamma = 1.0$ when (a) $R = 10.3458$ and, (b) $R = 10.1242$, on the upper branch of the solution.

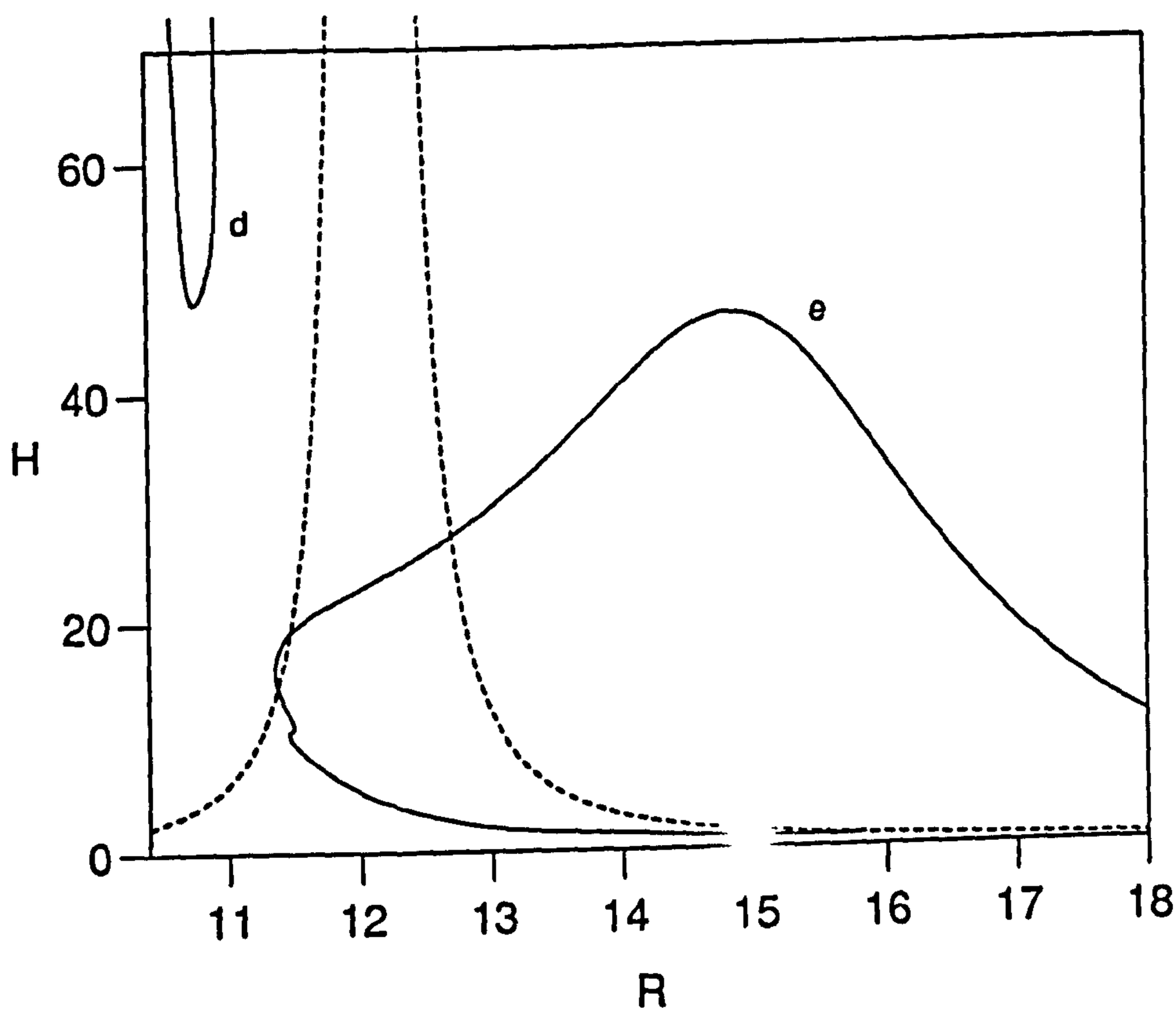

Figure 6.20: The nonlinear evolution of the second most unstable linear solution when $\Gamma = 1.0$. H against R for the basic state (- - -) and this solution (——).

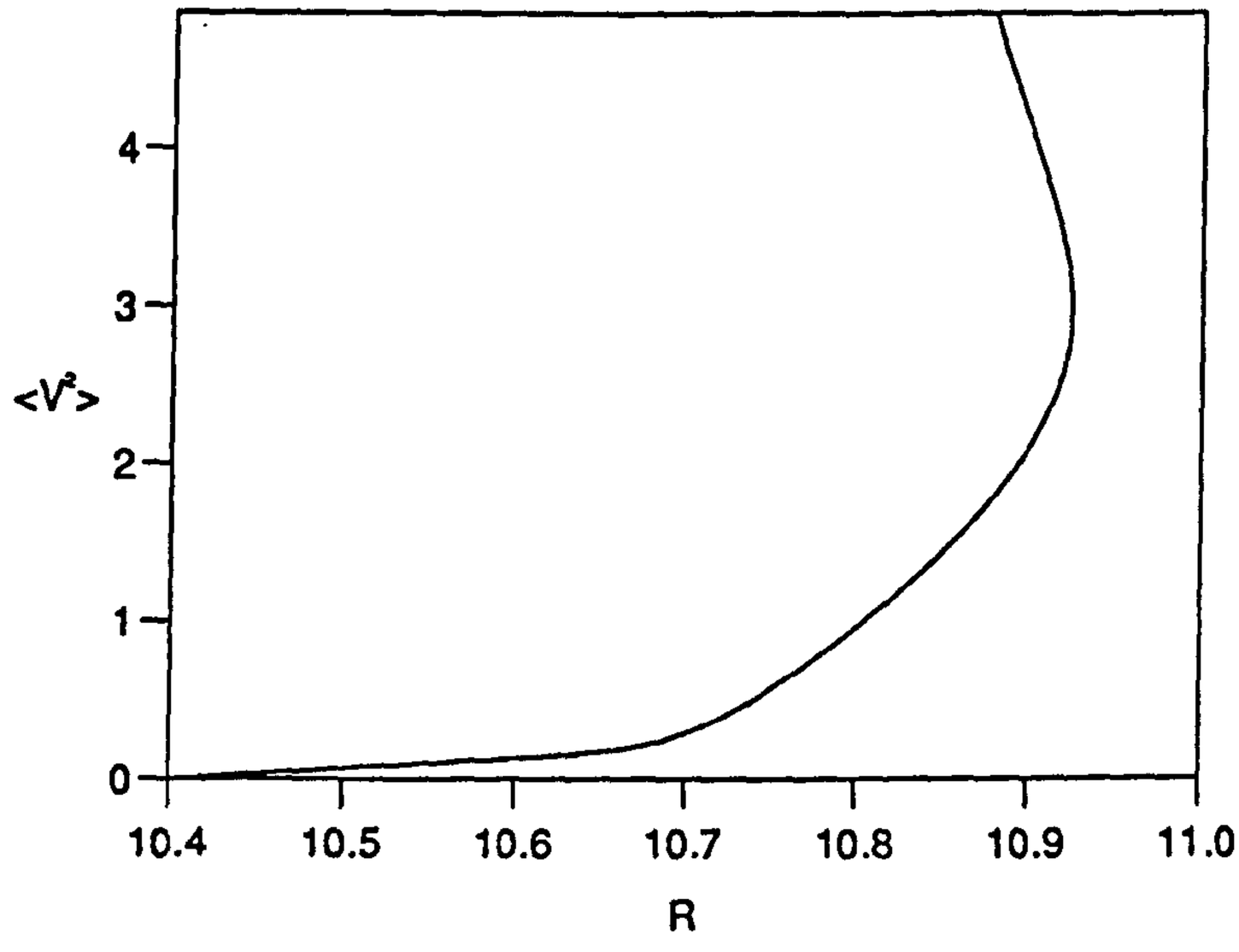

(a)

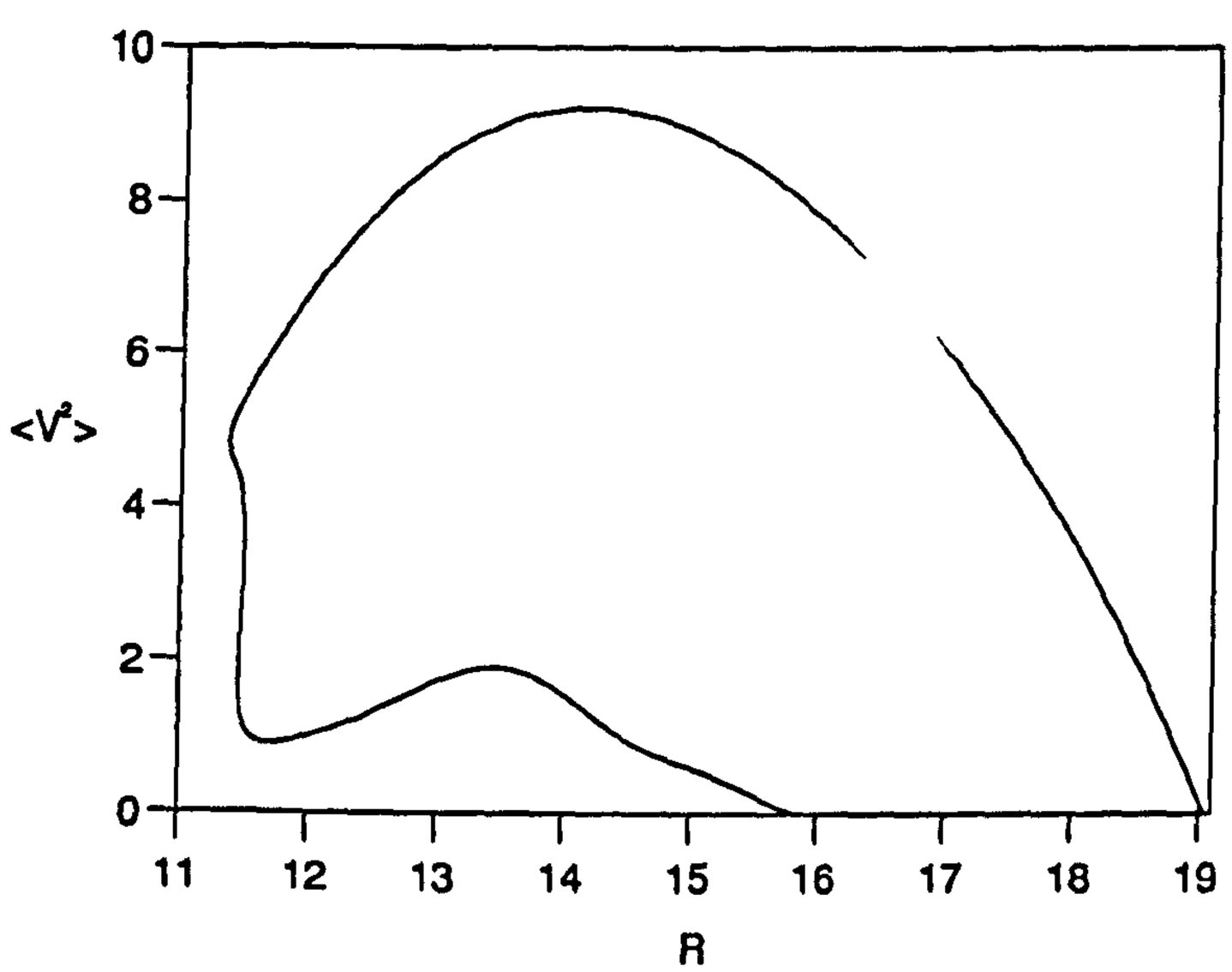

(b)

Figure 6.21: The amplitude of the geostrophic flow associated with the second nonlinear solution when $\Gamma = 1.0$. (a) $< V^2 >$ against R for branch d, and (b) $< V^2 >$ against R for branch e.

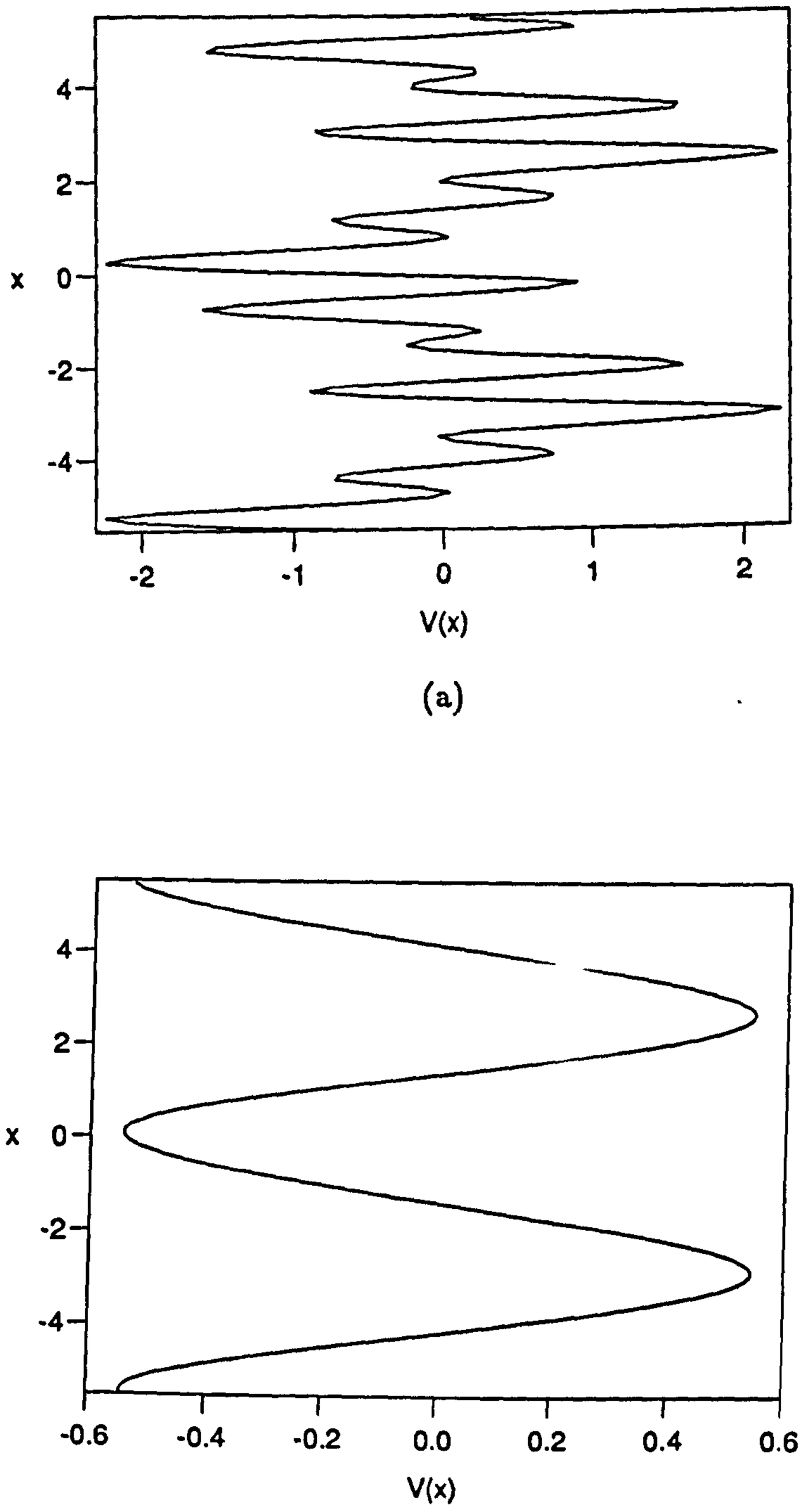

Figure 6.22: (a) Geostrophic flow profile for branch d at the point $R = 10.7402$ when $\Gamma = 1.0$ (b) Geostrophic flow profile for branch e at the point $R = 15.7313$ when $\Gamma = 1.0$ on the upper. branch of the solution.

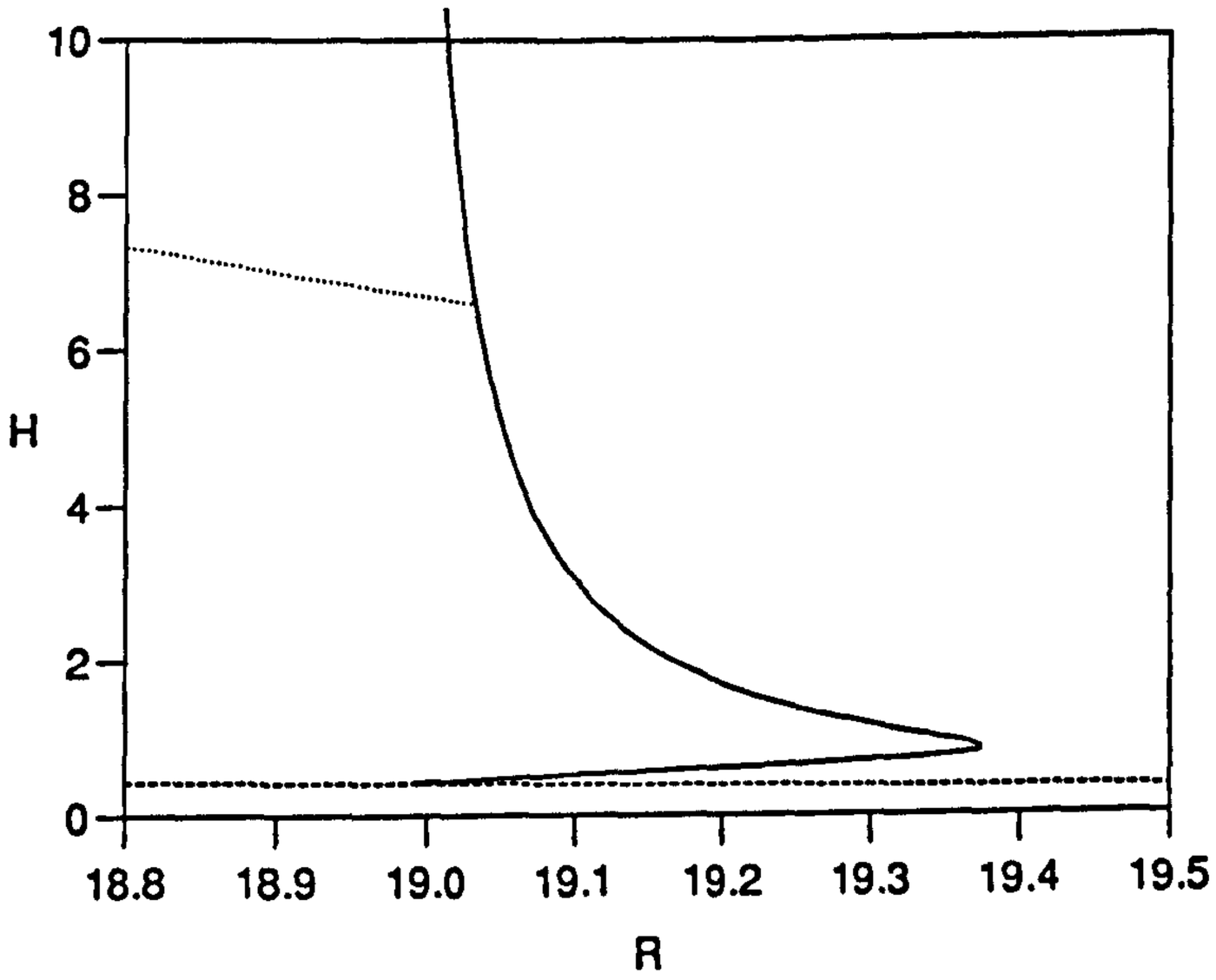

(a)

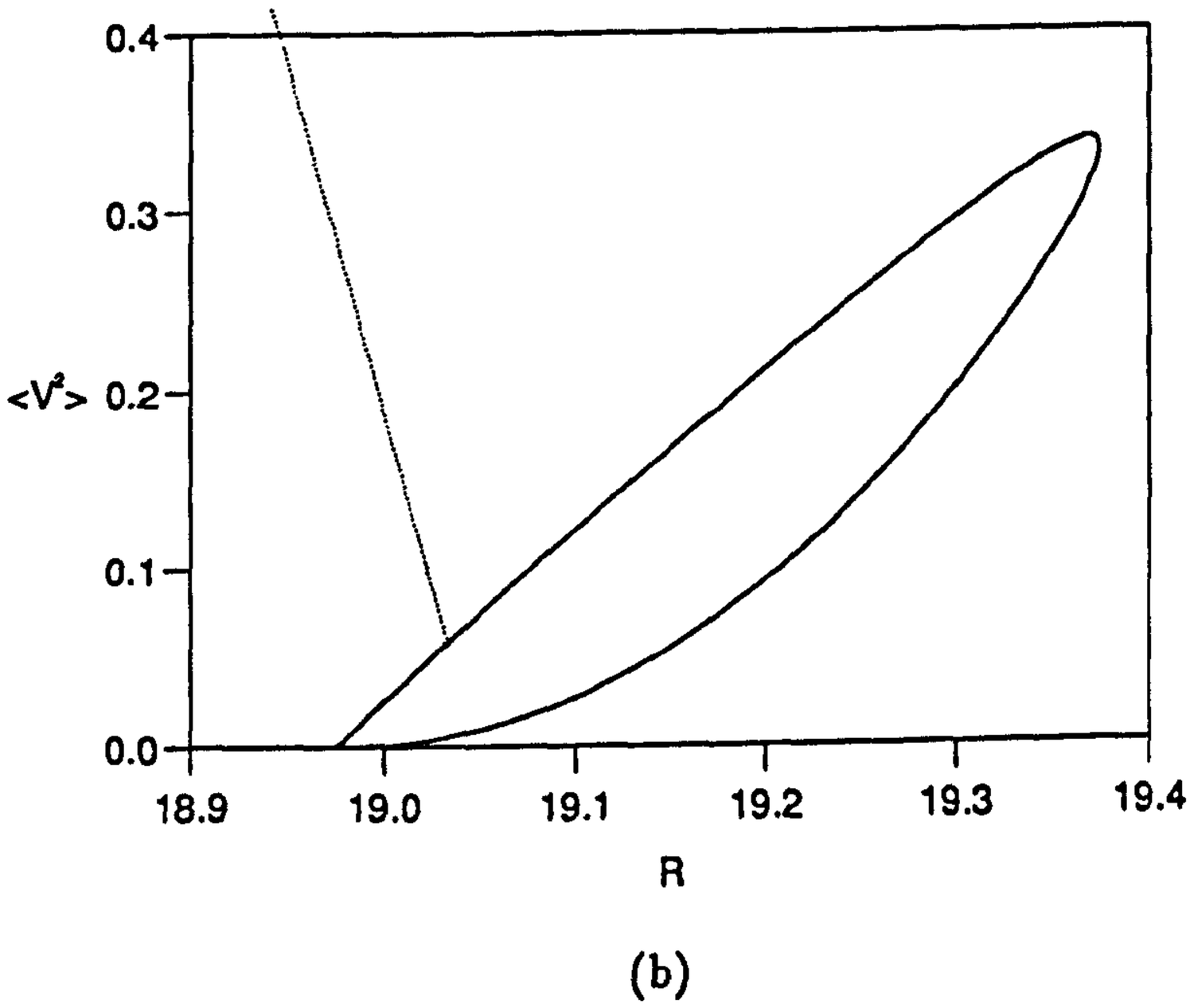

(b)

Figure 6.23: The nonlinear evolution of the solution (6.25) when $\Gamma = 1.0$.
(a) H against R for the basic state (- - -) and this solution (——). The dotted curve (.....) is branch e of the second nonlinear solution. (b) $< V^2 >$ against R for this solution. Again, the dotted curve is associated with branch e of the second nonlinear solution.

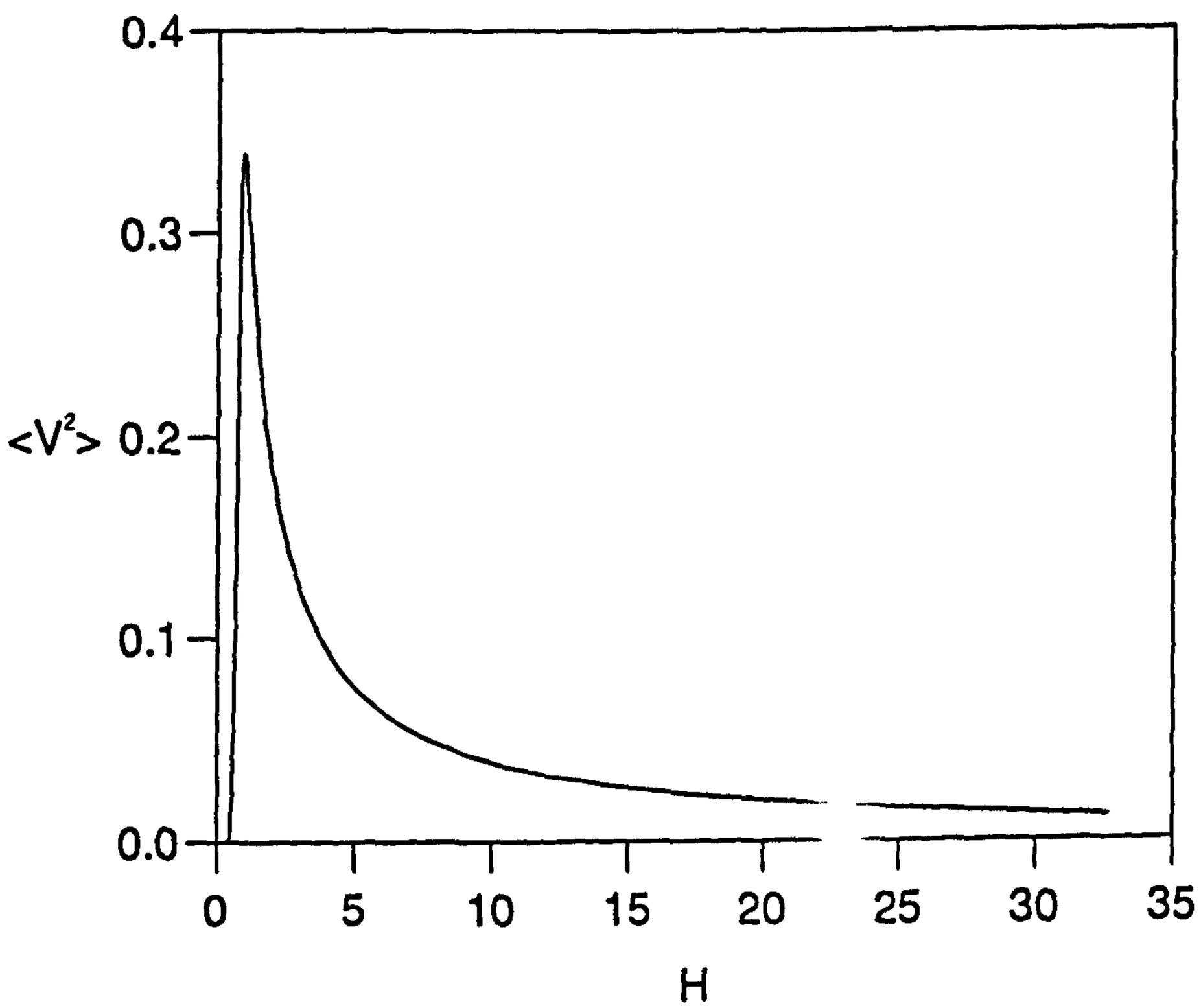

Figure 6.24: A plot of $< V^2 >$ against H for the solution (6.25) when $\Gamma = 1.0$.

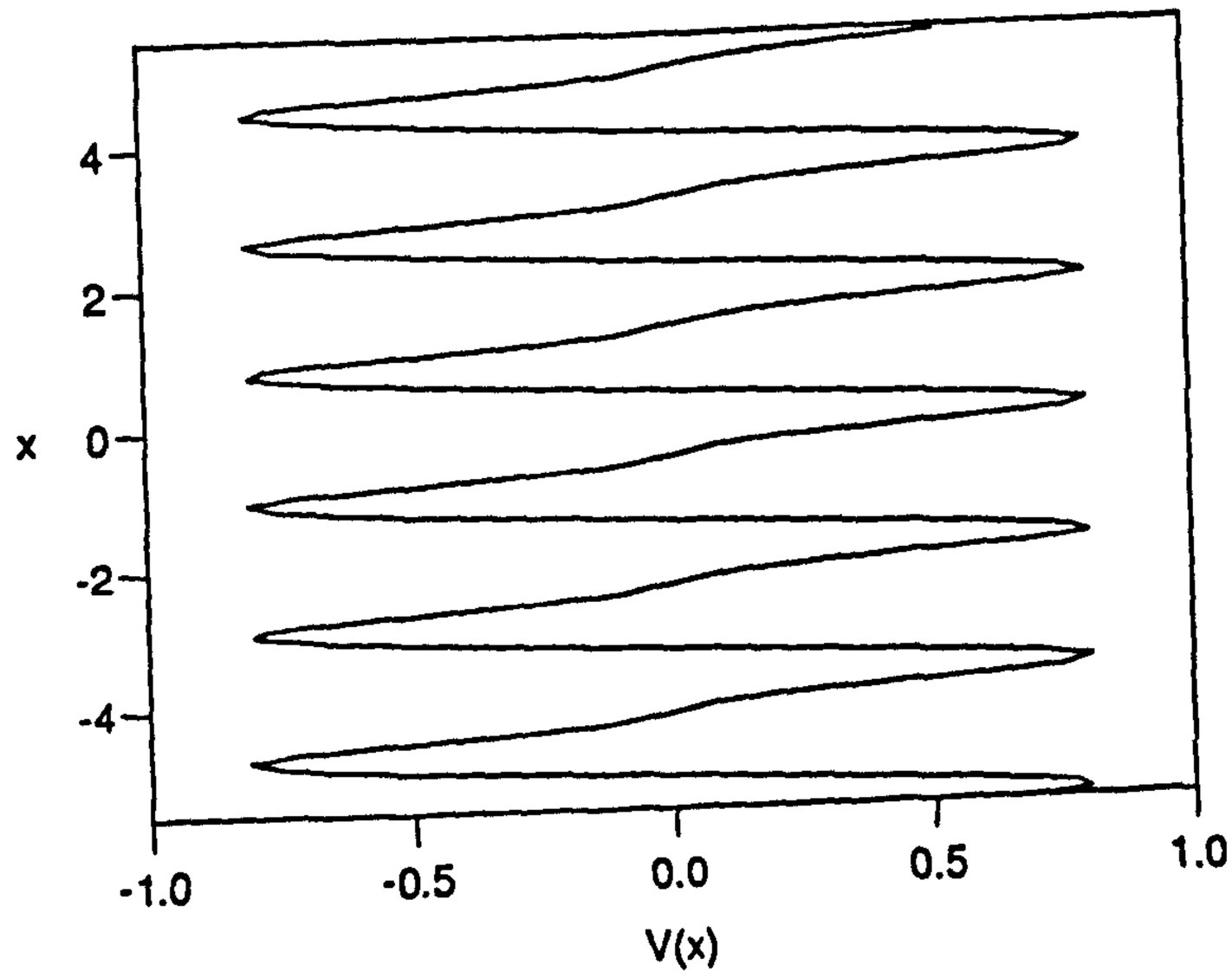

(a)

(b)

Figure 6.25: Geostrophic flow profiles for the solution (6.25) for $\Gamma = 1.0$ when (a) $R = 19.1100$ and, (b) $R = 19.37444$ on the upper branch of the solution.

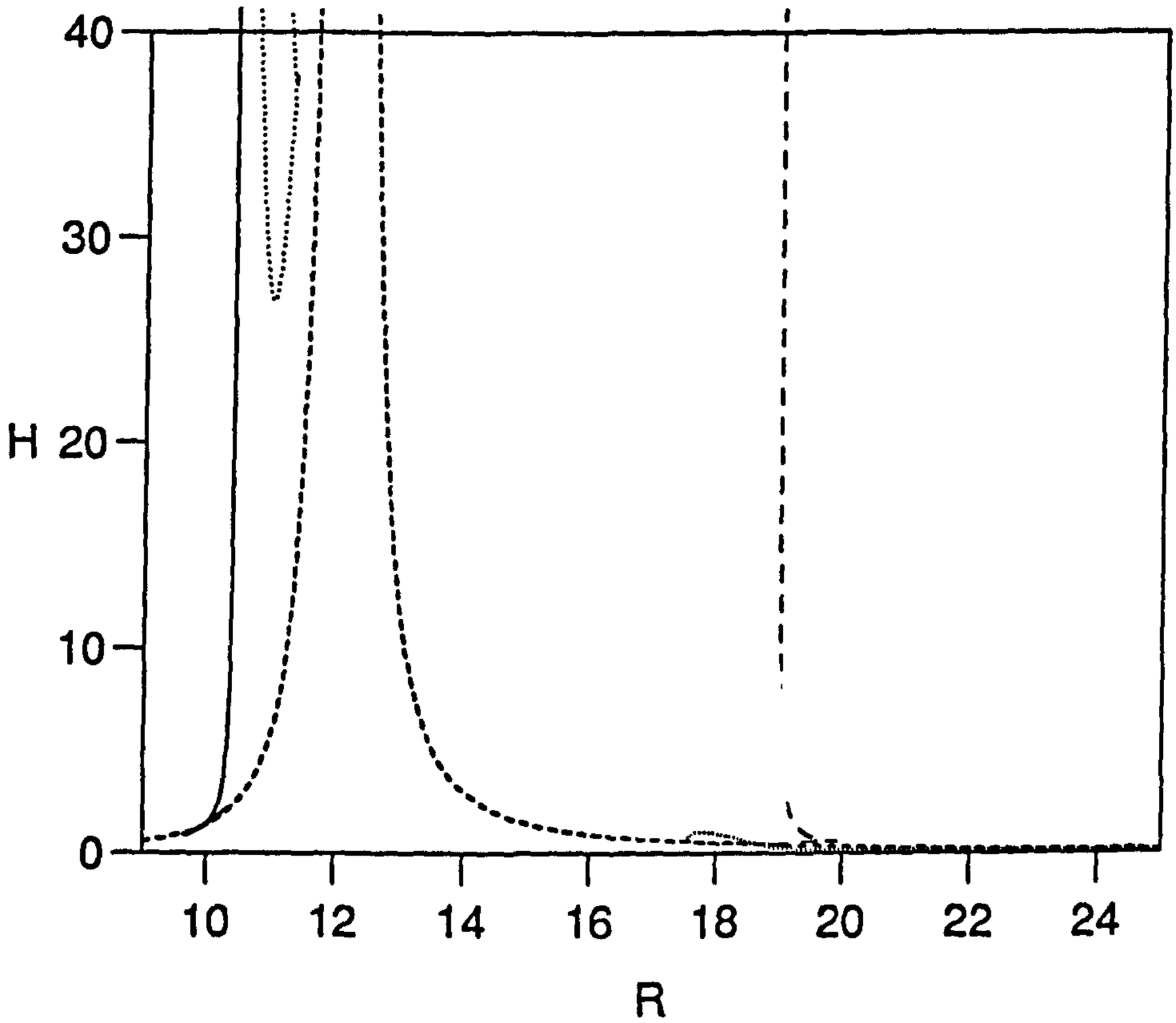

Figure 6.26: The bifurcation structure of the nonlinear solutions for the case $\Gamma = 10.0$. The curve (- - -) is the basic state, while all the other curves represent nonlinear solutions.

PAGE
MISSING
IN
ORIGINAL

At the point $R_c^{(5)}$, the solution has the form

$$\mathbf{X} = \sum_{n=-N}^{N} \mathbf{X}_{3n}(z) \exp(3inlx + imy) + c.c., \tag{6.25a}$$

$$V = \sum_{n=-N}^{N} V_{3n} \exp(3inlx) + c.c., \tag{6.25b}$$

and the double dashed curve in figure 6.1 shows this solution. The region of the bifurcation of (6.25) is shown enlarged in figure 6.13(a), while 6.13(b) shows the amplitude of the geostrophic flow associated with (6.25). These curves represent the nonlinear evolution of a linear solution of the form

$$\mathbf{X} = \sum_{n=-1}^{1} \left\{ \delta^{|n|} \mathbf{X}_{3n}(z) \right\} \exp(3inlx + imy) + c.c.. \tag{6.26}$$

The major difference between the solution (6.25) and the others described is that the lenghtscale of the convection in the x direction has been made shorter by a factor of 3. This smaller scale convection is not the preferred mode of convection, that being given by the solutions described previously, and larger values of R are needed to force it.

The solution (6.25) bifurcates supercritically off the basic state at the point $R_c^{(6)} = 18.9752$, which is the critical Rayleigh number associated with (6.26). The solution exists for $18.9752 \leq R \leq 19.0661$. For each value of R in this range, two solutions exist, one at a larger value of H than the other. The larger amplitude solutions constitute the upper branch of the graph shown in figure 6.14(a). The large amplitude solutions evolve to a Taylor state at $R_T^{(4)} = 18.9752$ via the same mechanism as the first nonlinear solution described. That is, the geostrophic flow amplitude decays to zero as $R \downarrow R_T^{(4)}$, removing the shear that controls the amplitude of the solution, and allowing Taylor's constraint to be met at $R = R_T^{(4)}$.

The Taylor solution at $R = R_T^{(4)}$ consists of a (+3)-roll whose amplitude is diverging (the amplitude of the other oblique modes decaying to zero) together with the finite amplitude transverse roll forced in the layer by the bumps. This occurs because as $R \downarrow R_T^{(4)}$, the +3 harmonic dominates the solution, while the amplitudes of the other oblique harmonics decay to zero.

6.4.2 The Case $\Gamma = 1.0$.

Increasing the value of Γ leads to a stronger geostrophic flow through the modified Taylor's constraint. The enhanced nonlinearity in this case suppresses the convection even more strongly, and as a consequence the amplitudes of the nonlinear solutions for this case (and for larger values of Γ) are smaller.

Figure 6.16 shows the bifurcation structure of the nonlinear solutions obtained when $\Gamma = 1.0$. Each curve on the diagram represents the same solution as found in the $\Gamma = 0.1$ case. Hence, the dashed curve (- - -) represents the basic state, the solid curve (——) is the nonlinear evolution of the most unstable linear solution, the dotted curve (.....) represents the nonlinear evolution of the second most unstable linear solution, and the double dashed curve (– –) is the solution (6.25) for this value of Γ.

As figures 6.17 and 6.18 show, the nonlinear evolution of the most unstable linear solution is qualitatively the same for $\Gamma = 1.0$. The solution bifurcates at the same point, $R_c^{(1)} = 10.3923$, and has a Taylor state at the same point, $R_T^{(1)} = 10.3923$ as the $\Gamma = 0.1$ case. The Taylor state, and the mechanism by which it is brought about are also similar. That is to say, the Taylor state consists of a (+)-roll with diverging amplitude, together with the finite amplitude transverse roll in the layer by the bumps.

The nonlinear solution (6.25) also behaves in a similar manner when $\Gamma = 1.0$, as figures 6.23 and 6.24 show, so it will not be discussed.

The major difference between the $\Gamma = 0.1$ solutions and the $\Gamma = 1.0$ solutions lies in the nonlinear evolution of the second most unstable linear solution. This is the dotted curve in figure 6.16, which is shown enlarged in figure 6.20. Instead of the three branch connected solution obtained previously, two distinct seperate branches are obtained, an upper branch (labelled d) and a lower branch (labelled e). As Γ is increased from 0.1 to 1.0, branch a of the $\Gamma = 0.1$ solution breaks into two parts. It's large amplitude part combines with branch b of the $\Gamma = 0.1$ solution to form branch d of this solution, while it's small amplitude part combines with branch c of the $\Gamma = 0.1$ solution to form branch e of this solution. The exact value of Γ at which the break occurs has not been determined. The amplitude of the geostrophic flow associated with branch d is shown in figure 6.21(a), while that associated with branch e is shown in figure 6.21(b).

The solutions on branch d of this solution are unusual in that they are not connected to the basic state in any way. Rather, branch d connects two (probable) Taylor states, one at $R_T^{(2)} = 10.3923$ and the other at $R_T^{(3)} = 10.8787$. The Taylor state at $R = R_T^{(1)}$ has it's origin in the Taylor state found on branch a of the $\Gamma = 0.1$ solution. It consists of a (-)-roll with diverging amplitude (the amplitude of the other oblique modes decaying to zero), together with the finite amplitude transverse roll forced by the bumps, aligned so that Taylor's constraint is met. As figure 6.21(a) shows, there is no geostrophic flow associated with this Taylor state. On the other hand, as $R \uparrow R_T^{(3)}$, the solution diverges to infinity and appears to enter a Taylor state. However, as figure 6.21(a) shows, the amplitude of the geostrophic flow is now *diverging* as this occurs and so this result needs to be treated with caution. As in the $\Gamma = 0.1$ case, it is very likely that the solution is not fully converged here, and an increase in the truncation of the solution is required to clarify matters. Again, this was not possible as the computing power was not available.

The solutions on branch e bifurcate off the basic state at the point $R_c^{(2)} = 15.8313$ (which is the critical Rayleigh number associated with the second most unstable linear solution when $\Gamma = 1.0$). The bifurcation is subcritical, and so the solutions exist for values of the Rayleigh number less than those predicted by linear stability theory. Each solution on branch e is an Ekman solution - no Taylor solutions were found. Branch e comes to an end at the point $R_c^{(3)} = 19.0230$, where it bifurcates onto the nonlinear solution (6.25) in the same manner as described in the $\Gamma = 0.1$ case: the amplitude of each harmonic that is not of the form

$$\exp(3inlx + imy)$$

(where n is an integer) decays to zero as $R \uparrow R_c^{(3)}$. It is interesting to see that the Taylor states for this solution (which lie on branch d) cannot be reached from the initial bifurcation of this solution (which occurs on branch e). This sort of solution, where the initial bifurcation is not connected to the Taylor states of the solution, has been seen before. Soward and Jones (1983) call this a type II Ekman solution. They have also been seen in models of kinematic dynamos (see for example Barenghi and Jones 1991, α^2 case).

6.4.3 The Case $\Gamma = 10.0$

The results for this value of Γ are shown in figure 6.26, which shows the bi-

furcation structure of the nonlinear solutions for this case. Since the behaviour of the solutions in the case $\Gamma = 10.0$ is qualitatively the same as that of the $\Gamma = 1.0$ case, they will not be discussed.

6.5 The Post Taylor Equilibrium

In each of the nonlinear solutions found in this chapter, the amplitude of the solution diverged to infinity as Taylor's constraint became satisfied. This was the Malkus-Proctor scenario, where the geostropic flow evolved to the eigenflow whose effect on the magnetic field through the induction equation was precisely that needed to satisfy Taylor's constraint. As V evolves to this eigenflow, the nonlinearity of the problem (the Taylor integral) vanishes. The amplitude of the solution cannot be determined once this occurs, and the solution diverges to infinity.

In the Taylor state, the solution is outside the asymptotic limit in which the governing equations (6.5) are valid. To follow the solution further, all the nonlinearities neglected in the derivation of (6.5) must be restored to the problem. These nonlinearities (e.g. the advective terms in the heat and induction equations) then become responsible for equilibrating the solution. The solutions of the full problem will also satisfy Taylor's constraint (having evolved through the Ekman states described here). Such solutions have been found in models of kinematic dynamos (see Abdel-Aziz and Jones 1988; Barenghi 1992a; Barenghi 1992b), but this procedure is not carried out here.

Chapter VII

Conclusions

The main theme of this work has been determining the effect of adding bumps to a rapidly rotating fluid layer containing a strong azimuthal magnetic field. The configuration of the layer is chosen so that the layer rotates about the vertical z direction, and has an applied magnetic field aligned in the horizontal y direction (which is chosen to represent the azimuthal direction in the core). Gravity is chosen to act in the negative z direction, and thermal forcing is used to drive the convection in the layer.

Since the main interest lies in isolating the key mechanisms by which the bumps effect the convection, the bumps themselves are assumed to take a simple form, namely a sinusoidal undulation which varies in the y direction. The axis of the bumps is chosen to be perpendicular to the applied magnetic field, and lies in the x direction. Such a simple form of topography has also been used by Kelly and Pal (1977), Kuang and Bloxham (1993) and Bell and Soward (1995) as a model of the topography on the core mantle boundary.

The bumps are assumed to be small in the sense that the bump size parameter γ satisfies

$$\gamma \ll 1.$$

To check that this is a valid assumption, γ must be calculated for the core. Taking

$$r_{\mathrm{CMB}} = 3481\mathrm{km}, \quad r_{\mathrm{ICB}} = 1221\mathrm{km},$$

as the radii of the core mantle boundary and the inner core boundary respectively, and assuming a bump height of 1km (see Hide 1967, 1969), then

$$\gamma = 4.42 \times 10^{-4}, \tag{7.1}$$

in the core. This value is certainly small enough to justify making the small bump approximation.

In chapter 2 the equations governing the topographic convection in the layer are derived from the full MHD equations governing convection in the core (i.e. the magnetogeostrophic equations). The derivation makes use of the fact that γ is small, and neglects all terms of $O(\gamma^2)$ or smaller from the problem. The resulting system of equations, namely equations (2.35), contain the parameter

$$\Gamma = \frac{\gamma^2}{E^{\frac{1}{2}}},$$

which is a modified bump size parameter. Γ is the key parameter which measures the effect of the bumps upon the convection. It also arises in the non-magnetic case (see Bell and Soward 1995; Bell 1994). In chapter 2, it is argued that Γ is a finite parameter. Again, this can be checked for the core using the values of γ and E in the core. These values give

$$\Gamma = 19.53, \tag{7.2}$$

which is certainly finite. Γ appears in the modified Taylor's constraint used to determine the geostrophic flow. It has the role of measuring the strength of the geostrophic flow, and hence, the effectiveness of the geostrophic nonlinearity in equilibrating the convection.

The boundaries of the layer are assumed to be rigid, isothermal and perfectly electrically conducting. The fact that γ is small is used to simplify the boundary conditions on the bumpy top boundary. These boundary conditions are Taylor expanded in γ, and only the $O(1)$ and $O(\gamma)$ terms are retained. In this way, a set of inhomogeneous boundary conditions on $z = \pi$ is obtained.

The presence of the bumps distorts the horizontal applied magnetic field, creating a small correction $\mathbf{b}$ to the main magnetic field. This small correction ensures that the main magnetic field fits into the bumpy layer, and is also responsible for accelerating the geostrophic flow through the modified Taylor's constraint. Similarly, the bumps create a small corrective velocity $\mathbf{u}$, which ensures that the geostrophic flow (which is aligned parallel to the applied magnetic field) also fits into the bumpy layer. This small velocity field represents the topographic convection that

is the subject of this work. Because the top boundary is an isotherm, the isotherms close to the top boundary are distorted from the horizontal. This effect is quite important, since it means that a hydrostatic balance is no longer possible in the bumpy layer.

Hence, in addition to the thermal forcing present on the bottom boundary, the fluid is also thermally forced by the bumps on the top boundary by the distortion of the isotherms. This topographic forcing is completely absent in the standard plane layer model, and gives this problem its' character.

As discussed in chapter 2, the boundary conditions on the top boundary do not reflect the true physics at the core mantle boundary. More accurate boundary conditions would reflect the fact that the lower mantle is (to a high approximation) electrically insulating, and not perfectly electrically conducting. Similarly, a condition on the heatflux through the core mantle boundary would be more realistic than arbitrarily imposing an isothermal core mantle boundary. However, as has been said already, of primary concern is isolating the mechanisms by which the bumps effect the convection. For this reason, the simpler boundary conditions are applied, in the hope that the essential physics of the problem are retained, and that the qualitative behaviour of the system remains the same.

As has been noted already, a hydrostatic balance is not possible in the bumpy layer. Hence, motion is forced by the bumps. This motion is investigated in chapter 4, and is there found to take the form of a steady transverse convection roll, whose axis is parallel to that of the bumps, and perpendicular to the applied magnetic field. This motion is not the preferred mode of convection in a plane layer for $O(1)$ values of the Elsasser number. As the results of chapter 3 and Roberts and Stewartson (1974) indicate, the preferred motion takes the form of oblique rolls, whose axes are not perpendicular to the applied magnetic field. The transverse roll is the free mode of the system, i.e. it is forced by the presence of the bumps.

The transverse roll is found to obey Taylor's constraint, and so does not accelerate a geostrophic flow. Consequently, the results of chapter 4 are independent of Γ. The roll exists for all values of the Rayleigh number R (confirming that it is indeed forced by the bumps) except for one value: it does not exist at that value of R for which the corresponding homogeneous problem in the standard plane layer has a solution. Close to this critical value of R, the amplitude of the forced transverse roll diverges to infinity. This phenomenon is called resonant wavelength excitation, and has also been found by Kelly and Pal (1977).

The stability of this transverse roll solution to perturbations which consist of a pair of oblique rolls aligned at equal but opposite angles to the applied magnetic field, together with the concomitant geostrophic flow accelerated by the interaction of these rolls with the transverse roll, is considered. The resulting linear stability problem is solved in chapter 5 (see also Appendix B).

The results of chapter 5 show that the stability characteristics of the transverse roll in the bumpy layer are identical to those found by Roberts and Stewartson (1974) for the hydrostatic conduction solution in the standard plane layer (when perturbed by oblique rolls). The reason for this was traced to the form of the most unstable perturbations in the bumpy layer. These are given by a pair of oblique rolls, which align themselves with the transverse roll in such a way that no mean Maxwell stress is generated by their interaction with the transverse roll. That is, Taylor's constraint continues to be satisfied in the perturbed state.

The vanishing of the Maxwell stress means that no geostrophic flow is accelerated by the interaction of these rolls with the transverse roll. The perturbations can then assume a simple sinusoidal z structure. Also, the stability results become independent of Γ. That the stability results are identical to those found by Roberts and Stewartson (1974) can easily be seen, since with no geostrophic flow present, the equations for the perturbations in the bumpy layer (namely equations (5.10)) become identical to those solved in Roberts and Stewartson (1974) and chapter 3 for oblique convection rolls in the standard plane layer (namely, equations (3.12)). This is shown more exactly in Appendix B, where the analytic form of the most unstable perturbations is found from equations (5.10).

These perturbations are the preferred mode of instability in the bumpy layer for two reasons. The first is that there is no shear present to inhibit these convection rolls form going unstable, since there is no geostrophic flow accelerated. The second reason is that these rolls have very simple z structures which are easier to excite in the layer. Both of these factors lead to a lower critical Rayleigh number for these perturbations than those associated with the other types of perturbations found in chapter 5, making these perturbations the preferred mode of instability in the bumpy layer.

In chapter 6, the nonlinear evolution of the linear solutions found in chapter 5 is considered. In the nonlinear regime, Taylor's constraint is violated, and the resulting non-zero Maxwell stress accelerates a geostrophic velocity. The solutions are then in an Ekman state, where their amplitudes are controlled by the shear

generated by this geostrophic flow. The nonlinear solutions found have a complicated structure. In some cases, as many as three distinct nonlinear solutions can exist at one value of the Rayleigh number.

The most unstable linear solution typically evolves nonlinearly as a type I Ekman solution (see Soward and Jones 1983). After the initial (subcritical) bifurcation, these solutions evolve through an Ekman regime where the Malkus-Proctor scenario enables the geostrophic flow to adjust so that it's effects upon the magnetic field $\mathbf{b}$ eventually satisfy Taylor's constraint. The amplitude of the solution diverges to infinity as the Taylor state is approached. This behaviour occurs for all the values of Γ considered. By contrast, the nonlinear evolution of the second most unstable linear solution is different. For small values of Γ, type I Ekman solutions are found, but as Γ is increased, the solutions become type II Ekman solutions. Here, the Taylor states of the solutions lie on an upper branch, which is not connected to the initial bifurcation of the solution. For all values of Γ, a branch of these solutions is connected to a third type of nonlinear solution, for which the lengthscale of the convection in the x direction is smaller. In general, the evolution of the nonlinear solutions found is quite similar to the evolution of several mean field dynamo models incorporating a geostrophic nonlinearity (see for example Abdel-Aziz and Jones 1988).

Two distinct types of Taylor solution are found. In the first, the amplitude of the geostrophic flow decays to zero as it adjusted via the Malkus-Proctor scenario to enable Taylor's constraint to be met. These Taylor solutions can be associated with the single oblique roll Taylor solutions found by Roberts and Stewartson (1974). For instance, the Taylor state reached in the nonlinear evolution of the most unstable linear solution consists of a large amplitude (+)-roll together with the finite transverse roll forced by the bumps, aligned so that no Maxwell stress is generated. Hence, there is an interesting connection between the large amplitude Taylor solutions in the bumpy layer and the Taylor solutions of the standard layer.

The second type of Taylor solution is different. There, the amplitude of the geostrophic flow remains finite as the Taylor state is approached i.e. it evolves towards an eigenflow (Malkus and Proctor 1975). These Taylor solutions cannot be associated with any Roberts and Stewartson Taylor solutions, as all the harmonics of the solution remain. However, as noted in chapter 6, it is not known for certain whether these solutions do evolve to a Taylor state, since the convergance of the solutions are in doubt. Hence, these results must be treated with caution. The

doubt could be removed by increasing the truncation of the relevant solutions, but as the computing power to do this was not available, this was not attempted.

In conclusion therefore, it has been shown that even small scale topography can have an effect upon the dynamics of a rotating plane layer. The presence of the bumps lead to inhomogeneities which create an imperfect configuration. This necessitates the calculation of an inhomogeneous basic state in the layer, which takes the form of a transverse roll. This transverse roll has a large effect upon the stability characteristics of the preferred mode of convection of the layer (i.e. the oblique rolls) and upon their subsequent nonlinear bifurcation structure.

However, the effects of the bumps only really have an effect in the asymptotic regime considered in this work i.e. when the amplitude of the convection forced is small, of the same magnitude of the bumps themselves. As we have shown, the solutions quickly evolve to large amplitude Taylor states, outside this regime. In this large amplitude regime, it is probable that the bumps will not have any real effect save through the presence of the finite amplitude transverse roll, which is always forced by the bumps.

However, a lot more work needs to be done on this problem. For instance, the question of the stability of the nonlinear solutions found was not considered. Of more importance perhaps, is the Post-Taylor regime, where Taylor's constraint is satisfied by the solutions. In this regime, all the nonlinearity neglected in this model would be restored. These new nonlinearities would become responsible for equilibrating the amplitude of the fully three dimensional convection that would ensue in this regime. Of larger interest is the question of how topography effects convection in a spherical shell. The results of such a study would have many implications for the geodynamo problem itself, and is the ultimate goal of this preliminary work.

Appendix A

The Tau Method - Example

Consider the following simple problem. Solve the ODE

$$D^2 f - k^2 f = 0, \tag{A.1}$$

(where k is a real constant) subject to the boundary conditions

$$f = 0 \quad \text{on} \quad z = 0, \tag{A.2a}$$

$$f = 1 \quad \text{on} \quad z = \pi. \tag{A.2b}$$

Now, this problem has a well defined, analytic solution, given by

$$f(z) = \frac{\sinh(kz)}{\sinh(k\pi)}. \tag{A.3}$$

However, to solve it using the Tau method, f is expanded in terms of Legendre polynomials as

$$f(z) = \sum_{n=0}^{M+2} f_n P_n(z'), \tag{A.4}$$

where M is a positive integer, and the f_n are constants. There are $M+3$ coefficients to be determined. Substituting (A.4) into (A.1) using (5.16b) yields the equation

$$\sum_{n=0}^{M} \left\{ \frac{2(2n+1)}{\pi^2} \sum_{\substack{p=n+2 \\ p+n \text{ even}}}^{M+2} [p(p+1) - n(n+1)] f_p \right\} P_n(z') - \sum_{n=0}^{M+2} k^2 f_n P_n(z') = 0. \tag{A.5}$$

Now, for each $m \in \{0, 1, ..., M\}$, equation (A.5) is multiplied by $P_m(z')$, and integrated from -1 to 1 in z'. Using the orthogonality condition (5.15), this process yields the following system of equations

$$\frac{2(2n+1)}{\pi^2} \sum_{\substack{p=n+2 \\ p+n \text{ even}}}^{M+2} [p(p+1) - n(n+1)] f_p - k^2 f_n = 0 \quad (0 \leq n \leq M). \qquad (A.6)$$

Note that the solution of (A.6) does not satisfy (A.5) *exactly*. Rather, the solution of (A.6) implies the modified equation,

$$\sum_{n=0}^{M} \left\{ \frac{2(2n+1)}{\pi^2} \sum_{\substack{p=n+2 \\ p+n \text{ even}}}^{M+2} [p(p+1) - n(n+1)] f_p \right\} P_n(z') - \sum_{n=0}^{M} k^2 f_n P_n(z') = 0. \quad (A.7)$$

However, the difference between the solution of (A.7) and the exact equation (A.5) tends to zero as $M \to \infty$, provided that the expansion (A.4) converges to the solution of (A.1) as $M \to \infty$.

Now, (A.6) defines $M+1$ algebraic equations for the f_n. But there are $M+3$ spectral coefficients. To close the system, two extra equations are needed. These equations are obtained from the boundary conditions (A.2). Substituting (A.4) into (A.2) using (5.17) yields the equations

$$\sum_{n=0}^{M+2} (-1)^n f_n = 0, \qquad (A.8a)$$

$$\sum_{n=0}^{M+2} f_n = 1. \qquad (A.8b)$$

Together, (A.6) and (A.8) define $M+3$ algebraic equations for the $M+3$ spectral coefficients f_n. In matrix notation, these equations take the form

$$\mathbf{LY} = \mathbf{R},$$

where $\mathbf{Y}$ and $\mathbf{R}$ are $(M+3) \times 1$ vectors defined by

$$\mathbf{Y}^T = \begin{bmatrix} f_0 & f_1 & f_2 & .... & f_{M+2} \end{bmatrix},$$

$$\mathbf{R}^T = \begin{bmatrix} 0 & 0 & 0 & .... & 0 & 1 \end{bmatrix},$$

and $\mathbf{L}$ is an $(M+3) \times (M+3)$ matrix of the form

$$\mathbf{L} = \begin{bmatrix} -k^2 & 0 & x & 0 & x & ... & . \\ 0 & -k^2 & 0 & x & 0 & ... & . \\ 0 & 0 & -k^2 & 0 & x & ... & . \\ 0 & 0 & 0 & -k^2 & 0 & ... & . \\ . & . & . & . & . & ... & . \\ . & . & . & . & . & ... & . \\ 1 & -1 & 1 & -1 & 1 & ... & (-1)^{M+2} \\ 1 & 1 & 1 & 1 & 1 & ... & 1 \end{bmatrix},$$

where x denotes a nonzero entry. This matrix equation may be set up numerically and solved using NAG routine F04ADF at given values of M. To ensure convergence, it is necessary to check that

$$\left| f(z) - \sum_{n=0}^{M+2} f_n P_n(z') \right| \to 0 \quad \text{as} \quad M \to \infty,$$

for each $z \in [0, \pi]$, where f is given by (A.3). In the case where the exact analytic form of $f(z)$ is not known, the test for convergence is slightly different. In such a case (as is considered in the work), define

$$f_M(z) = \sum_{n=0}^{M+2} f_n P_n(z').$$

Then, the method converges if

$$\left| f_{M+1}(z) - f_M(z) \right| \to 0 \quad \text{as} \quad M \to \infty.$$

A sequence of functions satisfying this criterion is said to Cauchy, and it can be shown that a Cauchy sequence converges in the usual sense (see any textbook on

analysis). Note that the Tau method can be easily adapted to deal with systems of equations with multiple boundary conditions.

Appendix B

Analytic Solutions Of The Perturbation Equations In The Limit $\Gamma \ll 1$

B.1 A New Notation

While it is necessary to solve the equations for the z-structure of the perturbations numerically, analytic results can be obtained in the limit of small Γ, i.e. when Γ satisfies

$$0 < \Gamma \ll 1. \tag{B.1}$$

The left hand inequality is necessary since solutions of the perturbation equations are only valid for non-zero values of Γ. In order to obtain the results, it is helpful to write the equations that are to be solved (namely, equations (4.6) for the z-structure of the basic state, and equations (5.10) and (5.11) for the z-structure of the perturbations) in a more compact form. This will be done using matrix notation. Throughout the following, r is assumed to take the values -1, 0 or 1.

Let the z-structures of the unknowns be given (as usual) by the vectors

$$\mathbf{X}_r^T(z) = \Big[T_r(z) \quad W_r(z) \quad B_r(z) \quad X_r(z) \quad Z_r(z)$$

$$B_{xr}(z) \quad B_{yr}(z) \quad U_{xr}(z) \quad U_{yr}(z)\Big].$$

Then, all the derivatives that act upon the $\mathbf{X}_r$ in equations (4.6) and (5.10) can be collected together to form the following 9×9 linear differential operator

$$\mathbf{D}_r(R) =$$

$$\begin{bmatrix}
0 & 2D & 0 & \Lambda im & 0 & 0 & 0 & 0 & 0 \\
k_r^2 R & 0 & -\Lambda im(D^2 - k_r^2) & 0 & 2D & 0 & 0 & 0 & 0 \\
0 & im & D^2 - k_r^2 & 0 & 0 & 0 & 0 & 0 & 0 \\
0 & 0 & 0 & D^2 - k_r^2 & im & 0 & 0 & 0 & 0 \\
D^2 - k_r^2 & 1 & 0 & 0 & 0 & 0 & 0 & 0 & 0 \\
0 & 0 & -irlD & -im & 0 & k_r^2 & 0 & 0 & 0 \\
0 & 0 & -imD & irl & 0 & 0 & k_r^2 & 0 & 0 \\
0 & -irlD & 0 & 0 & -im & 0 & 0 & k_r^2 & 0 \\
0 & -imD & 0 & 0 & irl & 0 & 0 & 0 & k_r^2
\end{bmatrix} \tag{B.2}$$

where $D = \frac{d}{dz}$, and

$$k_r^2 = r^2 l^2 + m^2.$$

Now, the terms in equations (5.10) that describe the interaction of the perturbations with the basic state take the form

$$\mathcal{U}\mathbf{I}_{-1}^*, \quad \mathcal{U}\mathbf{I}_1,$$

where $\mathcal{U}$ is the coefficient of the perturbation geostrophic flow, and $\mathbf{I}_{\pm 1}$ is a 9×1 vector defined by

$$\mathbf{I}_{\pm 1} = \begin{bmatrix}
0 \\
0 \\
qimB_0 \\
q\{imX_0 + l^2 B_{x0} \mp lmB_{y0}\} \\
imT_0 \\
0 \\
0 \\
0 \\
0
\end{bmatrix}. \tag{B.3}$$

Similarly, the terms of (5.10) that involve the complex number

$$\lambda = s + i\omega,$$

(where s is the growth rate and ω is the frequency of the perturbations) take the form

$$\lambda \mathbf{J} \mathbf{X}_{\pm 1},$$

where $\mathbf{J}$ is a 9×9 matrix defined by

$$\mathbf{J} = \begin{bmatrix} 0 & 0 & 0 & 0 & 0 & 0 & 0 & 0 & 0 \\ 0 & 0 & 0 & 0 & 0 & 0 & 0 & 0 & 0 \\ 0 & 0 & q & 0 & 0 & 0 & 0 & 0 & 0 \\ 0 & 0 & 0 & q & 0 & 0 & 0 & 0 & 0 \\ 1 & 0 & 0 & 0 & 0 & 0 & 0 & 0 & 0 \\ 0 & 0 & 0 & 0 & 0 & 0 & 0 & 0 & 0 \\ 0 & 0 & 0 & 0 & 0 & 0 & 0 & 0 & 0 \\ 0 & 0 & 0 & 0 & 0 & 0 & 0 & 0 & 0 \\ 0 & 0 & 0 & 0 & 0 & 0 & 0 & 0 & 0 \end{bmatrix}. \qquad (B.4)$$

From these definitions, the equations for the z-structures of the unknowns can be written in the form

$$\mathbf{D}_0(R)\mathbf{X}_0 = 0, \qquad (B.5a)$$

$$\left\{\mathbf{D}^*_{-1}(R) - \lambda \mathbf{J}\right\}\mathbf{X}_{-1} = \mathcal{U}\mathbf{I}^*_{-1}, \qquad (B.5b)$$

$$\left\{\mathbf{D}_1(R) - \lambda \mathbf{J}\right\}\mathbf{X}_1 = \mathcal{U}\mathbf{I}_1, \qquad (B.5b)$$

where $\mathcal{U}$ is determined from the equation

$$\mathcal{U} = \Gamma \frac{ilq\Lambda}{2\pi} \int_0^\pi (B_{x0}^* B_{y1} + B_{x0} B_{y,-1} + B_{x,-1} B_{y0} + B_{x1} B_{y0}^*) dz. \qquad (B.6)$$

The matrix equation equation (B.5a) represents equations (4.6) for the z-structure of the basic state (which is given by $\mathbf{X}_0$, as in chapter 4), while (B.5b) and (B.5c) represent the equations for the z-structure of the perturbations (which are given by $\mathbf{X}_{\pm 1}$, as in chapter 5). Equation (B.6) is for the coefficient of the perturbation geostrophic flow, V_p. These equations are to be solved subject to the boundary conditions

$$W_0 = B_0 = DX_0 = T_0 = 0 \quad \text{on} \quad z = 0, \qquad (B.7a)$$

$$W_0 = B_0 - \frac{im}{2q} = DX_0 = T_0 - \frac{1}{2} = 0 \quad \text{on} \quad z = \pi, \qquad (B.7b)$$

$$W_{-1} = B_{-1} = DX_{-1} = T_{-1} = 0 \quad \text{on} \quad z = 0, \qquad (B.7c)$$

$$W_{-1} + \frac{im\mathcal{U}}{2} = B_{-1} = DX_{-1} = T_{-1} = 0 \quad \text{on} \quad z = \pi, \qquad (B.7d)$$

$$W_1 = B_1 = DX_1 = T_1 = 0 \quad \text{on} \quad z = 0, \qquad (B.7e)$$

$$W_1 - \frac{im\mathcal{U}}{2} = B_1 = DX_1 = T_1 = 0 \quad \text{on} \quad z = \pi. \qquad (B.7f)$$

As usual, the stability of the basic state to the perturbations is decided by the sign of s. If s is negative, then the basic state is stable to the perturbations, but if s is positive, then the basic state is unstable to the perturbations. The critical Rayleigh number, at which the basic state loses stability to the perturbations, is defined to be that value R_c of R for which

$$s(R_c) = 0.$$

The value of ω at R_c, denoted by ω_c, says how the basic state loses stability. If ω_c is zero, then the basic state loses stability through the exchange of stabilities; but, if ω_c is non-zero, then the basic state loses stability through overstability. To find R_c and ω_c, s is set to zero in (B.5). This yields the following equations

$$\mathbf{D}_0(R_c)\mathbf{X}_0 = 0, \tag{B.8a}$$

$$\left\{\mathbf{D}^*_{-1}(R_c) - i\omega_c\mathbf{J}\right\}\mathbf{X}_{-1} = \mathcal{U}\mathbf{I}^*_{-1}, \tag{B.8b}$$

$$\left\{\mathbf{D}_1(R_c) - i\omega_c\mathbf{J}\right\}\mathbf{X}_1 = \mathcal{U}\mathbf{I}_1, \tag{B.8c}$$

$$\mathcal{U} = \Gamma\frac{ilq\Lambda}{2\pi}\int_0^\pi (B^*_{x0}B_{y1} + B_{x0}B_{y,-1} + B_{x,-1}B_{y0} + B_{x1}B^*_{y0})dz. \tag{B.8d}$$

Equations (B.8) must be solved subject to (B.7) to obtain $\mathbf{X}_0$, $\mathbf{X}_{-1}$, $\mathbf{X}_1$ and ω_c at $R = R_c$.

B.2 The Method Of Solution

In the limit being considered, i.e. (B.1), the fact that

$$\Gamma \ll 1,$$

can be used to obtain analytic solutions of equations (B.8). This is done by expanding the unknowns as power series in Γ. Hence, a solution of (B.8) is sought of the form

$$\mathbf{X}_r(z) = \sum_{n=0}^{\infty} \Gamma^n \mathbf{X}_{rn}(z), \tag{B.9a}$$

$$\mathcal{U} = \sum_{n=1}^{\infty} \Gamma^n \mathcal{U}_n, \tag{B.9b}$$

$$R_c = \sum_{n=0}^{\infty} \Gamma^n R_{cn}, \tag{B.9c}$$

$$\omega_c = \sum_{n=0}^{\infty} \Gamma^n \omega_{cn}. \tag{B.9d}$$

(The expansion for $\mathcal{U}$ arises as a consequence of (B.8d), which says that $\mathcal{U}$ is $O(\Gamma)$ at leading order). These expansions are substituted into equations (B.8) and boundary conditions (B.7). Using standard methods for manipulating infinite series, the following equations for the coefficients of the expansions are obtained

$$\mathbf{D}_0(R_{c0})\mathbf{X}_{0n} = \mathbf{F}_{0n} \quad (n = 0, 1, 2...), \tag{B.10a}$$

$$\left\{\mathbf{D}^*_{-1}(R_{c0}) - i\omega_{c0}\mathbf{J}\right\}\mathbf{X}_{-1n} = \mathbf{F}_{-1n} \quad (n = 0, 1, 2, ...), \tag{B.10b}$$

$$\left\{\mathbf{D}_1(R_{c0}) - i\omega_{c0}\mathbf{J}\right\}\mathbf{X}_{1n} = \mathbf{F}_{1n} \quad (n = 0, 1, 2, ...), \tag{B.10c}$$

$$\mathcal{U}_{n+1} = \sum_{m=0}^{n} \left[\frac{il\Lambda q}{2\pi} \int_0^{\pi} (B^*_{x0m} B_{y1,n-m} + B_{x0m} B_{y-1,n-m} \right.$$

$$\left. + B_{x-1,m} B_{y0,n-m} + B_{x1m} B^*_{y0,n-m}) dz\right] \quad (n = 0, 1, 2, ...), \tag{B.10d}$$

where the right hand sides of these equations are given by

$$\mathbf{F}_{0n} = \sum_{m=1}^{n} \left\{ -\hat{\mathbf{D}}_0(R_{cm})\mathbf{X}_{0,n-m} \right\}(1-\delta_{0n}), \qquad (B.11a)$$

$$\mathbf{F}_{-1n} = \sum_{m=1}^{n} \left\{ \mathcal{U}_m \mathbf{I}^*_{-1,n-m} - \{\hat{\mathbf{D}}^*_{-1}(R_{cm}) - i\omega_{cm}\mathbf{J}\}\mathbf{X}_{-1,n-m} \right\}(1-\delta_{0n}), \quad (B.11b)$$

$$\mathbf{F}_{1n} = \sum_{m=1}^{n} \left\{ \mathcal{U}_m \mathbf{I}_{1,n-m} - \{\hat{\mathbf{D}}_1(R_{cm}) - i\omega_{cm}\mathbf{J}\}\mathbf{X}_{1,n-m} \right\}(1-\delta_{0n}). \qquad (B.11c)$$

In (B.11), δ_{nm} is the Kronecker delta, $\hat{\mathbf{D}}_r(R_{cn})$ is a 9×9 matrix defined by

$$\hat{\mathbf{D}}_r(R_{cn}) = \begin{bmatrix} 0 & 0 & 0 & 0 & 0 & 0 & 0 & 0 & 0 \\ k_r^2 R_{cn} & 0 & 0 & 0 & 0 & 0 & 0 & 0 & 0 \\ 0 & 0 & 0 & 0 & 0 & 0 & 0 & 0 & 0 \\ 0 & 0 & 0 & 0 & 0 & 0 & 0 & 0 & 0 \\ 0 & 0 & 0 & 0 & 0 & 0 & 0 & 0 & 0 \\ 0 & 0 & 0 & 0 & 0 & 0 & 0 & 0 & 0 \\ 0 & 0 & 0 & 0 & 0 & 0 & 0 & 0 & 0 \\ 0 & 0 & 0 & 0 & 0 & 0 & 0 & 0 & 0 \\ 0 & 0 & 0 & 0 & 0 & 0 & 0 & 0 & 0 \end{bmatrix} \quad (n = 1, 2, \ldots), \qquad (B.12)$$

and $\mathbf{I}_{\pm 1,n}$ is a 9×1 vector defined by

$$\mathbf{I}_{\pm 1,n} = \begin{bmatrix} 0 \\ 0 \\ qimB_{0n} \\ q\{imX_{0n} + l^2 B_{x0n} \mp lmB_{y0n}\} \\ imT_{0n} \\ 0 \\ 0 \\ 0 \\ 0 \end{bmatrix} \quad (n = 0, 1, 2, \ldots). \qquad (B.13)$$

The boundary conditions (B.7) are satisfied by (B.9) provided that

$$W_{0n} = B_{0n} = DX_{0n} = T_{0n} = 0 \quad \text{on} \quad z = 0 \quad (n = 0, 1, 2, ...), \qquad (B.14a)$$

$$W_{0n} = B_{0n} - \frac{im}{2q}\delta_{0n} = DX_{0n} = T_{0n} - \frac{1}{2}\delta_{0n} = 0 \quad \text{on} \quad z = \pi \quad (n = 0, 1, 2, ...), \qquad (B.14b)$$

$$W_{-1n} = B_{-1n} = DX_{-1n} = T_{-1n} = 0 \quad \text{on} \quad z = 0 \quad (n = 0, 1, 2, ...), \qquad (B.14c)$$

$$W_{-1n} + \frac{im\mathcal{U}_n}{2}(1 - \delta_{0n}) = B_{-1n} = DX_{-1n} = T_{-1n} = 0 \quad \text{on} \quad z = \pi \, (n = 0, 1, 2, ...), \qquad (B.14d)$$

$$W_{1n} = B_{1n} = DX_{1n} = T_{1n} = 0 \quad \text{on} \quad z = 0 \quad (n = 0, 1, 2, ...), \qquad (B.14e)$$

$$W_{1n} - \frac{im\mathcal{U}_n}{2}(1 - \delta_{0n}) = B_{1n} = DX_{1n} = T_{1n} = 0 \quad \text{on} \quad z = \pi \, (n = 0, 1, 2, ...). \qquad (B.14f)$$

Equations (B.10), (B.11) and (B.14) define a hierarchy of problems for the coefficients of the expansions (B.9), each of which may be solved successively, starting with the $n = 0$ problem. Examination of the equations reveals that R_{cn} and ω_{cn} appear in the equations for the $\mathbf{X}_{rn}$. These two quantities are determined to ensure that the n^{th} system of equations can be solved. This is done by applying solvability conditions to the relevant equations. These solvability conditions will be described later.

B.3 The n=0 Problem

The first problem to be considered is the $n = 0$ problem. This is the easiest problem to solve, since there is no coefficient of $\mathcal{U}$ to determine at this order. Hence, setting $n = 0$ in equations (B.10), (B.11) and (B.14), the following equations for the $O(1)$ terms of the expansions (B.9) are obtained

$$\mathbf{D}_0(R_{c0})\mathbf{X}_{00} = 0, \qquad (B.15a)$$

$$\left\{\mathbf{D}^*_{-1}(R_{c0}) - i\omega_{c0}\mathbf{J}\right\}\mathbf{X}_{-10} = 0, \qquad (B.15b)$$

$$\left\{\mathbf{D}_1(R_{c0}) - i\omega_{c0}\mathbf{J}\right\}\mathbf{X}_{10} = 0. \qquad (B.15c)$$

These are to be solved subject to

$$W_{00} = B_{00} = DX_{00} = T_{00} = 0 \quad \text{on} \quad z = 0, \qquad (B.16a)$$

$$W_{00} = B_{00} - \frac{im}{2q} = DX_{00} = T_{00} - \frac{1}{2} = 0 \quad \text{on} \quad z = \pi, \qquad (B.16b)$$

$$W_{-10} = B_{-10} = DX_{-10} = T_{-10} = 0 \quad \text{on} \quad z = 0, \qquad (B.16c)$$

$$W_{-10} = B_{-10} = DX_{-10} = T_{-10} = 0 \quad \text{on} \quad z = \pi, \qquad (B.16d)$$

$$W_{10} = B_{10} = DX_{10} = T_{10} = 0 \quad \text{on} \quad z = 0, \qquad (B.16e)$$

$$W_{10} = B_{10} = DX_{10} = T_{10} = 0 \quad \text{on} \quad z = \pi. \qquad (B.16f)$$

Now, the equations and boundary conditions for $\mathbf{X}_{-10}$ and $\mathbf{X}_{10}$ are identical to those solved in chapter 3 for the Roberts and Stewartson (-) and (+) oblique

convection rolls in a standard plane layer. Therefore, the solution of (B.15b,c) subject to the relevant boundary conditions is given by

$$\mathbf{X}_{-10}(z) = A_{-10}\mathbf{X}_{-1RS}(z), \quad \mathbf{X}_{10}(z) = A_{10}\mathbf{X}_{1RS}(z), \qquad (B.17)$$

where $\mathbf{X}_{-1RS}$ is defined by (3.49) and $\mathbf{X}_{1RS}$ is defined by (3.15). A_{-10} and A_{10} are arbitrary complex constants. This solution only exists provided that the following relation holds

$$4(qi\omega_{c0} + 1 + k^2)^2(i\omega_{c0} + 1 + k^2) + \Lambda^2 m^4(i\omega_{c0} + 1 + k^2)(1 + k^2)$$
$$-k^2\Lambda m^2(qi\omega_{c0} + 1 + k^2)R_{c0} = 0, \qquad (B.18)$$

where

$$k^2 = k_1^2 = k_{-1}^2 = l^2 + m^2.$$

In the context considered here, (B.18) provides a solvability condition which yields those values of R_{c0} and ω_{c0} for which (B.15) and (B.16) have a solution. Recall from chapter 3 that (B.18) has two possible solutions for oblique rolls. Either

$$\omega_{c0}^2 = 0, \qquad (B.19a)$$

$$R_{c0} = \frac{4(1 + k^2)^2}{\Lambda m^2 k^2} + \frac{\Lambda m^2(1 + k^2)}{k^2}, \qquad (B.19b)$$

or

$$\omega_{c0}^2 = \frac{(q-1)\Lambda^2 m^4(1 + k^2) - 4(q + 1)^2(1 + k^2)^2}{4q^2(1 + q)^2}, \qquad (B.20a)$$

$$R_{c0} = \frac{2}{q}\left\{\frac{4(1 + q)(1 + k^2)^2}{\Lambda m^2 k^2} + \frac{\Lambda m^2(1 + k^2)}{k^2(1 + q)}\right\}. \qquad (B.20b)$$

These are the only values of R_{c0} and ω_{c0} for which the $n = 0$ problem has a solution.

Using the values of R_{c0} in (B.15a), $\mathbf{X}_{00}$ can be found exactly as in chapter 4. It is given by

$$\mathbf{X}_{00}(z) = \begin{bmatrix} T_{00}(z) \\ W_{00}(z) \\ B_{00}(z) \\ X_{00}(z) \\ Z_{00}(z) \\ B_{x00}(z) \\ B_{y00}(z) \\ U_{x00}(z) \\ U_{y00}(z) \end{bmatrix} = \begin{bmatrix} \sum_{n=1}^{6} A_{00n} \exp(\lambda_n z) \\ \sum_{n=1}^{6} (m^2 - \lambda_n^2) A_{00n} \exp(\lambda_n z) \\ \sum_{n=1}^{6} imA_{00n} \exp(\lambda_n z) + \frac{im(1-q)}{2q \sinh(m\pi)} \sinh(mz) \\ \frac{2i}{\Lambda m} \sum_{n=1}^{6} \lambda_n (m^2 - \lambda_n^2) A_{00n} \exp(\lambda_n z) \\ \frac{2}{\Lambda m^2} \sum_{n=1}^{6} \lambda_n (m^2 - \lambda_n^2)^2 A_{00n} \exp(\lambda_n z) \\ \frac{-2}{\Lambda m^2} \sum_{n=1}^{6} \lambda_n (m^2 - \lambda_n^2) A_{00n} \exp(\lambda_n z) \\ -\sum_{n=1}^{6} \lambda_n A_{00n} \exp(\lambda_n z) + \frac{(q-1)m}{2q \sinh(m\pi)} \cosh(mz) \\ \frac{2i}{\Lambda m^3} \sum_{n=1}^{6} \lambda_n (m^2 - \lambda_n^2)^2 A_{00n} \exp(\lambda_n z) \\ \frac{i}{m} \sum_{n=1}^{6} \lambda_n (m^2 - \lambda_n^2) A_{00n} \exp(\lambda_n z) \end{bmatrix}, \tag{B.21}$$

where the λ_n are the zeros of the polynomial (4.9) at the point $R = R_{c0}$, and the A_{00n} are the solutions of the linear equations (4.10). The values of R_{c0} in (4.9) are given by (B.19b) or (B.20b), depending on which case is being considered. Both cases can be considered simultaneously by retaining the term involving ω_{c0} throughout the calculation.

B.4 The n=1 Problem

Having solved the $n = 0$ problem, the next step is to solve the $n = 1$ problem for the $O(\Gamma)$ terms in the expansions (B.9). It is at this order that the first effects of the perturbation geostrophic flow are felt. The equations to be solved at this order are

$$\mathbf{D}_0(R_{c0})\mathbf{X}_{01} = -\hat{\mathbf{D}}_0(R_{c1})\mathbf{X}_{00}, \qquad (B.22a)$$

$$\left\{\mathbf{D}^*_{-1}(R_{c0}) - i\omega_{c0}\mathbf{J}\right\}\mathbf{X}_{-11} = \mathcal{U}_1\mathbf{I}^*_{-10} - \left\{\hat{\mathbf{D}}^*_{-1}(R_{c1}) - i\omega_{c1}\mathbf{J}\right\}\mathbf{X}_{-10}, \qquad (B.22b)$$

$$\left\{\mathbf{D}_1(R_{c0}) - i\omega_{c0}\mathbf{J}\right\}\mathbf{X}_{11} = \mathcal{U}_1\mathbf{I}_{10} - \left\{\hat{\mathbf{D}}_{10}(R_{c1}) - i\omega_{c1}\mathbf{J}\right\}\mathbf{X}_{10}, \qquad (B.22c)$$

$$\mathcal{U}_1 = \frac{il\Lambda q}{2\pi}\int_0^\pi (B^*_{x00}B_{y10} + B_{x00}B_{y,-10} + B_{x,-10}B_{y00} + B_{x10}B^*_{y00})dz. \qquad (B.22d)$$

These equations are to be solved subject to the boundary conditions

$$W_{01} = B_{01} = DX_{01} = T_{01} = 0 \quad \text{on} \quad z = 0, \qquad (B.23a)$$

$$W_{01} = B_{01} = DX_{01} = T_{01} = 0 \quad \text{on} \quad z = \pi, \qquad (B.23b)$$

$$W_{-11} = B_{-11} = DX_{-11} = T_{-11} = 0 \quad \text{on} \quad z = 0, \qquad (B.23c)$$

$$W_{-11} + \frac{im\mathcal{U}_1}{2} = B_{-11} = DX_{-11} = T_{-11} = 0 \quad \text{on} \quad z = \pi, \qquad (B.23d)$$

$$W_{11} = B_{11} = DX_{11} = T_{11} = 0 \quad \text{on} \quad z = 0, \qquad (B.23e)$$

$$W_{11} - \frac{im\mathcal{U}_1}{2} = B_{11} = DX_{11} = T_{11} = 0 \quad \text{on} \quad z = \pi. \qquad (B.23f)$$

Now, all the quantities on the right hand side of (B.22d) are known, having been found in the previous section. It is therefore easy to perform the relevant integrations to find $\mathcal{U}_1$. It transpires that

$$\mathcal{U}_1 = a_1 A_{10} + a_2 A_{-10}, \tag{B.24}$$

where A_{10} and A_{-10} are the arbitrary complex constants that arose in the solution of the $n = 0$ problem, and the a_n are complex constants, defined by

$$a_1 = \frac{\Lambda q l}{2m}\left\{\frac{-m^2}{k^2(1+k^2+iq\omega_{c0})} + \frac{2l}{\Lambda k^2 m}\right\}(1+k^2+i\omega_{c0})I_2^*$$

$$+\frac{\Lambda q l}{2m}\left\{\frac{-lm}{k^2(1+k^2+iq\omega_{c0})} - \frac{2}{\Lambda k^2}\right\}(1+k^2+i\omega_{c0})I_1^*, \tag{B.25a}$$

$$a_2 = \frac{-\Lambda q l}{2m}\left\{\frac{-m^2}{k^2(1+k^2+iq\omega_{c0})} - \frac{2l}{\Lambda k^2 m}\right\}(1+k^2+i\omega_{c0})I_2$$

$$-\frac{\Lambda q l}{2m}\left\{\frac{lm}{k^2(1+k^2+iq\omega_{c0})} - \frac{2}{\Lambda k^2}\right\}(1+k^2+i\omega_{c0})I_1, \tag{B.25b}$$

where

$$I_1 = \frac{1}{\pi}\int_0^\pi DB_{00}\cos(z)dz, \tag{B.26a}$$

$$I_2 = \frac{1}{\pi}\int_0^\pi X_{00}\cos(z)dz. \tag{B.26b}$$

Two problems now arise. The first is that R_{c1} and ω_{c1} must be known a priori before equations (B.24a), (B.24b) and (B.24c) can be solved. The second problem relates to the operators defined by

$$\mathcal{L}_{-1} = \mathbf{D}^*_{-1}(R_{c0}) - i\omega_{c0}\mathbf{J}, \tag{B.27a}$$

$$\mathcal{L}_1 = \mathbf{D}_1(R_{c0}) - i\omega_{c0}\mathbf{J}. \tag{B.27b}$$

The normal method used to solve the equations

$$\mathcal{L}_{-1}\mathbf{X}_{-11} = \mathcal{U}_1\mathbf{I}^*_{-10} - \left\{\hat{\mathbf{D}}^*_{-1}(R_{c1}) - i\omega_{c1}\mathbf{J}\right\}\mathbf{X}_{-10}, \tag{B.28a}$$

$$\mathcal{L}_1\mathbf{X}_{11} = \mathcal{U}_1\mathbf{I}_{10} - \left\{\hat{\mathbf{D}}_{10}(R_{c1}) - i\omega_{c1}\mathbf{J}\right\}\mathbf{X}_{10}, \tag{B.28b}$$

subject to

$$W_{-11} = B_{-11} = DX_{-11} = T_{-11} = 0 \quad \text{on} \quad z = 0, \tag{B.29a}$$

$$W_{-11} + \frac{im\mathcal{U}_1}{2} = B_{-11} = DX_{-11} = T_{-11} = 0 \quad \text{on} \quad z = \pi, \tag{B.29b}$$

$$W_{11} = B_{11} = DX_{11} = T_{11} = 0 \quad \text{on} \quad z = 0, \tag{B.29c}$$

$$W_{11} - \frac{im\mathcal{U}_1}{2} = B_{11} = DX_{11} = T_{11} = 0 \quad \text{on} \quad z = \pi, \tag{B.29d}$$

is to write the solutions in the form

$$\mathbf{X}_{-11}(z) = \mathbf{X}^{\mathrm{f}}_{-11}(z) + \mathbf{X}^{\mathrm{pi}}_{-11}(z),$$

$$\mathbf{X}_{11}(z) = \mathbf{X}^{\mathrm{f}}_{11}(z) + \mathbf{X}^{\mathrm{pi}}_{11}(z),$$

where $\mathbf{X}^{\mathrm{f}}_{\pm 11}$ are the free solutions, which satisfy the equations

$$\mathcal{L}_{-1}\mathbf{X}^{\mathrm{f}}_{-11} = 0, \tag{B.30a}$$

$$\mathcal{L}_{1}\mathbf{X}^{\mathrm{f}}_{11} = 0, \tag{B.30b}$$

subject to the boundary conditions (B.29), while $\mathbf{X}^{\mathrm{pi}}_{\pm 11}$ are the particular integrals, which are chosen to satisfy the inhomogeneous equations

$$\mathcal{L}_{-1}\mathbf{X}^{\mathrm{pi}}_{-11} = \mathcal{U}_1\mathbf{I}^{*}_{-10} - \left\{\hat{\mathbf{D}}^{*}_{-1}(R_{c1}) - i\omega_{c1}\mathbf{J}\right\}\mathbf{X}^{\mathrm{pi}}_{-10}, \tag{B.31a}$$

$$\mathcal{L}_{1}\mathbf{X}^{\mathrm{pi}}_{11} = \mathcal{U}_1\mathbf{I}_{10} - \left\{\hat{\mathbf{D}}_{10}(R_{c1}) - i\omega_{c1}\mathbf{J}\right\}\mathbf{X}^{\mathrm{pi}}_{10}. \tag{B.31b}$$

However, because R_{c0} and ω_{c0} obey the solvability condition (B.18), solutions of the equations (B.30) will only obey homogeneous boundary conditions - that is, R_{c0} and ω_{c0} are the *eigenvalues* of the operators $\mathcal{L}_{\pm 1}$ at which homogeneous solutions exist. Therefore, (B.30) cannot be solved subject to (B.29), since the boundary conditions (B.29) are inhomogeneous. Thus, a solution of (B.28) will only exist provided that the particular integrals $\mathbf{X}^{\mathrm{pi}}_{\pm 11}$ satisfy the boundary conditions (B.29) as well as satisfying (B.31).

Both problems would be eliminated if R_{c1} and ω_{c1} could be chosen in such a way that $\mathbf{X}^{\mathrm{pi}}_{\pm 11}$ obeyed (B.29) as well as satisfying (B.31). The conditions that ensure that this occurs are called the solvability conditions. To find them, the adjoint problem to (B.30) must be considered. Henceforth, $\mathbf{X}_{\pm 11}$ shall be written for $\mathbf{X}^{\mathrm{pi}}_{\pm 1}$.

B.4.1 The Adjoint Problems

Consider the following homogeneous problem. Solve the equations

$$\mathcal{L}_{1}\mathbf{X}_{11} = \left\{\mathbf{D}_1(R_{c0}) - i\omega_{c0}\mathbf{J}\right\}\mathbf{X}_{11} = 0, \tag{B.32}$$

subject to the boundary conditions

$$W_{11} = B_{11} = DX_{11} = T_{11} = 0 \quad \text{on} \quad z = 0 \quad \text{and} \quad z = \pi. \tag{B.33}$$

Define the adjoint vector $\mathbf{X}_{11}^{A}$ by

$$\mathbf{X}_{11}^{A^T}(z) = \Big[T_{11}^{A}(z) \quad W_{11}^{A}(z) \quad B_{11}^{A}(z) \quad X_{11}^{A}(z) \quad Z_{11}^{A}(z)$$

$$B_{x11}^{A}(z) \quad B_{y11}^{A}(z) \quad U_{x11}^{A}(z) \quad U_{y11}^{A}(z)\Big], \tag{B.34}$$

and an inner product $< .,. >$ by

$$< \mathbf{Y}, \mathbf{Z} >= \frac{1}{\pi}\int_0^{\pi} \mathbf{Y}.\mathbf{Z}dz. \tag{B.35}$$

Now, the inner product of (B.32) with $\mathbf{X}_{11}^{A}$ yields the equation

$$< \mathbf{X}_{11}^{A}, \mathcal{L}_1\mathbf{X}_{11} >= 0. \tag{B.36}$$

Evaluating this inner product, and using the formulae

$$\frac{1}{\pi}\int_0^{\pi} yDxdz = \frac{1}{\pi}\Big[xy\Big]_0^{\pi} - \frac{1}{\pi}\int_0^{\pi} xDydz,$$

$$\frac{1}{\pi}\int_0^{\pi} yD^2xdz = \frac{1}{\pi}\Big[yDx - xDy\Big]_0^{\pi} + \frac{1}{\pi}\int_0^{\pi} xD^2ydz,$$

the following condition (which is equivalent to (B.36)) is obtained

$$0 =< \mathcal{L}_1^{A}\mathbf{X}_{11}^{A}, \mathbf{X}_{11} > +$$

$$\frac{1}{\pi}\Big[W_{11}(T_{11}^{A} + U_{y11}^{A} + U_{x11}^{A}) - B_{11}(DW_{11}^{A} + DB_{11}^{A} - B_{x11}^{A} - B_{y11}^{A})$$

$$-T_{11}(DZ_{11}^{A}) - X_{11}^{A}(DX_{11}) + W_{11}^{A}(Z_{11} + DB_{11}) + B_{11}^{A}(DB_{11})$$

$$-X_{11}(DX_{11}^{A}) + Z_{11}^{A}(DT_{11})\Big]_0^{\pi}, \tag{B.37}$$

where

$$\mathcal{L}_1^A \mathbf{X}_{11}^A = \begin{bmatrix} (D^2 - k^2 - i\omega_{c0}) Z_{11}^A + k^2 R_{c0} W_{11}^A \\ -2DT_{11}^A + imB_{11}^A + Z_{11}^A + ilDU_{x11}^A + imDU_{y11}^A \\ (D^2 - k^2)\{B_{11}^A - \Lambda imW_{11}^A\} - iq\omega_{c0} B_{11}^A + ilDB_{x11}^A + imDB_{y11}^A \\ (D^2 - k^2 - iq\omega_{c0}) X_{11}^A + \Lambda imT_{11}^A - imB_{x11}^A + ilB_{y11}^A \\ -2DW_{11}^A + imX_{11}^A - imU_{x11}^A + ilU_{y11}^A \\ k^2 B_{x11}^A \\ k^2 B_{y11}^A \\ k^2 U_{x11}^A \\ k^2 U_{y11}^A \end{bmatrix}. \tag{B.38}$$

Using the boundary conditions (B.33), the condition (B.37) becomes

$$0 =< \mathcal{L}_1^A \mathbf{X}_{11}^A, \mathbf{X}_{11} > + \frac{1}{\pi} \Big[W_{11}^A (Z_{11} + DB_{11}) + B_{11}^A (DB_{11}^A) - DX_{11}^A (X_{11}) + Z_{11}^A (DT_{11}) \Big]_0^\pi. \tag{B.39}$$

Equation (B.39) is satisfied provided that $\mathbf{X}_{11}^A$ is chosen to be the solution of

$$\mathcal{L}_1^A \mathbf{X}_{11}^A = 0, \tag{B.40}$$

subject to the boundary conditions

$$W_{11}^A = B_{11}^A = DX_{11}^A = Z_{11}^A = 0 \quad \text{on} \quad z = 0 \quad \text{and} \quad z = \pi. \tag{B.41}$$

(B.40) and (B.41) define the adjoint problem to (B.32) and (B.33). To define the solvability conditions, only a particular solution of the adjoint problem is required. One such solution is given by

$$\mathbf{X}^A_{11}(z) = \begin{bmatrix} T^A_{11}(z) \\ W^A_{11}(z) \\ B^A_{11}(z) \\ X^A_{11}(z) \\ Z^A_{11}(z) \\ B^A_{x11}(z) \\ B^A_{y11}(z) \\ U^A_{x11}(z) \\ U^A_{y11}(z) \end{bmatrix} = \begin{bmatrix} \frac{-2(1+k^2+iq\omega_{c0})}{\Lambda m^2}\cos(z) \\ \sin(z) \\ \frac{\Lambda im(1+k^2)}{1+k^2+iq\omega_{c0}}\sin(z) \\ \frac{-2i}{m}\cos(z) \\ \left\{\frac{4(1+k^2+iq\omega_{c0})}{\Lambda m^2} + \frac{\Lambda m^2(1+k^2)}{1+k^2+iq\omega_{c0}}\right\}\sin(z) \\ 0 \\ 0 \\ 0 \\ 0 \end{bmatrix}. \qquad (B.42)$$

This solution exists provided that the following relation holds

$$4(qi\omega_{c0}+1+k^2)^2(i\omega_{c0}+1+k^2)+\Lambda^2 m^4(i\omega_{c0}+1+k^2)(1+k^2)$$
$$-k^2\Lambda m^2(qi\omega_{c0}+1+k^2)R_{c0}=0,$$

which is precisely the relation defining R_{c0} and ω_{c0}. This merely says that the eigenvalues of $\mathcal{L}^A_1$ are the same as those of $\mathcal{L}_1$.

In a similar manner, the adjoint problem for the homogeneous equations

$$\mathcal{L}_{-1}\mathbf{X}_{-11} = \left\{\mathbf{D}^*_{-1}(R_{c0}) - i\omega_{c0}\mathbf{J}\right\}\mathbf{X}_{-11} = 0, \qquad (B.43)$$

with boundary conditions

$$W_{-11} = B_{-11} = DX_{-11} = T_{-11} = 0 \quad \text{on} \quad z = 0 \quad \text{and} \quad z = \pi, \qquad (B.44)$$

can be set up. The details are ommitted, but the following particular solution of the resulting adjoint problem is found

$$\mathbf{X}^A_{-11}(z) = \begin{bmatrix} T^A_{-11}(z) \\ W^A_{-11}(z) \\ B^A_{-11}(z) \\ X^A_{-11}(z) \\ Z^A_{-11}(z) \\ B^A_{x,-11}(z) \\ B^A_{y,-11}(z) \\ U^A_{x,-11}(z) \\ U^A_{y,-11}(z) \end{bmatrix} = \begin{bmatrix} \frac{-2(1+k^2+iq\omega_{c0})}{\Lambda m^2}\cos(z) \\ \sin(z) \\ \frac{-\Lambda im(1+k^2)}{1+k^2+iq\omega_{c0}}\sin(z) \\ \frac{2i}{m}\cos(z) \\ \left\{\frac{4(1+k^2+iq\omega_{c0})}{\Lambda m^2} + \frac{\Lambda m^2(1+k^2)}{1+k^2+iq\omega_{c0}}\right\}\sin(z) \\ 0 \\ 0 \\ 0 \\ 0 \end{bmatrix}. \qquad (B.45)$$

Again, this solution only exists provided that (B.18) is satisfied.

The adjoint vectors $\mathbf{X}^A_{\pm 11}$ given by (B.42) and (B.45) will now be used to define the solvability conditions for equations (B.31), which will ensure that the particular integrals satisfying (B.31) also obey the boundary conditions (B.29)

B.4.2 The Solvability Conditions

Consider now the inhomogeneous equations

$$\mathcal{L}_{-1}\mathbf{X}_{-11} = \left\{\mathbf{D}^*_{-1}(R_{c0}) - i\omega_{c0}\mathbf{J}\right\}\mathbf{X}_{-11} = \mathbf{F}_{-11}, \qquad (B.46)$$

where

$$\mathbf{F}_{-11} = \mathcal{U}_1 \mathbf{I}^*_{-10} - \left\{ \hat{\mathbf{D}}^*_{-1}(R_{c1}) - i\omega_{c1}\mathbf{J} \right\} \mathbf{X}_{-10}. \qquad (B.47)$$

The solution of these equations is required to obey the boundary conditions

$$W_{-11} = B_{-11} = DX_{-11} = T_{-11} = 0 \quad \text{on} \quad z = 0, \qquad (B.48a)$$

$$W_{-11} + \frac{im\mathcal{U}_1}{2} = B_{-11} = DX_{-11} = T_{-11} = 0 \quad \text{on} \quad z = \pi. \qquad (B.48b)$$

Form the inner product of (B.46) with the adjoint vector $\mathbf{X}^A_{-11}$. This yields the equation

$$< \mathbf{X}^A_{-11}, \mathcal{L}_{-1}\mathbf{X}_{-11} > = < \mathbf{X}^A_{-11}, \mathbf{F}_{-11} > . \qquad (B.49)$$

Equation (B.49) is the required solvability condition for (B.46).

Using (B.37), together with the boundary conditions obeyed by $\mathbf{X}^A_{-11}$ and $\mathbf{X}_{-11}$, the left hand side of (B.49) yields

$$< \mathbf{X}^A_{-11}, \mathcal{L}_{-1}\mathbf{X}_{-11} > = < \mathcal{L}^A_{-1}\mathbf{X}^A_{-11}, \mathbf{X}_{-11} > +$$

$$\frac{1}{\pi}\Big[W_{-11}T^A_{-11} + \text{terms that vanish at } z = 0, \pi \Big]_0^\pi .$$

Now, using the equation satisfied by $\mathbf{X}^A_{-11}$, i.e.

$$\mathcal{L}^A_{-1}\mathbf{X}^A_{-11} = 0,$$

together with the definition of T^A_{-11} in (B.45), this becomes

$$< \mathbf{X}^A_{-11}, \mathcal{L}_{-1}\mathbf{X}_{-11} > = \frac{1}{\pi}\left[W_{-11}\left\{ \frac{-2(1 + k^2 + iq\omega_{c0})}{\Lambda m^2} \cos(z) \right\} \right]_0^\pi ,$$

which together with the boundary conditions satisfied by W_{-11} yields

$$< \mathbf{X}^{A}_{-11}, \mathcal{L}_{-1}\mathbf{X}_{-11} >= -\frac{i(1+k^2+iq\omega_{c0})}{\pi\Lambda m}\mathcal{U}_1. \qquad (B.50)$$

It is a straightforward (but tedious) task to form the inner product of $\mathbf{F}_{-11}$ with $\mathbf{X}^{A}_{-11}$. Using the definitions of $\mathbf{X}_{\pm 10}$, and performing the relevant integrations, the right hand side of (B.49) yields

$$< \mathbf{X}^{A}_{-11}, \mathbf{F}_{-11} >= \left\{\frac{-1}{2}k^2 R_{c1} + \chi i\omega_{c1}\right\}A_{-10} + \left[\frac{-q\Lambda m^2(1+k^2)}{1+k^2+iq\omega_{c0}}I_3^* \right.$$

$$\left. + \frac{2q}{m^2}\left\{k^2 I_2^* + lmI_1^*\right\} - im\left\{\frac{4(1+k^2+iq\omega_{c0})}{\Lambda m^2} + \frac{\Lambda m^2(1+k^2)}{1+k^2+iq\omega_{c0}}\right\}I_4^*\right]\mathcal{U}_1, \qquad (B.51)$$

where

$$\chi = \frac{2(1+k^2+iq\omega_{c0})}{\Lambda m^2} + \frac{\Lambda m^2(1+k^2)}{2(1+k^2+iq\omega_{c0})}$$

$$- \frac{\Lambda m^2 q(1+k^2)(1+k^2+i\omega_{c0})}{2(1+k^2+iq\omega_{c0})^2} + \frac{2q(1+k^2+i\omega_{c0})}{\Lambda m^2}, \qquad (B.52)$$

and

$$I_3 = \frac{1}{\pi}\int_0^{\pi} B_{00}\sin(z)dz, \qquad (B.53a)$$

$$I_4 = \frac{1}{\pi}\int_0^{\pi} T_{00}\sin(z)dz. \qquad (B.53b)$$

Equating (B.50) and (B.51), the following equation is obtained

$$a_3\mathcal{U}_1 - \mu A_{-10} = 0, \qquad (B.54)$$

where μ and a_3 are complex constants defined by

$$\mu = \frac{1}{2}k^2 R_{c1} - \chi i\omega_{c1}, \tag{B.55}$$

and

$$a_3 = \frac{-q\Lambda m^2(1+k^2)}{1+k^2+iq\omega_{c0}} I_3^* + \frac{2q}{m^2}\left\{k^2 I_2^* + lmI_1^*\right\} - im\left\{\frac{4(1+k^2+iq\omega_{c0})}{\Lambda m^2} + \frac{\Lambda m^2(1+k^2)}{1+k^2+iq\omega_{c0}}\right\} I_4^* + \frac{i(1+k^2+iq\omega_{c0})}{\pi\Lambda m}. \tag{B.56}$$

Now, consider the inhomogeneous equations

$$\mathcal{L}_1 \mathbf{X}_{11} = \left\{\mathbf{D}_1(R_{c0}) - i\omega_{c0}\mathbf{J}\right\}\mathbf{X}_{11} = \mathbf{F}_{11}, \tag{B.57}$$

where

$$\mathbf{F}_{11} = \mathcal{U}_1 \mathbf{I}_{10} - \left\{\hat{\mathbf{D}}_1(R_{c1}) - i\omega_{c1}\mathbf{J}\right\}\mathbf{X}_{10}. \tag{B.58}$$

The solution of these equations is required to obey the boundary conditions

$$W_{11} = B_{11} = DX_{11} = T_{11} = 0 \quad \text{on} \quad z = 0, \tag{B.59a}$$

$$W_{11} - \frac{im\mathcal{U}_1}{2} = B_{11} = DX_{11} = T_{11} = 0 \quad \text{on} \quad z = \pi. \tag{B.59b}$$

To find the solvability condition for (B.57), the inner product of (B.57) with $\mathbf{X}_{11}^A$ is formed. This yields the equation

$$< \mathbf{X}_{11}^A, \mathcal{L}_1 \mathbf{X}_{11} > = < \mathbf{X}_{11}^A, \mathbf{F}_{11} > . \tag{B.60}$$

Repeating the analysis carried out on equation (B.49), (B.60) yields the equation

$$a_4 \mathcal{U}_1 - \mu A_{10} = 0, \tag{B.61}$$

where μ is given by (B.55) and a_4 is another complex constant defined by

$$a_4 = \frac{-q\Lambda m^2(1+k^2)}{1+k^2+iq\omega_{c0}} I_3 + \frac{2q}{m^2}\Big\{k^2 I_2 - lmI_1\Big\} + im\Big\{\frac{4(1+k^2+iq\omega_{c0})}{\Lambda m^2}$$

$$+\frac{\Lambda m^2(1+k^2)}{1+k^2+iq\omega_{c0}}\Big\} I_4 - \frac{i(1+k^2+iq\omega_{c0})}{\pi\Lambda m}. \qquad (B.62)$$

Finally, the solvability conditions for equations (B.31) take the form

$$a_4\mathcal{U}_1 - \mu A_{10} = 0, \qquad (B.63a)$$

$$a_3\mathcal{U}_1 - \mu A_{-10} = 0. \qquad (B.63b)$$

Recalling that

$$\mathcal{U}_1 = a_1 A_{10} + a_2 A_{-10},$$

equations (B.63) can be written in matrix notation as

$$\mathbf{CA} = \mu\mathbf{A}, \qquad (B.64)$$

where $\mathbf{C}$ is a 2×2 complex matrix defined by

$$\mathbf{C} = \begin{bmatrix} a_1 a_4 & a_2 a_4 \\ a_1 a_3 & a_2 a_3 \end{bmatrix}, \qquad (B.65)$$

and $\mathbf{A}$ is a 2×1 complex vector defined by

$$\mathbf{A} = \begin{bmatrix} A_{10} \\ A_{-10} \end{bmatrix}. \qquad (B.66)$$

Hence, R_{c1} and ω_{c1} are obtained from the eigenvalues of $\mathbf{C}$, while A_{10} and A_{-10} are obtained from the eigenvectors of $\mathbf{C}$.

The two eigensolutions of (B.64) are given by

$$\mu = 0, \quad \mathbf{A} = \begin{bmatrix} -a_2 \\ a_1 \end{bmatrix}, \tag{B.67}$$

and

$$\mu = a_2 a_3 + a_1 a_4, \quad \mathbf{A} = \begin{bmatrix} a_4 \\ a_3 \end{bmatrix}. \tag{B.68}$$

Just as in the $n = 0$ case, where two possible values for R_{c0} and ω_{c0} existed so that the $n = 0$ equations had a solution, so here two possible values for R_{c1} and ω_{c1} exist (obtained from the two possible values of μ) at which the $n = 1$ equations have a solution. These two cases will be discussed seperately.

B.4.3 The Eigensolution (B.67)

The first eigensolution is given by (B.67). Using the definitions of μ and $\mathbf{A}$, (B.67) yields

$$\frac{1}{2}k^2 R_{c1} - \chi i \omega_{c1} = 0, \tag{B.69a}$$

$$\begin{bmatrix} A_{10} \\ A_{-10} \end{bmatrix} = \begin{bmatrix} -a_2 \\ a_1 \end{bmatrix}. \tag{B.69b}$$

Now, provided that l and m are non zero, then k^2 and χ are also non zero, whence the real and imaginary parts of (B.69a) yield

$$R_{c1} = 0, \quad \omega_{c1} = 0, \tag{B.70}$$

respectively. Similarly, (B.69b) yields

$$A_{10} = -a_2, \quad A_{-10} = a_1. \tag{B.71}$$

These values may be used in equation (B.24) for $\mathcal{U}_1$, to obtain

$$\mathcal{U}_1 = a_1(-a_2) + a_2(a_1) = 0. \qquad (B.72)$$

Having obtained R_{c1}, ω_{c1} and $\mathcal{U}_1$, equations (B.22a,b,c) can now be solved. Substituting (B.70) and (B.72) into (B.22a,b,c) gives

$$\mathbf{D}_0(R_{c0})\mathbf{X}_{01} = 0, \qquad (B.73a)$$

$$\left\{\mathbf{D}^*_{-1}(R_{c0}) - i\omega_{c0}\mathbf{J}\right\}\mathbf{X}_{-11} = 0, \qquad (B.73b)$$

$$\left\{\mathbf{D}_1(R_{c0}) - i\omega_{c0}\mathbf{J}\right\}\mathbf{X}_{11} = 0, \qquad (B.73c)$$

while the boundary conditions (B.23) become

$$W_{01} = B_{01} = DX_{01} = T_{01} = 0 \quad \text{on} \quad z = 0 \quad \text{and} \quad z = \pi, \qquad (B.74a)$$

$$W_{-11} = B_{-11} = DX_{-11} = T_{-11} = 0 \quad \text{on} \quad z = 0 \quad \text{and} \quad z = \pi, \qquad (B.74b)$$

$$W_{11} = B_{11} = DX_{11} = T_{11} = 0 \quad \text{on} \quad z = 0 \quad \text{and} \quad z = \pi. \qquad (B.74c)$$

A particular integral of (B.73) and (B.74) is

$$\mathbf{X}_{01}(z) = 0, \quad \mathbf{X}_{-11}(z) = 0, \quad \mathbf{X}_{11}(z) = 0, \qquad (B.75)$$

and this is the solution of the $n = 1$ equations for this case.

In fact, examination of equations (B.10) and (B.11) reveals that by choosing

$$\mathbf{X}_{rn}(z) = 0 \quad (n = 2, 3, ...), \tag{B.76a}$$

$$\mathcal{U}_n = 0 \quad (n = 2, 3, ...), \tag{B.76b}$$

$$R_{cn} = 0 \quad (n = 2, 3, ...), \tag{B.76c}$$

$$\omega_{cn} = 0 \quad (n = 2, 3, ...), \tag{B.76d}$$

an *exact*, *analytic* solution of (B.8) and (B.7) may be obtained! This analytic solution is given by

$$\mathbf{X}_0(z) = \mathbf{X}_{00}(z), \tag{B.77a}$$

$$\mathbf{X}_{-1}(z) = a_1 \mathbf{X}_{-1RS}(z), \tag{B.77b}$$

$$\mathbf{X}_1 = -a_2 \mathbf{X}_{1RS}(z), \tag{B.77c}$$

$$\mathcal{U} = 0, \tag{B.77d}$$

where $\mathbf{X}_{00}$ is defined by (B.21), a_1 and a_2 are defined by (B.25), and $\mathbf{X}_{\pm 1RS}$ are the Roberts and Stewartson ($\pm$) oblique roll solutions defined in chapter 3. This solution is discussed further in chapter 5.

B.4.4 The Eigensolution (B.68)

Attention is now turned to the second eigensolution of (B.64), which is (B.68). To compare with the numerics, only the case

$$\Lambda = 4,$$

will be considered, for which

$$R_{c0} = 6\sqrt{3}, \quad \omega_{c0} = 0, \quad l^2 = 2 - \frac{\sqrt{2}}{2}, \quad m^2 = \frac{\sqrt{3}}{2}.$$

At these values, a_1 and a_2 are given by (5.46), while a_3 and a_4 become

$$a_3 = -2\sqrt{3}qI_3^* + \frac{4}{\sqrt{3}}q(2I_2^* + lmI_1^*) + im(\frac{\sqrt{3}}{2\pi} - 4\sqrt{3}I_4^*), \qquad (B.78a)$$

$$a_4 = -2\sqrt{3}qI_3 + \frac{4}{\sqrt{3}}q(2I_2 - lmI_1) - im(\frac{\sqrt{3}}{2\pi} - 4\sqrt{3}I_4). \qquad (B.78b)$$

Now, because the basic state satisfies the condition (4.21), the integrals I_j must satisfy

$$I_1 = -I_1^*, \quad I_2 = -I_2^*, \quad I_3 = -I_3^*, \quad I_4 = I_4^*.$$

For the parameter values being considered, this fact implies that the a_j satisfy the conditions

$$a_1 = -a_1^*, \quad a_2 = -a_2^*, \quad a_3 = -a_3^*, \quad a_4 = -a_4^*,$$

and hence, that μ satisfies

$$\mu = \mu^*. \qquad (B.86)$$

Therefore, the imaginary part of μ vanishes, and so

$$2\sqrt{3}\omega_{c1} = 0 \quad \Rightarrow \quad \omega_{c1} = 0. \qquad (B.79)$$

The real part of μ gives

$$R_{c1} = a_1a_4 + a_2a_3. \qquad (B.80)$$

Using (B.68) together with the definition of **A** yields

$$\begin{bmatrix} A_{10} \\ A_{-10} \end{bmatrix} = \begin{bmatrix} a_4 \\ a_3 \end{bmatrix} \quad \Rightarrow \quad A_{10} = a_4, \quad A_{-10} = a_3. \tag{B.81}$$

Using this result in equation (B.24) for $\mathcal{U}_1$ gives

$$\mathcal{U}_1 = a_1 a_4 + a_2 a_3. \tag{B.82}$$

Hence, a second set of values for R_{c1}, ω_{c1} and $\mathcal{U}_1$ have been found to ensure that the $n = 1$ equations have a solution. These values may be substituted into (B.24a,b,c) and the relevant particular integral found. Denote the solution of (B.24a,b,c) with these values of R_{c1}, ω_{c1} and $\mathcal{U}_1$ by

$$\mathbf{X}_{01}(z), \quad \mathbf{X}_{-10}(z), \quad \mathbf{X}_{10}(z).$$

The actual form taken by the $\mathbf{X}_{r1}$ is very complicated, and is not very enlightening.

Bibliography

Abdel-Aziz, M.M. and Jones, C.A., '$\alpha\omega$ dynamos and Taylor's constraint', *Geophys. Astrophys. Fluid Dynamics* **44**, 117-139, (1988).

Barenghi, C.F., 'Nonlinear plantary dynamos in a rotating spherical shell II: The post Taylor equilibrium for α^2 dynamos', *Geophys. Astrophys. Fluid Dynamics* **67**, 27-36, (1992a).

Barenghi, C.F., 'Nonlinear planetary dynamos in a rotating spherical shell III: $\alpha^2\omega$ models and the geodynamo', *Geophys. Astrophys. Fluid Dynamics* **71**, 163-185, (1992b).

Barenghi, C.F. and Jones, C.A., 'Nonlinear planetary dynamos in a rotating spherical shell I: Numerical methods', *Geophys. Astrophys. Fluid Dynamics* **60**, 211-243, (1991).

Bell, P.I., 'The effect of bumps upon convection in the Earth's core', *PhD. dissertation, University of Newcastle Upon Tyne*, (1993).

Bell, P.I. and Soward, A.M., 'The influence of surface topography upon rotating convection', submitted, (1995).

Bloxham, J. and Gubbins, D., 'Thermal core-mantle interactions', *Nature* **325**, 511-513, (1987).

Braginsky, S.I., 'Magnetic waves in the Earth's core', *Geomag. Aeron.* **7**, 851-859, (1967a).

Braginsky, S.I., 'Nearly axially symmetric model of the hydromagnetic dynamo of the Earth I', *Geomag. Aeron.* **15**, 122-128, (1975).

Braginsky, S.I., 'Nearly axially symmetric model of the hydrodynamic dynamo of the Earth', *Geomag. Aeron.* **18**, 225-231, (1978).

Braginsky, S.I., 'The z model of the geodynamo with magnetic friction', *Geomag. Aeron.* **28**, 407-412, (1988).

Busse, F.H., 'Thermal instabilities in rapidly rotating systems', *J. Fluid Mech.* **44**, 441-460, (1970).

Busse, F.H. and Wicht, J., 'A simple dynamo caused by conductivity variations', *Geophys. Astrophys. Fluid Dynamics* **64**, 135-144, (1991).

Chandrasekhar, S., *Hydrodynamical and Hydromagnetic Stability*, Dover Publications inc., Oxford (1961).

Cowling, T.G., 'The magnetic field of sunspots', *Mon. Not. R. Astr. Soc.* **94**, 39-48, (1934).

Eltayeb, I.A. and Kumar, S., 'Hydromagnetic convective instbilities of a rotating self-gravitating fluid sphere containing a uniform distribution of heat sources', *Proc. R. Soc. Lond.* A**353**, 145-162, (1977).

Fearn, D.R., 'Thermally driven hydromagnetic convection in a rapidly rotating sphere', *Proc. R. Soc. Lond.* A**369**, 227-242, (1979a).

Fearn, D.R., 'Thermal and magnetic instabilities in a rapidly rotating fluid sphere', *Geophys. Astrophys. Fluid Dynamics* **14**, 103-126, (1979b).

Fearn, D.R., 'Differential rotation and thermal convection in a rapidly rotating hydromagnetic system', *Geophys. Astrophys. Fluid Dynamics* **49**, 173-193, (1989).

Fearn, D.R., 'Nonlinear planetary dynamos' in *Stellar and Planetary Dynamos*, (eds. M.R.E. Proctor and A.D. Gilbert), Cambridge University Press, (1994).

Fearn, D.R. and Proctor, M.R.E., 'Hydromagnetic waves in a differentially rotating sphere', *J. Fluid Mech.* **128**, 1-20, (1983a).

Fearn, D.R. and Proctor, M.R.E., 'The stabilising role of differential rotation on hrdromagnetic waves', *J. Fluid Mech.* **128**, 21-36, (1983b)

Fearn, D.R. and Proctor, M.R.E., 'Dynamically consistent magnetic fields produced by differential rotation', *J. Fluid Mech.* **178**, 521-534, (1987).

Fearn, D.R. and Proctor, M.R.E., 'Magnetogeostrophic balance in non axisymmetric, non-standard dynamo models', *Geophys. Astrophys. Fluid Dynamics* **67**, 117-128, (1992).

Fearn, D.R., Proctor, M.R.E. and Sellar, C.C., 'Nonlinear magnetoconvection in a rotating sphere and Taylor's constraint', *Geophys. Astrophys. Fluid Dynamics*,

77, 111-132, (1994).

Fearn, D.R., Roberts, P.H. and Soward, A.M., 'Convection, stability and the dynamo' in *Energy, Stability and Convection*, (eds G.P. Galdi and B. Straughan), Pittman Research Notes in Mathematics **168**, Longman, (1988).

Greenspan, H.P., *The Theory of Rotating Fluids*, Cambridge University Press, (1969).

Gottlieb, D. and Orzag, S.A., *Numerical Analysis of Spectral Methods*, SIAM, (1977).

Gubbins, D. and Richards, M., 'Coupling of the core dynamo and mantle: thermal or topographic?', *Geophys. Res. Lett.* **13**, 1521-1524, (1986).

Gubbins, D. and Bloxham, J., 'Morphology of the geomagnetic field and implications for the geodynamo', *Nature* **325**, 509-511, (1987).

Hide, R., 'Motions of the Earth's core and mantle and variations of the main geomagnetic field', *Science* **157**, 55-56, (1967).

Hide, R., 'Interaction between the Earth's liquid core and solid mantle', *Nature* **222**, 1055-1056, (1969).

Hide, R., 'Towards a theory of irregular variations in the length of day and core-mantle coupling', *Phil. Trans. R. Soc.* **A284**, 547-554, (1977).

Hide, R., 'Fluctuations in the Earth's rotation and the topography of the core-mantle interface', *Phil. Trans. R. Soc. Lond.* **A328**, 351-363, (1989).

Hollerbach, R. and Ierley, G.R., 'Macrodynamics of α^2 dynamos', *Geophys. Astrophys. Fluid Dynamics* **56**, 133-158, (1991).

Hollerbach, R., Barenghi, C.F. and Jones, C.A., 'Taylor's constraint in a spherical $\alpha\omega$ dynamo', *Geophys. Astrophys. Fluid Dynamics* **67**, 3-25, (1992).

Ierley, G.R., 'Macrodynamics of α^2 dynamos', *Geophys. Astrophys. Fluid Dynamics* **34**, 143-173, (1991).

Geomagnetism II, ed. J.A. Jacobs, London: Academic, (1987).

Jault, D. and Le Moeul, J.-L., 'The topographic torque associated with a tangentially geostrophic motion at the core surface and inferences on the flow inside the core', *Geophys. Astrophys. Fluid Dynamics* **48**, 273-296, (1989).

Jones, C.A., 'Dynamo models and Taylor's constraint' in *Advances in Solar System MHD* (eds. E.R. Priest and A.W. Hood), 25-50, Cambridge University Press, (1991).

Jones, C.A. and Roberts, P.H., 'Magnetoconvection in rapidly rotating Boussinesq and compressible fluids', *Geophys. Astrophys. Fluid Dynamics* **55**, 263-308, (1990)

Jones, C.A. and Soward, A.M., 'Magnetohydrodynamic dynamo action', *Sci. Prog. Oxford* **74**, 529-557, (1990).

Jones, C.A. and Wallace, S.G., 'Periodic, chaotic and steady solutions in $\alpha\omega$ dynamos', *Geophys. Astrophys. Fluid Dynamics* **67**, 37-64, (1992).

Kelly, R.E. and Pal, D., 'Thermal convection with spatially periodic boundary conditions: resonant wavelength excitation', *J. Fluid Mech.* **86**, 433-456, (1977).

Kuang, W. and Bloxham, J., 'On the effect of boundary topography on flow in the Earth's core', *Geophys. Astrophys. Fluid Dynamics* **72**, 161-195, (1993).

Lanczos, C., *Applied Analysis*, Prentis-Hall, (1956).

Malkus, W.V.R and Proctor, M.R.E., 'The macrodynamics of α-effect dynamos in rotating fluids', *J. Fluid Mech.* **67**, 417-443, (1975).

Moffat, H.K., *Magnetic Field Generation in Conducting Fluids*, Cambridge University Press, (1978).

Moffat, H.K., 'Topographic coupling at the core-mantle interface', *Geophys. Astrophys. Fluid Dynamics* **9**, 279-288, (1978).

Proctor, M.R.E., 'Numerical solution of the nonlinear α-effect dynamo equations', *J. Fluid Mech.* **80**, 769-784, (1977).

Roberts, P.H., 'On the thermal instability of a highly rotating fluid sphere', *Astrophys. J.* **141**, 240-250, (1965).

Roberts, P.H., 'On the thermal instability of a rotating fluid sphere containing heat sources', *Phil. Trans. R. Soc. Lond.* **A263**, 93-117, (1968).

Roberts, P.H., 'The future of geodynamo theory', *Geophys. Astrophys. Fluid Dynamics* **44**, 3-31, (1988).

Roberts, P.H., 'On topographic core-mantle coupling', *Geophys. Astrophys. Fluid Dynamics* **44**, 181-187, (1988).

Roberts, P.H., 'From Taylor state to model z?', *Geophys. Astrophys. Fluid Dynamics* **49**, 143-160, (1989).

Roberts, P.H. and Stewartson, K., 'On finite amplitude convection in a rotating magnetic system', *Phil. Trans. R. Soc. Lond.* A**277**, 93-117, (1974).

Roberts, P.H. and Stewartson, K., 'On double roll convection in a rotating magnetic system', *J. Fluid Mech.* **68**, 447-466, (1975).

Rotating Fluids in Geophysics, eds. P.H. Roberts and A.M. Soward, Academic Press, (1978).

Roberts, P.H. and Soward, A.M., 'Dynamo Theory', *Annu. Rev. Fluid Mech.* **24**, 459-512, (1992).

Skinner, P.H. and Soward, A.M., 'Convection in a rotating magnetic system and Taylor's constraint', *Geophys. Astrophys. Fluid Dynamics* *44*, 91-116, (1988).

Skinner, P.H. and Soward, A.M., 'Convection in a rotating magnetic system and Taylor's constraint II: numerical results', *Geophys. Astrophys. Fluid Dynamics* **60**, 335-356, (1990).

Soward, A.M., 'Thermal and magnetically driven convection in a rapidly rotating fluid layer', *J. Fluid Mech.* **90**, 669-684, (1979).

Soward, A.M., 'Finite amplitude thermal convection and geostrophic flow in a rotating magnetic system', *J. Fluid Mech.* **98**, 449-471, (1980).

Soward, A.M., 'Nonlinear marginal convection in a rotating magnetic system', *Geophys. Astrophys. Fluid Dynamics* **35**, 329-371, (1986).

Soward, A.M., 'The Earth's dyanamo', *Geophys. Astrophys. Fluid Dynamics* **62**, 191-209, (1991).

Soward, A.M. and Jones, C.A., 'α^2 dynamos and Taylor's constraint', *Geophys. Astrophys. Fluid Dynamics* **27**, 87-122, (1983).

Sun, Z.P., Schubert, G. and Glatzmaier, G.A., 'Numerical simulations of thermal convection in a rapidly rotating spherical shell cooled inhomogeneously from above', *Geophys. Astrophys. Fluid Dynamics* **75**, 199-226, (1994).

Taylor, J.B., 'The magnetohydrodynamics of a rotating fluid and the Earth's dynamo problem', *Proc. R. Soc. Lond.* A**274**, 274-283, (1963).

Voorhies, C.V., 'Coupling an inviscid core to an electrically insulating mantle', *J. Geomagn. Geoelectr.* **43**, 131-156, (1991).

Zhang, K.K., 'Convection in a rapidly rotating spherical shell at infinite Prantl number: steadily drifting rolls', *Phys. Earth Planet. Interiors* **68**, 156-169, (1991).

Zhang, K.K. and Gubbins, D., ' On convection in the Earth's core driven by lateral temperature variations', *Geophys. J. Int.* **108**, 247-255, (1992).

Zhang, K.K. and Gubbins, D., 'Convection in a rotating spherical shell with an inhomogeneous temperature boundary at infinite Prantl number', *J. Fluid Mech.* **250**, 209-232, (1993).